INVESTIGATION OF SOIL ARCHING UNDER DIFFERENT MODES OF SOIL MOVEMENT AND SURFACE LOADING

By

Mahdi Abbas Mahdi Al-Naddaf

M.Sc., the University of Kansas, Kansas, USA, 2017

B.Sc., Al-Nahrain University, Baghdad, Iraq, 2011

Submitted to graduate degree program in Civil, Environmental, and Architectural Engineering and the Graduate Faculty of the University of Kansas in partial fulfillment of the requirements for the degree of Doctor of Philosophy

_____

Chairperson: Dr. Jie Han, Professor

_____

Dr. Masoud Darabi, Assist. Professor

_____

Dr. Robert L. Parsons, Professor

_____

Dr. Steven D. Schrock, Professor

_____

Dr. Chi Zhang, Assist. Professor

Date Defended: June 10, 2019

The Dissertation Committee for Mahdi Al-Naddaf certifies that this is the approved version of the following dissertation:

INVESTIGATION OF SOIL ARCHING UNDER DIFFERENT MODES OF SOIL MOVEMENT AND SURFACE LOADING

_____

Chairperson: Dr. Jie Han, Professor

Date Approved: June 10, 2019

ABSTRACTS

Soil arching exists in many geotechnical applications, including tunnels, buried pipes and culverts, and Geosynthetic-Reinforced Pile-Supported (GRPS) embankments. The existence of these buried structures or structural elements within soil masses causes redistribution of stresses, which is referred to as soil arching. The relative stiffness and differential settlement between these buried structures and their surrounding soils affect the magnitude and distribution of vertical stresses. Soil arching has been mostly investigated using trapdoor tests under soil self-weight and/or uniform surcharge. In real applications, localized surface loading, such as traffic loading, may be applied onto soil and affect or degrade soil arching. Also, additional stresses caused by traffic loading on a buried structure may cause excessive deformations and even failure of the buried structure. Geosynthetics have been used in GRPS embankments or over buried pipes and may have effects on soil arching mobilization and degradation under localized surface loading. Expanded Polystyrene (EPS) geofoam, a lightweight material, has been increasingly used above buried structures as a compressible inclusion to reduce vertical stresses acting on the buried structures. The effects of surface traffic loading and geosynthetics on soil arching have not yet been well investigated. Therefore, the main objective of this study was to investigate soil arching under different modes of soil movement and surface loading.

To fulfill the above research objective, a comprehensive experimental study and numerical analysis were conducted. The experimental study included two experimental series. The first experimental series consisted of reduced-scale models of a buried box culvert that were constructed in a test box under a plane-strain condition. This study adopted the Induced Trench Installation (ITI) method to place the concrete culvert overlaid with an EPS geofoam and investigated the effects of EPS geofoam, including geofoam stiffness and thickness, on the

distribution of vertical stresses above a rectangular concrete culvert under surface footing loading. The second experimental series utilized the trapdoor test setup to investigate the effects of localized surface loading on soil arching mobilization and degradation in geosynthetic-reinforced and unreinforced embankments under a plane-strain condition. The trapdoor was supported by compressible springs of a known stiffness and could move under fill self-weight and surface loading to simulate soil subsidence and/or consolidation of foundation (soft) soil between rigid supports. In both experimental series, the backfill material was a dry, poorly-graded Kansas River sand. The footing load was applied parallelly to the culvert or the trapdoor axes. Earth pressure cells were used to monitor the vertical stress distributions above the culvert, the trapdoor, and the surrounding soil. To comprehensively assess the effects of localized surface loading with different configurations, numerical models simulating trapdoor tests were built and validated against the results of the experimental tests. A series of parametric studies were conducted to investigate: the effects of fill height, the most critical condition of the surface loading (as for the footing width and location), and the effects of non-uniform trapdoor displacements by multi-segment trapdoors on soil arching mobilization.

The experimental results of the buried box culvert show that the EPS geofoam reduced the vertical stresses on the buried structure due to the mobilization of soil arching. However, soil arching was found to be partially mobilized based on the measured soil arching ratio due to the low modulus ratio of soil to geofoam that caused limited compression of the geofoam. The lower stiffness and thin geofoam had more effect on the vertical stress reduction. Cyclic loading minimized the soil arching effect induced by the compressible geofoam. This study also examines the test results with available analytical solutions. The effects of soil arching and the induced

vertical stresses above the rigid structure under static footing loading were considered separately. The analytical solutions were found to match well with the experimental results.

The trapdoor test results show that the displacement of the trapdoor during the fill placement induced progressive mobilization of soil arching and geosynthetic reinforcement minimized soil arching mobilization due to the change of the soil deformation. Localized surface loading increased the degree of soil arching at low applied pressure (approximately 50 kPa); however, under higher footing loading, soil arching degraded or stress recovered due to larger trapdoor displacement. Single and double layers of geosynthetic reinforcement helped maintain soil arching under localized surface loading. Geosynthetic reinforcement increased the applied surface load required to fully degrade soil arching and eliminate the benefit of the geosynthetic. Soil arching exhibited arching degradation and even collapse under static loading; however, arching degradation was less pronounced under cyclic loading as the applied pressure increased beyond 80 kPa due to larger differential settlement within the fill.

The results of the numerical simulations show that the degree of soil arching increased as the fill height (H) increased due to the additional shear forces mobilized throughout the fill material. Consequently, less pressure was applied on the trapdoor and more pressure transferred to the supports as the fill height increased from H/B of 1 to 3 (B is the trapdoor width). The model with a footing width of 0.5B was the most critical width and had the highest vertical pressure on the trapdoor for H/B of 2; however, the model with a footing width of 1B had the highest pressure on the trapdoor for both H/B of 1 and 3. The model with a footing offset of 0.0B from the centerline of the trapdoor had the highest vertical pressure on the centerline of the trapdoor. Also, as the footing offset increased to 1B, less pressure reached the trapdoor and more pressure transferred onto the support.

In this study, an analytical solution was proposed based on Terzaghi's theory but for localized footing loading along the centerline of the trapdoor. This solution well predicted the measured vertical pressures on the trapdoor under localized footing loading as compared with the trapdoor test results obtained in this study. In addition to the experimental tests, eight numerical models with different fill height to trapdoor width ratios (H/B = 1, 2, and 3) and different footing widths (0.25B, 0.5B, 1B, 1.5B, 2B, and 5B (uniform)) were selected and their numerical results were compared well with the proposed solution. The numerical results further validated the proposed solution for soil arching over a trapdoor or a yielding soil zone under localized footing loading.

ACKNOWLEDGMENTS

I would like to express my sincere appreciation for my advisor and mentor, Professor Jie Han, for his invaluable academic and personal guidance and support throughout my journey as a Ph.D. student. Prof. Jie Han gave priceless time and efforts helping me conducting my research. I had learned much from his knowledge and wisdom in the past five years when I studied under him, and my learning will continue. His advice and encouragement during this period will always be in my memory, and his instructions will be a guide for the rest of my career. It has been a great pleasure and privilege to be one of Prof. Han's students.

I would like to thank my Ph.D. committee members, Dr. Masoud Darabi, Dr. Robert L. Parsons, Dr. Steven D. Schrock, and Dr. Chi Zhang for their guidance and help in improving this dissertation.

I would like to thank all members of the Geotechnical Society at the University of Kansas (KUGS), especially Dr. Mustapha Rahmaninezhad, Dr. Panpan Shen, and Saif Jawad, for their help and support in conducting the experimental work of this research.

Furthermore, I would like to express my gratitude to the lab technician, Kent Dye, in the Department of Civil, Environmental, and Architectural Engineering at the University of Kansas for his outstanding technical help in conducting the laboratory work.

Finally, my sincere gratitude goes to my family, especially my precious wife for her countless supports and love. She sacrificed a lot during my time as a Ph.D. student and made my Ph.D. study possible. I want to thank her again for her patient and being a precious mother to my gorgeous girl. Also, my sincere gratitude goes to my beloved parents for their unlimited support, encouragement, and sacrifices during my study.

TABLE OF CONTENTS

LIST OF TABLES

LIST OF FIGURES

CHAPTER 1 INTRODUCTION

This chapter provides a brief background about soil arching as a load transfer mechanism in several geotechnical applications and the importance of studying the stability of soil arching and presents problem statements, research objectives, the methodology for the study as well as the organization of the dissertation.

1.1 BACKGROUND

Soil arching is a phenomenon describing the pressure re-distribution associated with a relative displacement between a yielding soil mass and a stable soil mass (Terzaghi, 1943). Soil arching mobilizes when differential stiffness, differential settlement, or complete loss of support causes a relative displacement within the fill material. Arching commonly exists when soil interacts with structural elements, for example, tunnels, retaining walls, culverts or pipes, and piles in pile-supported embankments. Soil arching is a key mechanism of load transfer in these geotechnical applications. The performance of these applications highly depends on the stability of soil arching.

Terzaghi (1936) investigated the soil arching phenomenon using a trapdoor experiment under a plane-strain condition. His test results implied that as the trapdoor displacement increased, soil arching was mobilized. A plane of equal settlement, defined as the plane above which no differential settlement exists, was observed at a height of 1.5 to 2.5 times the width of the trapdoor. McNulty (1965) conducted a series of trapdoor experiments in an axisymmetric configuration. In his experiments, air pressure was applied on the surface of the dry sand in addition to the self-weight of sand over the trapdoor. In McNulty' study, a lower height of the plane of equal settlement was observed, which varied between 1.0 and 1.5 times the diameter of the trapdoor.

1.1.1 Pile-Supported Embankment

Suitable ground to support highway or railway embankments has become less available. Many of these embankments have been built on soft soils, which are considered as technically unsuitable or challenging for construction because of their low shear strength and high compressibility potential (Demerdash, 1996; Han, 1999). In order to enhance the ground stability and reduce anticipated settlement, piles have been increasingly used to support embankments on such problematic soils (Han and Gabr, 2002). In Pile-Supported (PS) embankments, load transfer mechanism plays an important role in the behavior of the system. In this system, soil arching is responsible for transferring the embankment load to the piles. The modulus difference between the soil and the piles under embankment loading causes differential settlement, which leads to the mobilization of soil arching within the embankment fill (Han et al., 2011). To minimize the differential settlement, geosynthetics have been successfully used as a basal reinforcement in PS embankments. The basal reinforcement would enhance the load transfer mechanism through the geosynthetic tensioned membrane effect and help transfer more load onto the piles (Han, 2015). This construction technique has been referred to as the geosynthetic-reinforced pile-supported (GRPS) embankments (Han and Gabr, 2002). Reid and Buchanan (1984) reported the early construction of a GRPS embankment using a single layer of geomembrane for a bridge approach embankment in Scotland in 1983. The geosynthetic reinforcement helped minimize the differential settlement and prevented the formation of a bump between the embankment and the bridge. Since then, a widespread use of GRPS embankments in Europe, the USA, Asia, and Australia led to several researchers to investigate this construction technique (e.g., Han and Gabr, 2002; Van Eekelen et al., 2003; Almeida et al., 2007; Chen et al., 2008; Filz et al., 2012; King et al., 2017). The use of geosynthetic as a basal reinforcement is also applicable to handle the problems imposed

by an existing large sinkhole under a planned highway or railway (Wang et al., 2009). Geosynthetic reinforcement has been used to bridge over voids without piles (Giroud et al., 1990; Gourc and Villard, 2000; Villard et al., 2000). GRPS embankments for highways and railways or buried pipes are often subjected to surface traffic loading, which may have some effect on the stability of soil arching thus affecting the load transfer mechanisms (Al-Naddaf et al. 2017); however, this effect has not been well understood and investigated.

Moreover, Jenck et al. (2007) conducted two-dimensional (2D) physical and numerical modeling of a pile-supported earth platform over soft soil. In their study, a soft and compressible foam was used to allow the development of differential settlement between piles, and an analogical soil of steel rods was used as the backfill. This study concluded that the backfill shear strength had the most important influence on the load transfer onto the piles and the surface settlement reduction. Bhandari (2010) and Bhandari and Han (2018) investigated the development of soil arching and the effects of geosynthetic reinforcement and cyclic loading on soil arching using 2D physical models and the discrete element method (DEM). Van Eekelen et al. (2012) conducted three-dimensional (3D) physical model tests in the laboratory to investigate the load transfer in geosynthetic-reinforced pile-supported embankments. Based on these tests, Van Eekelen et al. (2012) pointed out that the vertical embankment load is carried through three parts: P_A (arching) directly to the piles, P_B by the geosynthetic reinforcement to the piles, and P_C to the soft subsoil between the piles. Iglesia et al. (2014) conducted centrifuge tests to investigate the evolution of soil arching with the displacement of the trapdoor and proposed a ground reaction curve (GRC), which is divided into four stages: initial soil arching, maximum soil arching (i.e. the minimum stress on the trapdoor), stress recovery, and ultimate state. Han et al. (2017) simplified the GRC into three linear lines and found that Terzaghi's solution (Terzaghi, 1943) predicted the ultimate

state well at the trapdoor displacement equal to 10% the trapdoor width. Rui et al. (2016) investigated the evolution of soil arching in sand using 2D physical models and found that the patterns of soil arching depended on fill height, trapdoor width, and trapdoor displacement. Rui et al. (2019) conducted 2D trapdoor model tests without and with geosynthetic reinforcement and observed a concentric deformation pattern when geosynthetic reinforcement was used. This pattern is consistent with the soil arching model proposed Van Eekelen et al. (2013).

1.1.2 Buried Structures

When a structure (e.g., pipe, conduit, or culvert) is buried in the ground, it interacts with its surrounding soil, causing redistribution of geostatic stresses. This redistribution affects the level of the stresses transferred onto the structure. The geometry of the buried structure and its relative stiffness to the surrounding soil have a significant effect on the magnitude and distribution of the vertical stresses above this structure. When the stiffness of the buried structure is higher than that of the surrounding soil (i.e., buried rigid structure), the settlement of the surrounding soil is larger than that of the central soil column above the buried structure (Chen and Sun, 2013a). The relative settlement generates shear stresses between the surrounding soil and the soil column above the structure, resulting in vertical stress concentration on the buried structure (Spangler, 1948; Penman et al., 1975; Dasgupta and Sengupta, 1991; Bennett et al., 2005). Therefore, the vertical stresses on the top of the rigid structure buried under a relatively high embankment are higher than the weight of the soil column above the structure as a result of negative soil arching. On the contrary, when the stiffness of the buried structure is less than that of the surrounding soil (i.e., buried flexible structure), the vertical stresses on the top of the flexible structure are less than the weight

of the soil column above the structure as a result of positive soil arching due to higher settlement of the central soil column above the buried structure than the surrounding soil.

To reduce the vertical stresses on a rigid structure constructed under high embankment fill, several methods are commonly used in the construction process, among which the Induced Trench Installation (ITI) method is widely used in the embankment construction. The ITI (also known as Imperfect Ditch) method was initially proposed by Marston (1930). The ITI method includes a compressible layer with low stiffness installed above a rigid structure to reverse the relative displacement in the overlying soil. After construction of the embankment with a compressible material and during its service life, the low stiffness layer compresses more than the surrounding soil to generate positive soil arching, which can transfer part of the vertical stresses of the central soil column to the adjacent soil.

1.1.3 Trapdoor Model Test

Trapdoor test has been commonly used to demonstrate and investigate the soil arching mobilization above yielding soil. Terzaghi (1936) conducted the first trapdoor test to investigate the arching effect. Many researchers (e.g., McNulty 1965; Ladanyi and Hoyaux 1969; Harris 1974; Evans 1983, Chen et al. 2008; Al-Naddaf et al. 2017) replicate Terzaghi's trapdoor tests. A typical trapdoor test setup is shown in Figure 1.1. The trapdoor is set to allow for differential settlement within the soil mass after the trapdoor being lowered; therefore, soil arching mobilizes. When the fill soil is high enough, the differential settlement generated within the fill soil extends to a specific plane that is called equal settlement plane, above which no soil arching exists.

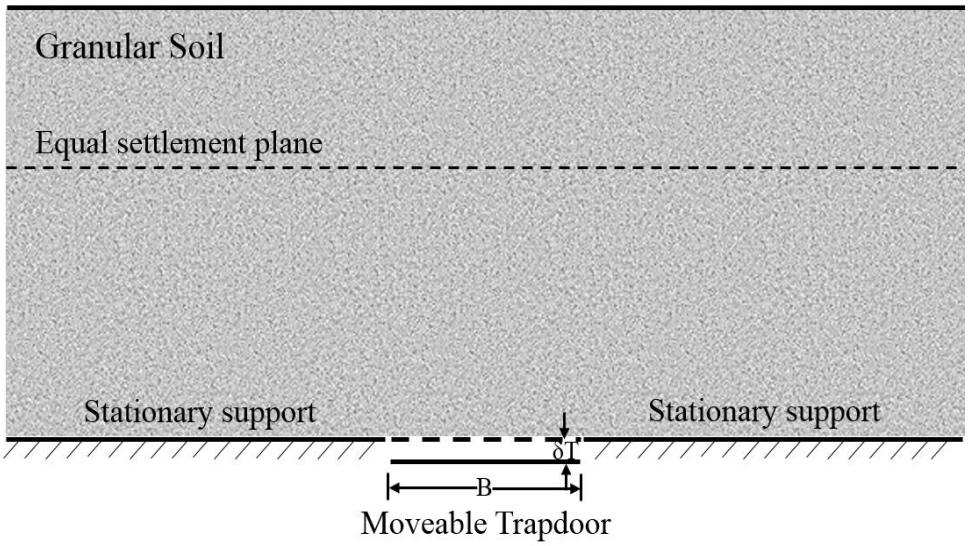

Figure 1.1 Schematic of a typical trapdoor test setup.

1.2 PROBLEM STATEMENTS

Past research work has provided an essential level of knowledge of the load transfer mechanisms associated with underground structures in geotechnical engineering, yet most studies have been conducted under specific or limited loading conditions. For example, researchers have used trapdoor tests to investigate the soil arching phenomenon (Terzaghi 1936; McNulty 1965; Ladanyi and Hoyaux 1969; Harris 1974). However, most trapdoor tests have been conducted in considerably small-scale models under soil self-weight or soil self-weight plus uniform surcharge (static surface loading). Scale effects of small model tests may have influenced the accuracy of the test results. In addition, a uniform surcharge may not be representative of most surface loading and the critical situation for soil arching stability since smaller differential settlement may develop in the soil under a uniform surcharge than a localized load.

Moreover, earth structures or buried structures are often subjected to cyclic surface loading (due to moving vehicles and railroad crossings) and dynamic-in-depth loading (due to pile driving, blast waves, and earthquakes). Unfortunately, the knowledge of cyclic or dynamic loading on soil

arching stability lacks, even though Terzaghi (1943) pointed out that vibrations might have a significant impact on soil arching, and degradation of soil arching would result in an increase of stresses applied on the buried structures and increase the chance of structure damages. Very limited research has been conducted to investigate the soil arching behavior under cyclic loading. Chen et al. (1991) studied soil arching based on impact loading on a flexible trapdoor, yet limited soil arching developed in their test because the trapdoor underwent no movement, but it deformed due to its flexibility. Al-Naddaf (2017) investigated the soil arching stability under cyclic loading in a trapdoor test; however, the trapdoor was fixed under the load application which affected the mobilization of soil arching.

The mode of soil deformation (uniform versus non-uniform) within the yielding soil zone would also affect the distribution of the shear forces within the embankment fill and change the degree of soil arching mobilization. Different modes of soil deformation have not been comprehensively investigated prior to this study and are not entirely understood. Most previous soil arching investigations utilized the traditional trapdoor which consisted of the one-segment plate that would settle uniformly. This is a simplified condition of the soil movement and does not represent the actual displacement mode of foundation soil. For instance, in pile-supported embankments, the displacements of foundation soil between rigid supports are not uniform and exhibit a concave (parabola)-like shape. In this study, a three-segment trapdoor was utilized to better simulate the displacement condition of the foundation soil.

Furthermore, current design methods for geosynthetic-reinforced earth structures involving soil arching, such as geosynthetic over voids and geosynthetic-reinforced pile-supported embankments, were mostly developed based on the findings from trapdoor studies without any geosynthetic. This extrapolation lacks appropriate theoretical and experimental justifications. The

influence of geosynthetic reinforcement on soil arching is not entirely understood. This study is expected to provide an insight into the effect of the geosynthetic on the mobilization and degradation of soil arching

1.3 RESEARCH OBJECTIVES

The objectives of this study are: (1) to investigate the soil arching phenomenon under soil self-weight as a result of differential movement without and with geosynthetic reinforcement; (2) to study the progressive change of soil arching under static and cyclic footing loading; (3) to investigate the stability (degradation and even collapse) of the mobilized soil arching under static and cyclic surface footing loading; (4) to assess the effects the soil deformation modes on the degree of soil arching; and (5) to evaluate the benefit of geosynthetics (biaxial geogrid over a yielding base and geofoam over a buried box culvert) on soil arching under surface footing loading.

1.4 RESEARCH METHODOLOGY

The following methodologies have been adopted in this research to achieve the above objectives: (1) an extensive literature review on load transfer mechanisms, such as soil arching and tensioned membrane, responsible for the stress redistribution around underground structures; (2) an experimental study with reduced-scale model tests of a buried box culvert under relatively low embankment fill with an emphasis on the benefit of a compressible inclusion, such as expanded polystyrene geofoam, above the culvert under static and cyclic surface loadings; (3) an experimental study with spring-based trapdoor tests to evaluate the mobilization and degradation of soil arching under static and cyclic surface loadings; (4) an assessment for the benefit of geosynthetics reinforcement above a self-yielding base using the trapdoor model test simulating

the condition of soil subsidence or consolidation of soft foundation soil between stationary supports; (5) a numerical analysis using a finite difference software to simulate trapdoor tests and to study the most critical surface loading on the soil arching mobilization and degradation; and (6) an analytical solution to account for the localized surface loading on the soil arching mobilization.

1.5 ORGANIZATION OF THIS DISSERTATION

This dissertation consists of seven chapters. Chapter 1 presents a brief introduction to this study followed by Chapter 2, which presents a literature review on load transfer mechanisms in underground structures, definition and overview of soil arching, relevance and applications related to soil arching, soil arching and tensioned membrane theories, and soil arching investigations under static and cyclic loading. Chapter 3 discusses the test setups and describes the experimental work details including embankment material properties, reinforcement properties, instrumentation, test procedure, and loading types used in this study. Chapter 4 presents the test results of the experimental study on arching mobilization over a buried box culvert and discusses the benefit of expanded polystyrene geofoam installed above the buried structure in reducing the vertical pressure on it. Chapter 5 presents the test results of the experimental study on soil arching with a spring-based trapdoor and discusses the effects of reinforcement and loading on the mobilization and degradation of soil arching. Chapter 6 introduces and validates a numerical model for the trapdoor problem using a three-dimensional finite difference software against the experimental results and then presents a parametric study based on the validated numerical model. Chapter 7 draws the conclusions of this study and provides recommendations for future research.

CHAPTER 2 LITERATURE REVIEW

The primary objective of the literature review is to summarize the accumulated knowledge on the subject, draw attention to the areas where research is required, and subsequently define the aim of this study. This literature review covers the following subjects:

- ✓ Load transfer mechanisms above underground structures
- ✓ Definition and overview of soil arching
- ✓ Relevance and applications related to soil arching
- ✓ Soil arching theories
- ✓ Tensioned membrane theories
- ✓ Soil arching investigations under static and cyclic loading

2.1 LOAD TRANSFER MECHANISMS ABOVE UNDERGROUND STRUCTURES

Earth structures constructed on very soft soils are potentially subjected to considerable total and/or differential settlement. These displacements must be controlled to a limited value to sustain the stability, structural integrity, and durability of these structures. For construction of roads including highways and railways, and industrial buildings, the use of traditional foundation options may lead to high costs and long delays. During the last few decades, rigid inclusions have become an attractive alternative to traditional methods. This technique utilizes a network of piles, a granular load-transfer layer (platform) located above the piles, and if needed, geosynthetic reinforcement placed in the middle or at the base of the granular layer (such as geogrid or geotextile sheet). The primary function of this technique is to increase the load transferred to the piles and reduce the

vertical load acting on the soft soil and consequently avoid bearing failure and reduce the surface settlement.

Other rigid structures, such as pipes, conduits, and culverts, are extensively used for transportation applications and buried within granular soil. The existence of these structures within the granular soil mass causes a redistribution of stresses. The stiffness of the buried structure relative to the surrounding soil affects the magnitude and distribution of vertical stresses. Since the stiffness of the buried structure is often higher than that of the surrounding soil, the settlement of the surrounding soil is larger than that of the central soil column above the buried structure (Chen and Sun, 2013a). The relative settlement generates shear stresses between the surrounding soil and the soil column above the structure, resulting in vertical stress concentration on the buried structure.

In the above geotechnical applications, soil arching is a key load transfer mechanism. However, soil arching does not act alone as a load transfer mechanism when geosynthetic is used. Both soil arching and geosynthetic tensioned membrane are responsible for the load transfer. Geosynthetics have been widely used in many of geotechnical applications, such as geosynthetic-reinforced pile-supported (GRPS) embankment and geosynthetic over cavities.

The following sections will examine both soil arching and geosynthetic tensioned membrane effects to have a better understanding of these load transfer mechanisms.

2.2 DEFINITION AND OVERVIEW OF SOIL ARCHING

Soil arching is a transfer of stresses from a yielding soil mass onto its adjoining stationary soil mass in response to a relative displacement between these two masses (Terzaghi 1943). If only a specific area of support for a soil mass yields, the soil above the yielding region would have a

tendency to settle with the yielding soil while the rest remains stationary. In the transition plane between the moving and stationary soil masses, shear stresses are developed to counteract the relative movement of the two masses. Since the shear resistance tries to keep the yielding mass in its original position, it reduces the stress on the yielding part and, subsequently, increases the stress on the stationary part. Figure 2.1 shows a schematic of the soil arching phenomenon above a yielding base.

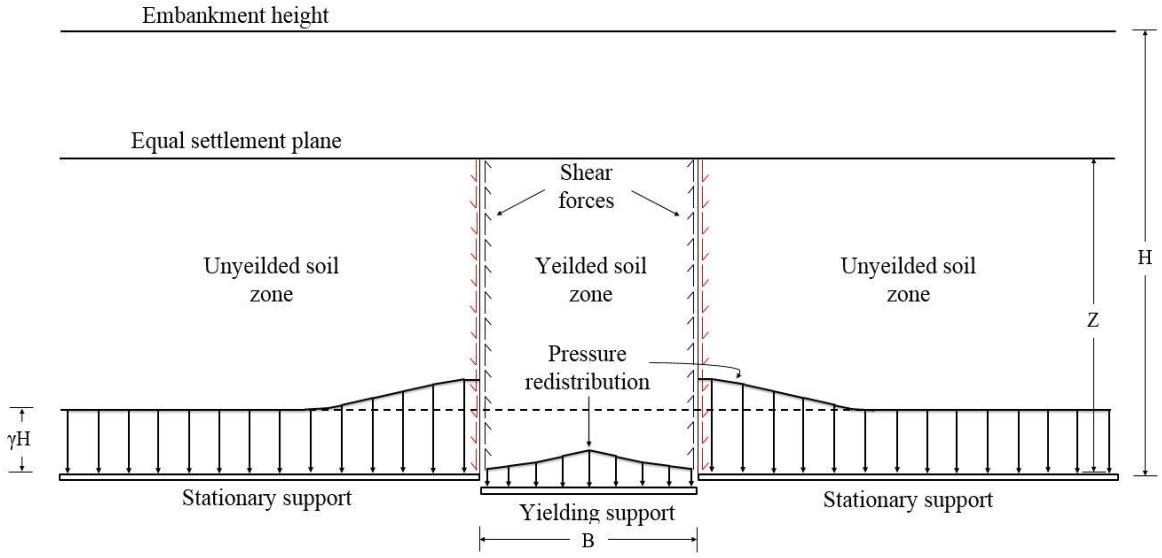

Figure 2.1 Schematic of the soil arching phenomenon above a yielding base (Al-Naddaf, 2017).

The mechanism, in which the stresses are transferred and redistributed, results from a series of shear stresses generated along the vertical planes that separate the yielding soil mass and the adjoining stationary mass as shown in Figure 2.1. These shear stresses are the counteracting forces depending on frictional characteristics of the soil to resist the relative movement. If the yielding soil moves downward, the induced frictional stresses have an uplift effect on the moving soil, so they reduce the stresses on the yielding mass and redistribute them to the stationary mass as shown in Figure 2.2(a). This phenomenon is called “active or positive” soil arching, and it can be

generated with only a small movement (Terzaghi 1936). On the contrary, if the movement occurs in the reverse direction (i.e., the yielding surrounding soil mass moves downward with respect to the central part), down-drag frictional forces are generated to impede that movement. These down-drag forces will increase the stress on the yielding soil and reduce it on the surrounding soil. Such type of soil arching is referred to as "passive or negative" soil arching as shown in Figure 2.2(b).

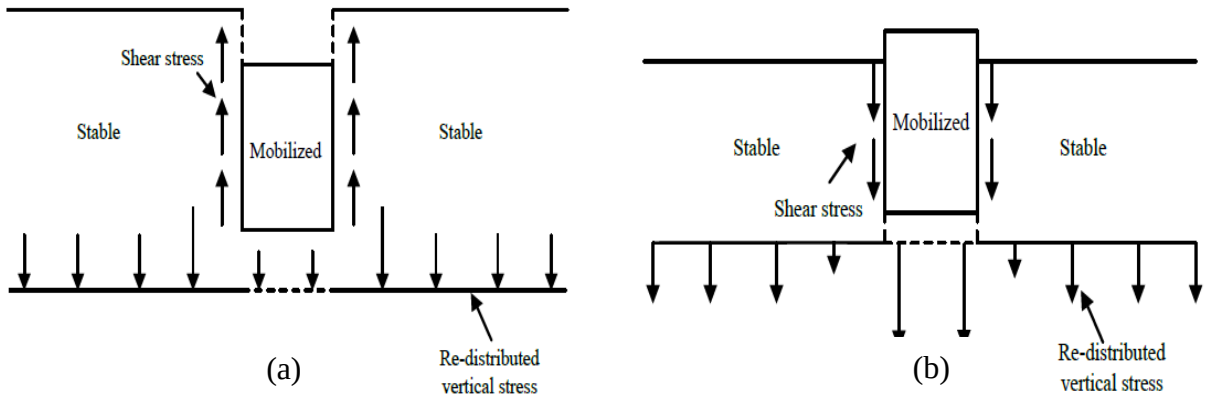

Figure 2.2 Different types of soil arching: (a) active or positive soil arching and (b) passive or negative soil arching (Han et al. 2016).

Stress redistribution (i.e., soil arching) in a medium is also associated with the soil-structure interaction. Soil arching may cause a significant change in the stresses throughout the soil medium because the structure has different compressibility from the surrounding soil (McNulty 1965). McNulty (1965) stated that the main factors contributing to the level of stress redistribution include: the physical properties of the structure (particularly its compressibility characteristics), the properties of the surrounding soil (mainly its ability to transfer loads through mobilization of shear stresses as a consequence of relative displacements); and the free field state of the stresses which exists if a structure is not present.

The degree of load transfer can be evaluated by a soil arching ratio (ρ) as proposed by McNulty (1965), which is defined as the average vertical stress above the yielding base (σ_v) to the overburden pressure (γH) plus the surcharge (q) if available, as expressed in Equation (2.1):

$$\rho = \frac{\sigma_v}{\gamma H + q} \tag{2.1}$$

where ρ = 0 represents complete soil arching while ρ = 1 represents no soil arching.

Terzaghi (1943) stated that "arching effect is one of the most universal phenomena encountered in soils both in the field and in the laboratory." The arching phenomenon has been investigated over a century in geotechnical and non-geotechnical fields. In France, military engineers found that the silo base carried a fraction of grain weight while the silo walls carried more than one would expect (Feld 1948). The "Silo Theory" was proposed by Janssen (1895) to design silos based on the observed behavior.

In the United States, a large number of drainage projects were carried out in 1910, and many structural failures happened to the designed pipes after the installation and backfilling (Spangler and Handy 1973). These failures were believed related to load redistribution (i.e., the arching phenomenon) on the underground conduits which were also investigated by Marston (1930) at Iowa State University. Depending upon the flexibility of conduits, the load on the conduit can vary from a portion of the overburden weight to several times the overburden weight (Marston 1930; Spangler 1964).

Engineers also observed arching around tunnels, i.e., the load carried by a tunnel was lower than the overburden pressure, and accurate predictions were necessary for a better design. Terzaghi (1943) developed a theoretical solution to quantify this load based on his experimental research

(i.e., the use of trapdoor test) in 1936. Atkinson and Potts (1977) investigated soil arching related to the stability of tunnels. In the 1960s, the US Department of Defense sponsored considerable research for protection of infrastructures and the soil-structure interaction topic gained great attention. Researchers showed that soil arching would contribute to the protection of underground facilities from nuclear attacks during war, which would demolish any surface building (Evans 1983).

Since the 1960s, columns have been increasingly used to support embankments over soft soils to control and reduce their settlement (Magnan 1994). Construction of embankments for highway applications on soft ground is hard to achieve without ground improvement techniques. Use of piles or columns is often an economical solution to reduce soft soil compressibility and enhance ground stability (Han and Gabr 2002). In these pile-supported embankments, there exist two distinct supports – rigid pile caps and soft soil. Differential settlement easily develops between the supports. Soil arching develops between the pile caps as a result of the differential settlement. Thus, embankment weight can be transferred onto an adequate stratum below the soft soil through piles as pointed out by Holtz and Massarsch (1976), Holmberg (1979), Broms and Wong (1985) and studied by Hewlett and Randolph (1988) and Low et al. (1994).

Trapdoor test has been commonly used to evaluate soil arching developing above the yielding part. Terzaghi (1936) conducted the first trapdoor test to investigate the arching effect. Many researchers (e.g., McNulty 1965; Ladanyi and Hoyaux 1969; Harris 1974; Evans 1983) replicate Terzaghi's trapdoor tests. These trapdoor studies have been performed under soil self-weight or soil self-weight plus uniform surcharge (static surface loading). A uniform surcharge configuration may not be the critical situation for soil arching stability as compared with the locally loaded situation since less differential settlement may develop in the soil.

2.3 RELEVANCE AND APPLICATIONS RELATED TO SOIL ARCHING

Soil arching is considered as a universal phenomenon in geotechnical engineering because it is encountered in many geotechnical applications including sinkholes, mining subsidence, tunneling, landfill liner systems over voids, buried conduits and structures, pile-supported embankments, fill behind retaining walls, slope stabilizing piles, and soil tunnel by animals or insects. Figure 2.3 depicts some of these applications.

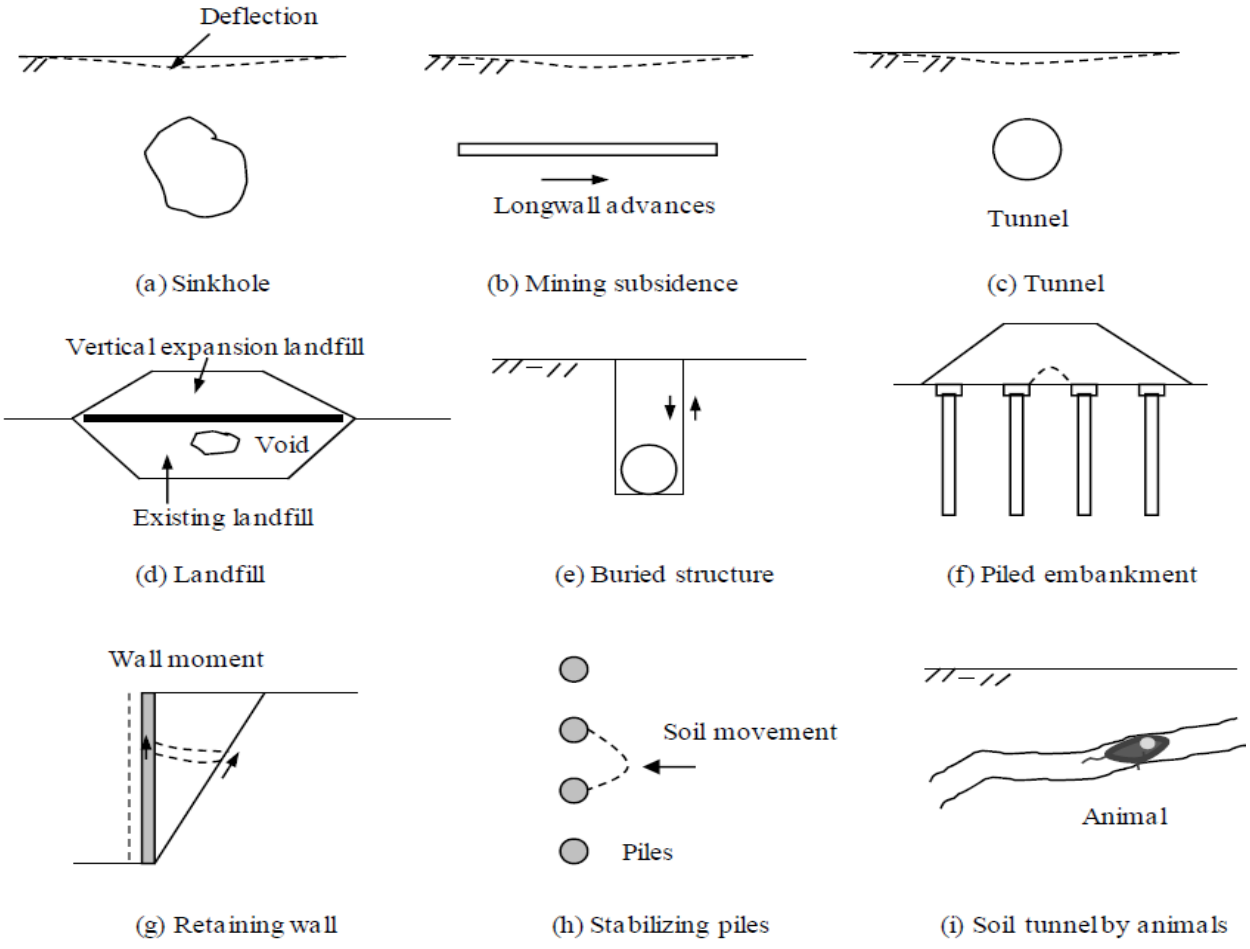

Figure 2.3 Soil arching phenomena in various applications (Han, personal communication).

In the above applications, soil arching develops as a result of relative movement between soil and support in either vertical or lateral direction. Sinkholes, mining subsidence, tunneling, and landfill liner systems over voids are examples of relative vertical movement. Lateral movement of support, such as outward yielding of retaining walls, results in soil arching which forms a semi-arch between the wall and a slip plane and significantly reduces lateral earth pressures. Soil arching in retaining walls initiates from a rough wall when rotation of principal stresses at the wall takes place (Handy 1985). A slope stabilizing pile system is another example of lateral movement where soil arching develops as the soil tends to move through between the stabilizing piles that are often embedded in firm foundations (Bosscher and Gray 1986).

In addition to the relative movement, a relative stiffness difference between the support and the surrounding soil may also mobilize soil arching which results in transfer of the load to a stiffer support. Buried conduits were one of the early applications considering soil arching as a result of relative stiffness (Marston 1930). Wu and Leonards (1985) indicated that soil arching above buried pipes (conduits) could be positive or negative depending on the stiffness of the pipe relative to that of the surrounding backfill. Also, Einstein and Schwartz (1979) presented a simplified analysis to account for the load redistribution on tunnel supports as subsequence to the relative stiffness difference.

The following sections will further discuss three most common geotechnical applications involving soil arching.

2.3.1 Reinforced Fill Systems over Cavities

Construction takes place on the natural ground that may include mining areas, karstic terrains, landfills, and non-saturated cohesive soils, which are susceptible to the danger of collapse because

these areas more likely develop cavities or sinkholes during their lifetime. Groundwater flows through soil masses that contain limestones, or gypsum contents can create significantly large sinkholes of a diameter ranging from one to several meters (Giroud et al. 1990). Sinkholes may develop when collapsible soils, which are dry or partially-saturated cemented soils, lose their cementation upon wetting and under loading (Agaiby and Jones 1996). In addition, some cavities are formed during the progress of longwall mining or tunnels excavated by animals or insects. Thus subsidence likely develops during such processes (Tsur-Lavie et al. 1988; Reichman and Smith 1990). Also, vertical expansions to existing landfills have become an attractive alternative for expanding usable space. However, there is a concern that overstretching of liners and leachate collection systems may occur above voids in the old landfill areas created by progressive degradation of waste and collapse of large objects (Jang and Montero 1993). Agaiby and Jones (1996) pointed out that the term "cavity" is relative. For example, a thin compressible layer of very soft soil embedded in a much stiffer stratum can be considered as a cavity due to its incapability to provide the same support to loads as its surroundings.

The existence of a cavity, in general, in soil would induce either differential settlement or complete loss of support. Thus soil arching would transfer the loads above (i.e., soil self-weight and surface loading) onto the sides of the cavity. However, if the shear resistance of the soil forming the roof and the sides of a cavity is not strong enough to support the exerted loads, sudden collapse may occur. Therefore, geosynthetic reinforcement may be used to bridge over a cavity and carry the loads to reduce the risks of collapse. Geosynthetics have been used to stabilize the soil above cavities (Giroud et al. 1990; Agaiby and Jones 1995; Wang et al. 1996). Depending on the cavity size and the geosynthetic stiffness, the geosynthetic may touch the bottom of the cavity (especially for a shallow or low height cavity) and transfer some of the load to the soil underneath

it or support the load without touching the bottom of the cavity (especially for a deep cavity and a strong and stiff geosynthetic) (Giroud et al. 1990).

Much research, related to the load transfer mechanisms of such systems, has been done, including theoretical derivations, analytical methods, and experimental investigations. Terzaghi (1943) and Kezdi (1975) derived theoretical solutions for soil arching over an infinitely long trench and circular voids, respectively. These solutions were adopted by Giroud (1984) and Giroud et al. (1990) as well as the tensioned membrane theory to assess the load-carrying capacity and to provide a design method for geosynthetic-reinforced soil layer systems spanning voids, such as sinkholes, tension cracks, dissolution cavities, and depressions.

2.3.2 Buried Structures

Buried structures (e.g., pipe, conduit, or culvert) are commonly used to provide safe and relatively economical structures for the transport of water, vehicles, utilities, or pedestrians. Although these structures are rather simple and widely used, the loadings applied to these structures during their construction and subsequent service life can be complex. A buried structure causes a redistribution of stresses in the surrounding soil layers and the nature of this redistribution influences the load that reaches the structure. The load that reaches the structure is governed by the characteristics of the soil, and the geometry and stiffness of the structure itself. Marston (1930) pointed out that the load on a buried structure is affected by installation conditions in addition to the height of fill over the structure. Spangler (1950) stated that the primary factors influencing the load are associated with the installation conditions that control the magnitude and direction of settlement of the central soil column over the structure relative to settlement of the adjacent soil. Therefore, when a buried structure is rigid (i.e., has a higher stiffness than the surrounding soil), the vertical stresses on the

top of the structure buried under a relatively high embankment are higher than the weight of the soil column above the structure as a result of negative soil arching. Generally, soil arching occurs due to a relative displacement between a yielding soil mass and a stable soil mass (Terzaghi, 1943). The degree of soil arching varies with the relative displacement. Han et al. (2016 and 2017) studied fully and partially mobilized soil arching. They concluded that if the displacement of the soil is limited, the shear stresses in the soil medium are lower than its shear strength, and soil arching at this state is referred to as partially mobilized soil arching. Also, Han (2015) pointed out that the soil-arching effect could not be fully mobilized when the elastic modulus ratio of the buried structure to the soil is lower than 100. The reason is that a low modulus ratio may not induce sufficient relative displacement between a buried structure and soil to achieve fully mobilized soil arching.

The fill load transferred to a buried structure is largely dependent on the type of installation as well as the height of the fill over the structure (Marston and Anderson, 1913; Brown, 1967). There are four installation methods commonly used in practice: (1) Trench method; (2) Positive Projecting Embankment; (3) Negative Projecting Embankment; and (4) Jacked or Tunneled method (ACPA, 2011). Positive projection embankment (PPE) is widely used in the North America when a buried structure is installed in a relatively flat stream bed under a high embankment. In the PPE, the generated shear stresses increase the vertical stresses on the buried structure. Higher vertical stresses on the buried structure may cause excessive deformations and even failure of the buried structure (Chen and Sun, 2013a and 2013b).

To reduce the vertical stresses on a rigid structure constructed under high embankment fill, several methods are commonly used in the construction process, among which the Induced Trench Installation (ITI) method is widely used in the embankment construction. The ITI (also known as

Imperfect Ditch) method was initially proposed by Marston (1930). The ITI method includes a compressible layer with low stiffness installed above a rigid structure to reverse the relative displacement in the overlying soil. Baled straw, leaves, compressive soil, or Expanded Polystyrene geofoam (EPS geofoam) are examples of lightweight materials used as a compressible layer above rigid structures in practice. After construction of the embankment with a compressible material and during its service life, the low stiffness layer compresses more than the surrounding soil to generate positive soil arching, which can transfer part of the vertical stresses of the central soil column to the adjacent soil. Therefore, the use of the compressible material can reduce the vertical stresses on the culvert or pipe, and allow it to be buried at a greater depth.

Figure 2.4 illustrates the differential settlement within the embankment and the direction of the mobilized shear stresses along the central column of soil above the culvert for both the PPE and the ITI. For a high fill embankment, the shear stresses may extend up to a horizontal plane within the embankment, called as the plane of equal settlement. Above which no relative settlement occurs, and there is no soil arching effect. Based on Marston's (1930) research, Spangler (1950) used the field measurements of the settlement over various types of culverts to propose a settlement ratio. The settlement ratio describes the magnitude of the relative displacement of the soil column above the culvert and the adjacent soil and is used to calculate the load on the culvert. Brown (1967) quantified the pressure reduction effect of hay blocks above a rigid culvert based on the finite element method. Vaslestad et al. (1993) studied the long-term load reduction on rigid culverts under high fill using the ITI method. Furthermore, the performance of the ITI method was investigated by field and laboratory tests (Sladen and Oswell, 1988; Liedberg, 1997; Sun et al., 2011; Oshati et al., 2012), as well as numerical analysis (Kim and Yoo, 2005; Kang et al., 2008; Sun et al., 2009; McGuigan and Valsangkar, 2010; McGuigan and Valsangkar, 2011). Kim and

Yoo (2005) conducted a numerical study to investigate the effect of several factors (i.e., the width, thickness, location, and stiffness of the compressible layer) on the performance of the box culvert under a high fill embankment. Kim and Yoo (2005) pointed out that the width of the compressible layer should not be greater than 1.5 times the box culvert width and the most significant load reduction occurred when the compressible layer was placed immediately on the culvert top.

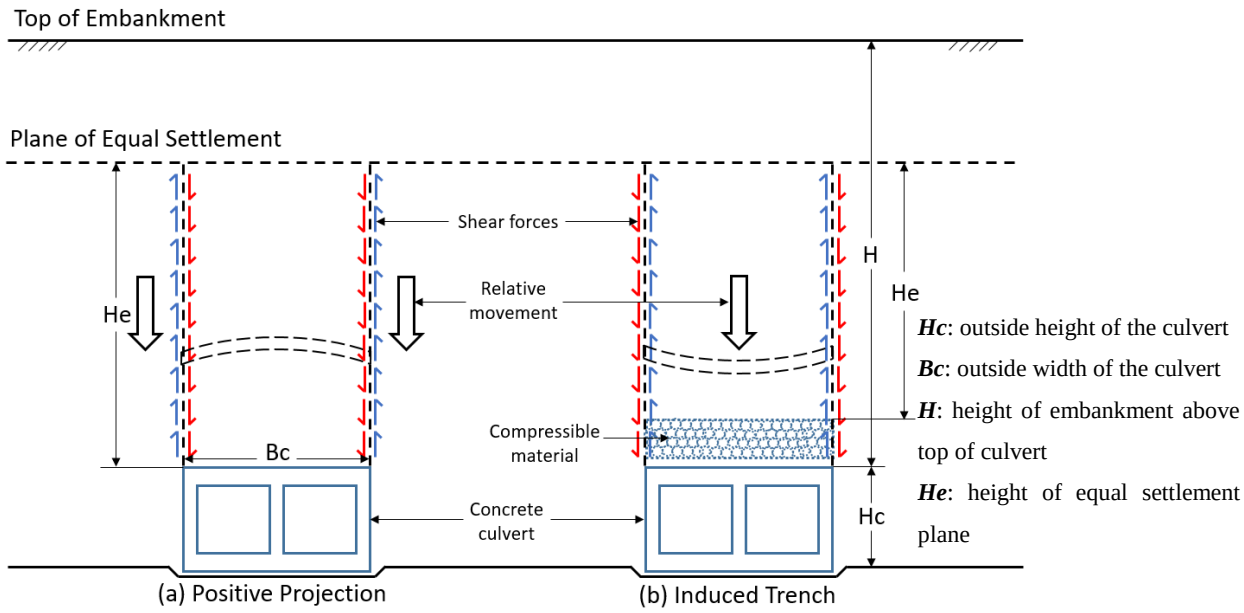

Figure 2.4 Simplified arching mechanism of (a) PPE and (b) ITI (Reprinted from McGuigan and Valsangkar (2010), © Canadian Science Publishing).

Although the knowledge about the buried structure installed under a high fill embankment by the ITI has been accumulated from the past research, limited studies have been conducted to evaluate the behavior of the buried structure installed under a relatively low fill embankment by the ITI method, especially under surface loading. Under these circumstances, additional stresses induced by traffic loading may extend to the level of the buried structure, which is different from the situation for a high fill embankment where these induced stresses may diminish at a greater

depth. Moreover, most of the previous studies have been conducted under soil self-weight or soil self-weight plus uniform static surface surcharge. Limited studies have been conducted to evaluate the pressure distribution induced by a footing load (e.g., traffic loading). Most of the previous investigations focused on stress transfer due to localized internal displacement under embankment overburden pressure instead of that due to localized surface loading (Al-Naddaf et al., 2017). Also, there is a lack of knowledge on the effects of footing loading on the mobilization of soil arching, which is the primary load transfer mechanism controlling the pressure distribution on buried structures.

2.3.3 Pile-Supported Embankments

Piles have been used to increase soft foundation bearing capacity and minimize post-construction settlements in many embankments since the early 1960s (Magnan 1994). When piles are used, they carry a large percent of the embankment weight up to 60% with as little as 10% of pile coverage area, by virtue of soil arching induced from the differential settlements between piles and soft soil (Hewlett and Randolph 1988). Therefore, a single stage of embankment construction is possible without the risk of soft soil undrained bearing failure. Another advantage of using piles is that installation may densify and stiffen soil, thus reducing the settlement of the foundation soil (Hewlett and Randolph 1988). These embankments are mainly used to support highway or railway systems.

Geosynthetics have been introduced in pile-supported (PS) embankments as basal reinforcement to assist the load transfer and to reduce the differential settlement (Han and Gabr 2002). Figures 2.5(a) and 2.5(b) show typical cross-sections of PS and GRPS embankments, respectively. Moreover, by introducing geosynthetic in a PS embankment, piles can be constructed

with larger spacing and smaller caps, thus reducing the cost of piling (Jones et al. 1990). Bell et al. (1994) pointed out that primary and long-term secondary settlements can be minimized by using geosynthetic. In addition, using geosynthetic allows for thick or high embankments to be built, and thus preventing the differential settlements at the base being reflected to the crest of the embankment (Broms and Wong 1985).

Due to these advantages, many GRPS embankments have been built. In Scotland, one of the earliest GRPS embankments was constructed with a single layer of geomembrane for a bridge approach embankment (Reid and Buchanan 1984). Also, multiple layers of geosynthetic were used to support a roadway embankment in London, England 1989 (Card and Carter 1995). In Philadelphia, PA in 1994, a large diameter storage tank was built on a geosynthetic-reinforced column-supported platform (Collin 2003).

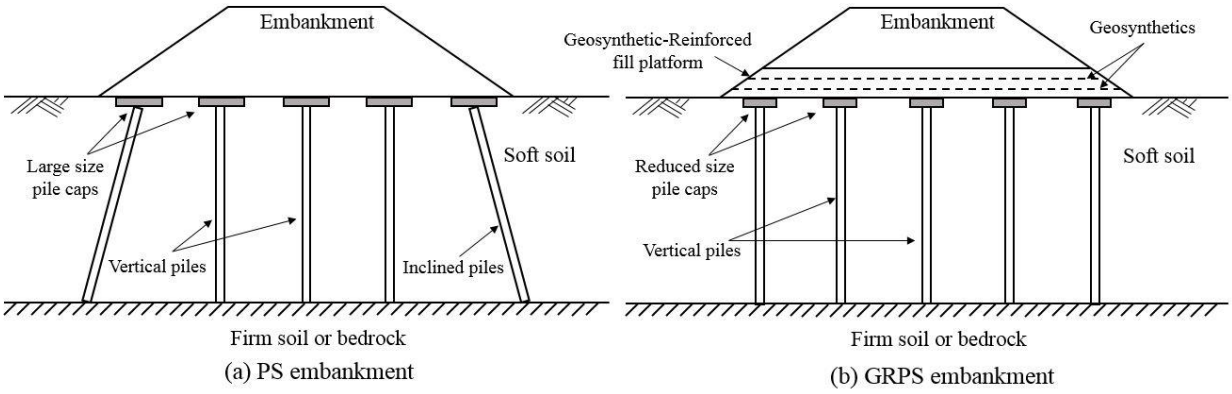

Figure 2.5 Typical cross-sections of PS and GRPS embankments (Han, 2015).

In GRPS embankments, the geosynthetic-reinforced fill platform acts as a unit to reduce the load on soft soil (i.e., foundation soil) and transfer it to stiffer piles through soil arching and tensioned membrane effects. Figure 2.6 illustrates these two mechanisms under a plane strain condition. If there are no piles within the foundation soil, the embankment soil should settle evenly,

and the vertical pressure at the embankment base is equal to the total overburden stress (γH). When piles are incorporated, the embankment fill above the soft soil would have a tendency to settle relative to the stationary adjoining fill above the piles. As the differential settlement (Δ*S*) occurs, soil arching mobilizes and transfers the embankment load to the piles.

Simultaneously, the geosynthetic sheet extending across the span of the two piles deforms as the soil mass moves downwards. A tangential tensile force (T) develops within the geosynthetic sheet. The vertical component of the tensile force counteracts the downward moving soil mass and applies additional load on the piles. As the tension develops in the geosynthetic sheet, the embankment weight is transferred from the foundation soil to the piles. This is called the tensioned membrane effect. The load transfer mechanism in GRPS embankments is a combination of soil arching and tensioned membrane effects. However, soil arching dominates the mechanisms through which the embankment weight and the surface loadings are transferred to the piles (Han et al. 2011). Soil arching is the only mechanism which is responsible for the load transfer in PS embankments.

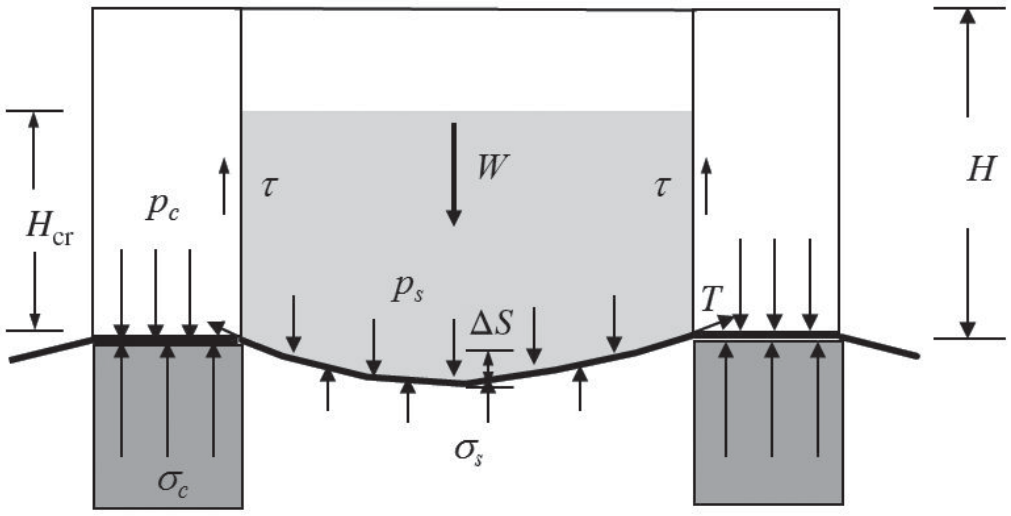

Figure 2.6 Load transfer mechanisms in GRPS embankments (Han, 2015).

2.4 SOIL ARCHING THEORIES

Soil arching theories are essential for discussing the arching effect and providing a path for further development in related arching studies. Soil arching phenomenon has been studied for decades; many experimentally and analytically-based theories have been proposed (e.g., Janssen 1895; Terzaghi 1936; Finn 1963; Hewlett and Randolph 1988; Low et al. 1994). Similar to many geotechnical problems, soil arching has been investigated by scholars in two distinctly different methods: limit equilibrium and continuum mechanics-based methods (Agaiby and Jones 1995). These two approaches are different in their assumptions, formulations, and consequences.

The formulations for the behavior of any geotechnical problems are either indeterminate or complex to some extent; therefore, commonly a simplified constitution for the soil behavior is favorable. Limit equilibrium methods facilitate the soil arching problem by assuming a failure state with certain shapes and ranges of slip surfaces, which make the problems easily solved (Agaiby and Jones 1995). The presumed shape of soil arching is the primary difference among all the limit equilibrium methods, such as a flat arch acting like a lintel or a curved mode like an arch, a ring or a dome (Getzler et al. 1968; Handy 1985; Hewlett and Randolph 1988).

Han (2015) classifies soil arching theories according to the proposed models by researchers in the following to study GRPS embankments: (a) vertical slip surfaces (Russell and Pierpoint 1997; Chen et al. 2008; British Standard 8006 2010); (b) semispherical dome (Hewlett and Randolph 1988; Kempfert et al. 2004); and (c) triangular wedge (Carlsson 1987; Miki 1997; Collin 2003). An illustration of these different models is shown in Figure 2.7.

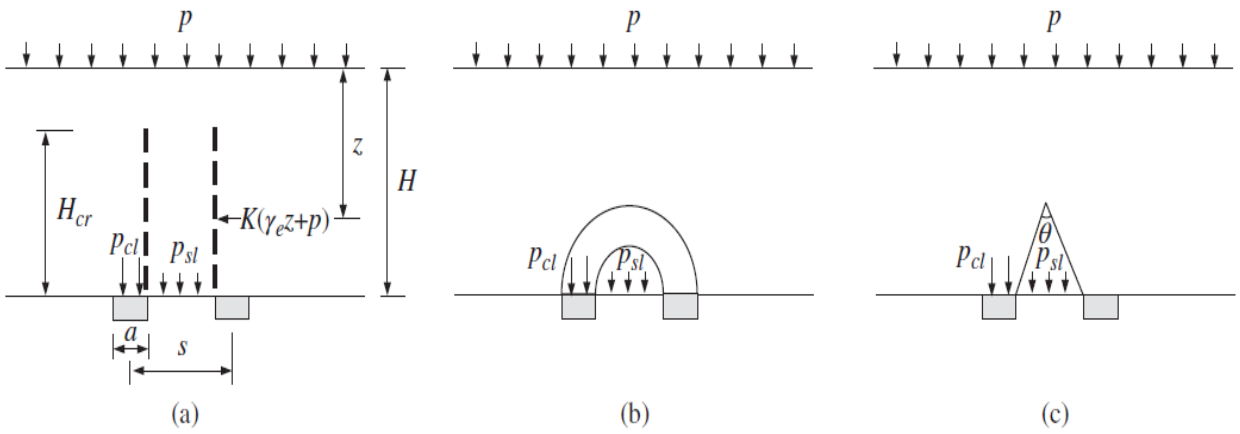

Figure 2.7 Soil arching models: (a) vertical slip surface, (b) semispherical dome, and (c) triangular wedge (Han, 2015).

2.4.1 Terzaghi's Investigation of Soil Arching

A series of trapdoor tests were conducted by Terzaghi (1936) as the first experimental investigation of the arching phenomenon. Terzaghi's trapdoor tests were performed under a plane-strain condition. Based on his results and observations, he proposed a theoretical solution to describe the soil arching phenomenon in 1943. He also developed an equation to calculate the vertical stress above a yielding trapdoor.

In Terzaghi's experimental work, a trapdoor of 73 mm wide and 463 mm long was fixed on the base of a 310 mm sand container. It was allowed to move downwards gradually. Meanwhile, the total load on the trapdoor and its displacement were measured. As the displacement was just started, the load on the trapdoor decreased rapidly as indicated by the test results, and the shear stresses induced by soil arching increased with an increase in the displacement. Subsequently, the pressure on the trapdoor reached a constant value at a displacement of approximately 10% of the trapdoor width.

The adopted model in Terzaghi's investigation is similar to the one proposed by Janssen (1895) to study the pressure distribution in silos. As shown in Figure 2.8(a), Terzaghi (1943)

observed that the slip surfaces are curved (i.e., **ac** and **bd** curves**)** when the trapdoor was lowered. However, he assumed for the simplification and calculation purposes that two vertical planes passing through the outer edges of the trapdoor (i.e., **ae** and **bf** planes) restrained the yielding soil and there was a horizontal plane (**e_1f_1**), above which no relative displacement happened. Such a plane is called the equal settlement plane. The soil mass above the equal settlement plane was treated as a surcharge (i.e., no arching effect available above that plane).

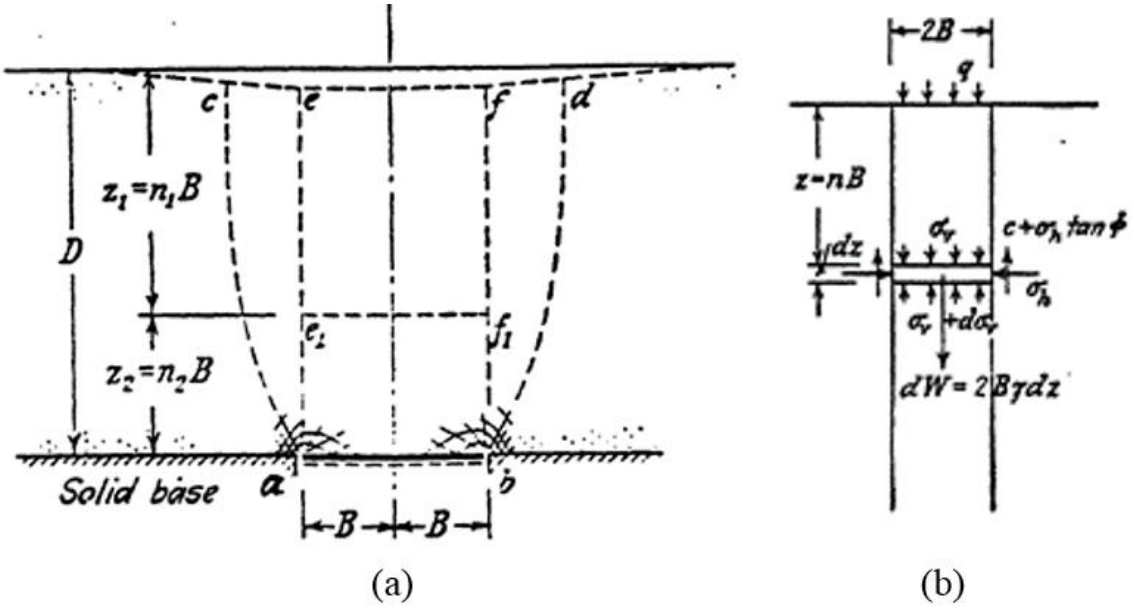

Figure 2.8 Terzaghi's investigation of arching effect in sand: (a) proposed failure of downward movement in a trapdoor test and (b) free body diagram for a slice of soil within the yielding zone (Terzaghi, 1943).

Figure 2.8(b) shows the free body diagram for a slice of soil within the yielding zone examined by Terzaghi (1943), in which he assumed that normal stresses were uniform across the horizontal sections and the coefficient of lateral stress (K) was a constant. Cohesion (c) was assumed to exist along the slip surfaces. By satisfying the force equilibrium vertically for the free

body diagram in Equation (2.2), he derived the following equations to estimate the vertical stress (σ_v) as in Equation (2.3) and the soil arching ratio as in Equation (2.4).

$$2B\gamma dz = 2B(\sigma_v + d\sigma_v) - 2B\sigma_v + 2cdz + 2\sigma_h dz \tan\phi \tag{2.2}$$

$$\sigma_v = \frac{B\left(\gamma - c/B\right)}{K\tan\phi}\left(1 - e^{-Kz\tan\phi/B}\right) + qe^{-Kz\tan\phi/B} \tag{2.3}$$

$$\rho = \frac{\sigma_v}{\gamma H + q} = \frac{B\left(\gamma - c/B\right)}{\left(\gamma H + q\right)K\tan\phi}\left(1 - e^{-Kz\tan\phi/B}\right) + \frac{qe^{-Kz\tan\phi/B}}{\gamma H + q} \tag{2.4}$$

where $2B$ = width of the trapdoor; γ = unit weight of soil; z = depth from the equal settlement plane; σ_v = vertical stress; σ_h = horizontal stress ($\sigma_h = K\sigma_v$); K = coefficient of lateral earth pressure; c = cohesion of soil; ϕ = friction angle of soil; and q = surcharge at the soil surface.

2.4.2 Hewlett and Randolph's Soil Arching Theory

Hewlett and Randolph (1988) studied the mechanism by which the load is carried by a square grid of piles or continuous walls and is transferred from a granular embankment fill based on laboratory model tests. They suggested a model of arched shape based on their observations of deformations within the fill as shown in Figure 2.9. Then, a solution for the soil arching effect, by considering limiting equilibrium of stresses within the arch, was proposed for a plane-strain and three-dimensional conditions.

For the plane-strain condition, as shown in Figure 2.9(a), Hewlett and Randolph (1988) considered that long arches are formed within the arching zone and supported by continuous walls. These arches are responsible for transferring the embankment weight to the supports in a similar action to that of the masonry arches in cathedrals. They assumed that arches are semi-circular and

have the same thickness, and no overlap of arches happens above the supports to satisfy the static equilibrium requirement. Also, they ignored the self-weight of the soil within the soil arching zone and considered no mobilization of the shear stresses for the soil below and between the formed arches. Considering that the limit equilibrium would reach first at the crown, a differential equation in terms of equilibrium in the radial direction was obtained as shown in Equation (2.4). By satisfying the boundary conditions at the crown of the arch, the stress just below the inner boundary of the arch is expressed in Equation (2.5).

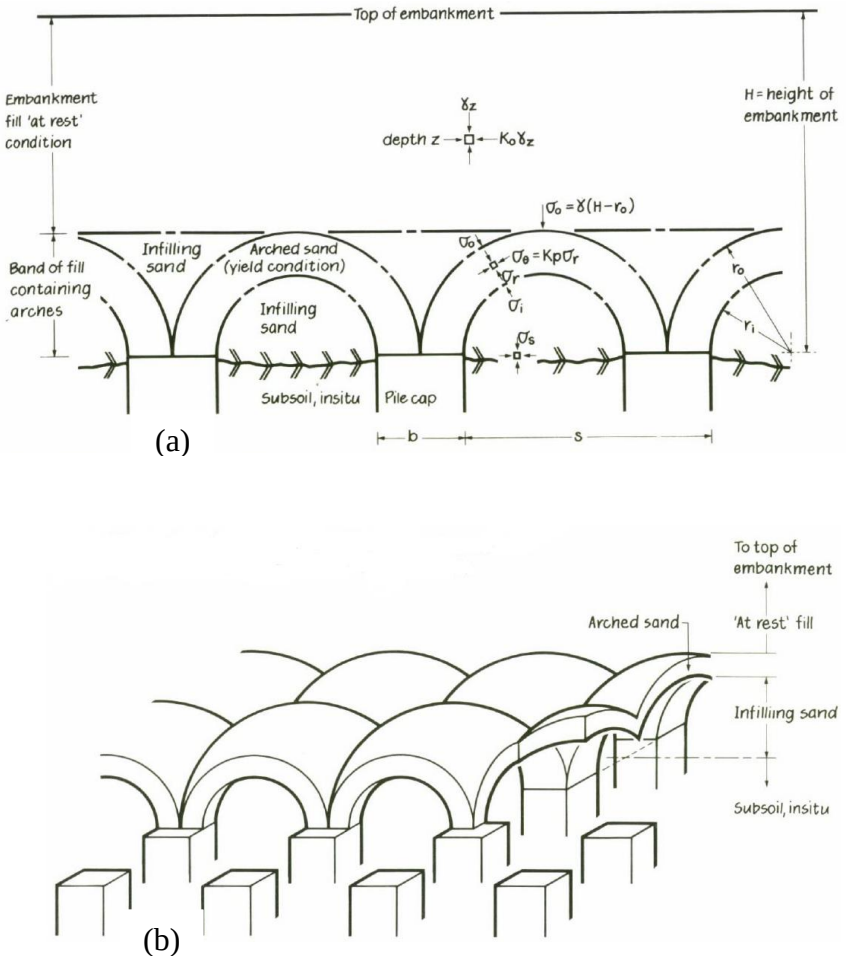

Figure 2.9 Soil arching in (a) a plane-strain condition (above continuous supports) and (b) a three-dimensional condition (above the grid of piles in a square pattern) (Hewlett and Randolph, 1988).

$$\frac{d\sigma_r}{dr} - \frac{(\sigma_r - \sigma_\theta)}{r} = 0 \tag{2.5}$$

$$\sigma_i = \gamma\left(H - \frac{s}{2}\right)\left(\frac{s-b}{s}\right)^{(K_P - 1)} \tag{2.6}$$

$$\rho = \frac{\sigma_i}{\gamma H} = \frac{1}{H}\left(H - \frac{s}{2}\right)\left(\frac{s-b}{s}\right)^{(K_P - 1)} \tag{2.7}$$

where σ_r = the radial stress, σ_θ = the tangential stress, r = the arch radius, σ_i = the vertical stress on the inner side of the arch, which equals to the vertical stress at $r = (s-b)/2$, γ = the soil unit weight, H = the height of the embankment, s = the center to center spacing of the support, b = the width of the support, and K_P = Rankine's passive earth pressure coefficient.

Hewlett (1984) considered the self-weight of soil within the arching zone and obtained the differential equation in the radial direction as shown in Equation (2.6). By solving the differential equation and applying the boundary conditions, the inner stress (σ_i) below the boundary of the arch is expressed in Equation (2.7). This analysis is only valid when the embankment height is more than half the spacing of the supports (i.e., $H > s/2$):

$$\frac{d\sigma_r}{dr} - \frac{(\sigma_r - \sigma_\theta)}{r} = -\gamma \tag{2.8}$$

$$\sigma_i = \gamma\left(\frac{s-b}{2(K_P - 2)}\right) + \gamma\left(H - \frac{s-b}{4} - \frac{s}{2(K_P - 2)}\right)\left(\frac{s-b}{s}\right)^{(K_P - 1)} \tag{2.9}$$

$$\rho = \frac{\sigma_i}{\gamma H} = \left(\frac{s-b}{2H(K_P - 2)}\right) + \left(1 - \frac{s-b}{4H} - \frac{s}{2H(K_P - 2)}\right)\left(\frac{s-b}{s}\right)^{(K_P - 1)} \tag{2.10}$$

For the embankments that are supported by piles, the most representative analysis for studying the soil arching is a three-dimensional analysis. In a three-dimensional condition and when piles are in a grid of square pattern, Hewlett and Randolph (1988) found that soil arching

would form in a series of domes based on their experimental tests as shown in Figure 2.9(b). They also observed that the vaults do not necessarily fail only at the crown of the domes, but also they might fail at the pile cap location as an inverted bearing capacity failure because of the highly concentrated stresses above the limited area of the caps. Therefore, first failure at either location determines the arching capacity, and the analysis should be done for both locations to determine which one has a lower capacity. By considering the equilibrium at the crown of the arch and satisfying the boundary conditions into the following differential equation (Equation (2.11)), the inner stress (σ_i) below the boundary of the arch is expressed in Equation (2.12).

$$\frac{d\sigma_r}{dr}+\frac{\left(\sigma_r-\sigma_\theta\right)}{r}=-\gamma \tag{2.11}$$

$$\sigma_i=\left[\gamma\left(1-\frac{b}{s}\right)^{2(K_P-1)}\right]\times\left[H-\frac{s}{\sqrt{2}}\left(\frac{K_P-2}{2K_P-3}\right)\right]+\gamma\frac{s-b}{\sqrt{2}\left(2K_P-3\right)} \tag{2.12}$$

$$\rho=\frac{\sigma_i}{\gamma H}=\left(1-\frac{b}{s}\right)^{2(K_P-1)}\times\left[1-\frac{s}{\sqrt{2}H}\left(\frac{K_P-2}{2K_P-3}\right)\right]+\frac{s-b}{\sqrt{2}H\left(2K_P-3\right)} \tag{2.13}$$

The soil arching ratio when failure happens at the pile cap location is given in Equation (2.14):

$$\rho=1/\left[\left(\frac{2K_p\left(K_p\delta+1-(1-\delta)^{K_p}\right)}{\left(K_p+1\right)\left(\delta+1\right)}-1\right)\left(\delta^2-1\right)\right] \tag{2.14}$$

where: $\delta = b/s$.

2.4.3 British Standard BS 8006

Two design methods based on two arching theories are adopted in the British Standard BS 8006 (2010) for strengthened/reinforced soils and other fills. The first method adopted in the BS 8006

was originally established based on the simplified analysis methods developed by Jones et al. (1990). Jones et al. (1990) modified Marston's formula for the positive projecting subsurface conduits to the three-dimensional condition of piles in PS or GRPS embankments to estimate the amount of load carried by the piles. Based on this method, BS 8006 assumes that shear stresses developed around vertical slip surfaces are responsible for the soil arching. The ratio of the vertical stress exerted on top of the pile (p_c) to the average vertical stress at the base of the embankment ($\sigma_v = \gamma H$) may be estimated from Equation (2.15).

$$\frac{p_c}{\gamma H} = \left[\frac{C_c\, a}{H}\right]^2 \tag{2.15}$$

where γ = the soil unit weight, H = the embankment height, a = the width of the pile cap, and C_c = the arching coefficient and can be calculated: $C_c = 1.95H/a - 0.18$ for end-bearing piles and $C_c = 1.5H/a - 0.07$ for floating piles.

Also, BS 8006 considered two different arching conditions: (1) the partial arching condition, where $0.7(s-a) \leq H \leq 1.4(s-a)$ and (2) the full arching condition, where $H > 1.4(s-a)$. The degree of soil arching which is commonly expressed by a soil arching ratio (ρ) or stress reduction ratio (SRR) is presented in Equations (2.16) and (2.17). These equations were derived for both arching conditions using the method presented by Russell and Pierpoint (1997).

$$SRR = \frac{2s}{(s+a)(s^2-a^2)}\left[s^2 - a^2\left(\frac{p_c}{\gamma H}\right)\right] \quad \text{For partial arching} \tag{2.16}$$

$$SRR = \frac{2.8s}{(s+a)^2 H}\left[s^2 - a^2\left(\frac{p_c}{\gamma H}\right)\right] \quad \text{For full arching} \tag{2.17}$$

where s = the center to center distance between piles.

The above equations can be used to calculate the SRR when PS or GRPS embankment is designed. However, for some embankments, these equations yielded SRRs greater than one, which is impossible. The main reason for this is that BS 8006 does not satisfy the vertical equilibrium when calculating the line load on the geosynthetic layer. Jones et al. (1990) made this choice to guarantee sufficient safety so that the stress on the geosynthetic is overpredicted and the outcome is a stronger design. However, this leads to unrealistic results for some embankment problems as discussed by Ariyarathne and Liyanapathirana (2015). Recently, Van Eekelen et al. (2011) proposed some modifications to BS 8006 in order to eliminate the shortcomings when calculating the line load on the geosynthetic layer. The modified equations satisfy the vertical equilibrium for the partial arching condition, but not for the full arching condition. However, they give more realistic values. The modified equations for the SSR are given below.

$$SRR = \frac{1}{(s^2-a^2)}\left[s^2 - a^2\left(\frac{p_c}{\gamma H}\right)\right] \quad \text{For partial arching} \tag{2.18}$$

$$SRR = \frac{1.4}{(s+a)H}\left[s^2 - a^2\left(\frac{p_c}{\gamma H}\right)\right] \quad \text{For full arching} \tag{2.19}$$

It worth mentioning that the partial or full arching condition depends on the embankment height and the clear spacing between adjacent piles. Since embankment height changes with the placement of each fill layer, it is possible for a partial arch to convert into a full arch during the embankment construction.

The second method adopted in the BS 8006 is based on Hewlett and Randolph (1988) arching theory discussed in the previous section. This method determines the arching efficiency E

as the proportion of the embankment weight carried by the piles. Based on this theory, the system may fail at one of two critical locations, either at the crown E_{crown} of the arch or the pile cap E_{cap}. Generally, for low embankment heights (relative to the pile spacing), arching efficiency may be assumed to govern the design, and as the embankment height increase, pile cap arching efficiency may be assumed to govern. Equations (2.20) to (2.22) present the formula used to calculate the arching efficiency.

$$E_{crown} = 1 - \frac{(s^2 - a^2)}{s^2 \gamma H}\left[\sigma_i + \gamma\left(\frac{s-a}{\sqrt{2}}\right)\right] \tag{2.20}$$

$$E_{cap} = \frac{\beta}{1+\beta} \tag{2.21}$$

$$\beta = \frac{2K_p}{(K_p+1)\left(1+\frac{a}{s}\right)}\left[\left(1+\frac{a}{s}\right)^{-K_p} - \left(1+K_p\frac{a}{s}\right)\right] \tag{2.22}$$

where σ_i = the pressure acting at the inner surface of the hemispherical dome and K_p = the passive lateral earth pressure calculated as $K_p = (1+\sin\varphi)/(1-\sin\varphi)$.

2.4.4 Van Eekelen Arching Model

An arching model that was developed by Van Eekelen et al. (2013), to best describe the arching above a geosynthetic reinforcement layer in GRPS embankment, is called the concentric arching model. The significant difference of this model as compared to the model of Hewlett and Randolph (1988) is that this model (1) considers the arching development as the subsoil deforms, (2) finds the load that is localized on the segment of the geosynthetic reinforcement between two sequential piles, and (3) gives a physical explanation for the inverse triangular load distribution on the

geosynthetic reinforcement that was found in their experimental study. Figure 2.10 shows the concentric arching model. This model assumes that 3D concentric arches (hemispheres) are formed above the square between every four piles. These hemispheres transfer the load outward in all directions along the hemispheres towards the 2D arches across two sequential piles. The process continues with the further transfer of the load along the 2D arches toward the pile caps.

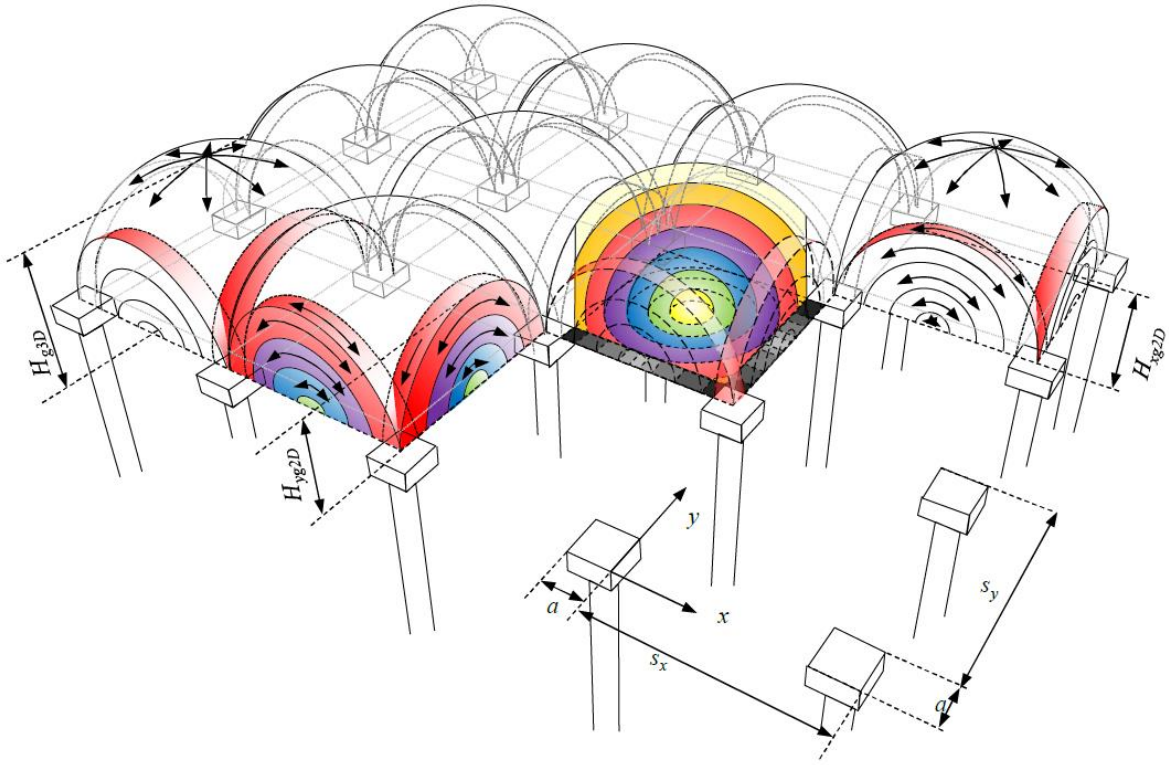

Figure 2.10 The concentric arching model (Van Eekelen et al. 2013).

The detailed description for the development of concentric arches can be found in Van Eekelen et al. (2013). This model assumes the development of an outer (larger) arch that bridges over piles as the subsoil deforms. With the continuous deformation of the subsoil, additional arches develop inside the outer one. This process of arches development results in a set of concentric

hemispheres as shown in Figure 2.10. In this model, the geosynthetic reinforcement is essential because, without geosynthetic reinforcement, there will be a more or less even settlement of the area between the piles and the concentric arches cannot develop.

Figure 2.11 shows the 2D concentric arches. The radial stress σ_r in the 2D arch is found by considering the radial equilibrium of the crown element of the 2D arch and assuming that the stress state in the arch is uniform around the semi-circle and that the limit state occurs in the entire arch, which gives the tangential stress $\sigma_\theta = K_p\,\sigma_r$. This leads, after some derivation can be found in Van Eekelen et al. (2013), to the following tangential stress for a 2D arch in the *x*-direction:

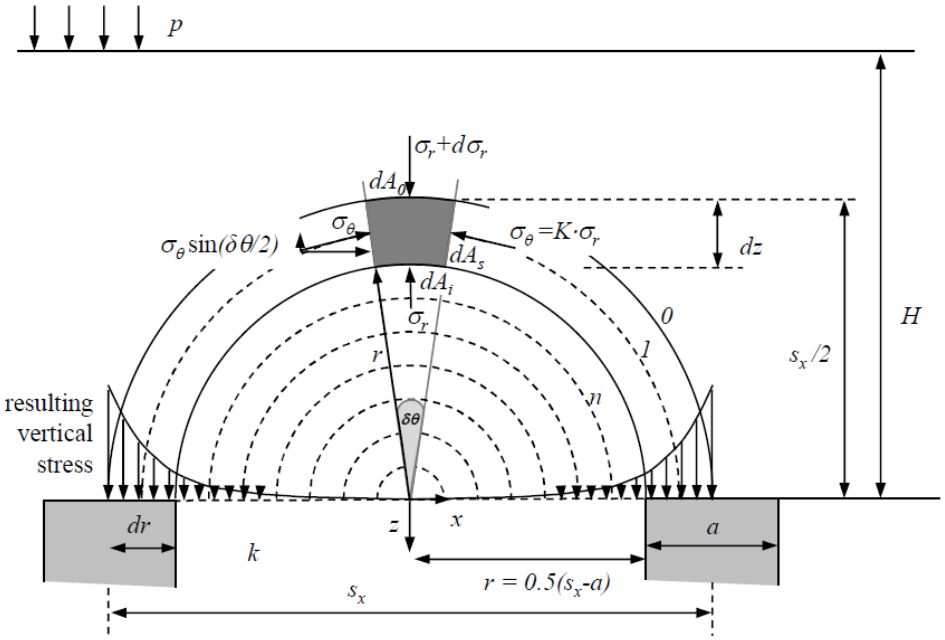

Figure 2.11 Forces in the 2D concentric arches (Van Eekelen et al. 2013).

$$\sigma_\theta = P_{x2D} r^{(K_P-1)} + Q_{2D} r \tag{2.23}$$

$$P_{x2D} = K_P {H_{xg2D}}^{1-K_P} \left[\gamma H + p - \gamma H_{xg2D} \frac{(K_P-1)}{(K_P-2)}\right] \tag{2.24}$$

$$Q_{2D} = K_P \frac{\gamma}{K_P - 2} \tag{2.25}$$

$$H_{xg2D} = \frac{s_x}{2} \qquad for\ H \geq \frac{s_x}{2} \quad \text{(Full arching)} \tag{2.26}$$

$$H_{xg2D} = H \qquad for\ H < \frac{s_x}{2} \quad \text{(Partial arching)} \tag{2.27}$$

$$K_P = \frac{1+\sin \emptyset}{1-\sin \emptyset} \tag{2.28}$$

where r = the radius of the 2D arch, γ = the fill unit weight, p = the uniformly distributed surcharge load on top of the fill, H_{xg2D} = the height of the largest 2D arch, s_x = the pile spacing parallel to the x-axis, and φ = the friction angle of soil.

Figure 2.12 shows the 3D concentric hemispheres. The tangential stress in the 3D arches is found in a similar way as for the 2D arches.

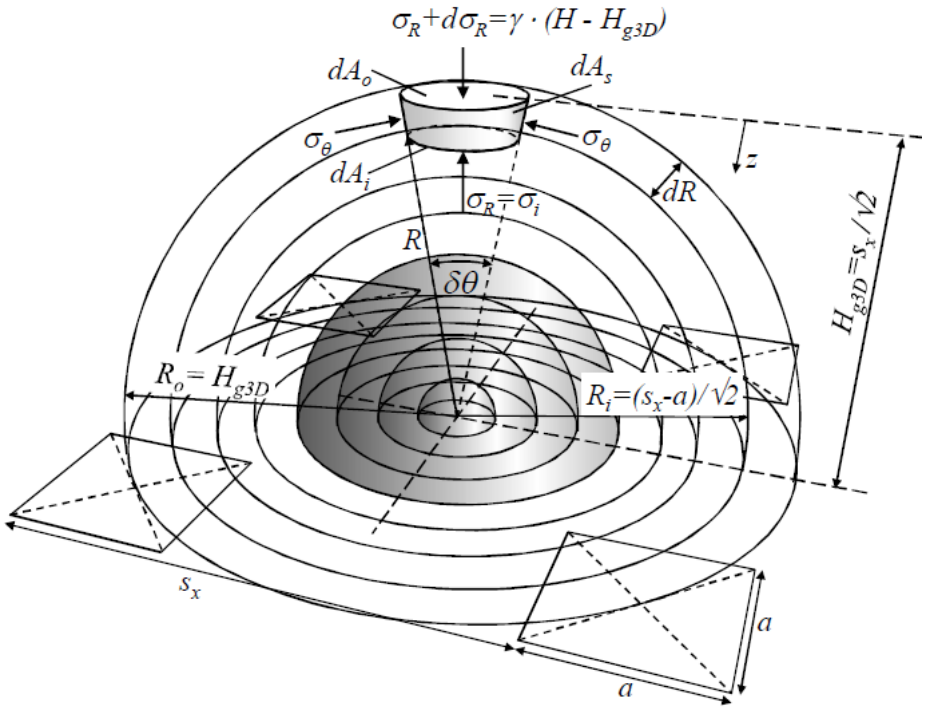

Figure 2.12 Forces in the 3D concentric hemispheres (Van Eekelen et al. 2013).

$$\sigma_{\theta(p=0)} = P_{3D}R^{2(K_P-1)} + Q_{3D}R \tag{2.29}$$

$$P_{3D} = \gamma K_P {H_{g3D}}^{2-2K_P}\left[H + H_{g3D}\frac{(2K_P-2)}{(2K_P-3)}\right] \tag{2.30}$$

$$Q_{3D} = K_P\frac{\gamma}{2K_P-3} \tag{2.31}$$

$$H_{g3D} = \frac{s_d}{2} \qquad for\ H \geq \frac{s_d}{2} \quad \text{(Full arching)} \tag{2.32}$$

$$H_{g3D} = H \qquad for\ H < \frac{s_d}{2} \quad \text{(Partial arching)} \tag{2.33}$$

$$\sigma_{\theta(p>0)} = \left(\frac{\gamma(H-z)+p}{\gamma(H-z)}\right)P_{3D}R^{2(K_P-1)} + Q_{3D}R \tag{2.34}$$

where R = the radius of the 3D hemisphere, H_{g3D} = the height of the largest 3D hemisphere, s_d = the diagonal center-to-center distance between piles, and z = the vertical distance between the considered point and the pile cap.

In the concentric arching model, the arch is extended downwards towards the subsoil, resulting in a set of concentric arches in 2D and hemispheres in the 3D. These arches and hemispheres exert a force on their subsurface. The larger the radius, the larger the force exerted on the subsurface.

2.5 TENSIONED MEMBRANE THEORIES

Geosynthetics have been widely used as a basal reinforcement in both pile-supported embankments and over existing sinkholes to better transfer the applied loads to the piles or surrounding soils, respectively. Thus, when a geosynthetic layer is extended over voids or compressible soils, the geosynthetic deforms and mobilizes its tension. This phenomenon is called a tensioned membrane effect. Gourc and Villard (2000) defined the membrane effect as "the ability

of a geosynthetic sheet to be deformed, thereby absorbing forces initially perpendicular to its surface through tension."

A few tensioned membrane theories have been proposed to account for the membrane effect. The available theories are based on a parabolic arc shape and a circular arc shape of the deformed geosynthetic. The directions of the stresses developing within the soil and applied on the geosynthetic are the reason for these two arc shapes. A parabolic arc shape is a result of considering that the stresses acting on the geosynthetic are only vertical at all the locations across the void width. However, assuming the geosynthetic deformed shape as a circular arc indicates that the stresses acting on the geosynthetic are normal to the geosynthetic surface when it deforms. Thus, the stresses on the geosynthetic have vertical and horizontal components at all locations except in the center of the void. It is noteworthy to mention that most of these theories were originally developed for the design of soil-geosynthetic systems over voids, such as sinkholes, dissolution cavities, and localized depression even though they have also been used for designing GRPS embankments. Two of the methods that have been commonly used to account for the tensioned membrane effect are Delmas (1979) and Giroud et al. (1990) and presented below.

2.5.1 Delmas' Method

The parabolic arc shape was proposed by Delmas (1979) in an analytical method to predict the tension-deformation relationship of a horizontal geosynthetic sheet above a void (e.g., cavity or trench) subjected to a uniformly distributed vertical load as shown in Figure 2.13. The assumptions for Delmas' method as stated by Gourc and Villard (2000) are:

- the problem is under a plane-strain condition,

- the geosynthetic sheet with an original length (L) is fixed at each end, and is subjected to a uniformly distributed vertical load (q),
- the stresses remain vertical and constant after deformation takes place,
- there is no horizontal displacement of any point on the geosynthetic during deflection, and
- the geosynthetic is assumed to have a linear elastic behavior (i.e., $T=J*\varepsilon$, where T = the tensile force in the sheet, ε = the strain and, J = the tensile stiffness defined by a unit width of the sheet).

The geosynthetic vertical deformation (Z) at any distance (y) from the edge of the void can be estimated from Equation (2.35).

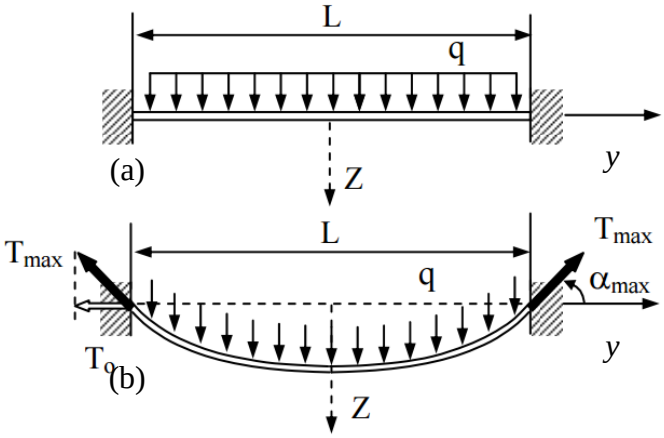

Figure 2.13 Delmas's tensioned membrane method: (a) before deflection and (b) after deflection (Gourc and Villard, 2000).

$$Z(y) = \frac{qL^2}{8T_0} - \frac{qx^2}{2T_0} \tag{2.35}$$

where T_0 is the horizontal component of the maximum tension, T_{max}, and can be calculated from the following equations:

$$T_0 = \frac{qL}{2\beta} \tag{2.36}$$

$$\frac{qL}{J} = \frac{3\left[\beta\sqrt{1+\beta^2} + ArgSh(\beta) - 2\beta\right]}{3+\beta^2} \tag{2.37}$$

While the maximum tension, T_{max}, and the maximum deformation, Z_{max}, can be calculated as:

$$T_{\max} = \frac{\sqrt{4T_0^2 + q^2L^2}}{2} \tag{2.38}$$

$$Z_{\max} = \frac{qL^2}{8T_0} \tag{2.39}$$

2.5.2 The Giroud et al. Method

An analytical solution to estimate the tension in the geosynthetic that bridges over a void and deforms in a circular arc shape was presented in Giroud et al. (1990). In addition to assuming the deformed geosynthetic as a circular arc as shown in Figure 2.14, they considered that the load is normally applied to the geosynthetic, which only stretches within the void span with a uniform strain along the portion of the geosynthetic overlying the void.

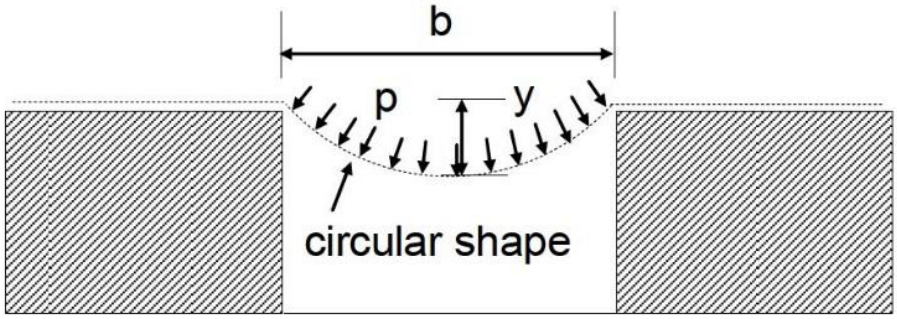

Figure 2.14 Deflected circular geosynthetic layer (Giroud et al., 1990).

The geosynthetic tensile force, T, over an infinitely long void, can be estimated using Equation (2.40).

$$T = pb\Omega \tag{2.40}$$

where p = the pressure normal to the geosynthetic, b = the void width, and Ω = a dimensionless factor, which can be determined by either Equation (2.41) or (2.42):

$$1+\varepsilon = 2\Omega \sin^{-1}\left(\frac{1}{2\Omega}\right) \qquad (y/b \le 0.5) \tag{2.41}$$

$$1+\varepsilon = 2\Omega\left[\pi - \sin^{-1}\left(\frac{1}{2\Omega}\right)\right] \qquad (y/b \ge 0.5) \tag{2.42}$$

where ε = the geosynthetic strain and y = the maximum deflection.

For a geosynthetic spanning a circular void, despite that the deflection shape is not a circular, Giroud et al. (1990) suggested using a diameter of, $2r$, instead of the width, b, in Equation (2.28) to calculate the tension, T, approximately.

2.6 SOIL ARCHING INVESTIGATIONS UNDER LOADING

2.6.1 Arching Under Self-Weight and Static Surface Loading

Soil arching has been commonly investigated using the trapdoor test approach since Terzaghi (1936). Terzaghi's tests were performed in a two-dimensional "plane-strain" box by using a rectangular trapdoor mounted to the box base under soil self-weight only, while McNulty (1965) used a circular trapdoor inside a cylindrical chamber to investigate the arching phenomenon under an axisymmetrical test setup. In addition, McNulty (1965) applied air pressure on the surface of the soil. Terzaghi (1936) and McNulty (1965) found that the shear stress induced by soil arching increased with an increase of the trapdoor displacement based on their test results. The Terzaghi (1936) tests indicated that the pressure on the trapdoor became constant when the deflection reached approximately 10% the width of the trapdoor, while the McNulty (1965) study showed a lower percentage of approximately 3% of deflection needed. They also found a plane of equal settlement, above which no soil arching or reduction of stress existed when the thickness of the soil mass was large enough. According to Terzaghi's observation, the equal settlement plane was at the height of 1.5 to 2.5 times the width of the trapdoor. However, McNulty (1965) found that the height of the equal settlement plane was from 1.0 to 1.5 times the trapdoor diameter under an axisymmetrical test condition.

Furthermore, trapdoor tests were carried out by Adachi et al. (1989) to investigate soil arching between piles that are used to stabilize landslide. Soil displacement and soil arching effect represented by the load applied on the piles were quantified by using displacement tracking marks buried in the soil and strain gauges attached to the piles, respectively. The soil arching phenomenon was observed by examining the pattern of soil particles' movement. Bertin (1978) conducted

centrifuge cavity collapse tests to investigate the effects of cavity diameter, soil properties, roof thickness, and surcharge on the collapse of the cavity.

Numerical methods have also been used to investigate soil arching behavior in different geotechnical problems. Koutsabeloulis and Griffiths (1989) simulated the trapdoor problem using a finite element method to study the stress distribution related to the active and passive modes of soil arching. In addition, plane-strain finite element analyses were conducted by Gabr and Hunter (1994) to investigate the contribution of geogrid in reducing the tensile strains induced in landfill liners over subsurface cavities. Han and Gabr (2002) studied the soil arching effects associated with the geosynthetic-reinforced pile-supported embankments using the finite difference program - Fast Lagrangian Analytical of Continua (FLAC). They found that the soil arching ratio depends on the stiffness difference between piles and soil, the pile spacing, and the existence of geosynthetic reinforcement.

Therefore, test configurations (e.g., plane-strain or axisymmetrical setup) and loading conditions (e.g., with or without surcharge or surface loading) affect the results and the applicability of their findings to the field condition. The load configuration effects have not yet been well investigated.

2.6.2 Arching Under Cyclic or Dynamic Loading

Several geotechnical applications are subjected to dynamic or cyclic surface loading, such as moving vehicles, railroad crossings, pile driving, impact due to falling of heavy objects, blast waves, and earthquakes.

Chen et al. (1991) performed simple impact tests using buried flexible plates, acrylic plates, as a trapdoor to evaluate the effects of impact or dynamic loading on soil arching. In their test

setup shown in Figure 2.15, a small-scale cylindrical sand tank was used. By using a steel ball that was dropped from a high of 0.6 m on an aluminum plate placed on the top of sand, the impact load was generated. Three different thicknesses of buried plates were used to represent different degrees of roof rigidity. In their tests, the ratio of soil cover thickness to opening diameter was kept to be 0.5. The earth pressures above and accelerations below the buried plate were measured. The test results demonstrated significant soil arching effects, and these effects depended on the deflection of the plate and the interaction between the soil and the plate. It worth mentioning that a limited soil arching degree was mobilized in Chen et al. (1991) tests since the trapdoor deflection was due to the flexibility of the acrylic plate itself and no movement was allowed for the trapdoor.

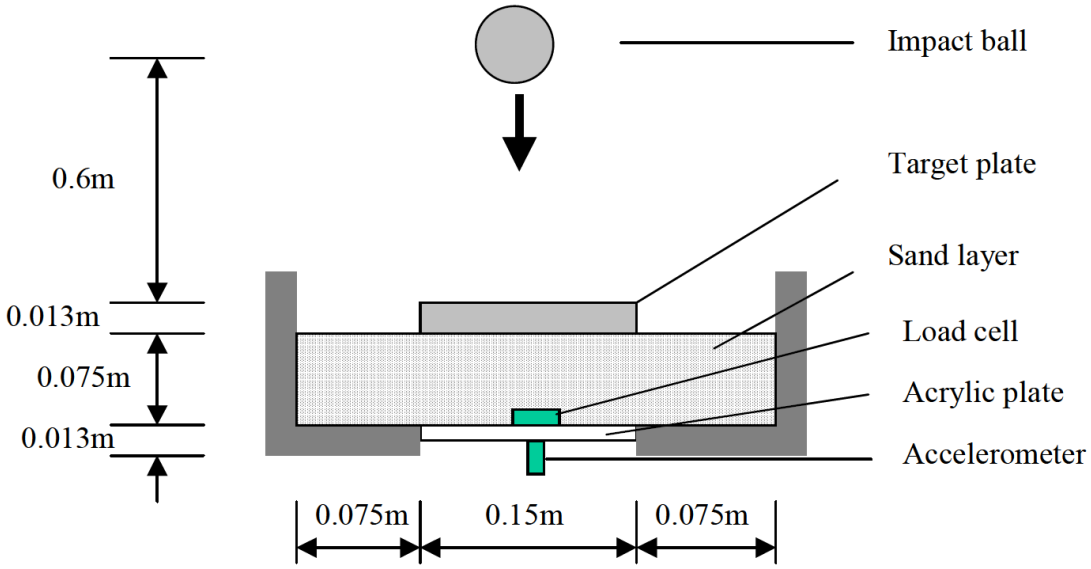

Figure 2.15 Chen et al. (1991) dynamic soil arching experimental setup (Han, personal communication).

Dancygier and Karinski (1999) also studied the soil arching contribution on the response of soil-buried structures under dynamic surface loading and proposed a simple, analytical model to evaluate the effect of shear stresses in soil. Their model assumed that the soil was subjected to

a uniformly distributed surface dynamic or impact load. The model also assumed the potential slip plane above the buried structure is vertical, which is the same as that proposed by Terzaghi (1943). Dancygier and Karinski (1999) defined the "arching ratio" as the ratio of the shear stress to the vertical displacement, which is different from the ratio proposed by McNulty (1965). Furthermore, Helwany and Chowdhury (2000) performed experimental studies to assess the change of lateral earth pressures on buried structures under dynamic loading considering soil arching effects.

Han and Bhandari (2009) and Bhandari (2010) conducted a numerical study using a discrete element method (DEM) to investigate soil arching and geogrid tension in geogrid reinforced and unreinforced pile-supported embankments under cyclic loading. In the unreinforced embankment shown in Figure 2.16(a), the contact force was oriented randomly after 25 cycles of loading through the footing on the surface, suggesting collapsing of soil arching. In the geosynthetic-reinforced embankment, however, the orientation and continuity of the contact forces suggested stable soil arching as shown in Figure 2.16(b). Bhandari (2010) found that the vertical stresses over the pile caps and the soft soil were constant for the reinforced embankment irrespective of the load cycles. On the other hand, the stresses over the pile caps decreased and the stresses on the soil increased with the load repetition for the unreinforced embankment. Consequently, one can conclude that the stresses above the pile caps and the soil may eventually approach to the same value if a sufficiently large number of load repetitions is applied, indicating the disappearance of soil arching.

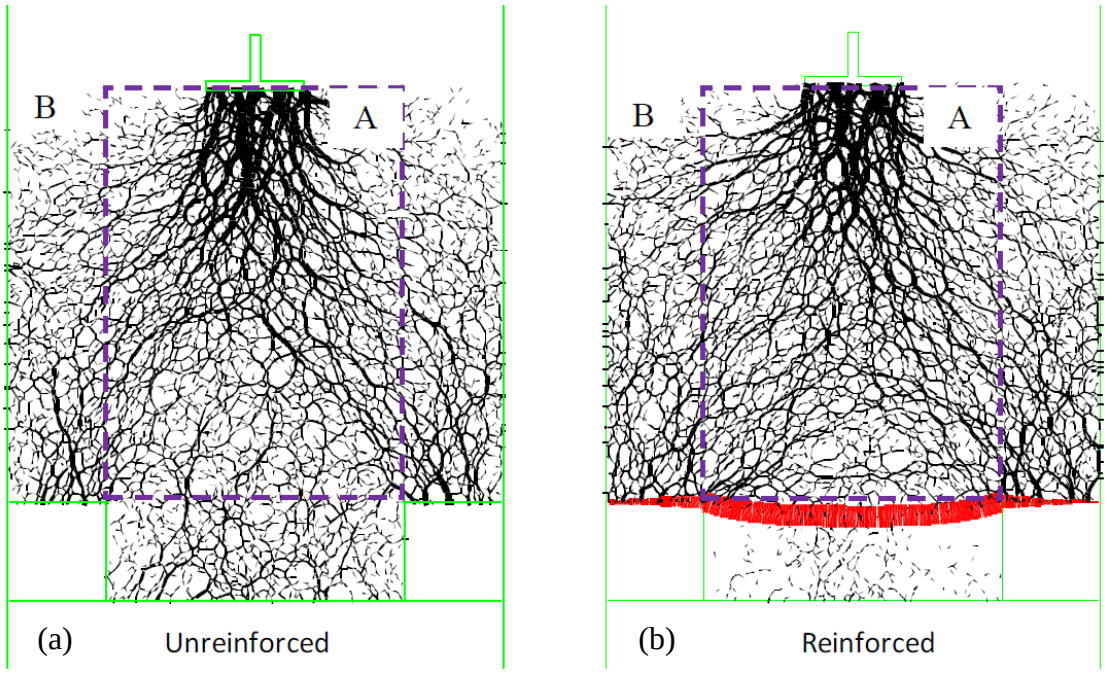

Figure 2.16 Contact force distribution for: (a) unreinforced and (b) reinforced embankment after 25 cycles of loading (Bhandari, 2010).

In general, soil arching under static loading is formed by shear stresses, which depend on the contact stresses between soil particles as a result of the interactional frictional forces. Under dynamic loading, however, the interactional frictional forces and the contact stresses may be reduced due to vibration effects so that soil arching tends to degrade, leading to the progressive reduction of interactional forces transmitting shear stresses. The factors that may affect the stability of the soil arching under dynamic or cyclic loading are, for example, the severity (i.e., number and intensity) of cyclic loading, the size of the load area, the distance between the load and the stable arch, and the presence of reinforcement.

CHAPTER 3 EXPERIMENTAL TESTS ON SOIL ARCHING WITH GEOFOAM ON CULVERT AND SPRING-BASED TRAPDOORS

In this research, two sets of experimental tests were conducted. The first set was to investigate the load transfer mechanism (i.e., soil arching) over a reduced-scale buried structure as well as the benefit of Expanded Polystyrene (EPS) geofoam installed above the buried structure to reduce the vertical pressure on it. The second set was to simulate soil subsidence and/or consolidation of foundation (soft) soil between two stationary supports, in which trapdoor tests were conducted to investigate both soil arching and geosynthetic tensioned membrane effects when geosynthetic was used. The following sections present the test setup and describe the experimental work details, including fill material properties, reinforcement properties, instrumentation, test procedure, and loading types.

3.1 EXPERIMENTAL TEST WITH BURIED STRUCTURE

3.1.1 Description of Experiments

Nine reduced-scale models were constructed in a test box under a plane-strain condition. One reference test with only a concrete culvert and no geofoam was conducted to simulate the positive projecting embankment (PPE). Other eight tests were constructed with a geofoam layer above the culvert to simulate the induced trench installation (ITI) method as outlined in Table 3.1.

Figure 3.1 shows the experimental setup used in this study, which consists of a twin-cell concrete culvert embedded in the center of the test box. The concrete culvert dimensions (height H_c = 0.2 m and width B_c = 0.36 m) were chosen to represent a 1.8 m twin-cell box culvert by a scale factor of 5.0.

Table 3.1 Buried box culvert test plan and parameters.

Test no.	Description	EPS geofoam		Loading type
		Type	*Thickness (mm)*	
T1	PPE	No geofoam		Static
T2	ITI	EPS12	0.2*Bc* (72)	Static
T3	ITI	EPS12	0.4*Bc* (144)	Static
T4	ITI	EPS12	0.8*Bc* (288)	Static
T5	ITI	EPS15	0.2*Bc* (72)	Static
T6	ITI	EPS15	0.4*Bc* (144)	Static
T7	ITI	EPS15	0.8*Bc* (288)	Static
T8	ITI	EPS12	0.2*Bc* (72)	Cyclic
T9	ITI	EPS15	0.2*Bc* (72)	Cyclic

Note: B_c = the outside width of the culvert as shown in Figure 3.1.

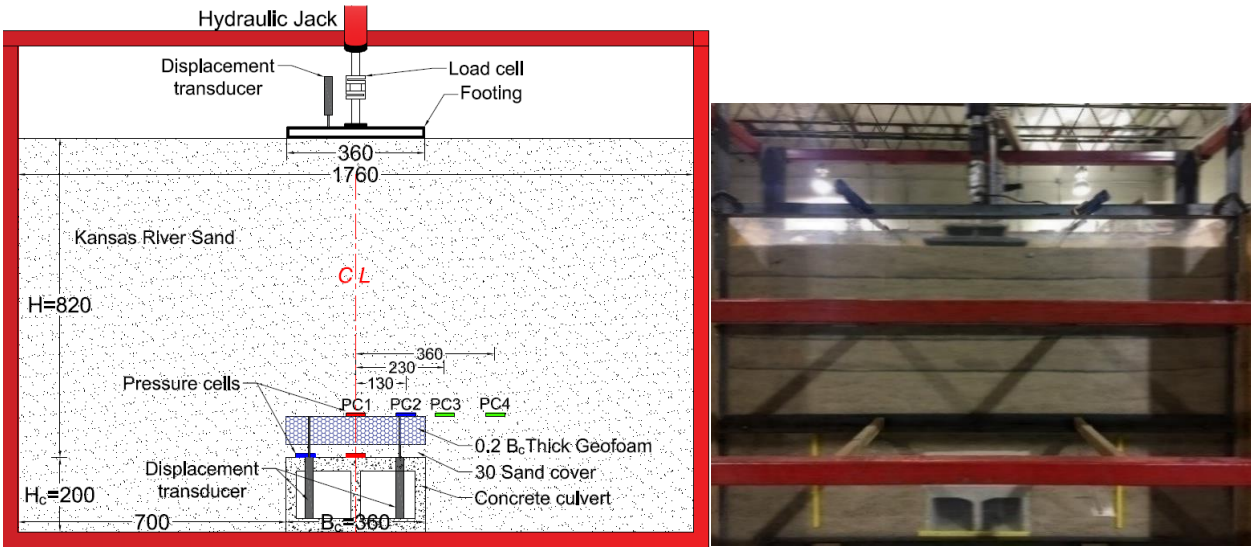

(a) (b)

Figure 3.1 Test box: (a) cross section showing locations and dimensions of the concrete culvert, EPS geofoam, footing, and instrumentation (units: millimeters) and (b) photo.

The test box was designed to accommodate a plane-strain condition with interior dimensions of 1.76 m long, 0.46 m wide, 1.50 m high. This box was made of three sides of plywood

and a Plexiglas on the front side to allow visual observation of soil deformations during the test. The walls were reinforced by steel square tubes all around the box to minimize the lateral deflections of its sides. Also, the Plexiglas plate was stiffened by four sections of steel angle along the front side. Three sides of the test box made of plywood were covered by a double layer of thick plastic sheet. The layer in contact with the box was fixed, while the layer in contact with the soil was free to move with minimum frictional resistance from the box walls. Using plastic sheets or lubricant for boundary treatment were successfully used by researchers in reduced-scale tests (Zarnani et al., 2011; Ahmed, 2016; Hong et al., 2016; Kakrasul et al., 2016). No treatment was made for the front Plexiglas plate because any treatment would smear the plate and make the visional observation of soil movement difficult. The friction between the Plexiglas plate and the soil might affect the measured data; however, such an effect was minimal because the measured pressures on the box base were approximately equal to the theoretical overburden pressure (γH) as discussed later in the result section. The length of the concrete culvert was the same as the width of the box. The culvert width, B_c = 0.36 m, was selected to be one-fifth of the test box width (i.e., the culvert placed far enough from the sidewalls) so that the boundary effect would be minimized. The distance from each side of the culvert to the box sidewall was 0.7 m, which is twice the width of the buried structure as recommended by Bloomquist et al. (2009). On the top of the embankment fill, a footing load was applied using a hydraulic jack attached to a rigid steel footing that had the same dimension as the culvert, i.e., 0.36 m wide and 0.46 m long, and was centered above the culvert as shown in Figure 3.1. The hydraulic jack had a load capacity of 25 tons and was modified to apply cyclic loading in addition to static loading with a maximum frequency of 0.5 Hz. The applied load was monitored using an S-shape load cell with a load capacity of 22.3 MN mounted above the footing.

3.1.2 Test Material

Dry Kansas River sand was used as a granular fill for the embankment material to investigate the distribution of vertical stresses above the concrete culvert. This material was selected because its properties were determined by the previous studies (Rahmaninezhad et al., 2016; Al-Naddaf, 2017). Based on the particle size distribution curve shown in Figure 3.2, this sand had a maximum particle size of 4.75 mm and a mean particle size of 0.6 mm. This sand was classified as poorly graded sand (SP) according to the Unified Soil Classification System (USCS) (ASTM, 2011). The coefficients of uniformity (Cu) and curvature (Cc) were 3.18 and 0.99, respectively. Kansas River Sand had minimum and maximum dry unit weights of 16.02 kN/m^3 and 18.85 kN/m^3, respectively, in accordance with ASTM D4254-14 and ASTM D4253-14.

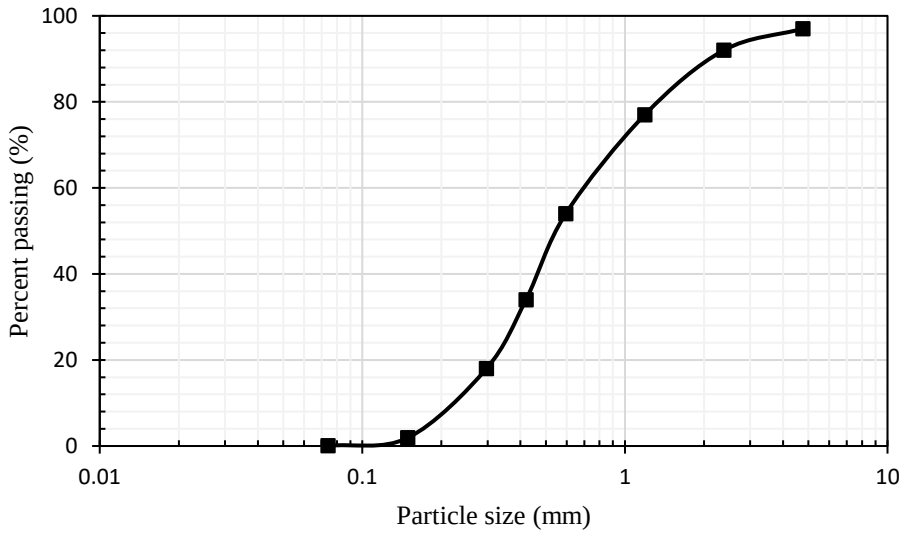

Figure 3.2 Particle size distribution curve for the Kansas River sand.

In this study, the embankment height (H=820 mm) was selected to represent a full-scale embankment of 4.1 m high by a scale factor of 5.0. This height is more than twice the width of the concrete culvert (i.e., H=820 mm, B_c=360 mm, and H/B_c=2.28) to allow the soil arching

mobilization. During the construction of the embankment, Kansas River sand was poured and then compacted to 75% relative density in lifts until the required embankment height was reached. A manual compactor, with a 150 mm drop height as shown in Figure 3.3, was used to compact each lift by evenly distributing 64 drops on the sand lift surface until a relative density of 75% was reached. The compacted sand at this density had a unit weight of 18.04 kN/m^3 and a peak friction angle of 38º based on triaxial shear tests. The initial elastic modulus of the sand was 25 MPa based on three confining pressures of 35, 70, and 100 kPa of triaxial shear tests.

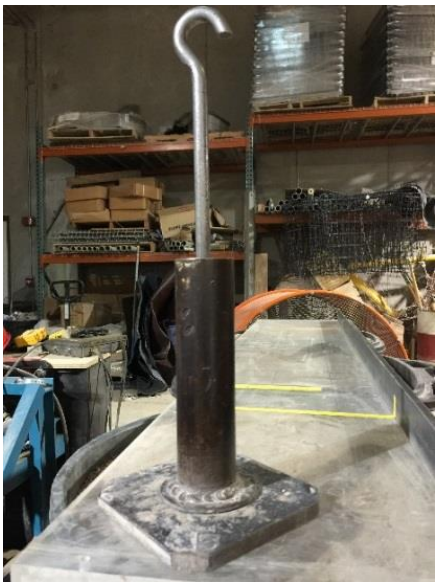

Figure 3.3 Manual steel compactor.

A lightweight material, EPS geofoam of two different densities, was used as a compressible layer above the concrete culvert to simulate the ITI method. Table 3.2 provides the EPS geofoam properties. EPS geofoams with densities of 12 and 15 kg/m^3 are commonly used in culvert and pipe applications, and therefore they were used in this study. These two densities represent the smallest densities available in the market with the lowest stiffness (highest compressibility). The relative stiffness values between soil and compressible material as defined by the ratio of soil

elastic modulus to geofoam elastic modulus (E_s/E_g) were 16.7 and 10 for EPS12 and EPS15, respectively. Since the elastic modulus ratio of the soil to the geofoam is relatively low as compared with that suggested by Han (2015), partially mobilized soil arching was expected in this study. The width of the EPS geofoam was chosen to be equal to that of the concrete culvert (B_c). Also, the geofoam thicknesses were chosen to represent $0.2B_c$, $0.4B_c$, and $0.8B_c$. These thicknesses were considered acceptable to allow the mobilization of soil arching by Vaslestad et al. (1993) and McGuigan and Valsangkar (2010).

Table 3.2 EPS geofoam physical properties.

Property	**Unit**	**Geofoam**	
		EPS12	***EPS15***
Density	kg/m^3	11.2	14.4
Compressive resistance @ 1% strain	kPa	15	25
Compressive resistance @ 5% strain	kPa	35	55
Compressive resistance @ 10% strain	kPa	40	70
Elastic modulus @ 1% strain	kPa	1500	2500

Note: Physical properties are based on manufacturer provided datasheet.

3.1.3 Instrumentation

To obtain the pressure distribution during the test, six earth pressure cells were used and placed in the middle of the culvert as depicted in Figure 3.4. In the PPE test (T1), pressure cells were installed symmetrically about the centerline of the culvert at distances of 0, 130, 230, and 360 mm, respectively, as shown in Figure 3.4(a). In the ITI tests (T2 to T9), two pressure cells were placed above the box culvert at distances of 0 and 130 mm from its centerline within a 30 mm thick sand cover, as shown in Figures 3.1 and 3.4(b). This cover was left between the culvert top and the EPS

geofoam bottom to simulate the common practice (McAffee and Valsangkar, 2005) and to accommodate the pressure cells used to measure the pressures above the culvert in these tests. Figure 3.4(c) shows that four more pressure cells were installed above the geofoam and adjacent soil at the right side of the test box centerline at distances of 0, 130, 230, and 360 mm, respectively. The pressure cells located on the top of the geofoam were used to measure the changes of the vertical earth pressures associated with the vertical compression of the geofoam induced by the footing load, while the other two cells were installed to measure the increase of the vertical earth pressures at the adjacent soil. These pressure cells had an outside diameter of 50 mm, a sensing-surface diameter of 46 mm, a thickness of 11.3 mm, and a maximum capacity of 200 kPa.

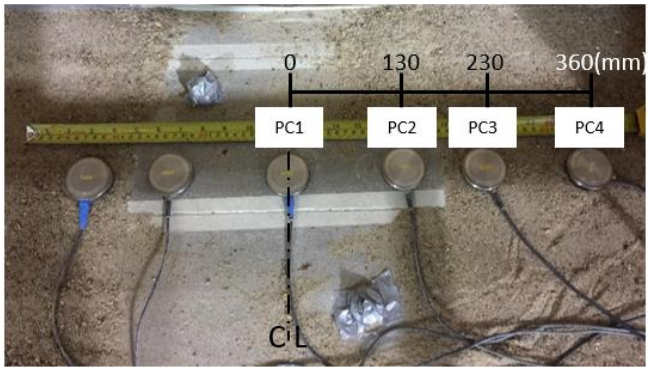

(a)

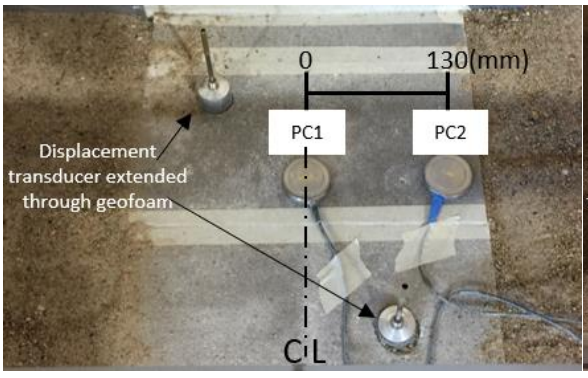

(b)

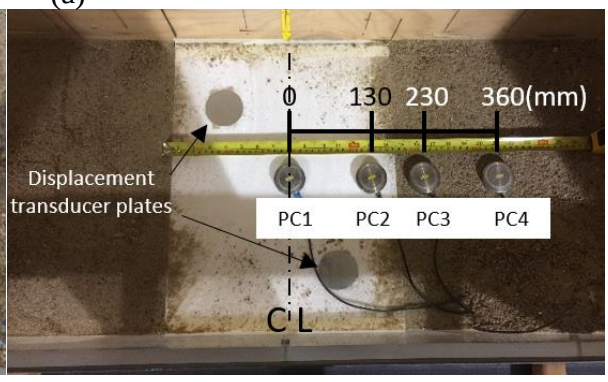

(c)

Figure 3.4 Layout of earth pressure cells: above the culvert in (a) test T1; (b) tests T2 – T9; and (c) above the geofoam in tests T2 – T9.

Geofoam compression and footing settlement were monitored using three displacement transducers (type TML CDP-50, manufactured by the Tokyo Sokki Kenkyujo Co., Ltd.) with a measuring capacity of 50 mm as shown in Figure 3.5(a). Two displacement transducers were placed under the geofoam, along with the diagonal line and at 100 mm away from the corner of the geofoam. A displacement transducer pin passed through a custom-made opening of 10 mm diameter cylindrical shape through the geofoam to be in contact with a 50 mm diameter aluminum plate as shown in Figures 3.4(b) and 3.4(c). Another displacement transducer was mounted above the footing to monitor the footing settlement during loading as shown in Figure 3.5(b). The pressure cells and the displacement transducers were connected to a data acquisition system, which consisted of three Smart Dynamic Strain Recorders (type DC-204R, manufactured by Tokyo Sokki Kenkyujo Co., Ltd.) to record the pressures and the displacements automatically with a scan frequency of 100 Hz as shown in Figure 3.6.

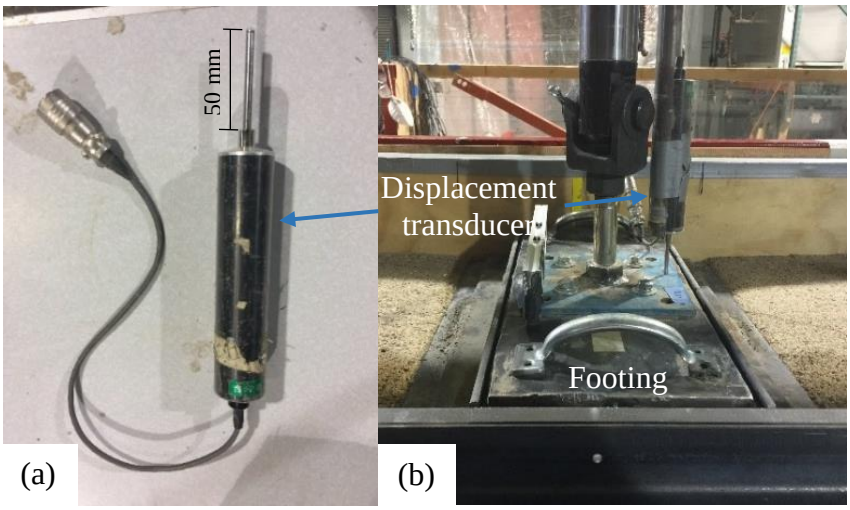

Figure 3.5 Displacement transducer: (a) in display and (b) above the footing.

Figure 3.6 Data acquisition systems consisted of three Smart Dynamic Strain Recorders type.

3.1.4 Test Procedure

In the model tests performed in this study, the culvert was placed directly on the box base to ensure no settlement beneath the culvert simulating an unyielding foundation. Therefore, this study excludes the effects of the foundation soil. Embankment construction continued in lifts around and over the culvert up to the desired height as shown in Figure 3.1. The construction was performed in eight lifts of approximately 100 mm thick per lift using a mass-volume control method. Kansas River sand was poured and then compacted using a manually-held steel compactor. The compacted soil had a relative density of 75%. The effect of compaction on the granular fill in reduced-scale models was discussed in Rahmaninezhad et al. (2009). In the ITI tests, the EPS geofoam was installed above the culvert over a 30 mm sand cover within the embankment. Pressure cells were placed above the culvert and the geofoam as described previously. After the embankment construction, the embankment surface was subjected to a static footing load. The load was applied in increments with each incremental pressure of approximately 7 kPa to study the re-distribution of additional stresses induced by the footing load above the buried structure in Tests T1 to T7. Also, incremental cyclic loading was utilized in tests T8 and T9 with a frequency of 0.1 Hz for a 100-cycle per each incremental pressure of approximately 9 kPa.

3.2 EXPERIMENTAL TEST WITH SPRING-BASED TRAPDOOR

3.2.1 Description of Experiments

A conventional trapdoor test is conducted by moving a rigid trapdoor gradually by a manual or automatic control; therefore, the trapdoor movement is not affected by the vertical stress on the trapdoor. This method of trapdoor movement does not represent the situation happening in the field, for example, in GRPS embankments. In the Al-Naddaf (2017) study, after being lowered to a certain level, the trapdoor was fixed during surface footing loading. This situation is also different from what happens in the field. To overcome these problems, a spring-based trapdoor test was proposed and conducted in this study.

To better evaluate the effect of localized surface loading on the soil arching mobilization and degradation while allowing the movement of the trapdoor, a spring-based trapdoor was used except for the reference tests. The test started with the placement of soil on and around the trapdoor (i.e., the fill placement stage), during which the trapdoor moved downward due to the vertical stress on the trapdoor and the compression of the springs, followed by the application of footing loading (i.e., the loading test stage). The experimental program, as outlined in Table 3.3**,** consisted of twelve physical model tests. These reduced-scale model tests were constructed in the test box under a plane-strain condition. Two reference tests (T10 and T18) with unreinforced fill were constructed and tested under static and cyclic footing loading, respectively, without the mobilization of soil arching (i.e., no trapdoor movement). These tests were conducted to evaluate and differentiate the pressure distribution on the test box base with other tests when the trapdoor was allowed to move (i.e., soil arching was mobilized). Seven trapdoor tests (T11-T17) were constructed with unreinforced and geosynthetic-reinforced fill and tested under static footing loading, while three other trapdoor tests (T19-T21) were constructed with unreinforced fill and

tested under static footing loading. Two different types of trapdoors with different spring stiffness were utilized in these tests to simulate different modes of soil movement (i.e., yielding soil) between two stationary supports and to assess the associated load transfer mechanisms.

The two trapdoor types were one-segment and three-segment trapdoors to simulate a uniform and a non-uniform soil displacement conditions of a yielding subsoil. Prior to this study, most soil arching investigations utilized only the one-segment trapdoor, which is a simplified condition of the soil movement and does not represent the actual displacement mode of a subsoil. In pile-supported embankments, the displacement of the subsoil between rigid supports is not uniform and exhibits a concave (parabola)-like shape. Therefore, a three-segment trapdoor was utilized in this study to better simulate the displacement condition of the subsoil. Since the one-segment trapdoor resulted in a uniform soil displacement, the pressure distribution above the trapdoor was not uniform but was close to that under a rigid footing on granular material. Therefore, the one-segment trapdoor will be referred to as a rigid trapdoor in this study. On the other hand, the three-segment trapdoor had a non-uniform displacement but a more uniform pressure distribution; therefore, it behaved more like a flexible footing on granular material. The three-segment trapdoor will be referred to as a "flexible" trapdoor in this study.

Table 3.3 Spring-based trapdoor test plan and parameters.

Test No.	Embankment type	Trapdoor		Loading type
		Type (Behavior)	K_T (kPa/m)	
T10	Unreinforced	No trapdoor movement (reference test)		Static
T11	Unreinforced	Four-Spring (Rigid)	1150	Static
T12	SL reinforced	Four-Spring (Rigid)	1150	Static
T13	DL reinforced	Four-Spring (Rigid)	1150	Static
T14	Unreinforced	Six-Spring (Rigid)	1725	Static
T15	SL reinforced	Six-Spring (Rigid)	1725	Static
T16	Unreinforced	Six-Spring ("flexible")	1725	Static
T17	SL reinforced	Six-Spring ("flexible")	1725	Static
T18	Unreinforced	No trapdoor movement (reference test)		Cyclic
T19	Unreinforced	Four-Spring (Rigid)	1150	Cyclic
T20	Unreinforced	Six-Spring (Rigid)	1725	Cyclic
T21	Unreinforced	Six-Spring ("flexible")	1725	Cyclic

Note: a geogrid was covered with a non-woven (NW) geotextile before dry sand was placed as fill.

3.2.2 Test Setup

In this study, three different conditions were investigated, which include unreinforced fill, single layer (SL) geosynthetic-reinforced fill, and double layer (DL) geosynthetic-reinforced fill. Complete test setup for each condition is depicted in Figure 3.7. The experimental setup used in this study consisted of a moveable trapdoor mounted on four or six compression springs, as shown in Figures 3.7 and 3.8, and embedded in the center of the test box between two stationary supports. The trapdoor with a width B = 0.36 m and a length L = 0.46 m was chosen to represent a yielding subsoil with a span of 1.8 m wide scaled by a factor of 5.0 between two supports. The trapdoor roof consisted of one piece of 20-mm thick plywood and a 13-mm thick aluminum plate. To ensure

that the trapdoor would settle evenly, the compression springs were distributed symmetrically about the trapdoor centerline and under its plate such that each spring would carry the same amount of load. In addition, a plastic washer was placed all around the trapdoor to reduce the frictional resistance of the trapdoor edges during its movement. The stationary supports that were made of wood blocks had a dimension of 0.46 m wide and 0.70 m long. The same test box and treatments described earlier in Section 3.1.1 were used to conduct these tests. The box was designed to create a plane-strain condition with interior dimensions of 1.76 m long, 0.46 m wide, and 1.50 m high. The length of the trapdoor was the same as the width of the box. The trapdoor width, B = 0.36 m, was selected to be one-fifth of the test box width (i.e., the trapdoor placed far enough from the sidewalls) so that the boundary effect would be minimized. The distance from each side of the trapdoor to the box sidewall was 0.7 m, which is twice the width of the trapdoor. On the top of the fill, a footing load was applied using a hydraulic jack attached to a rigid steel footing that had the same dimension as the trapdoor (i.e., 0.36 m wide and 0.46 m long) and was centered above the trapdoor as shown in Figure 3.7.

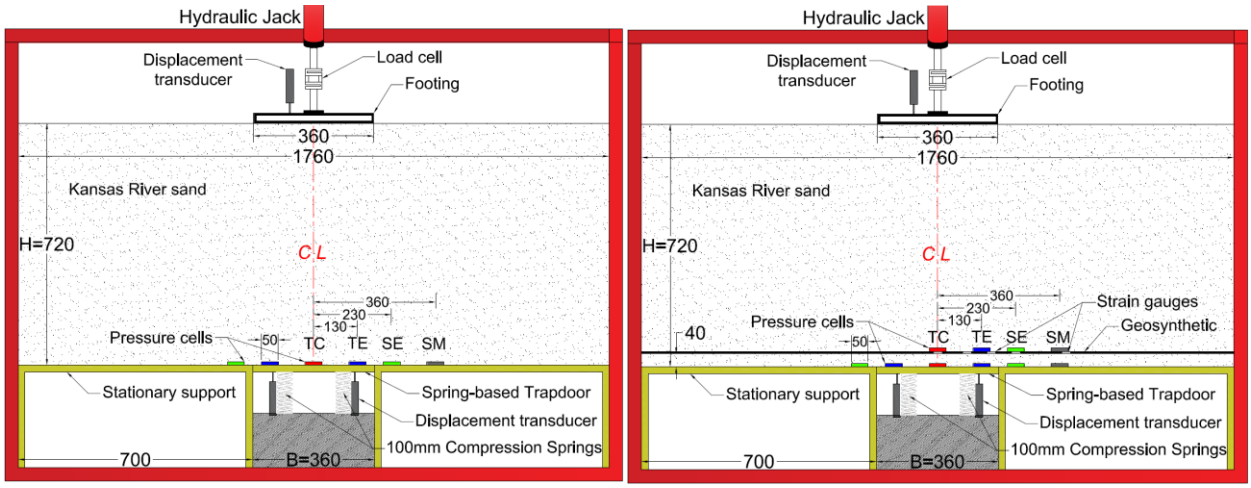

(a) (b)

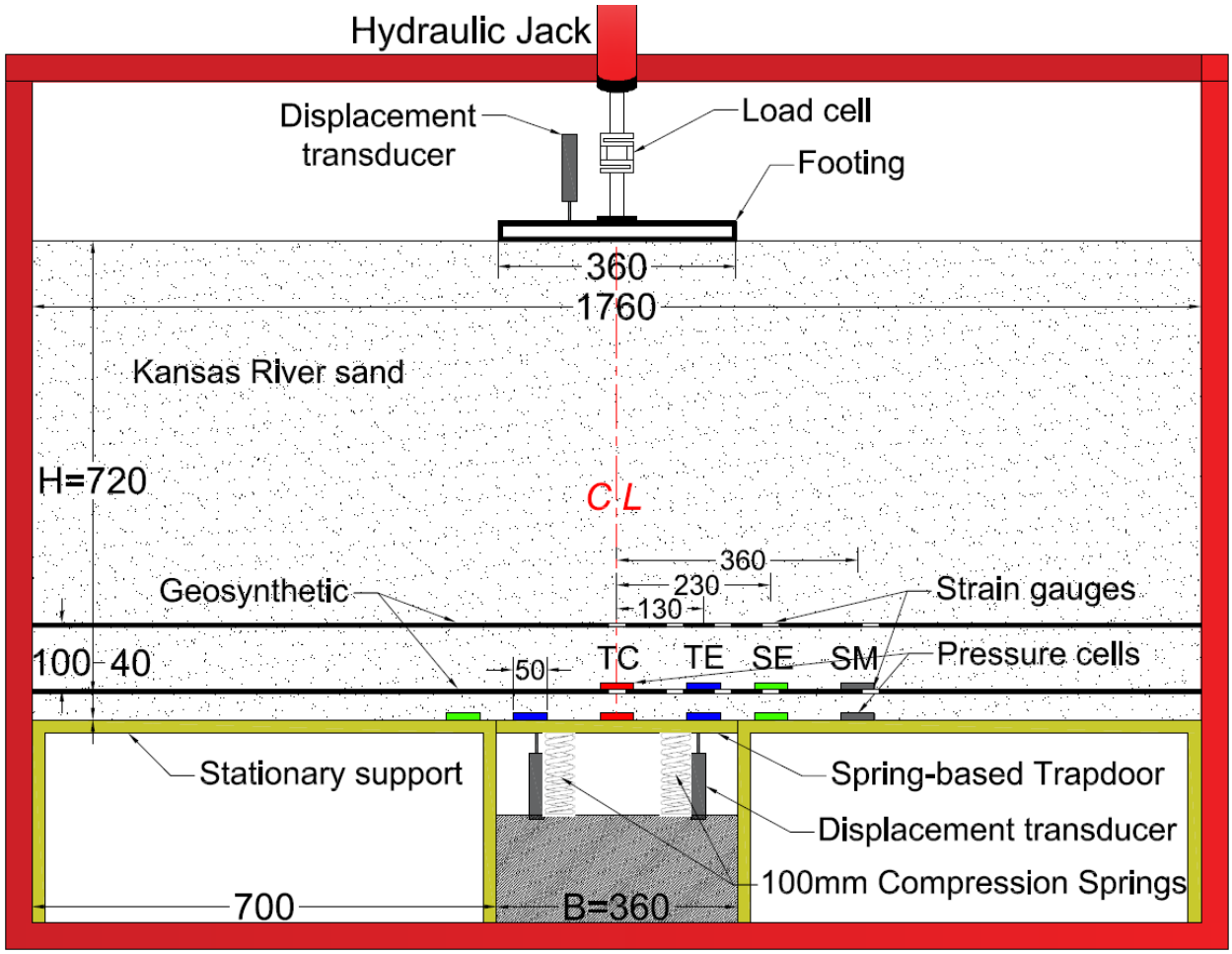

(c)

Figure 3.7 Cross-sectional view of the test setup showing locations and dimensions of the trapdoor and supports, reinforcement, footing, and instrumentations for: (a) unreinforced fill; (b) SL geosynthetic-reinforced fill; and (c) DL geosynthetic-reinforced fill (units: millimeters).

(a) (b)

Figure 3.8 Spring-based trapdoor layout: (a) rigid (one segment) trapdoor and (b) flexible (three-segment) trapdoor.

3.2.3 Fill Material

Granular material is commonly used as a fill material in many geotechnical applications, such as embankments, reinforced earth platforms, fill over buried pipes, and fill behind retaining walls, in which soil arching is an important mechanism of the load transfer. Therefore, the same Kansas River sand described earlier in Section 3.1.2 was selected as the granular fill material in this study to investigate the arching phenomenon. For all tests, the fill height (H=0.72 m) was selected to represent a full-scale embankment of approximately 3.6 m high scaled by a factor of 5.0. This height is twice the width of the trapdoor (i.e., H=0.72 m, B=0.36 m, and H/B=2) to allow for the soil arching mobilization. During placement of fill, sand was poured and then compacted to 75% relative density in lifts (controlled by mass and volume) until the required embankment height was

reached. This fill placement method is to simulate the method used in field. The compacted sand at this density had a unit weight of 18.04 kN/m^3 and a peak friction angle of 38^o based on triaxial shear tests. The initial elastic modulus of the sand was 25 MPa based on three confining pressures of 35, 70, and 100 kPa of triaxial shear tests.

3.2.4 Reinforcement

As pointed out in Chapter 2, geosynthetic reinforcement has been used in several geotechnical applications, such as GRPS embankments, geosynthetic bridging over cavities, and reinforced earth platforms. However, the effects of geosynthetic reinforcement on soil arching in trapdoor tests have rarely been investigated. Therefore, investigating the effects of the geosynthetic reinforcement on soil arching is valuable for practical applications.

This study investigated the effects of SL and DL of geosynthetic reinforcement on the soil arching mobilization and degradation. In the reinforced fill tests, a non-woven geotextile sheet was placed atop of a biaxial geogrid. Table 3.4 and Figure 3.9 provide the geosynthetic properties and shapes, respectively. Since the fill material was sand, the non-woven geotextile was utilized over the geogrid to prevent sand from flowing through the geogrid apertures, and to distribute the load from the embankment to the geogrid. The SL of geosynthetic reinforcement was placed over a sand layer of 40 mm thick over the trapdoor and the supports as shown in Figure 3.7(b). Also, the same thickness of sand layer was used under the first reinforcement layer in the DL of geosynthetic-reinforced fill test, and a distance of 100 mm was maintained between the first and second layers of reinforcement as shown in Figure 3.7(c).

Table 3.4 Geosynthetic properties.

Geosynthetic	Properties	Units	Values	
			MD	***XMD***
Biaxial geogrid	Aperture dimensions	mm	25	33
	Minimum rib thickness	mm	0.76	0.76
	Tensile strength @ 2% strain	kN/m	4.1	6.6
	Tensile strength @ 5% strain	kN/m	8.5	13.4
	Ultimate tensile strength	kN/m	12.4	19
Non-woven geotextile	Unit mass	g/m^2	119	
	Grab tensile strength	N	400	
	Grab elongation	%	50	
	Trapezoid tear	N	156	
	Puncture	N	245	
	Mullen burst	kN/m^2	1276	

Note: geosynthetic properties are based on the manufacturer provided datasheet; MD = machine direction and XMD = cross-machine direction.

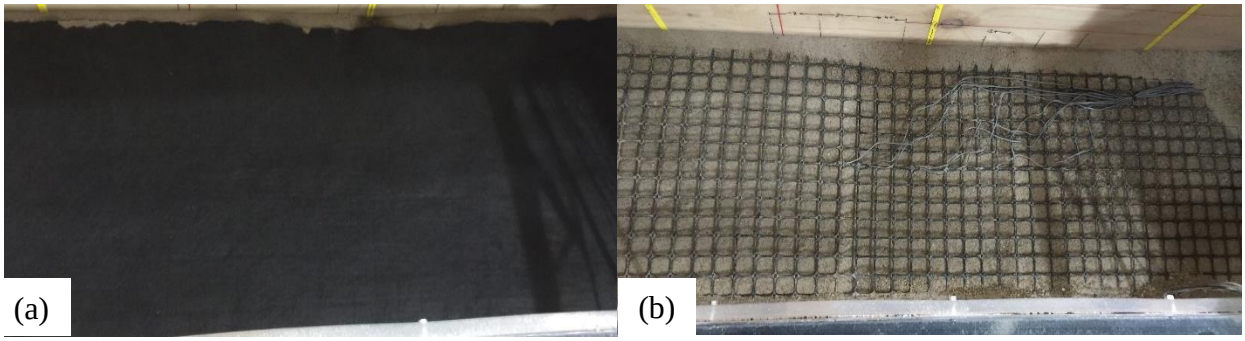

Figure 3.9 Geosynthetic: (a) non-woven geotextile; and (b) biaxial geogrid.

3.2.5 Instrumentation

In this study, four types of measurements were collected, which include earth pressures, footing and trapdoor displacements, geogrid strains, and embankment fill movement.

To obtain the pressure distribution during the test, eight earth pressure cells were used and placed in the middle of the test box as depicted in Figure 3.10. In unreinforced embankment tests, five pressure cells were installed symmetrically about the centerline of the trapdoor at distances of

0, 130, and 230 mm, respectively, as shown in Figure 3.10(a). The other three cells were distributed above the test box base for data assurance. In reinforced embankment tests, five pressure cells were placed below the reinforcement within a sand bedding layer of 40 mm thick and installed symmetrically about the centerline of the trapdoor at distances of 0, 130, and 230 mm, respectively, as shown in Figure 3.10(b). The sand bedding layer that was placed between the test box base and the reinforcement is to provide the required interlock with the single or first geosynthetic layer and to accommodate the pressure cells used to measure the pressures above the box base in these tests. Figure 3.10(c) show that three more pressure cells were installed above the single or first reinforcement layer to the right side of the trapdoor centerline at distances of 0, 130, and 230 mm, respectively. The pressure cells located above the trapdoor were used to measure the changes of the vertical earth pressures associated with the vertical movement of the trapdoor and during loading, while the other cells were installed to measure the increase of the vertical earth pressures above the stationary supports. The pressure cell placed at the centerline of the trapdoor is noted as TC, and the other two cells near the edges of the trapdoor are noted as TE-R and TE-L (R stands for the right, and L stands for the left). Also, the two pressure cells near the edges of the stationary supports are noted as SE-R and SE-L. Since these pressure cells were placed in a symmetrical layout, the average pressure from the pressure cells (TE-R and TE-L) and that from (SE-R and SE-L) will be presented in the test result section. Each pressure cell had an outside diameter of 50 mm, a sensing-surface diameter of 46 mm, a thickness of 11.3 mm, and a maximum capacity of 200 kPa.

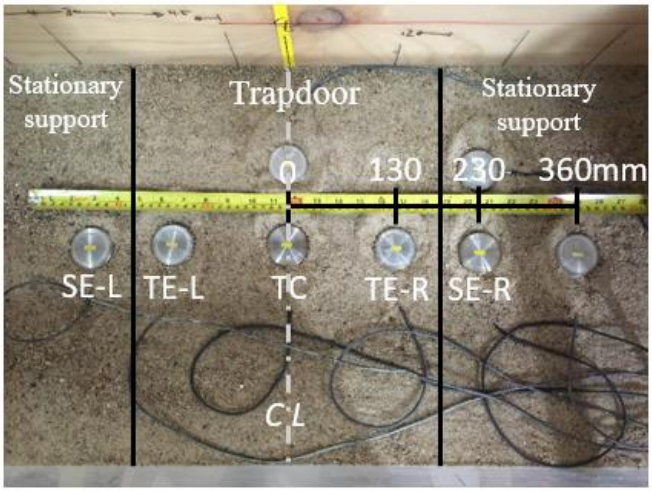

(a)

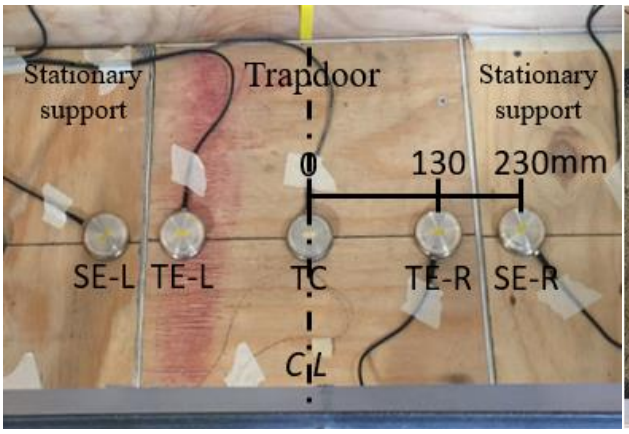

(b)

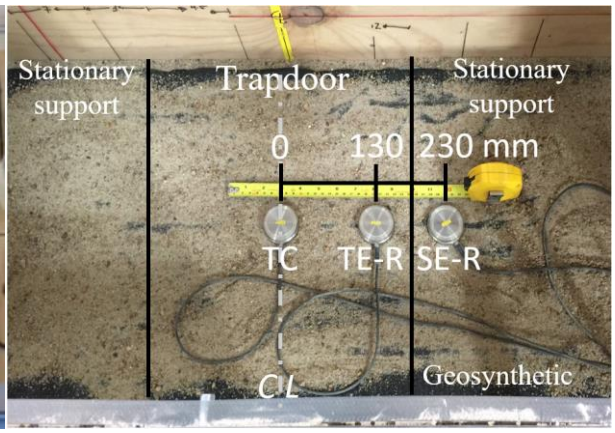

(c)

Figure 3.10 Layout of earth pressure cells: (a) above the test base in unreinforced fill tests; (b) below; and (c) above the first reinforcement layer in the reinforced fill tests.

To measure the geosynthetic strains in the reinforced fill tests, 5-mm long foil-strain gauges were attached to the biaxial geogrid at different locations using a plastic hardening bonding agent. On the biaxial geogrid, fourteen strain gauges were attached to the geogrid along the middle rib as shown in Figure 3.11. Among these strain gauges, eight gauges were attached to the upper and lower surfaces of the geogrid (shown with red color in Figure 3.11) while the other six were attached to the upper surface of the geogrid only (shown with white color in Figure 3.11). The strain gauges placed on both surfaces of the geogrid were at the expected location of high tensile forces and were to study the bending effect of the geogrid. Figure 3.12 depicts one of the strain

gauges which were supplied by Tokyo Sokki Kenkyujo Co., Ltd. and the bonding agent used for the strain gauges installation.

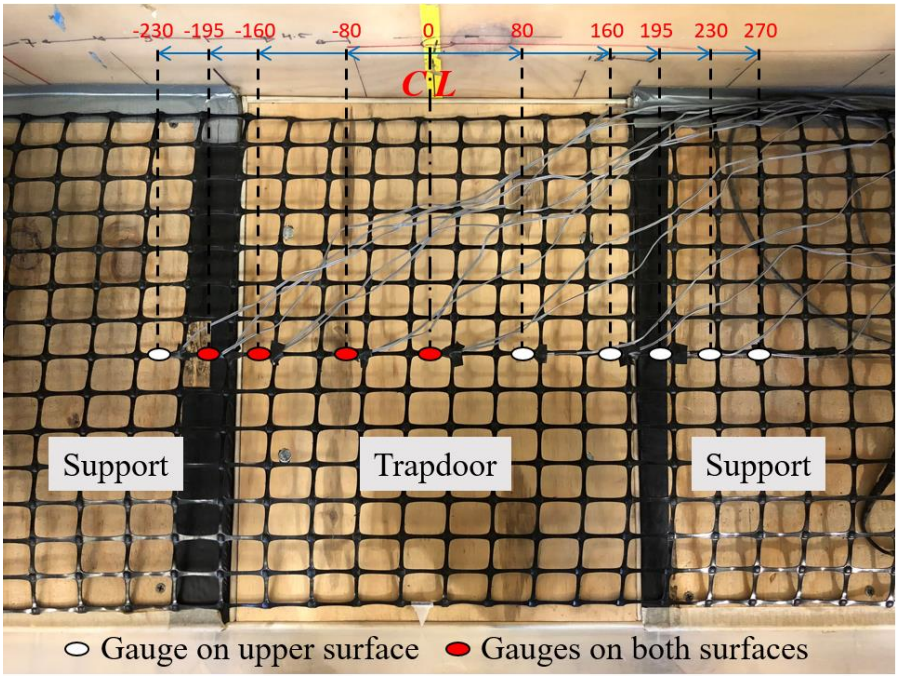

Figure 3.11 Strain gauge locations on the biaxial geogrid.

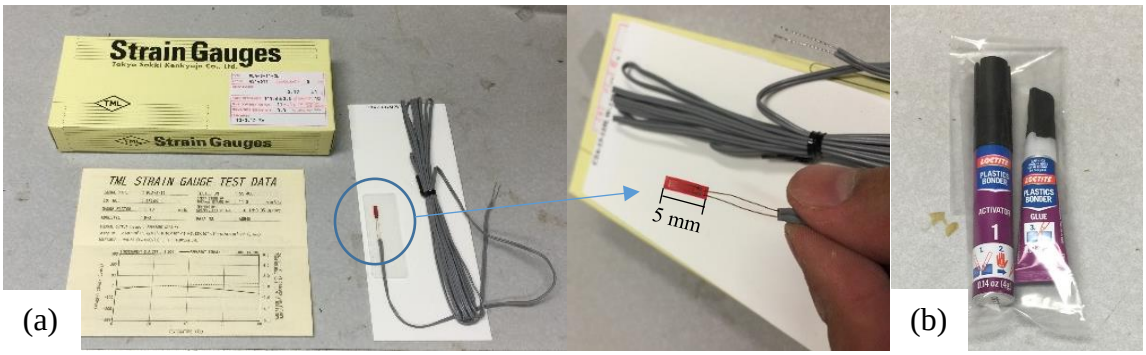

Figure 3.12 Materials for strain gauge installation: (a) strain gauge and (b) plastic bonding agent.

Trapdoor movement and footing settlement were monitored using four displacement transducers (type TML CDP-50, manufactured by the Tokyo Sokki Kenkyujo Co., Ltd.) with a measuring capacity of 50 mm. Three displacement transducers were placed under the trapdoor,

with one of them in the middle and the other two along with the diagonal line and at 100 mm away from the corner of the trapdoor. Another displacement transducer was mounted above the footing to monitor the footing settlement during loading. The displacement transducers and the pressure cells were connected to a data acquisition system, which consisted of four Smart Dynamic Strain Recorders (type DC-204R, manufactured by Tokyo Sokki Kenkyujo Co., Ltd.) to record the pressures and the displacements automatically with a scan frequency of 100 Hz. Another data acquisition system consisted of one CR-1000 Campbell Scientific data logger and two units of multiplexer, as depicted in Figure 3.13, were used to measure the strain in the geogrid.

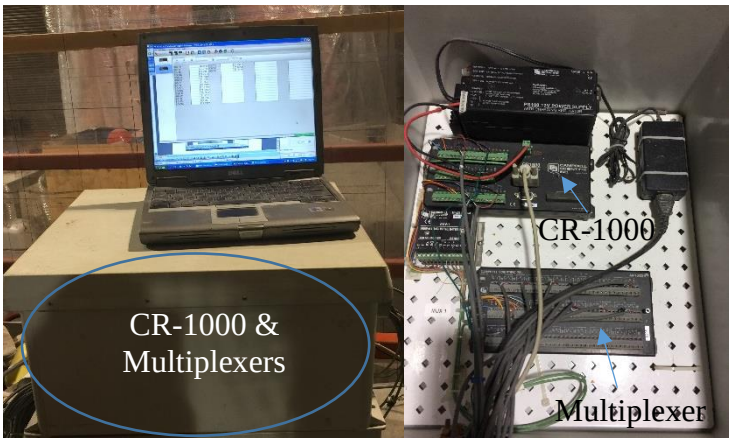

Figure 3.13 Data acquisition system consisting of one CR-1000 Campbell Scientific data logger and two units of multiplexer.

To monitor the fill movement during the test, a photogrammetric method was used to trace the black colored sand lines, which were placed between the sand lifts during the embankment construction. For the photogrammetric method, a camera was used and fixed in position during the test to record the fill movement. Figure 3.14 shows the setup for tracing the fill movement during the test.

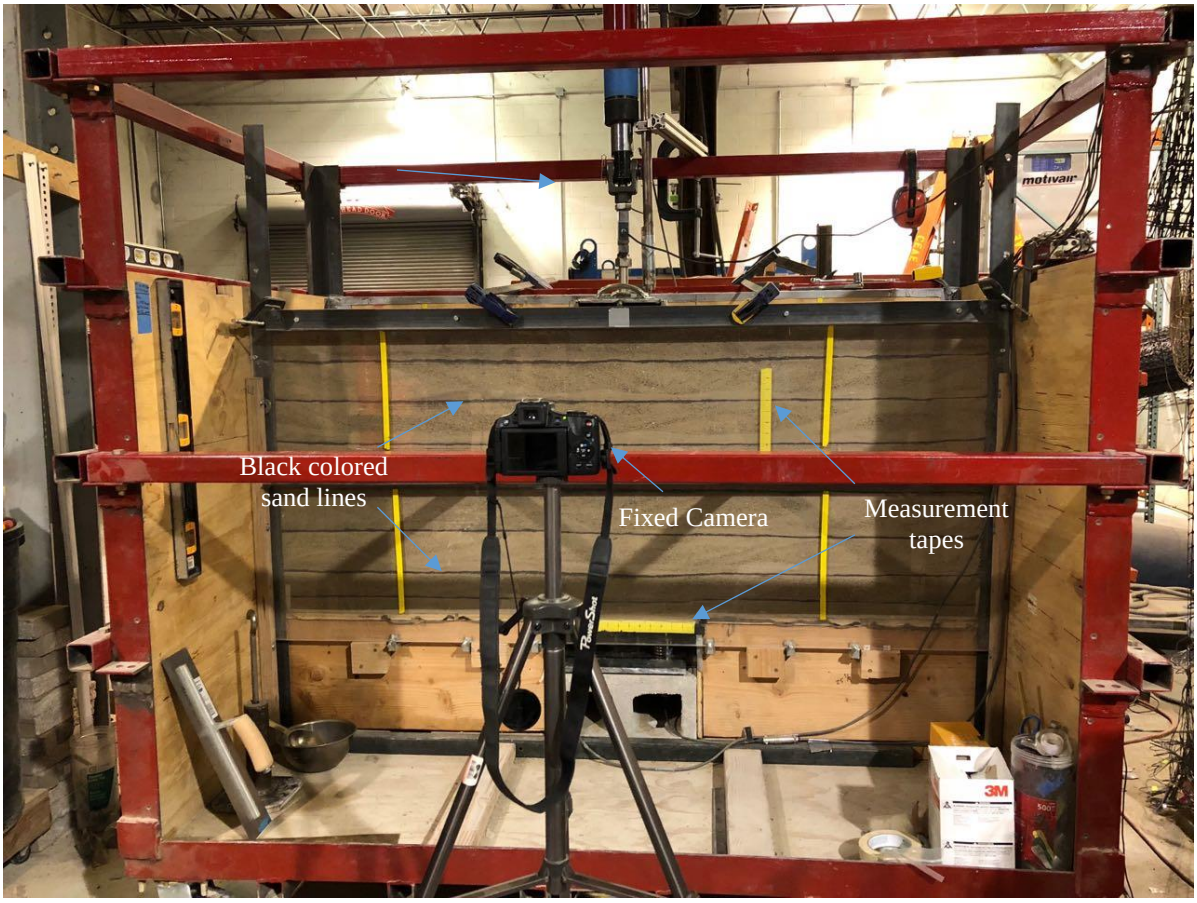

Figure 3.14 Setup for the photogrammetric method.

3.2.6 Test Procedure

In the model tests performed in this study, the spring-based trapdoor was placed in the center of the test box between two stationary supports to simulate a yielding subsoil. Fill placement continued in lifts over the trapdoor and the supports up to the desired height as shown in Figure 3.7. The construction was performed in seven lifts of approximately 100 mm thick per lift using a mass-volume control method. The sand was poured and then compacted using a manually-held steel compactor. The compacted soil had a relative density of 75%. In reinforced embankment tests, the single or first geosynthetic layer was installed over a 40-mm thick sand bedding layer within the embankment. Pressure cells were placed below and above this reinforcement layer as

described previously. A sand layer of 100 mm thick was placed between the first and second geosynthetic layers in the double reinforcement tests. All reinforcement layers were free at their ends and not fixed to the test box. Since the trapdoor was supported by compression springs, the trapdoor underwent vertical downward displacements during the fill placement. The total trapdoor displacement at the end of the fill placement stage varied with the trapdoor stiffness (i.e., numbers of the springs). Since the trapdoor underwent vertical displacements, soil arching mobilized during the fill placement. Following the fill placement, the fill surface was subjected to either static or cyclic footing loading, during which the trapdoor underwent further displacements. The load was applied in increments with each incremental pressure of approximately 7 kPa to study the re-distribution of additional stresses induced by the footing load and the mobilization and the degradation of soil arching. The loading test was terminated when the pressure on the center of the trapdoor exceeded the pressure on the stationary supports.

3.3 LOADING TYPE

Throughout the experimental tests with the buried box culvert and the spring-based trapdoor, both monotonic static and incremental cyclic loads were adopted to investigate the effect of localized surface loading on soil arching. The load was applied using a rigid footing which was centered along the test box centerline, as described earlier in the test setup Sections 3.1.1 and 3.2.2. During the application of static footing loading, the load was applied in increments with each incremental pressure of approximately 7 kPa and was held for approximately three minutes. Figure 3.15 shows a typical example of the monotonic loading sequence that was used for the tests under static loading.

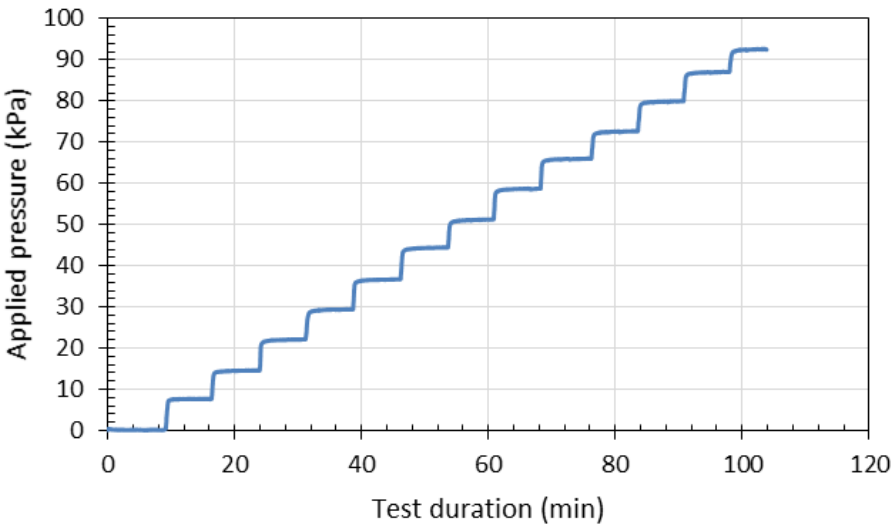

Figure 3.15 Example of the monotonic static loading.

During the application of cyclic footing loading, the soil arching phenomenon was investigated under incremental cyclic loading at a frequency of 0.1 Hz for 100 cycles per each loading increment of 9 kPa. Figure 3.16 shows a typical example of the incremental load applied during cyclic loading.

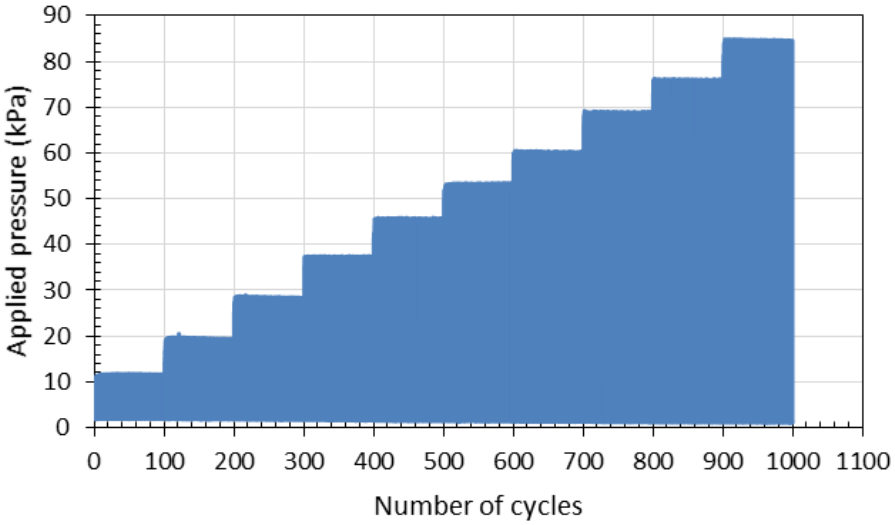

(a)

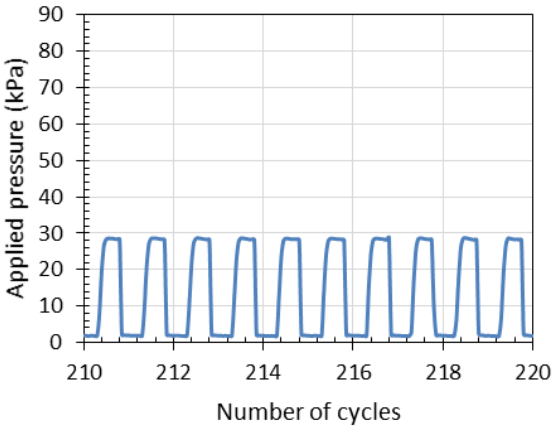

(b)

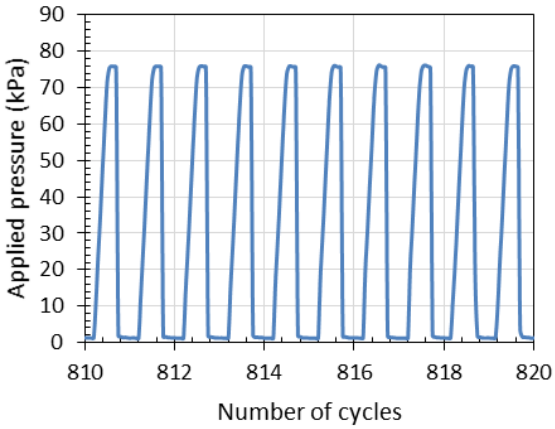

(c)

Figure 3.16 Example of incremental cyclic loading: (a) during the whole loading period; (b) from cycles No. 210 to 220; and (c) from cycles No. 810 to 820.

CHAPTER 4 TEST RESULTS AND ANALYSIS OF SOIL ARCHING WITH GEOFOAM ON CULVERT

This chapter aims to investigate the stress re-distribution over a buried structure (i.e., specifically box culvert) installed by both the positive projecting embankment (PPE) method and the induced trench installation (ITI) method under static and cyclic footing loads, examines the effects of Expanded Polystyrene (EPS) geofoam including its stiffness and thickness on the distribution of vertical stresses above a rectangular concrete using a series of physical model tests, and presents a comparison of the available analytical solutions with the test results.

4.1 EMBANKMENT CONSTRUCTION

Vertical earth pressures and geofoam compression were measured during the embankment construction. In the PPE test (T1), the measured vertical pressure on the culvert was higher than the overburden pressure (γH) during the embankment construction, and the increase in the measured pressure was approximately 13% due to negative soil arching at the end of the construction as shown in Figure 4.1(a). In the ITI tests (T2 to T9), although the geofoam underwent small compression (less than 0.10 mm on average, i.e., not enough deformation to mobilize positive soil arching) during the embankment construction, the measured vertical pressure was almost the same as the overburden pressure, for example, as shown in Figure 4.1(b) for test T2. Therefore, the EPS geofoam prevented the mobilization of negative soil arching induced by the embankment weight.

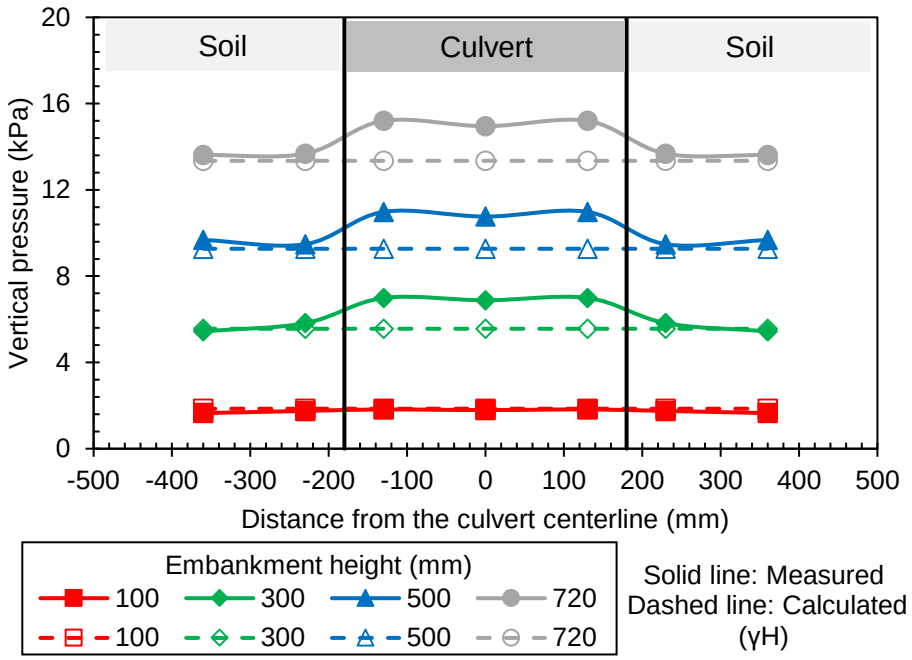

(a)

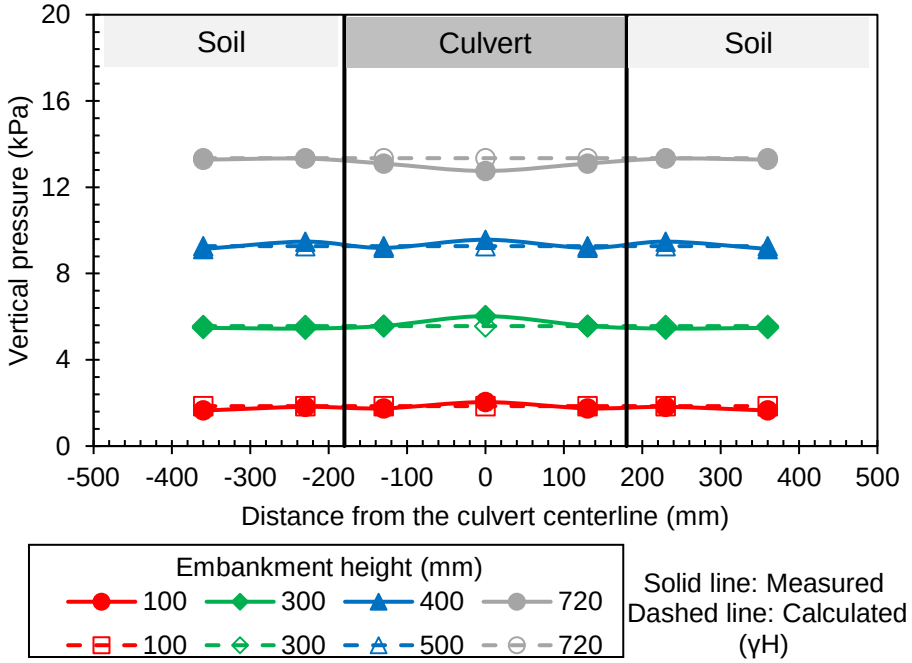

(b)

Figure 4.1 Measured and calculated vertical pressures on and around the culvert during the embankment construction in: (a) PPE test (T1); and (b) ITI test (T2).

4.2 PRESSURE DISTRIBUTION UNDER STATIC FOOTING LOAD

This section presents and discusses the earth pressure results from the PPE test (T1) and two ITI tests (T2 and T5) to illustrate the pressure distribution above the culvert with and without a compressible layer under static footing loading.

Figure 4.2 shows the measured vertical pressure distribution both on and besides the culvert in the PPE (T1). The measured maximum pressure was located under the centerline of the footing, which was also the centerline of the culvert in this study. Boussinesq's solution for a strip footing was used to calculate the pressure at the same depth of the culvert for comparison. The calculated pressure plotted in Figure 4.2 represents the sum of the overburden pressure (γH) and the additional vertical pressure induced by the footing load calculated using Boussinesq's solution. The calculated pressure simulates the case where no rigid inclusion exists. The difference between the calculated and measured pressure could be used to evaluate the effects of rigid inclusion and soil arching. The measured vertical pressure in the PPE test was significantly higher than the calculated pressure over the culvert, while the measured pressure was slightly lower than the calculated one over the surrounding soil. Therefore, majority of the additional stresses were concentrated over the culvert because of negative soil arching and stress concentration due to the relative stiffness of the culvert to the surrounding soil. As the footing load increased, the difference between the measured and the calculated pressures above the culvert became larger. This can be attributed to the fact that more negative soil arching was mobilized as the relative displacement between the soil column above the culvert and the surrounding soil increased. The relative displacement was generated due to more compression of soil around the culvert under the increased load of the footing.

Figure 4.3 shows the percentage of pressure increase above the culvert in the PPE test under static footing loading. This percentage was calculated as the difference between the average

measured pressure above the culvert and the average calculated one using Boussinesq's solution, divided by the average calculated pressure. The percentage of pressure increase grew from 13% at the end of the embankment construction to 37% at an applied footing pressure of 130 kPa as the negative soil arching was mobilized. This percentage is 12% higher than that reported by Meguid et al. (2017) (i.e., 25%) in their study for a hollow steel culvert constructed with the PPE under a uniform surcharge of 130 kPa. It should be noted that a similar embankment height to culvert width ratio was used in Meguid et al. (2017), but the modulus of elasticity of the hollow steel culvert reported in their study was 200 GPa. The hollow steel culvert was stiffer than the concrete culvert utilized in this study. Therefore, one may conclude that negative soil arching is more critical under footing loading located directly above the culvert than that induced by a uniformly distributed pressure or overburden pressure.

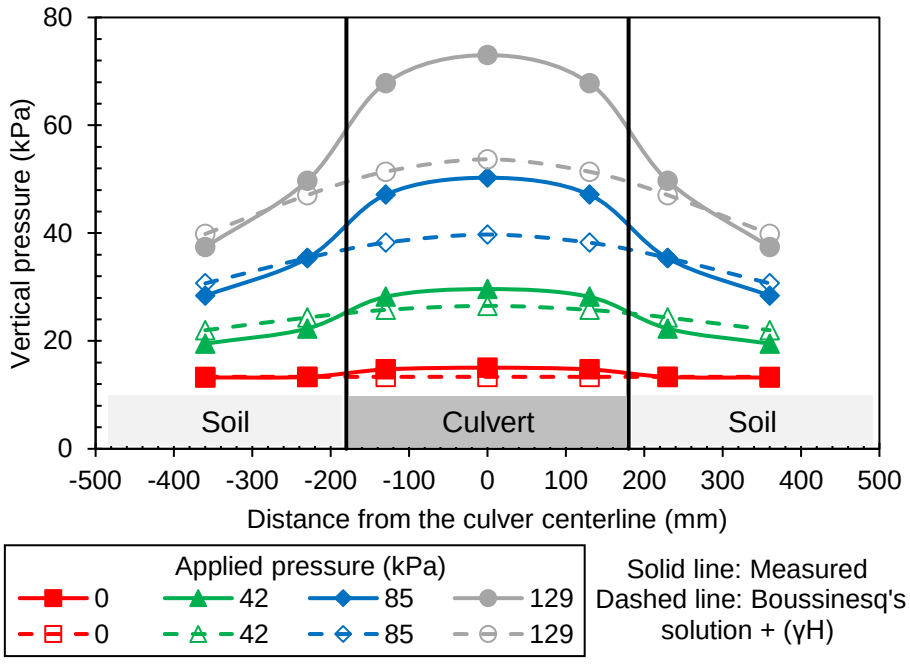

Figure 4.2 Cross-sectional pressure distribution under static footing loading in the PPE test (T1).

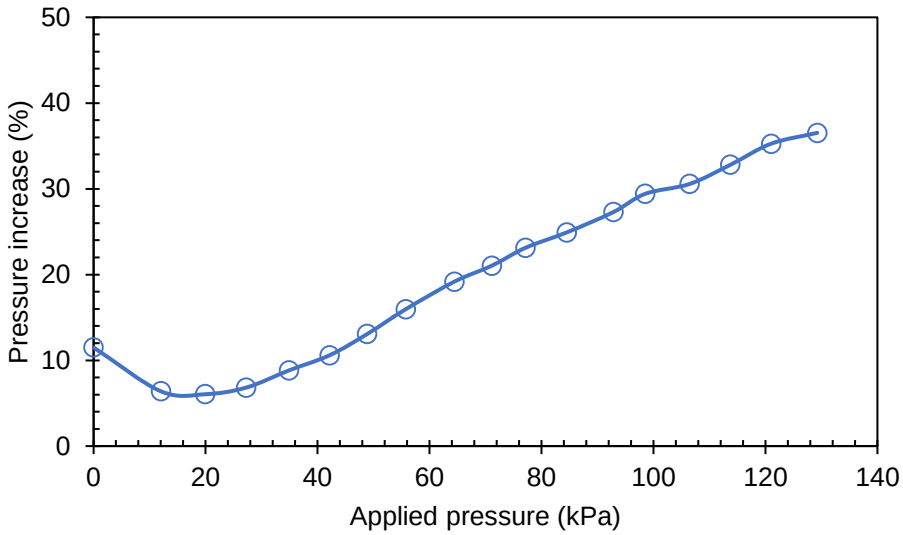

Figure 4.3 Percentage of increase between the measured and calculated pressures above the culvert under static footing loading in the PPE test (T1).

To investigate the soil arching mobilization under static footing loading associated with the ITI method, the pressure distribution at the level of the top of the geofoam is presented in Figure 4.4 since the maximum differential settlement was expected to happen at this level. Figure 4.4 presents the results of T2 and T5, in which geofoam EPS12 and EPS15 were utilized, respectively. Both geofoams had a thickness of $0.2B_c$. When no footing load was applied, the distribution of the measured vertical pressures was uniform on and besides the geofoam. As the applied pressure increased, a non-uniform distribution was observed across the embankment, where the pressures on the geofoam decreased and those on the surrounding soil increased as depicted in Figure 4.4. Moreover, the magnitude of the transferred pressure from the geofoam to the surrounding soil increased as more footing load was applied. This pressure re-distribution is associated with the mobilization of positive soil arching due to the relative displacement between the soil column above the geofoam and the surrounding soil. Figure 4.4 also compares the results of T2 and T5 with those of the reference test T1 (no geofoam was used). The percent of reduction

in the pressure on the geofoam in T2 and T5 as compared with that of T1 was 23% and 13%, respectively, at an applied pressure 130 kPa. On the surrounding soil (i.e., at 230 mm from the culvert centerline), however, the measured pressures in T2 and T5 increased 33% and 17%, respectively, as compared with that of T1 at the same applied pressure. This result confirms the mobilization of soil arching above the geofoam. A similar distribution was observed in all tests performed with the inclusion of an EPS geofoam (T2 to T7). However, the degree of the transferred pressure from the top of the culvert to the surrounding soil was different and affected mainly by the geofoam to soil stiffness ratio as discussed in the next sections.

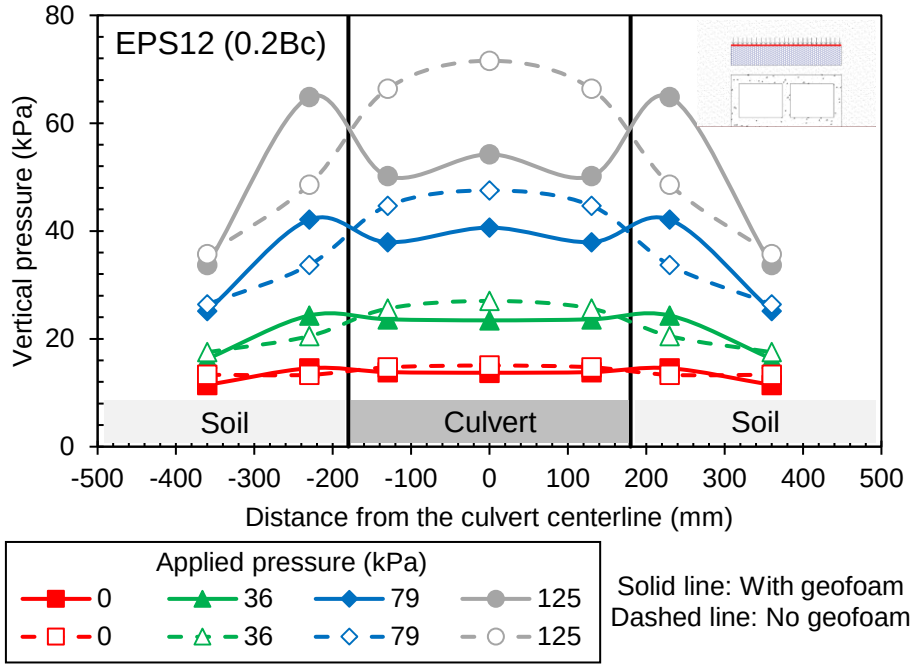

(a)

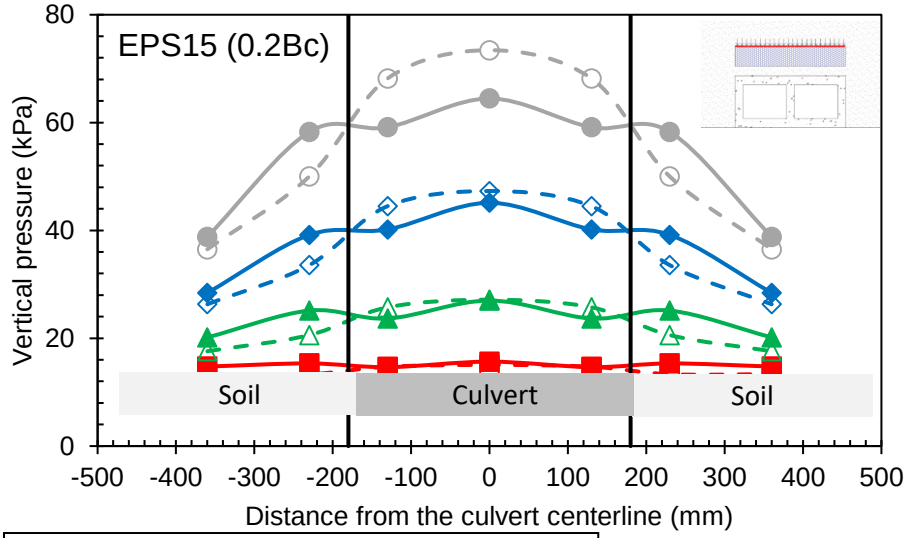

(b)

Figure 4.4 Cross-sectional pressure distribution under static footing loading at the top of geofoam: (a) EPS12; and (b) EPS15.

4.3 EFFECTS OF GEOFOAM STIFFNESS

Figure 4.5 shows the average measured vertical pressures on the top of the culvert in the ITI tests T2 to T5 under static footing loading, in which the culvert was overlaid by two types of geofoam, namely EPS12 and EPS15, with different densities as provided in Table 3.2. The results of the reference test with no geofoam are also provided for the comparison purposes in Figure 4.5. The measured vertical pressures generally increased with the increase of the applied footing load for all tests. However, the vertical pressures measured in the ITI tests were significantly lower than those measured in the PPE test. The effect of geofoam stiffness at the same thickness on the vertical pressure above the culvert can be clearly recognized in Figure 4.5. When pressures of lower than 40 and 60 kPa were applied on the backfill with the geofoams of $0.2B_c$ and $0.4B_c$ thick, respectively, these two test sections behaved similarly despite the geofoam densities were different. However, as the applied pressure increased, the average measured vertical pressure under the geofoam with lower stiffness, EPS12, was lower than that under the geofoam with the higher stiffness, EPS15. This result indicates that the geofoam with lower stiffness deformed more, resulting in a larger relative displacement between the soil column above the culvert and the surrounding soil. The larger relative displacement mobilized more soil arching and transferred lower pressure onto the culvert. At an applied pressure of approximately 130 kPa, the average measured vertical pressure above the culvert in the PPE test was 72 kPa. However, the use of EPS12 or EPS15 of 0.2*Bc* thick above the culvert reduced the measured pressure to 38 kPa (equivalent to 47% reduction) or 49 kPa (equivalent to 32% reduction) on the culvert, respectively. When EPS12 or EPS15 of 0.4*Bc* thick was used, the measured vertical pressure on the culvert decreased to 41 kPa (equivalent to 43% reduction) or 50 kPa (equivalent to 31% reduction), respectively, at the same applied pressure.

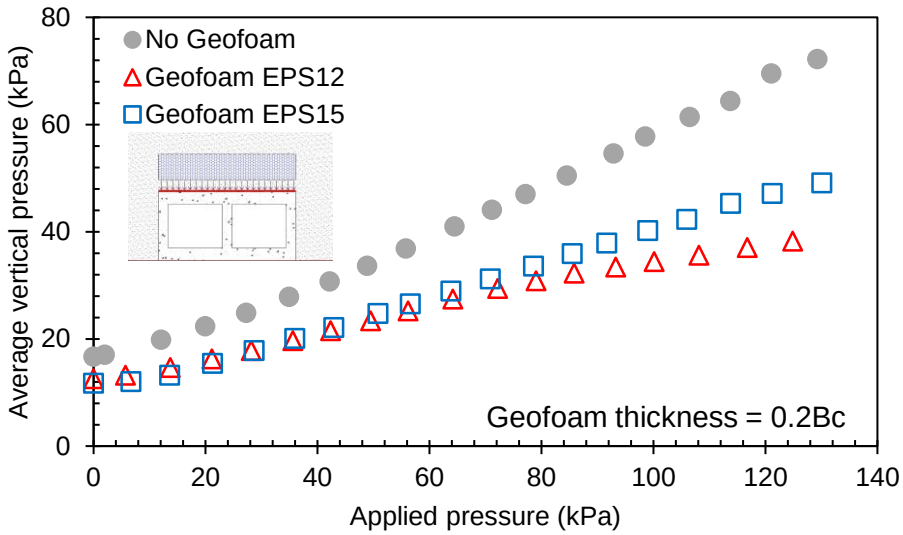

(a)

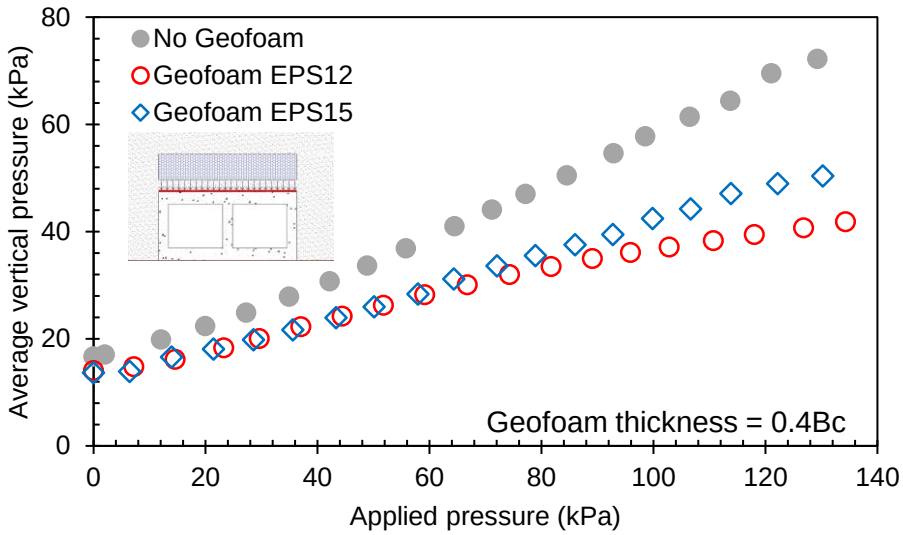

(b)

Figure 4.5 Average measured pressure on the culvert under static footing loading constructed with geofoam thickness of: (a) 0.2*Bc* and (b) 0.4*Bc*.

4.4 EFFECTS OF GEOFOAM THICKNESS

Figure 4.6 shows the normalized vertical pressures on the culvert in the ITI tests with respect to those measured in the PPE test. The results of the ITI tests show that pressure reduction happened under the increased static footing load for both EPS12 and EPS15. Figure 4.6 also shows the effects of the EPS geofoam thickness for both EPS12 and EPS15 on the vertical pressure. The measured vertical pressure on the culvert decreased more when a thin geofoam was used than when a thick geofoam was used. As the geofoam thickness was increased from $0.2B_c$ to $0.4B_c$, the percent of pressure reduction by EPS 12 decreased from 47% to 43% and by EPS15 decreased from 32% to 31% at an applied footing pressure of 130 kPa. Figure 4.6 indicates that the difference in the percent of the pressure reduction decreased as the applied pressure increased. This result is different from those reported by other researchers (Kim and Yoo, 2005; McGuigan and Valsangkar, 2010; Meguid et al., 2017), who found that thick geofoam was more effective in reducing the pressure on the culvert under a uniform distributed pressure.

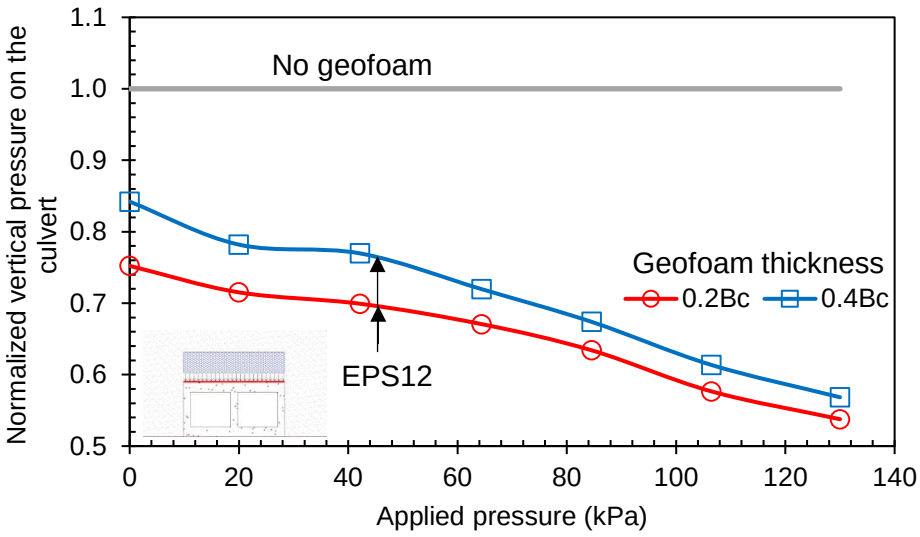

(a)

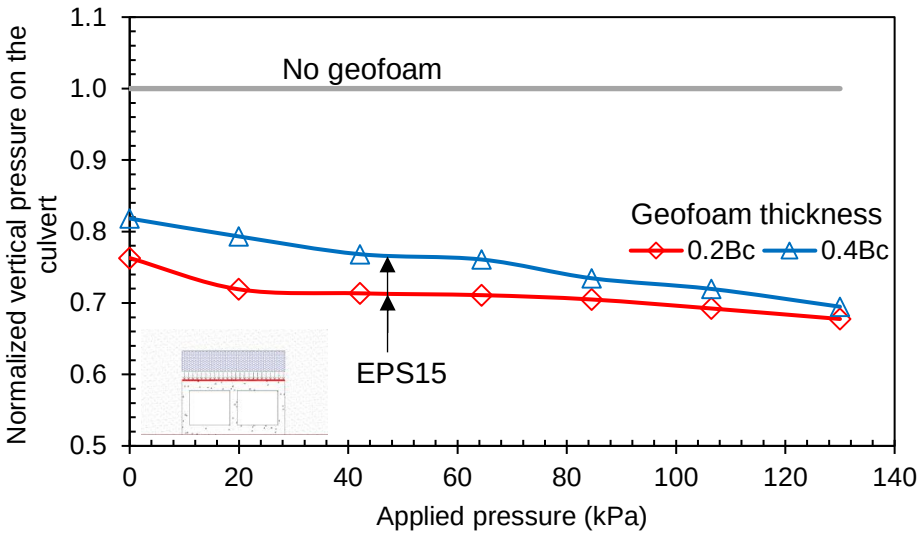

(b)

Figure 4.6 Comparison of measured pressures on the culvert in the ITI tests with the PPE test under static footing loading with geofoam: (a) EPS12; and (b) EPS15.

A possible explanation is illustrated in Figure 4.7, which reflects the results of the tests T2 to T7 using the geofoams with different densities (i.e., EPS12 and EPS15) under footing loading. By assuming the slip surface of the mobilized zone under the footing to be vertical for simplification, the thickness of the fill (H_s) above the thin geofoam layer (t = 0.2B_c) was larger

than that (H_s') above the thick geofoam (2t). In other words, the footing was further away from the top of the geofoam. Since the interface resistance between the geofoam and the fill is lower than the internal soil resistance, the resistance provided by the frictional forces along the interfaces (**ab** and **dc**) in the test with the thin geofoam was higher than those in the test with the thick geofoam (at **a'b'** and **d'c'**). Therefore, more load was transferred to the adjacent soil, and less load was applied on the top of the geofoam when the thin geofoam was used, as compared with the thick geofoam. This situation is different from that studied by most other researchers, in which self-weight and/or a uniform surcharge were applied and more soil arching developed above the thick geofoam.

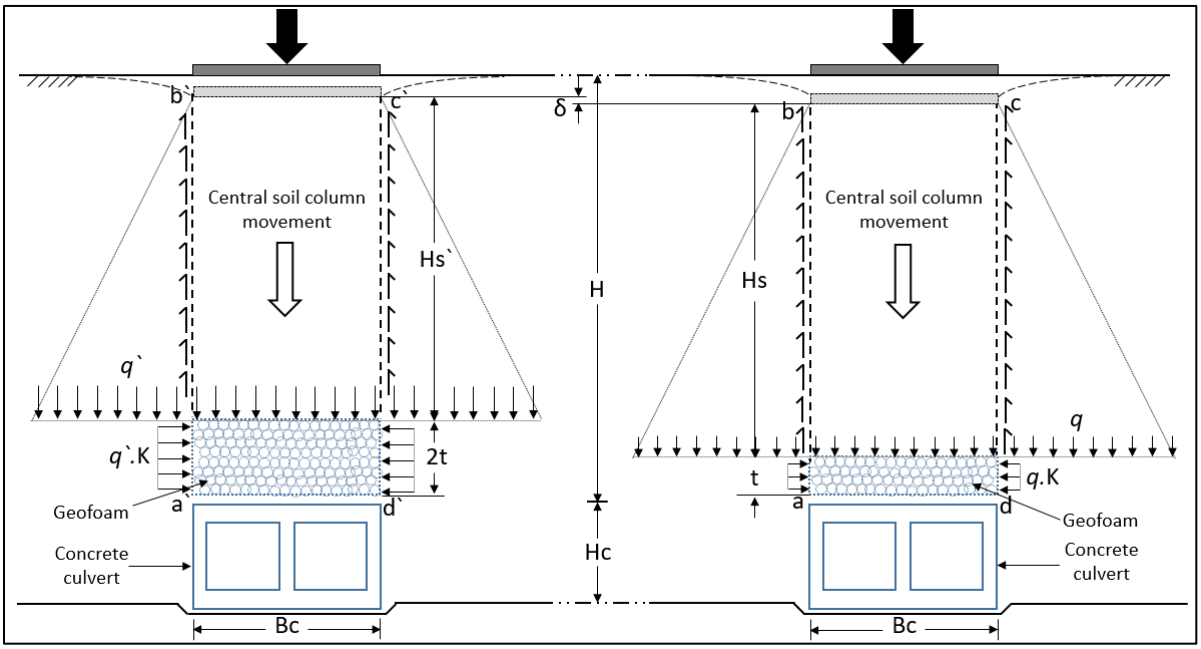

Figure 4.7 Effect of geofoam thickness on the measured pressure above the culvert under static footing loading.

Figure 4.8 shows the geofoam compression and the footing settlement under static footing loading in the tests performed with EPS12. Similar results were found for the tests with EPS15,

which are not shown here to save pages. The thin geofoam underwent less compression than the thick geofoam as shown in Figure 4.8(a), and the footing settlement in the test with the thin geofoam was larger than that with the thick geofoam at the same applied pressure, as shown in Figure 4.8(b). Therefore, the soil column above the thick geofoam underwent smaller compression than that above the thin geofoam. In other words, the region consisting of the soil and the thick geofoam over the culvert behaved as a stiffer composite than the region consisting of the soil and the thin geofoam. As a result, the shear stresses in the soil under the influence of the footing in the test with the thick geofoam was lower than that with the thin geofoam, and less soil arching was mobilized in the test with the thick geofoam.

To further investigate the effect of the geofoam thickness on its stiffness, a simple test was performed in an unconfined condition (i.e., in air) utilizing a triaxial test frame as shown in Figure 4.9. The test specimen size was determined based on the recommendation of ASTM-D1621 (2016). Two geofoam specimens of different thicknesses at the same density (EPS12 or EPS15) were tested, one with a thickness t = 50 mm and the other with a thickness 2t. All specimens had a cross-sectional dimension of 100 mm long and 100 mm wide. Figure 4.10 presents the results of the specimens tested in air as compared with those in the ITI tests T2-T3 and T5-T6, in which the geofoam was confined in soil. These results show that the thick geofoam had higher stiffness than the thin geofoam of the same density under both conditions (confined and unconfined). The unconfined tests confirm that the stiffness of the geofoam was affected by its thickness. At the same time, the effect of the geofoam thickness on its stiffness was magnified under the confined condition. Based on the test results, the moduli of the confined geofoams were approximately two to four times those of unconfined geofoams. Therefore, the vertical pressure difference on the top of the culvert when a thin or thick geofoam was used is attributed to their modulus difference.

However, when the geofoam thickness is equal to zero, it becomes a PPE case so that the vertical pressure on the top of the culvert should be higher. Therefore, there may be an optimum geofoam thickness, which will be further investigated in the future.

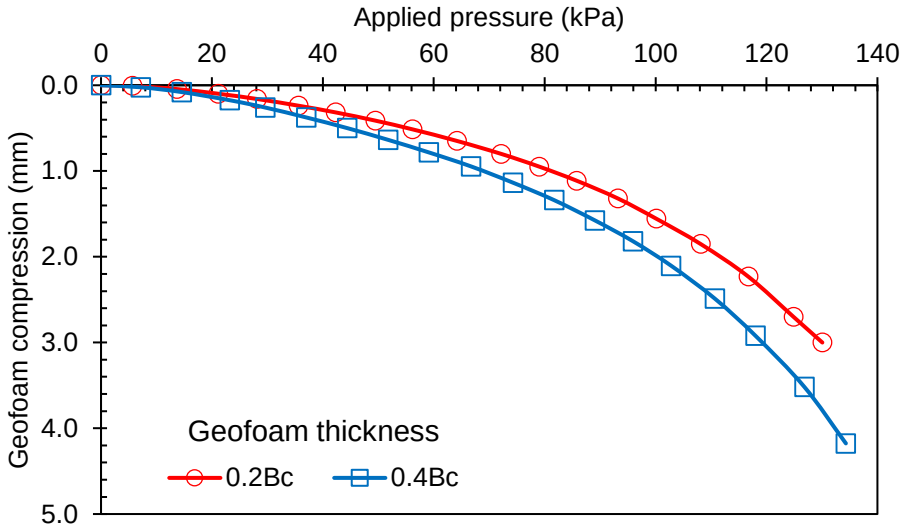

(a)

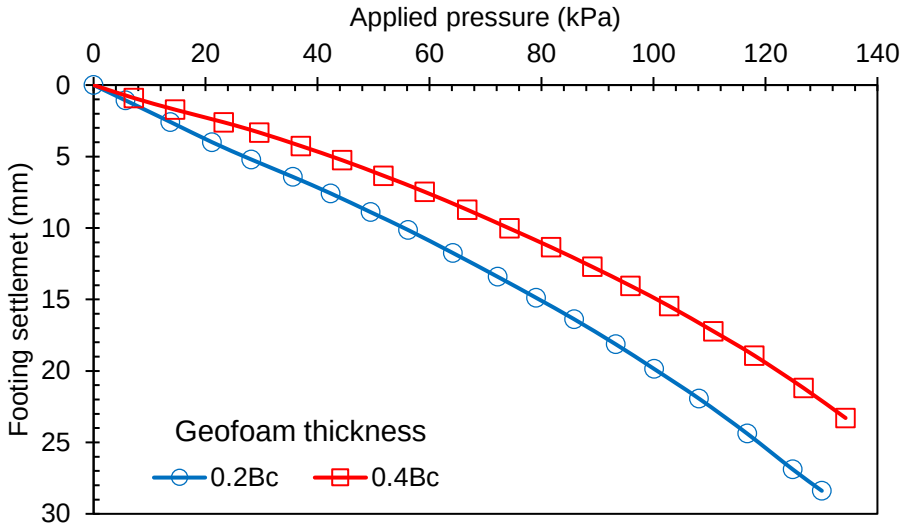

(b)

Figure 4.8 Effects of the thickness of geofoam EPS12 on (a) the geofoam compression and (b) the footing settlement under static footing loading.

(a) (b)

Figure 4.9 Test setup for the isolated EPS geofoam with a thickness of (a) t = 50 mm; and (b) 2t = 100 mm.

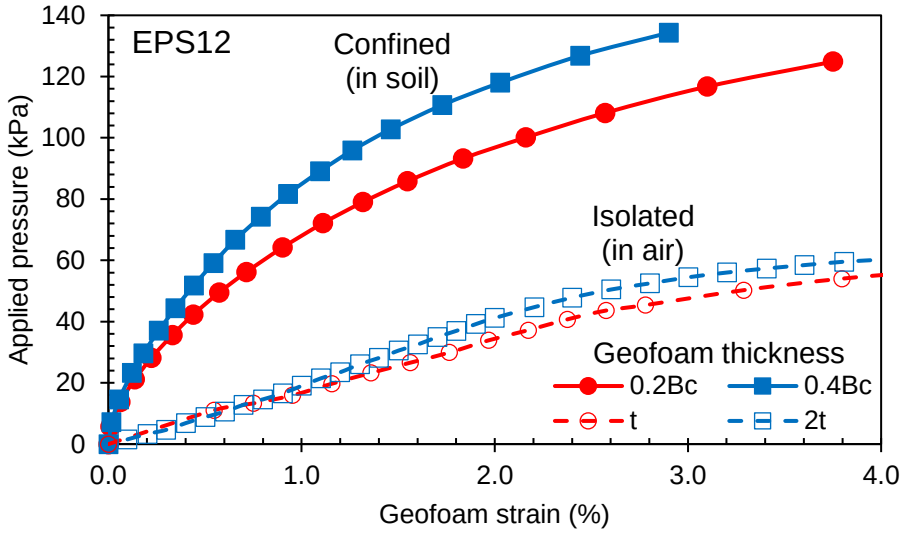

(a)

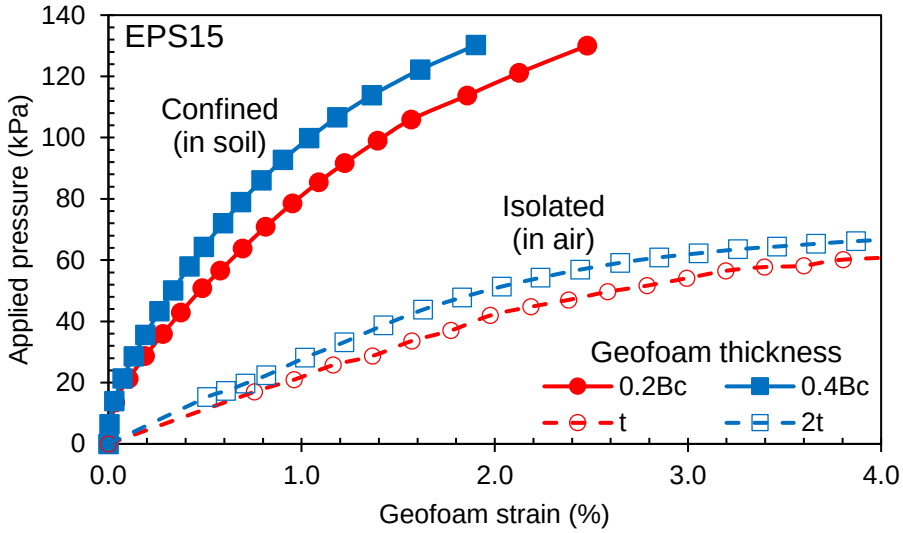

(b)

Figure 4.10 Effect of the geofoam thickness on the geofoam stiffness in confined and unconfined (i.e., isolated) conditions with: (a) EPS12; and (b) EPS15.

4.5 DEGREE OF SOIL ARCHING

McNulty (1965) proposed a soil arching ratio (ρ) to assess the degree of the load transferred from a yielding soil zone to the surrounding soil zone. This ratio, given in Equation (4.1), is calculated as the average vertical pressure above the yielding base (σ_v) (i.e., the geofoam in this study) to the overburden pressure (γH) plus the uniform surcharge (q) if applied.

$$\rho = \frac{\sigma_v}{\gamma H + q} \tag{4.1}$$

At the end of the ITI tests (T2 and T5), the measured pressures on the culvert were relatively uniform; therefore, the soil arching ratio was calculated based on the average pressure measured on the culvert. At the same time, the applied pressure, q, in Equation (1) was calculated using the Boussinesq solution for the location above the culvert. Figure 4.11 presents the soil arching ratio versus the applied footing pressure for both ITI tests (T2 and T5). In both tests, the soil arching ratio dropped from 1.0 to 0.84 as the footing pressure increased to 30 kPa. This drop in the arching ratio indicates the mobilization of soil arching. However, EPS geofoam stiffness affected the degree of soil arching mobilization as the footing pressure increased beyond 30 kPa. In T2, in which geofoam EPS12 was used, soil arching continued to mobilize, and the arching ratio dropped to 0.75 as the footing pressure increased to 130 kPa. In T5 with the use of geofoam EPS15, however, soil arching degraded (or stress recovered) and the arching ratio increased to 0.95 as the footing pressure increased to 130 kPa. To evaluate the mobilization of soil arching, the solution for the soil arching ratio developed by Terzaghi (1943) is presented below:

$$\rho = \frac{B_c}{2HK\,tan\emptyset}\left(1 - e^{-2K\,tan\emptyset\frac{H}{B_c}}\right) + \frac{q}{\gamma H + q}\left(e^{-2K\,tan\emptyset\frac{H}{B_c}}\right) \tag{4.2}$$

where B_c = the width of the culvert; H = the height of the embankment; K = the lateral earth-pressure coefficient (use K =1 as suggested by Terzaghi (1943) and recommended by Han et al. (2017) for the ultimate soil arching condition), ϕ = the friction angle of soil, and q = the applied pressure (calculated using the Boussinesq's solution for the location above the geofoam).

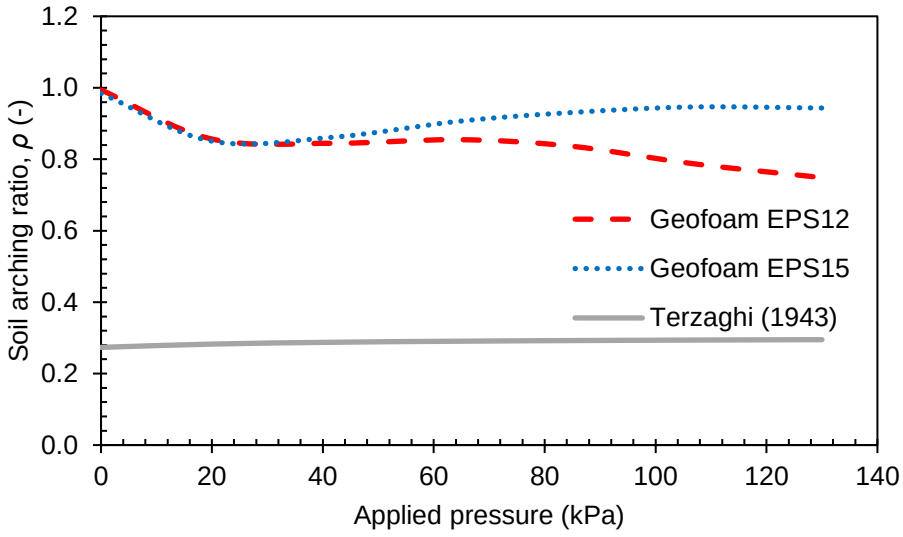

Figure 4.11 Soil arching ratio above the geofoam under static footing loading in ITI tests.

Figure 4.11 shows that the measured soil arching ratio is greater than that calculated by Terzaghi (1943), implying the partial mobilization of soil arching. It is worth mentioning that the geofoam densities used in this study represent the smallest densities available in the market with the lowest stiffness (highest compressibility). The relative stiffness values between soil and compressible material as defined by the ratio of soil elastic modulus to geofoam elastic modulus (E_s/E_g) were 16.7 and 10 for EPS12 and EPS15, respectively. This finding is consistent with the suggestion by Han (2015) mentioned earlier.

4.6 COMPARISON WITH ANALYTICAL SOLUTION

This section discusses the experimental results of the ITI tests (T2-T3 and T5-T6) as compared with the analytical solution. In this comparison, the vertical stresses above the culvert induced by soil arching and static footing loading were considered separately. The vertical stress induced by soil arching under soil self-weight was calculated based on Marston's theory while the vertical stress induced by footing loading was calculated using Boussinesq's solution or the 2:1 distribution mothed.

Marston's theory, initially published by Marston (1930), was developed for trench and embankment conditions. This method has been commonly used to determine loads on buried rigid structures to design these structures installed by the ITI method (McAffee and Valsangkar, 2008). This theory considers only the vertical pressure applied on the rigid structure induced by the embankment weight. The calculated pressure is basically the weight of the soil column immediately above the structure plus or minus the shear resistance due to the relative displacement between the central soil column and the adjacent soil. Figure 4.12 shows the schematic of the force equilibrium for a soil element above the culvert. The vertical force equilibrium of a soil element at depth *h* below the equal settlement plane is given by Eq. (4.3) (Marston, 1930).

$$\mathrm{d}W = -V + (V + \mathrm{d}V) + 2\mathrm{d}F = \mathrm{d}V + 2\mathrm{d}F \tag{4.3}$$

where dW = the self-weight of the soil element; V = the vertical forces on top of the soil element; V+dV = the vertical forces on the bottom of the soil element; and dF = the frictional force on the vertical slip plane of the soil column. The vertical stress acting on the top of the soil element q is assumed to be uniformly distributed, and it can be calculated by Eq. (4.4)

$$q = \frac{V}{B} = C_c \gamma B \tag{4.4}$$

where B = the culvert width; C_c = the load coefficient; and γ = the soil unit weight.

C_c can be calculated using Eq. (4.5) for the culvert under a complete condition (i.e., $H_e \geq H$) or Eq. (4.6) for the culvert under an incomplete condition (i.e., $H_e < H$) (McAffee and Valsangkar, 2008)

$$C_c = \frac{e^{-2K\mu(\frac{H}{B})} - 1}{-2K\mu} \qquad (H_e \geq H) \tag{4.5}$$

$$C_c = \frac{e^{-2K\mu(\frac{H_e}{B})} - 1}{-2K\mu} + \left(\frac{H}{B} - \frac{H_e}{B}\right) e^{-2K\mu(\frac{H_e}{B})} \qquad (H_e < H) \tag{4.6}$$

where H = the embankment height; H_e = the equal settlement plane height; K = the lateral earth pressure coefficient; and μ = the frictional coefficient (commonly calculated as μ = tan ϕ where ϕ = soil frictional angle).

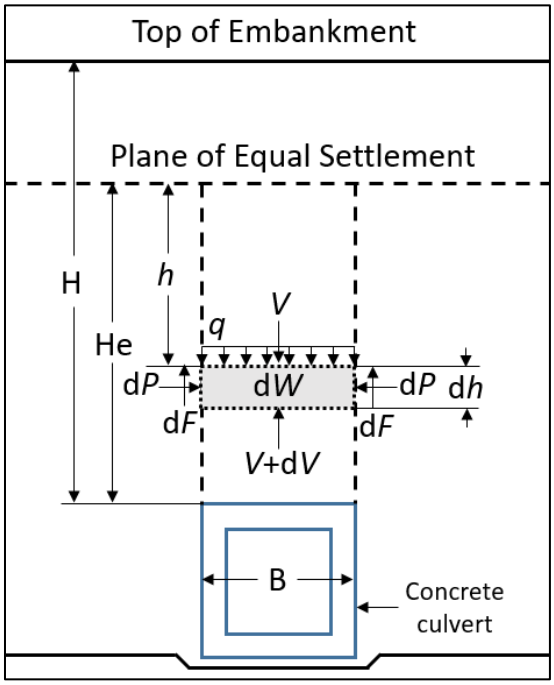

Figure 4.12 Forces on a soil element above a culvert based on Marston's theory.

The vertical pressure on the culvert due to the embankment weight was calculated using Eq. (4.4). In Eq. (4.4), the load coefficient C_c was considered for the case of a complete condition ($H_e \geq H$), which is shown in Eq. (4.5). In this study, soil arching was mobilized under the condition that the footing load was applied. Since the footing load induced a differential settlement at the embankment surface, the equal settlement plane exceeded the embankment hieght and a complete condition existed. The Rankine active earth pressure coefficient, K_a = (1- sin ϕ) / (1+ sin ϕ), was used here since the geofoam maximum compression observed in these tests was 1.10% of the geofoam width. This is consistent with Marston and Anderson's (1913) suggestion of using K_a when soil arching is triggered by a small deformation. Marston (1930) indicated that the effect of the frictional coefficient (μ) of the embankment material on the calculated pressure is relatively minor for the ITI method; therefore μ = tan ϕ was used therein. In addition to the vertical pressure induced by the embankment weight, the vertical pressure on the culvert caused by the footing load was calculated using either Boussinesq's solution or the 2:1 distribution mothed. Figure 4.13 shows the comparison of the measured pressures on the culvert in the ITI tests T2-T3 and T5-T6 with the calculated pressures. The measured vertical pressures are in good agreement with the calculated pressures.

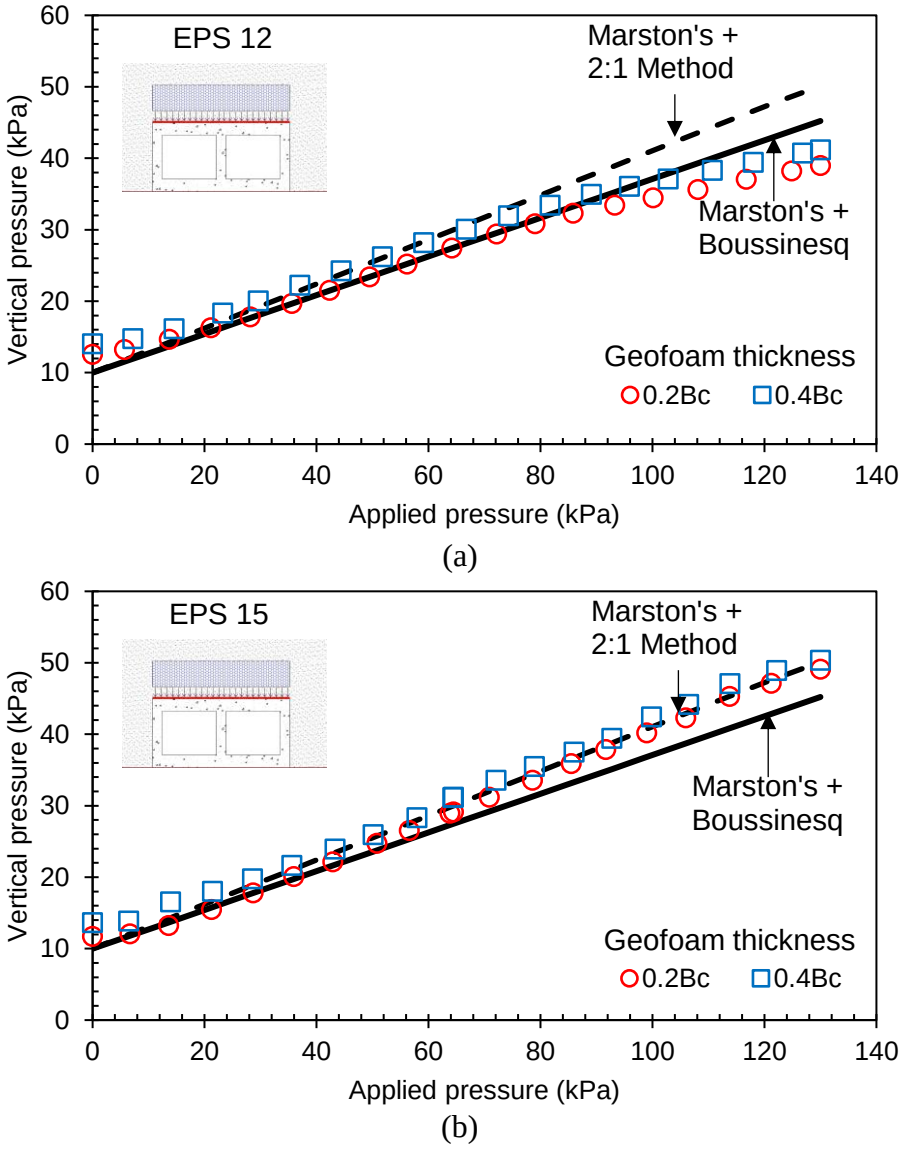

Figure 4.13 Measured versus calculated pressures above the culvert under static footing loading in the ITI tests with geofoam: (a) EPS12; and (b) EPS15.

4.7 EFFECTS OF LOADING TYPE

Buried structures used for transportation applications under low embankments are more susceptible to dynamic loading effects, such as traffic loading. This study simulated traffic loading with cyclic loading at a frequency of 0.1 Hz. A similar frequency was previously used by researchers to simulate traffic loading (Shenton, 1975; Key, 1999; Al-Naddaf, 2017). In this study,

Tests T8 and T9, with EPS12 and EPS15, respectively, of $0.2B_c$ thick were tested under cyclic loading for totally 1300 loading cycles, applied with each incremental pressure of approximately 9 kPa for 100 cycles. Figure 4.14 presents the maximum vertical pressures on the culvert measured in these tests at the end of the 100^{th} cycle of each increment of the applied pressure as compared with those under static loading. The results show that cyclic loading reduced the soil arching effect induced by the compressible geofoam. The soil arching effect (i.e., shear forces) generated within the mobilized zone was degraded by dynamic loading, which is similar to what was found by Al-Naddaf (2017). Thus higher vertical pressure on the culvert was measured under cyclic loading than that under static loading. However, geofoam density showed no effect on the measured vertical pressure on the culvert.

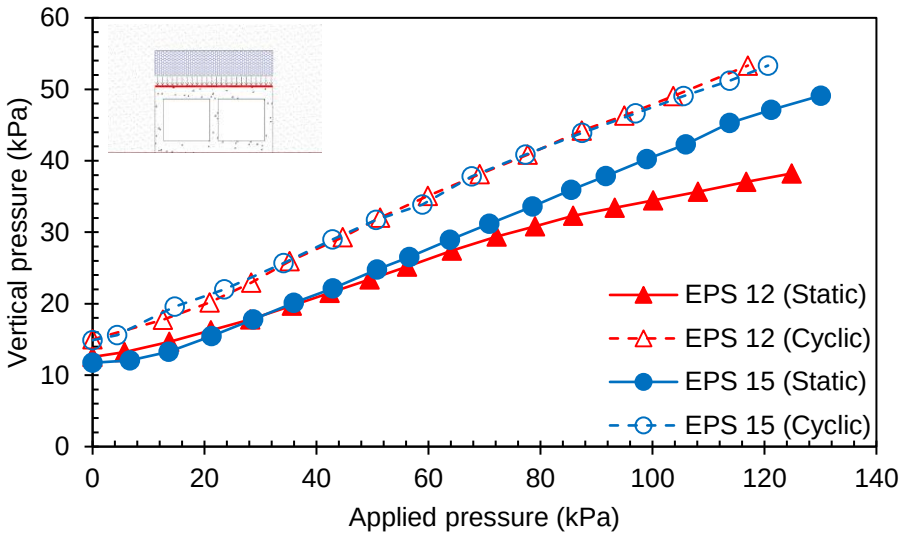

Figure 4.14 Measured vertical pressures on the culvert under static and cyclic footing loading with a geofoam thickness of $0.2B_c$.

CHAPTER 5 TEST RESULTS AND ANALYSIS OF SOIL ARCHING WITH SPRING-BASED TRAPDOOR

Trapdoor tests have been widely used by researchers to investigate soil arching behavior. However, soil arching has been commonly investigated using the conventional trapdoor test. In the conventional trapdoor test, the trapdoor movement is not governed by the vertical stress on the trapdoor but rather it forcibly moves gradually by a manual or automatic control. This method of trapdoor movement does not represent the situation happening in the field, for example, in GRPS embankments. To overcome this problem, a spring-based trapdoor test was proposed and conducted in this study. Moreover, soil arching has been commonly investigated under soil self-weight or soil self-weight plus a uniform surcharge. Uniform surcharge may not be representative for traffic loading and not be the critical condition for soil arching stability. Therefore, this chapter aims to investigate the soil arching mobilization and degradation under localized static and cyclic surface loading. Moreover, the influence of geosynthetic reinforcement on soil arching behavior under localized surface loading is not entirely understood. To better understand the effect of localized surface loading and the benefits of the geosynthetic reinforcement, this chapter presents the results of a series of plane-strain (2D) trapdoor tests as described in Section 3.2, to investigate the soil arching mobilization and degradation under static and cyclic footing loading without and with single layer (SL) or double layer (DL) of geogrid reinforcement. This chapter also presents an analytical solution for the soil arching problem based on Terzaghi's theory to estimate the pressure on the trapdoor under localized static footing loading.

5.1 PRESSURE DISTRIBUTION DURING FILL PLACEMENT

Overburden stresses (i.e., vertical earth pressures) of the fill on and besides the trapdoor were measured during the fill placement of all tests (T10-T21). Figures 5.1 to 5.4 present the vertical pressures on and besides the trapdoor during the placement of the unreinforced and reinforced fill (T10-T17), which was tested later under static footing loading. Since T18-T21 were constructed under the same condition of T10-T12, T14, and T16 but tested under different loading type (i.e., cyclic loading), their results during fill placement are not presented herein.

In T10 as a reference test, the trapdoor was fixed during placement and compaction of each fill layer and zero trapdoor displacement was measured by the three displacement transducers placed underneath the trapdoor. In this test, the measured pressures on and besides the trapdoor increased linearly with the fill height, and the pressures at TC, TE, and SE were approximately the same as shown in Figure 5.1. At the fill height of 720 mm, the vertical pressures over the trapdoor and the supports were approximately equal to the theoretical overburden pressure (γH). This implies that no soil arching was mobilized during fill placement of T10 and the pressure cells accurately measured soil pressures. On the other hand, tests (T11-T15) had a movable rigid trapdoor (i.e., one-segment trapdoor), which was free to move during the fill placement. In these tests, during fill placement, the soil pressure decreased on the trapdoor and increased on the supports due to the mobilization of soil arching with an increase in the relative displacement (δ) between the trapdoor and the stationary supports. The measured pressures on the trapdoor and especially at its edge (TE) deviated and decreased below the theoretical overburden pressure (γH) as the fill placement increased beyond 200 mm as shown in Figures 5.2 and 5.3. Meanwhile, the vertical pressure at SE gradually increased as the trapdoor progressively settled with the fill placement. Most importantly, a non-uniform pressure distribution over the trapdoor was observed

in these tests. In tests T16 and T17, when the flexible (i.e., three-segment) trapdoor was used, the measured pressures on the trapdoor at TC and TE as shown in Figures 5.4 were approximately the same, and thus a more uniform pressure on the trapdoor was observed since the outer trapdoor segments displaced less than the central one. The trapdoor displacement (δ) at the end of fill placement (i.e., 720 mm) for each test are also reported in Figures 5.1 to 5.4. In these tests, the maximum trapdoor displacement depended on (1) trapdoor stiffness (i.e., the number of springs), (2) trapdoor type or behavior (i.e., rigid or flexible), and (3) degree of soil arching and tensioned membrane mobilized in the test that controlled the magnitude of pressure on the trapdoor and that transferred onto the supports.

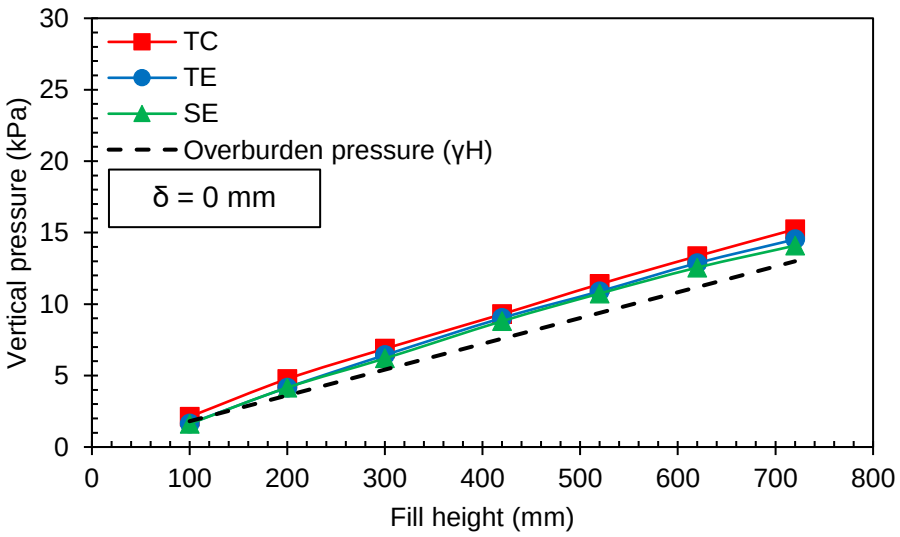

Figure 5.1 Measured vertical pressures on and besides the trapdoor during fill placement of T10.

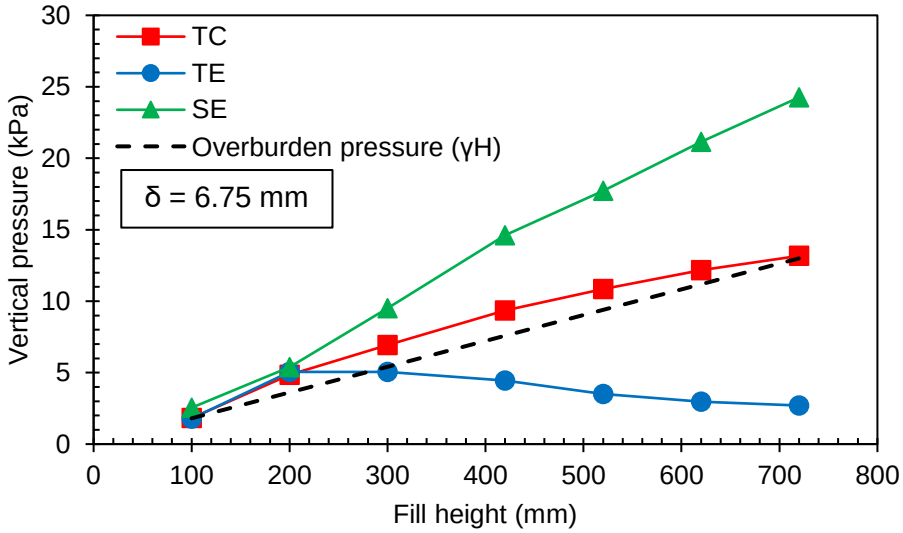

(a)

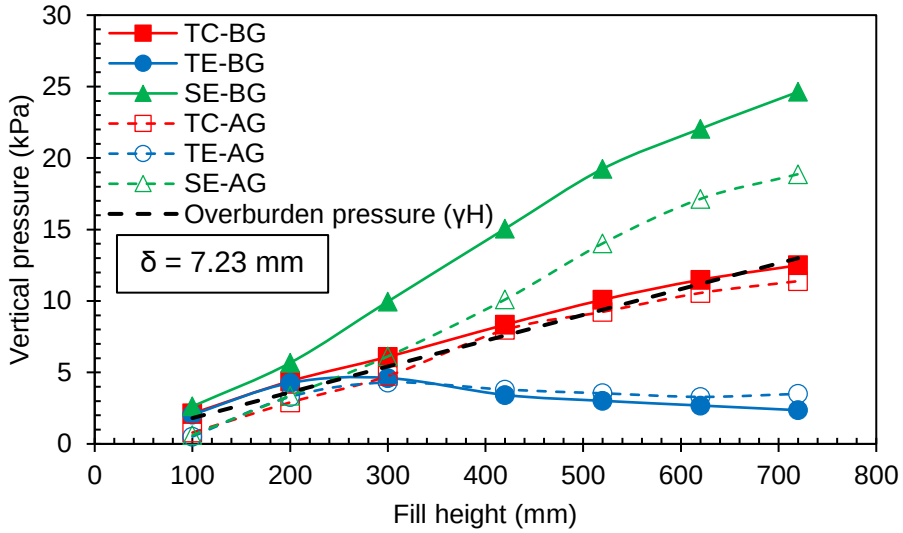

(b)

Figure 5.2 Measured vertical pressures on and besides the trapdoor during fill placement of: (a) T11; (b) T12; and (c) T13.

Note: BG: refers to the pressure measured below the geosynthetic and atop the test box base; AG: refers to the pressure measured above the single or first layer of geosynthetic.

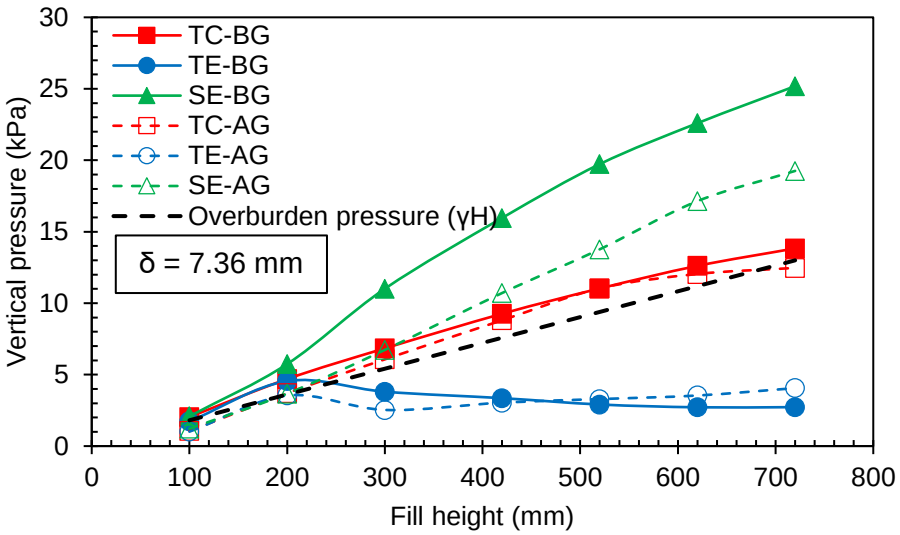

(c)

Figure 5.2 Measured vertical pressures on and besides the trapdoor during fill placement of: (a) T11; (b) T12; and (c) T13 (Continued).

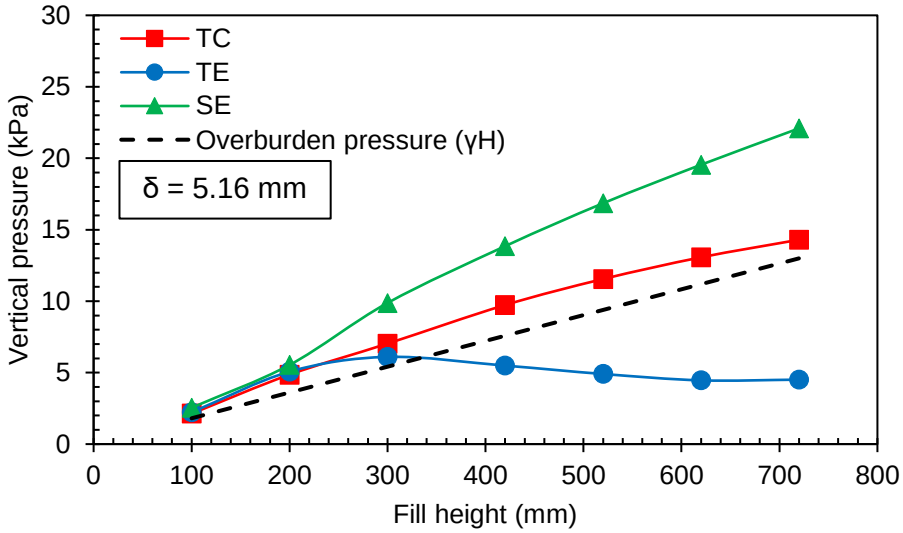

(a)

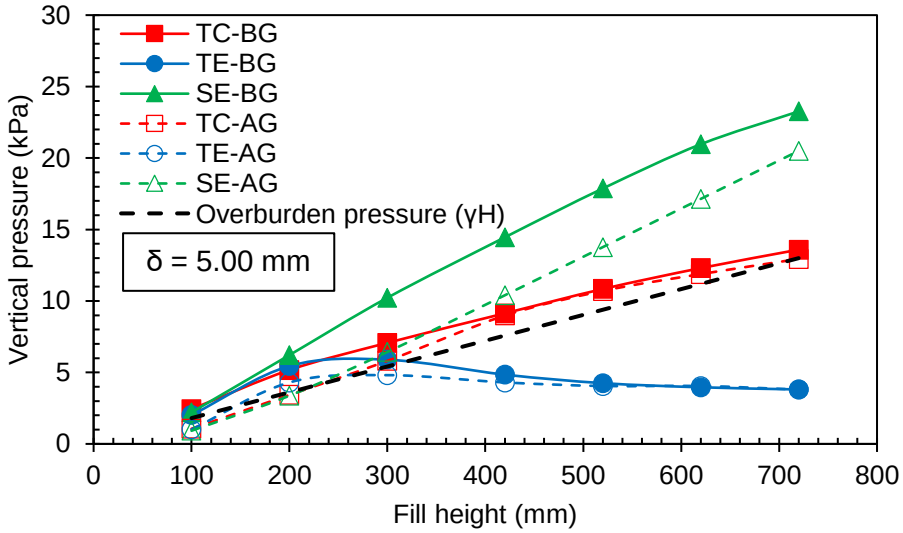

(b)

Figure 5.3 Measured vertical pressures on and besides the trapdoor during fill placement of: (a) T14; and (b) T15.

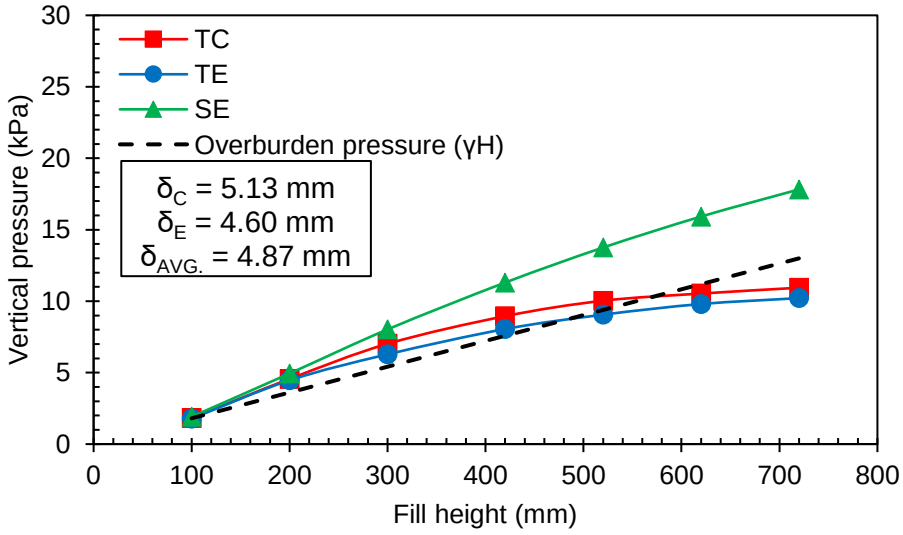

(a)

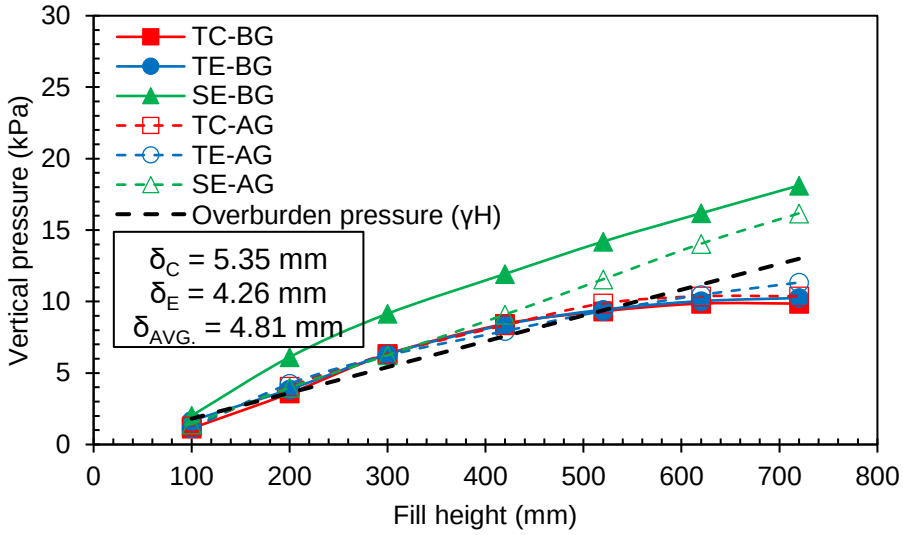

(b)

Figure 5.4 Measured vertical pressures on and besides the trapdoor during fill placement of: (a) T16; and (b) T17.

5.2 PRESSURE DISTRIBUTION UNDER STATIC FOOTING LOADING

When PS or GRPS embankments are constructed for roadway applications on soft soils, differential settlement likely occurs between the subsoil and the piles during their construction. Therefore, by the time when these embankments are ready for service, a considerable degree of soil arching is mobilized and partially responsible for the performance of the embankment during

the service. The effect of traffic loading on the stability of soil arching may affect the performance of the embankment during the service; therefore, it is of great importance but has not been well investigated. In this study, the effect of traffic loading on the stability of mobilized soil arching within the fill was investigated by utilizing a static footing load on the fill surface following the fill placement stage.

The results of the reference test T10, as shown in Figure 5.5, conducted on the unreinforced fill under static loading without any trapdoor movement (i.e., no soil arching) will be compared with those of T11-T17 with mobilized soil arching subjected to the footing load in the following section. It should be noted that the trapdoor in tests T11-T17 was free to move during the fill placement and surface loading stages. This condition is similar to that in pile-supported embankments where the subsoil between piles continues deforming under a surface load. The effect of the continuous soil deformation has not been fully understood and deserves a further study, which will be discussed here.

Figures 5.6 to 5.7 present the measured pressures over the trapdoor at the center, the edges, and the stationary supports during the surface loading stage of tests T11-T15. As the footing pressure increased in these tests, the measured pressure at TC slowly increased as compared to that at SE, even though TC was located under the footing centerline where the maximum applied pressure was measured in T10. Also, the pressure at TE increased at the slowest rate. However, the measured pressure at SE increased most rapidly as compared with those on the trapdoor at TC and TE. Therefore, the non-uniformity of the pressure distribution over the trapdoor increased under the application of static footing loading in these tests. When the flexible trapdoor was used in tests (T16 and T17), the measured pressures on the trapdoor at TC and TE as shown in Figure 5.8 were approximately the same as the applied footing pressure increased, and thus a more

uniform pressure distribution was developed over the trapdoor in these tests as compared to those in T11-T15.

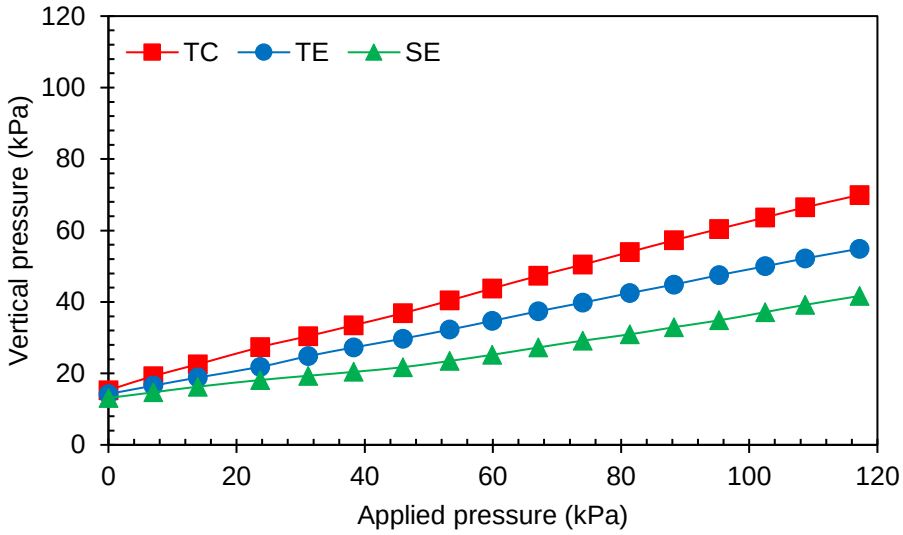

(a)

Figure 5.5 Measured vertical pressures on and besides the trapdoor under static footing loading of T10.

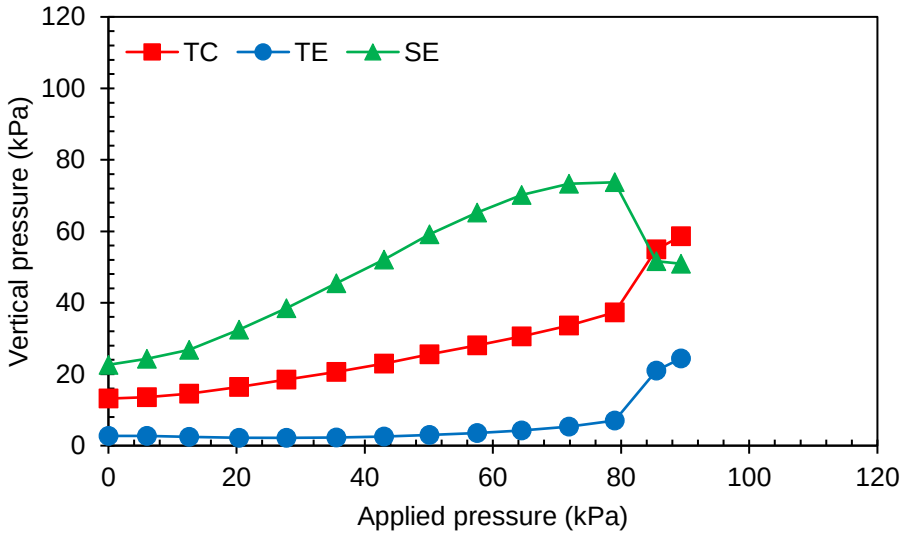

(a)

Figure 5.6 Measured vertical pressures on and besides the trapdoor under static footing loading in: (a) T11; (b) T12; and (c) T13.

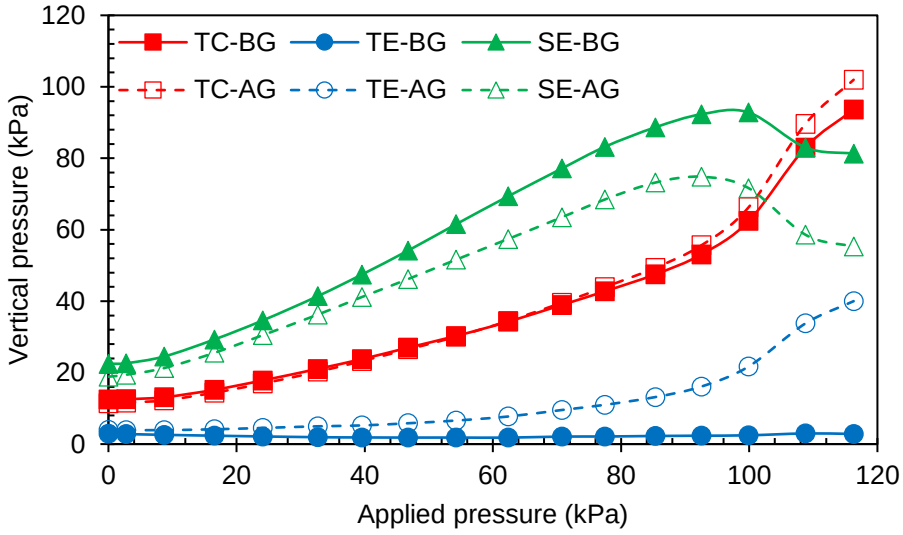

(b)

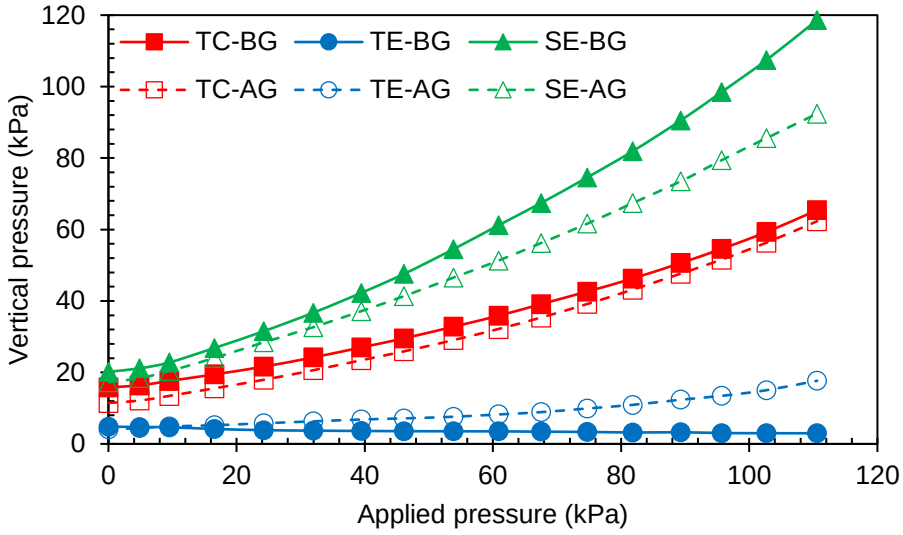

(c)

Figure 5.6 Measured vertical pressures on and besides the trapdoor under static footing loading in: (a) T11; (b) T12; and (c) T13;

Note: BG: refers to the pressure measured below the geosynthetic and atop the test box base; AG: refers to the pressure measured above the single or first layer of geosynthetic.

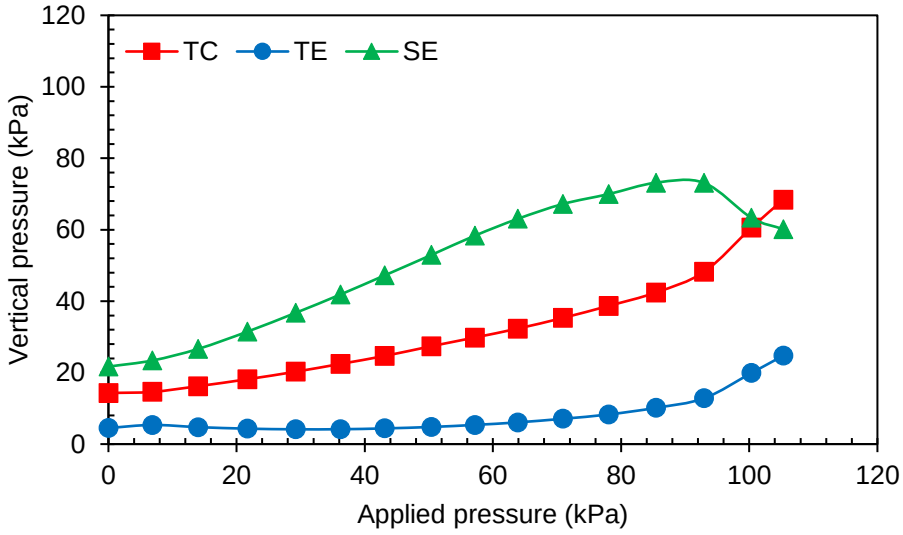

(a)

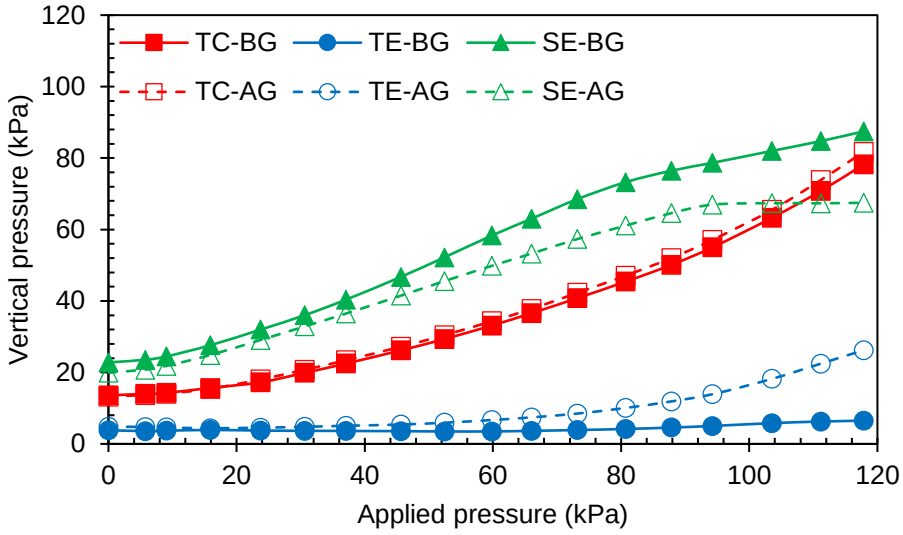

(b)

Figure 5.7 Measured vertical pressures on and besides the trapdoor under static footing loading in: (a) T14; and (b) T15.

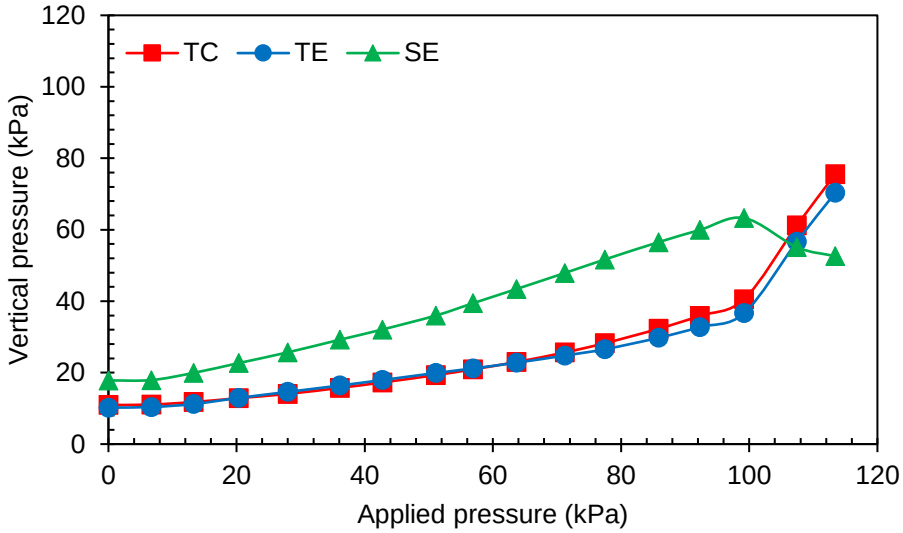

(a)

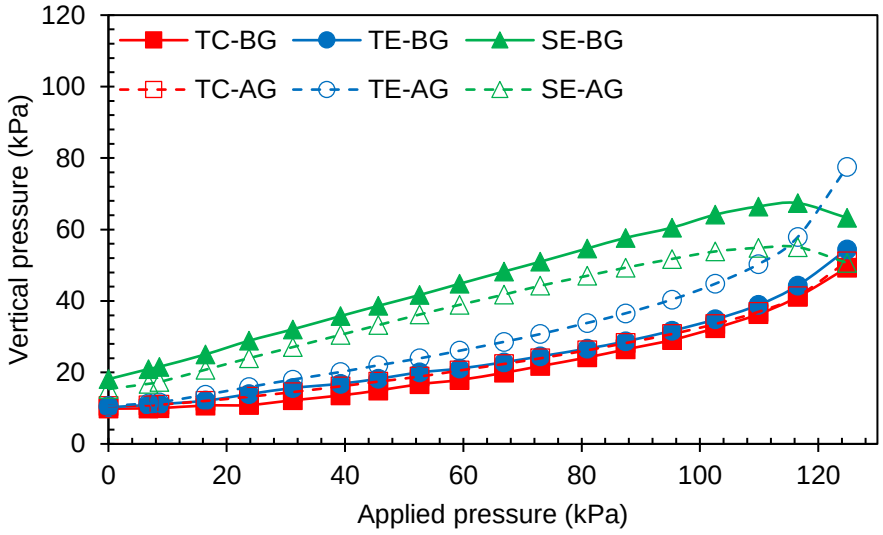

(b)

Figure 5.8 Measured vertical pressures on and besides the trapdoor under static footing loading in: (a) T16; and (b) T17.

5.3 STRAINS IN GEOGRID

This section presents and discusses the strain results of the reinforcement layers (i.e., geogrid) in tests T12 and T13 during the fill placement and surface loading stages. T12 and T13 were conducted with SL and DL of biaxial geogrid as reinforcement, respectively, with a four-spring-

supported rigid trapdoor. Strain results of T15 and T17, which were conducted with SL of biaxial geogrid on a six-spring-supported rigid trapdoor and a six-spring-supported flexible trapdoor, respectively, had similar distribution across the geogrid layers with smaller magnitudes than those in T12. These results are not presented herein. It is worth mentioning that in all reinforced tests, the geogrid was free at its two ends and not fixed to the test box. The mobilized strains in the geogrid were induced by the lateral movement of the above fill and the tensioned membrane effect due to trapdoor movement. In these tests, a string tell-tale was connected to the end rib of the geogrid (i.e., the geogrid rib at 0.8 m away from the trapdoor centerline) and no movement was observed at the geogrid end rib during all stages of the test, indicating no pullout tendency.

Figure 5.9 shows the distribution and change in the measured geogrid strains during the fill placement of T12 with SL biaxial geogrid. As the fill height increased to 720 mm, the geogrid was stretched, thus causing a maximum tensile strain of 0.12% at a distance of 195 mm away from the trapdoor centerline (i.e., at the support edges) as shown in Figure 5.9(a). This strain distribution is consistent with what Han and Gabr (2002) found from their numerical analysis and Bhandari and Han (2018) found from their experimental study. The higher tensile strains at the trapdoor edges confirm the effect of the tensioned membrane in transferring the vertical pressure on the reinforcement to the adjacent supports. Figure 5.9(a) shows that anchorage is required for the tensioned membrane effect. Figure 5.9(a) also shows that small and even negative (compressive) strains happened near the trapdoor edges and towards the middle portion of the geogrid. This compressive strain of -0.11% at a distance of 160 mm away from the trapdoor centerline (i.e., at the trapdoor edges) was the second highest strain along the biaxial geogrid. This result can be explained that soil particles above the geogrid moved or slid toward the centerline and generated

an inward shear stress to compress the geogrid when the trapdoor and the geogrid displaced downward during the fill placement.

At the distances of 0, 160, and 195 mm away from the trapdoor centerline, strain gauges were attached on both upper and lower surfaces of the biaxial geogrid to evaluate the bending behavior of the geogrid during the test. Even though the geogrid had a rib thickness of 0.76 mm (i.e., a thin geogrid and less susceptible for a bending effect), the geogrid experienced both tensile and compressive strains on upper and lower surfaces as shown in Figures 5.9(b) to 5.9(d). At two locations (0 and 195 mm from the trapdoor centerline), the measured tensile strains were higher than the compressive strains, and the net strain (the sum of positive and negative strains divided by 2) was positive and tensile; therefore, at these locations, the geogrid was overall under tension but subjected to bending. Meanwhile, at 160 mm from the trapdoor centerline, the measured tensile strain was equal to the compressive strain, and the net strain was zero; therefore, at this location, the geogrid was under pure bending.

Figure 5.10 shows the measured strain results for T13 with DL biaxial geogrid during fill placement. The lower geogrid layer was stretched to a maximum tensile strain of 0.16% at the support edges and underwent a maximum compressive (negative) strain of -0.08% at the trapdoor edges when the fill height increased to 720 mm as depicted in Figure 5.10(a). Also, a tensile strain of 0.04% existed at the trapdoor centerline in the lower geogrid layer. Meanwhile, the upper geogrid layer underwent much less tensile strain of 0.02% than that of the lower geogrid layer at the support edges as shown in Figure 5.10(b). However, across the trapdoor, the upper geogrid layer underwent more uniform compressive strain (approximately -0.06%) than that of the lower geogrid layer. The existence of the tensile strain at the support edges and trapdoor centerline in the lower geogrid layer and the compressive strain across the trapdoor in the upper geogrid layer

confirmed the beam behavior of the load transfer platform consisting of the DL geosynthetic reinforcement and the sand in-between as observed by Huang et al. (2005) in their numerical analysis of a three-layer geosynthetics-reinforced embankment over piles and Al-Naddaf et al. (2019) in their experiment work of a double layer geosynthetics-reinforced trapdoor test.

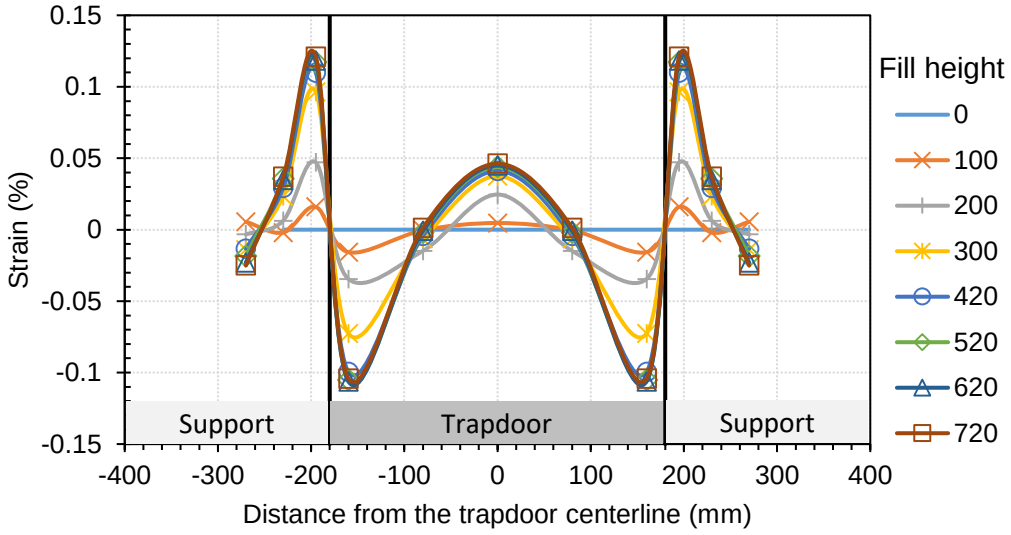

(a)

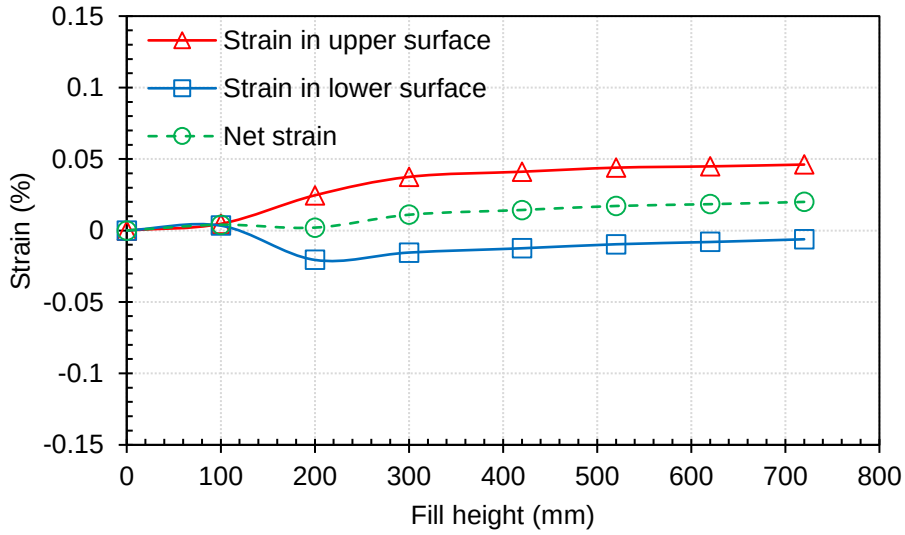

(b)

Figure 5.9 Measured geogrid strains during the fill placement of T12: (a) cross-sectional distribution; (b) at 0 mm; (c) 160 mm; and (d) at 195 mm away from the trapdoor centerline.

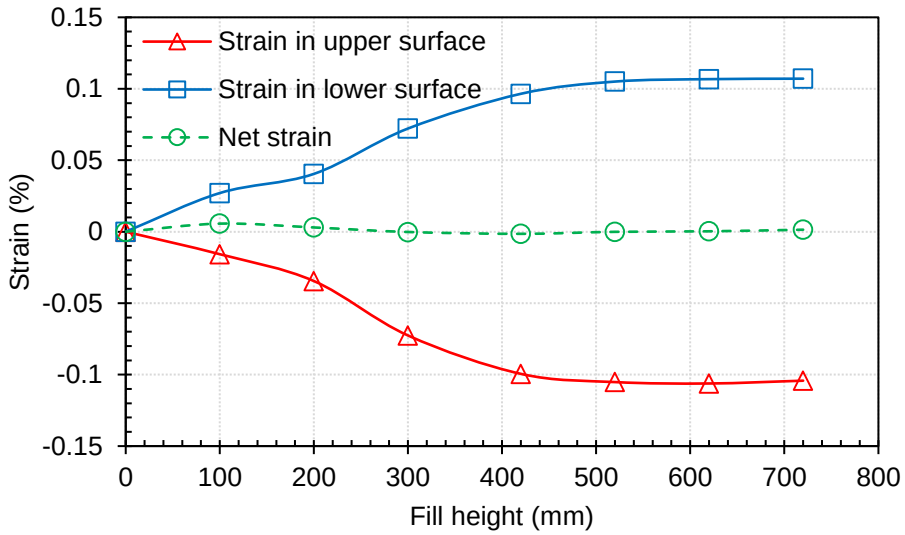

(c)

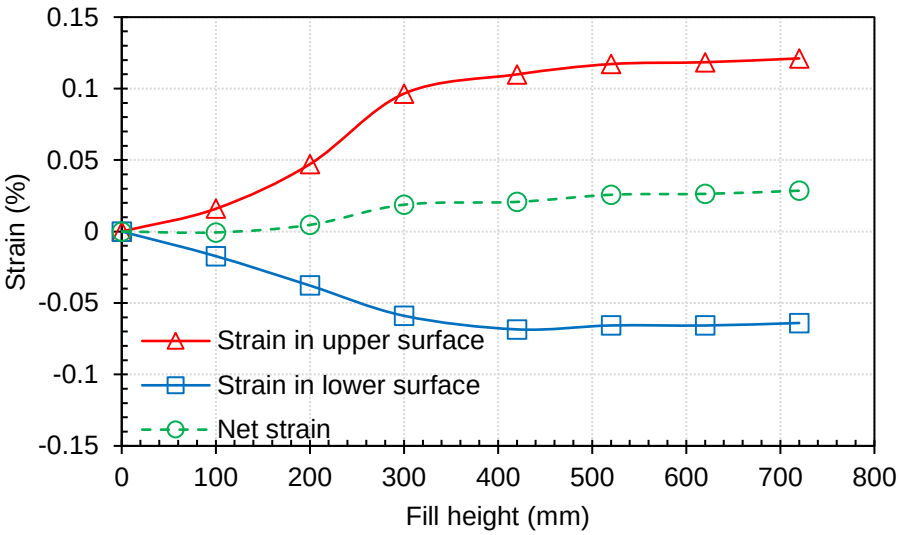

(d)

Figure 5.9 Measured geogrid strains during the fill placement of T12: (a) cross-sectional distribution; (b) at 0 mm; (c) 160 mm; and (d) at 195 mm away from the trapdoor centerline (Continued).

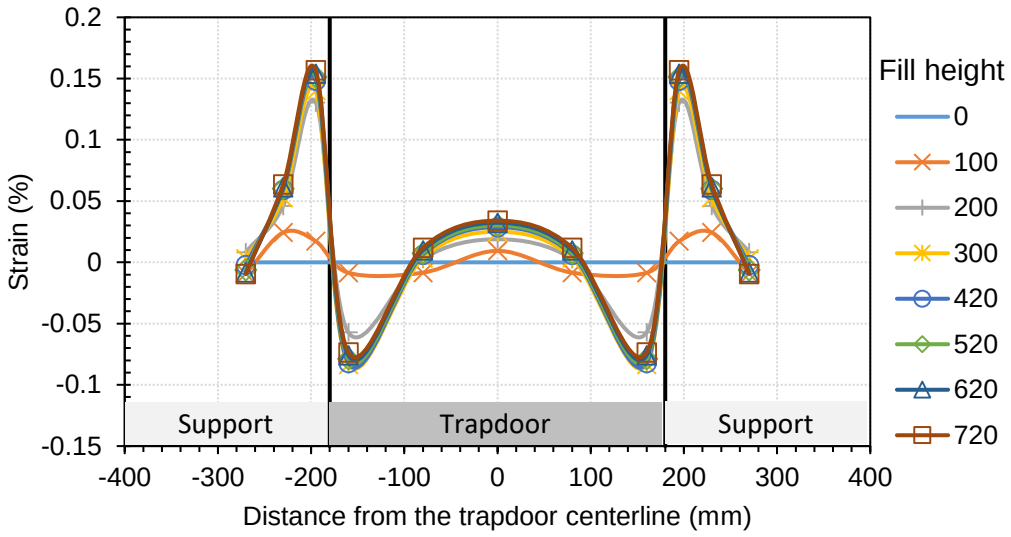

(a)

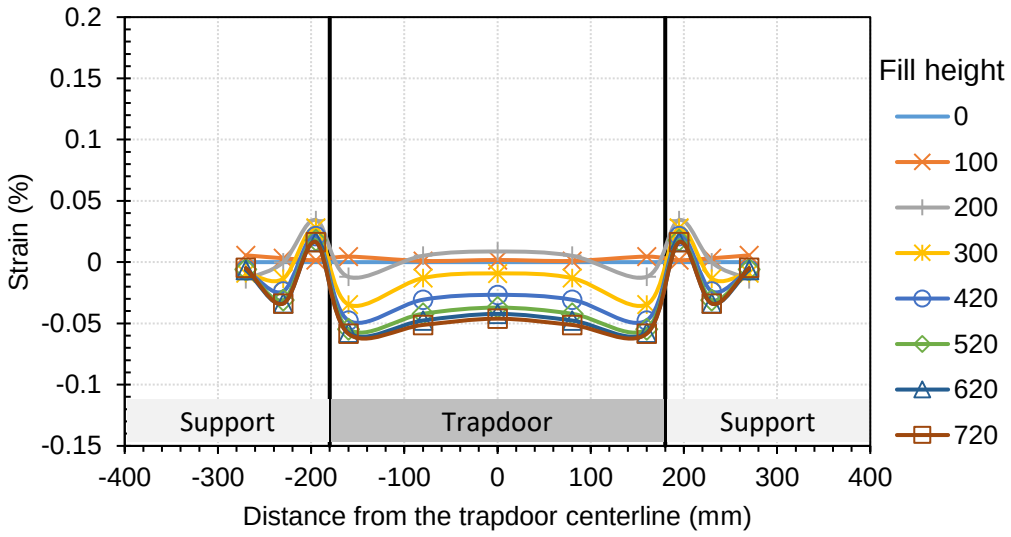

(b)

Figure 5.10 Measured geogrid strains during the fill placement of T13 with DL biaxial geogrid: (a) lower reinforcement layer; and (b) upper reinforcement layer.

Figures 5.11 and 5.12 show the distribution of the measured strains during the surface loading stages of T12 and T13 conducted with SL and DL biaxial geogrids, respectively. Figures 5.11 and 5.12 show that the applied footing loading eliminated the compressive strains and induced more tensile strains along the geogrid layers for both tests (T12 and T13). However, the biaxial geogrid experienced higher overall tensile strains in the SL reinforced test, T12, as compared with those in the DL reinforced test, T13. For instance, since the trapdoor was free to move during the surface loading stage, the geogrid in T12 underwent additional elongation and the tensile strain increased from 0.05% to 1.15% at the trapdoor centerline and from 0.12% to 2.00% at the support edges as the applied footing pressure increased from 0 to 116 kPa. For the same reason, the tensile strains in the DL geogrid test, T13, increased from 0.04% to 0.60% in the lower geogrid and from -0.05% to 0.21% in the upper geogrid at the trapdoor centerline as the applied footing pressure increased from 0 to 117 kPa. Similarly at the support edges of the DL geogrid test, where the tensile strains increased from 0.16% to 1.00% in the lower geogrid and from 0.02% to 0.70% in the upper geogrid as the applied footing pressure increased from 0 to 117 kPa. Therefore, the sum of the maximum tensile strains (i.e., at the support edges) of these two geogrid layers were 1.70%, which is slightly smaller than the maximum tensile strain of the single geogrid (i.e., 2.00%). Since the overall strains along the geogrid layers in both SL and DL reinforced tests under footing loading were tensile strains, with higher tensile strains at the support edges as compared with those over the trapdoor, the tensioned membrane was the dominating mechanism in the reinforcement layers that helped transfer the vertical load to the adjacent supports.

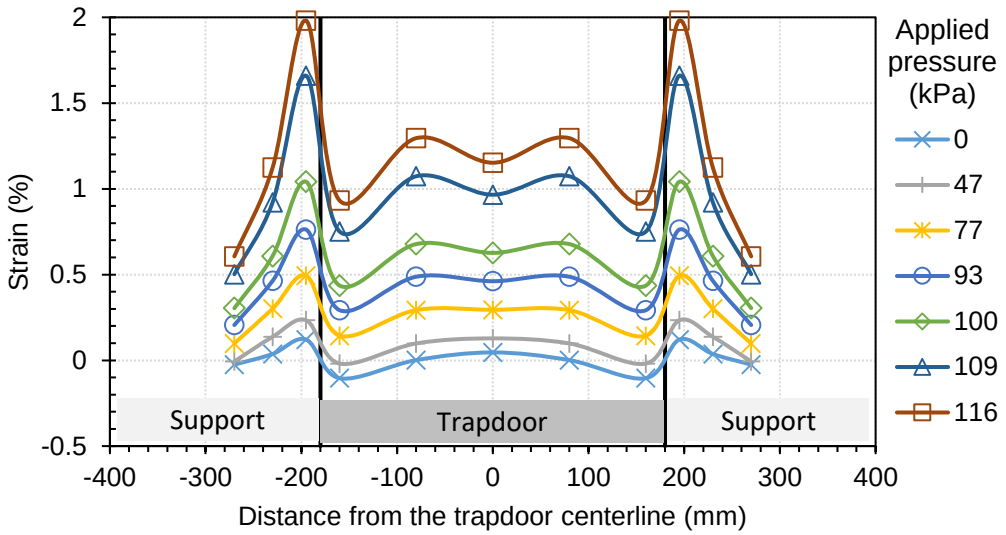

Figure 5.11 Cross-sectional distribution of the measured strains under static footing loading of T12 with SL biaxial geogrid.

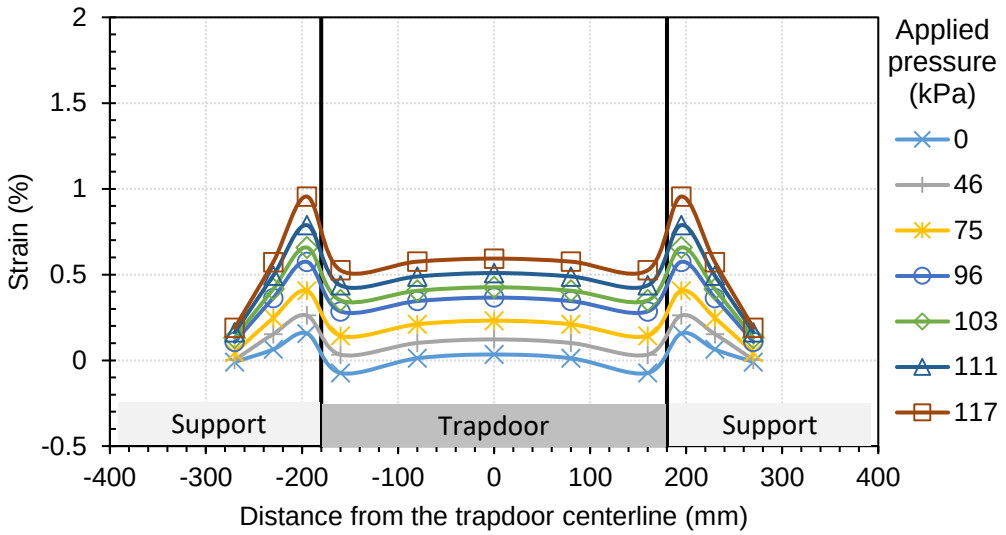

(a)

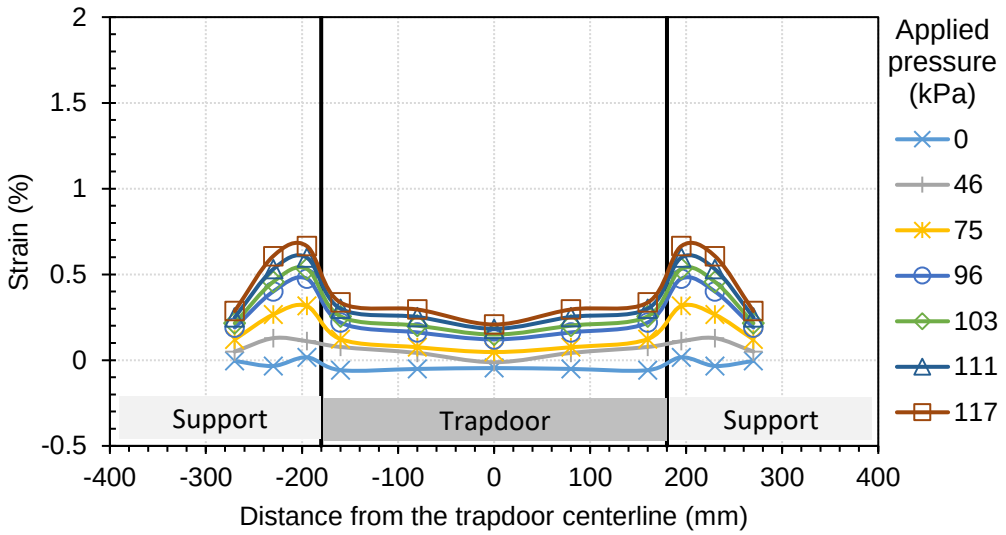

(b)

Figure 5.12 Measured geogrid strains under static footing loading of T13 with DL biaxial geogrid: (a) lower reinforcement layer; and (b) upper reinforcement layer.

5.4 DEGREE OF SOIL ARCHING AND STRESS REDUCTION

The degree of soil arching in pile-supported embankments is often evaluated in terms of a soil arching ratio (e.g., Han and Gabr 2002). Soil arching ratio (SAR), first proposed by McNulty (1965), is used to assess the degree of the load transferred from a yielding soil zone to the surrounding soil zone. This ratio, given in Equation (5.1), is calculated as the average vertical pressure above a yielding base (σ_v) (i.e., the trapdoor for an unreinforced test or the geosynthetic reinforcement for a reinforced test in this study) to the overburden pressure (γH) plus the uniform surcharge (q) if applied. SAR = 0 represents the complete soil arching while SAR = 1 represents no soil arching. On the other hand, a stress reduction ratio (*SRR*) (e.g., Low et al. 1994) is used to assess the combined effect of soil arching and tensioned membrane in GRPS embankments. *SRR* is defined as the ratio of the average measured pressure (σ_v') below the geosynthetic reinforcement and on the trapdoor to the overburden pressure plus the uniform surcharge ($\gamma H + q$). In unreinforced fill tests, SRR is equal to SAR.

$$SAR = \frac{\sigma_v}{\gamma H + q} \tag{5.1}$$

$$SRR = \frac{\sigma_v'}{\gamma H + q} \tag{5.2}$$

Since soil arching mobilized under soil self-weight during the fill placement stage for tests T11-T17, the applied surcharge, q, in Equations (5.1) and (5.2) was zero. Based on the definition of SAR or SRR, the denominator in Equations (5.1) or (5.2) represents the initial condition of pressure on the yielding base before the arching mobilization; therefore, during the surface loading stage of T11-T17, q for the SAR or SRR calculation was considered based on the average measured pressures on the trapdoor in the reference test, T10, in which no trapdoor movement was allowed.

Figures 5.13 and 5.14 present the variations in the SAR and SRR versus the normalized trapdoor displacement with respect to its width (i.e., δ/B) and the total pressure of the fill and the footing loading ($\gamma H+q$), respectively, for the four-spring-supported rigid trapdoor tests (T11-T13), six-spring-supported rigid trapdoor tests (T14 and T15), and six-spring-supported flexible trapdoor tests (T16-T17). In general, these figures show that soil arching mobilized as the fill height increased to 720 mm and followed by more mobilization in soil arching at an applied pressure of less than 50 kPa; however, as the footing pressure increased, soil arching degraded. The following sections will discuss the effects of reinforcement, trapdoor stiffness, and trapdoor type or behavior on soil arching in more details.

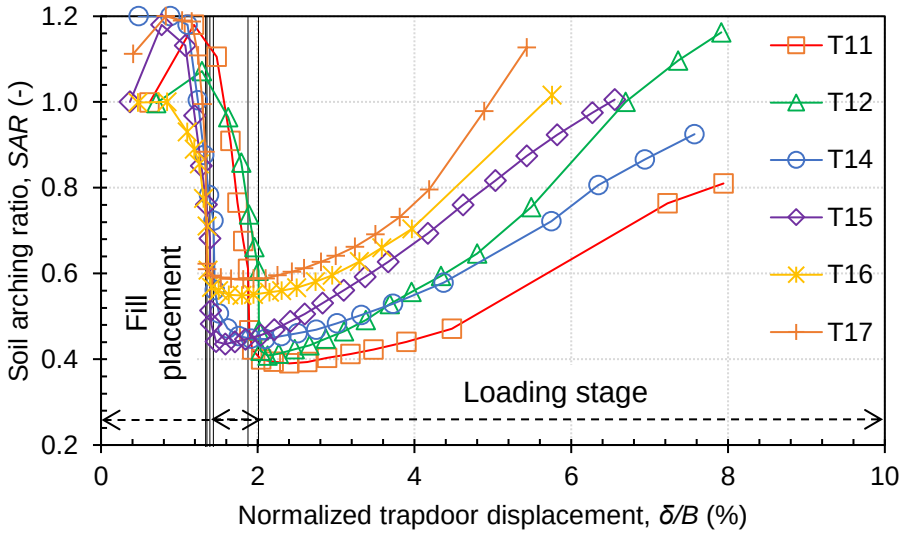

(a)

Figure 5.13 Soil arching and stress reduction ratios versus normalized trapdoor displacement for: (a) all tests T11-T17 except T13; (b) four-spring-supported rigid trapdoor tests (T11-T13); and (c) six-spring-supported rigid and flexible trapdoor tests (T14-T17).

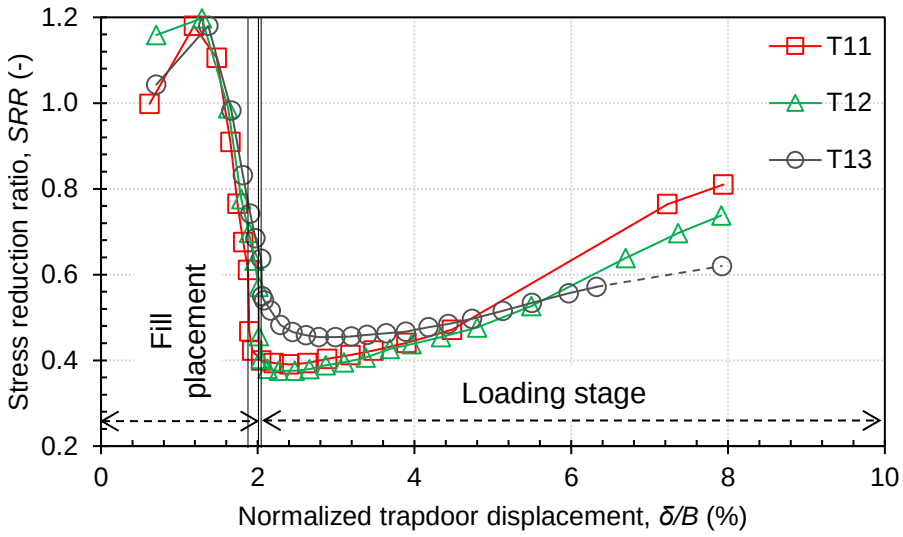

(b)

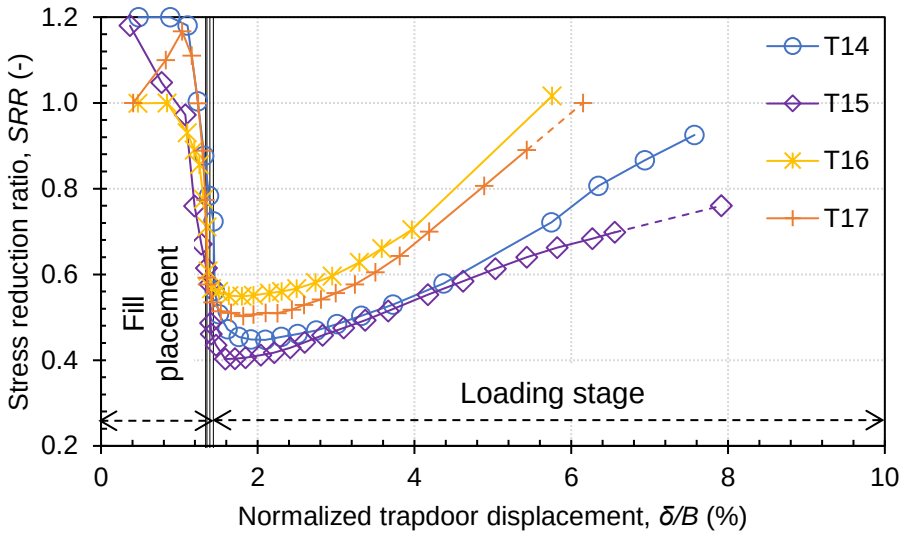

(c)

Figure 5.13 Soil arching and stress reduction ratios versus normalized trapdoor displacement for: (a) all tests T11-T17 except T13; (b) four-spring-supported rigid trapdoor tests (T11-T13); and (c) six-spring-supported rigid and flexible trapdoor tests (T14-T17) (Continued).

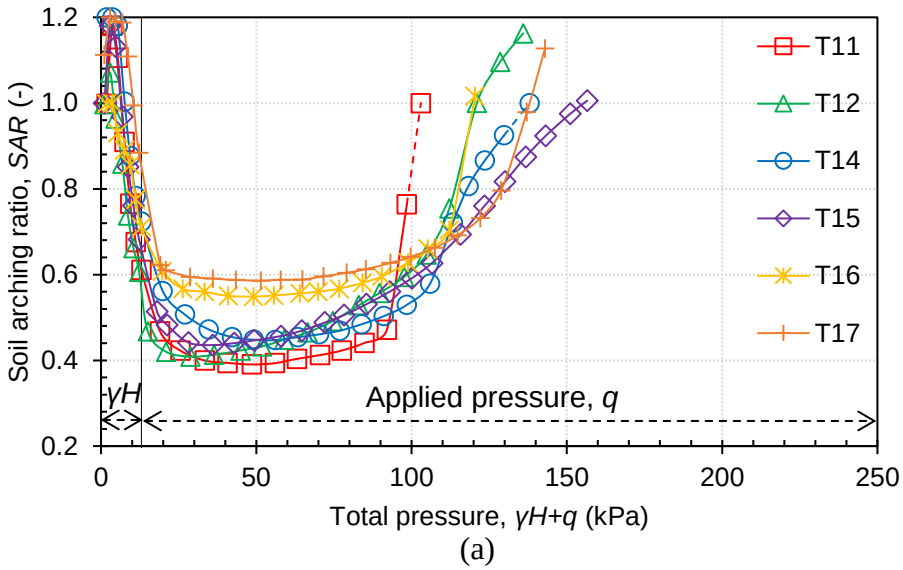

(a)

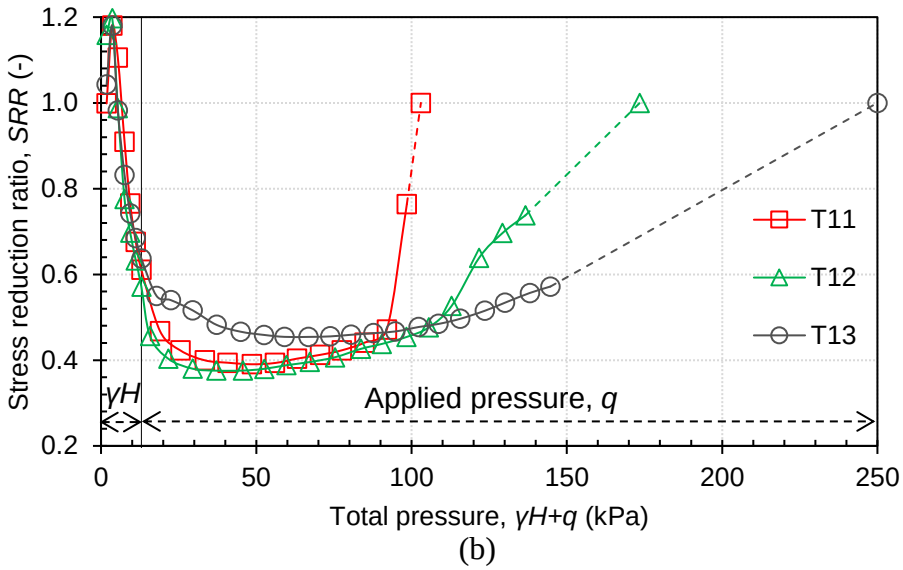

(b)

Figure 5.14 Soil arching and stress reduction ratios versus total pressure of the fill and the footing loading ($\gamma H+q$) for: (a) all tests T11-T17 except T13; (b) four-spring-supported rigid trapdoor tests (T11-T13); and (c) six-spring-supported rigid and flexible trapdoor tests (T14-T17).

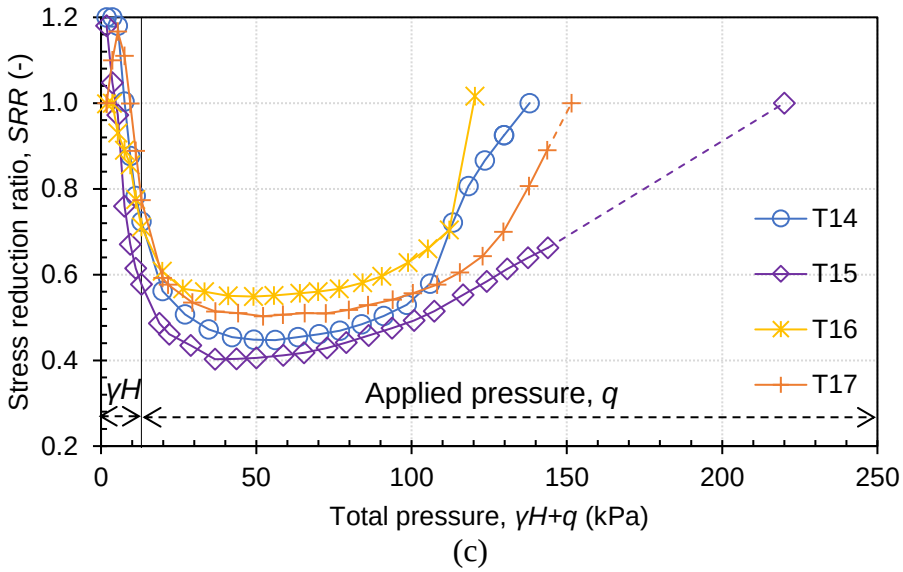

(c)

Figure 5.14 Soil arching and stress reduction ratios versus total pressure of the fill and the footing loading ($\gamma H+q$) for: (a) all tests T11-T17 except T13; (b) four-spring-supported rigid trapdoor tests (T11-T13); and (c) six-spring-supported rigid and flexible trapdoor tests (T14-T17) (Continued).

5.5 EFFECTS OF GEOSYNTHETIC REINFORCEMENT

To evaluate the effect of geosynthetic reinforcement on the soil arching mobilization and degradation, four tests (T12, T13, T15, and T17) were conducted with geosynthetic-reinforced fill as compared with the unreinforced fill tests (T11, T14, and T16). T11, T12, and T13 were conducted without reinforcement and with SL and DL of biaxial geogrid, respectively, using the four-spring-supported rigid trapdoor. T14 and T15 were conducted without reinforcement and with SL of biaxial geogrid, respectively, using the six-spring-supported rigid trapdoor. T16 and T17 were conducted without reinforcement and with SL of biaxial geogrid, respectively, using the six-spring-supported flexible trapdoor.

Figures 5.2 to 5.4 and 5.6 to 5.8 present the results during fill placement and surface loading stages, respectively, for these tests. As the fill height increased and the trapdoor displaced

downward, the pressures on the trapdoor in the reinforced fill tests were lower than those in the unreinforced fill tests as shown in Figures 5.2 to 5.4. At the same time, the geosynthetic reinforcement deformed, stretched, and underwent tension. Consequently, the measured pressures at SE in the geosynthetic-reinforced fill tests continued to increase and reached a higher value as compared with those in the unreinforced fill tests as the fill height increased to 720 mm. The decreased pressure over the trapdoor and the increased pressure over the supports are attributed to the tensioned membrane effect of the geosynthetic reinforcement. Figures 5.6 to 5.8 also demonstrate the benefits of geosynthetic reinforcement in reducing the pressure on the trapdoor and transferring it to the adjacent supports under static footing loading. Even though the pressures measured at TC were approximately the same in the unreinforced and reinforced fill tests, the pressures measured at TE and SE in the reinforced tests were significantly lower and higher, respectively, than those in the unreinforced tests. Therefore, the geosynthetics helped transfer the load from the trapdoor to the adjacent supports due to its tensioned membrane effect. It should be pointed out that the trapdoor was in contact with the reinforced soil mass and no separation was observed during all stages of the reinforced fill test. In other words, the weight of the soil mass above the geogrid layer and any additional force applied by the footing were not only carried by the geogrid but also transferred to the soil mass underneath the geogrid and then to the trapdoor.

Figures 5.13 and 5.14 present the variations of the soil arching and stress reduction ratios in T11-T17. As the fill height increased to 720 mm in the unreinforced fill tests, Figure 5.13(a) shows that the SAR dropped from approximately 1.20 to 0.61 in T11, 0.68 in T14, and 0.71 in T16 as the trapdoor moved downward by 1.88% of its width (i.e., δ/B) in the four-spring-supported rigid trapdoor test (T11) and 1.40% in the six-spring-supported rigid and flexible trapdoor tests (T14 and T16). While for the SL reinforced tests, the SAR dropped from approximately 1.20 to

0.61 in T12, 0.72 in T15, and 0.88 in T17 at a normalized trapdoor displacement (δ/B) of 2.00% for the four-spring-supported rigid trapdoor test (T12) and 1.36% for the six-spring-supported rigid and flexible trapdoor tests (T15 and T17). Figure 5.14(a) also shows the same drop in the SAR as the total pressure increased to 13 kPa. In general, this drop in the SAR indicates the mobilization of soil arching during the fill placement stage of these tests. Furthermore, with the continuous movement of the trapdoor under the applied static footing loading, the SAR continued to decrease and reach the minimum of 0.39 in T11, 0.41 in T12, 0.44 in T14, 0.45 in T15, 0.55 in T16, and 0.59 in T17 at a normalized trapdoor displacement (δ/B) of approximately 2.0% for all tests as shown in Figure 5.13(a). These minimum SARs were at approximately 50 kPa total pressure as shown in Figure 5.14(a). Beyond 2.0% of normalized trapdoor displacement or 50 kPa of total applied pressure, soil arching degraded (or stress recovered). Figures 5.13(a) and 5.14(a) show that the SAR had a slowly increasing rate followed by a faster increasing rate that caused SAR to increase and approach 1.00 at a normalized trapdoor displacement range from 5.0 to 10 % or a total pressure range from 100 to 160 kPa based on the test condition. During both fill placement and surface footing loading, the inclusion of the SL of geosynthetic reinforcement in T12, T15, and T17 reduced the degree of arching mobilization as compared with that in the unreinforced fill tests T11, T14, and T16, respectively. The higher SAR is because the deflected geosynthetic changed the shape of soil displacement above the geosynthetic and reduced the total amount of soil movement even though the trapdoor had approximately the same movement as that in the unreinforced fill test. Less amount of soil movement minimized soil arching mobilization. Unfortunately, no pressure cells were placed above the upper layer of geosynthetic in the DL reinforced test, T13; therefore, SAR was not calculated for this test.

Figures 5.13(b) and 5.14(b) present the SRRs in unreinforced, SL, and DL geosynthetic-reinforced fill tests that were conducted with a four-spring-supported rigid trapdoor. During the fill placement, the unreinforced fill test (T11) had the lowest SRR (i.e., soil arching mobilized most), the SL geosynthetic-reinforced fill test (T12) had a higher SRR (soil arching mobilized less), and the DL geosynthetic-reinforced fill test (T13) had the highest SRR (soil arching mobilized least). The reason is that geosynthetic reinforcement changed the fill deformation shape and minimized the average fill deformation magnitude. The SRRs at a normalized trapdoor displacement of approximately 2.0% were 0.61 (T11), 0.63 (T12), and 0.64 (T13). At this small displacement, the tensioned membrane effect was not significant enough (as shown in Figures 5.9 and 5.10 and discussed in the strain result section) to reduce the pressures underneath the geosynthetic reinforcement (also on the trapdoor). However, as the footing pressure increased, which induced additional trapdoor displacement, the tensioned membrane effect became important so that the pressures underneath the geosynthetic reinforcement decreased in the SL reinforced fill test, T12. At the same time, the pressure on the trapdoor in the unreinforced fill test increased due to the soil arching degradation. Therefore, the SRRs dropped to a minimum of 0.39 and 0.37 for unreinforced and SL reinforced tests, respectively. These minimum SRRs were at approximately 40 kPa total pressure as shown in Figures 5.14(b). However, since a different behavior was observed for the geosynthetic reinforcement in DL reinforced fill test (i.e., geogrids and sand in-between acted as a stiffened beam rather than tensioned membrane effect as discussed in the strain result section), the minimum SSR (0.45) and the corresponding total pressure (60 kPa) in the DL reinforced test were higher those in the unreinforced and SL reinforced tests. The higher total pressure is because the geogrids had the same property (i.e., tensile strength) in both SL and DL reinforced tests. As the total pressure increased beyond 90 kPa, it caused larger relative

displacements between the trapdoor and two supports in T11-T13 so that soil arching degraded and their SRRs increased toward unity. At the same time, the responses in the unreinforced, SL, and DL reinforced fill tests became much different, and more significant benefits of the geosynthetic reinforcement were observed.

Similarly, the unreinforced and SL reinforced fill tests with six-spring-supported rigid trapdoor or flexible trapdoor had the same behavior as those with four-spring-supported rigid trapdoor in the terms of the benefits of geosynthetic reinforcement as shown in Figures 5.13(c) and 5.14(c).

5.6 EFFECTS OF TRAPDOOR STIFFNESS

Four tests (T11, T12, T14, and T15) with two different trapdoor stiffness values were conducted to evaluate the effects of relative displacement (δ) between the trapdoor and the stationary supports (i.e., subsoil compressibility in PS or GRPS embankments) on the soil arching mobilization and degradation. The tests with a low-stiffness trapdoor (four-spring with spring stiffness of 1150 kN/m^3) had larger total trapdoor displacements during fill placement and under surface footing loading as compared with those in the tests with a high-stiffness trapdoor (six-spring with spring stiffness of 1725 kN/m^3) as shown in Figure 5.15. Also, both unreinforced fill tests with low and high-stiffness trapdoors (T11 and T14) and SL reinforced fill tests with low and high-stiffness trapdoors (T12 and T15) exhibited the same trends. Since the low-stiffness trapdoor had larger displacements than the high-stiffness trapdoor, the total pressures on the trapdoor in T11 and T12 were lower than those in T14 and T15, respectively, as shown in Figures 5.2, 5.3, 5.6, and 5.7 for these tests. Consequently, the low-stiffness trapdoor transferred more pressure to the supports than the high-stiffness trapdoor. Therefore, both SARs and SRRs in the low-stiffness trapdoor tests

were less than those in the high-stiffness trapdoor tests under the total applied pressure up to 90 kPa or its corresponding normalized displacement up to 4.5% as shown in Figures 5.13 and 5.14. As the total applied pressure increased beyond 90 kPa, the low-stiffness trapdoor had a much faster displacement rate, which caused soil arching to degrade and the SARs to increase faster than those in the high-stiffness trapdoor. This phenomenon was observed and described by several researchers (e.g., Iglesia et al. 2014; King et al. 2017; Han et al. 2017; and Al-Naddaf et al. 2019).

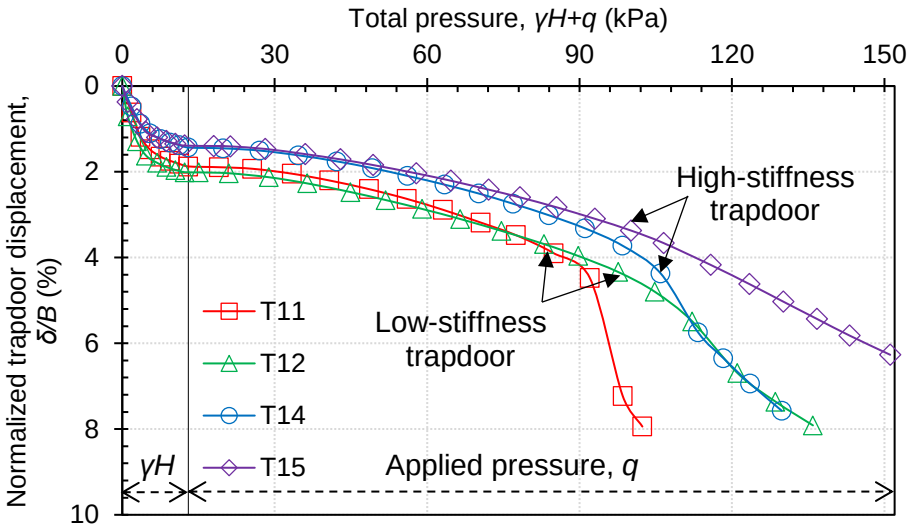

Figure 5.15 Normalized trapdoor displacement during fill placement and surface loading stages for T11, T12, T13, and T14.

5.7 EFFECTS OF TRAPDOOR TYPE

Based on the results of trapdoor tests T11 to T15, which were conducted with a one-segment rigid trapdoor, the pressure distribution on the trapdoor was not uniform, especially after the application of the footing loading because the trapdoor settled uniformly. This pressure distribution on the trapdoor was close to that under a rigid footing on granular material. Since the trapdoor should simulate the behavior of subsoil in real applications (e.g., PS or GRPS embankments), a uniform

displacement of the trapdoor does not represent the actual mode and simplifies the condition of soil movement between rigid supports. In PS or GRPS embankments, the displacement of subsoil between rigid supports exhibits a concave (parabola)-like shape; therefore, it is not uniform. To better simulate the subsoil displacement mode, a three-segment flexible trapdoor was utilized in this study. The pressure distribution on the three-segment trapdoor was uniform and more like a flexible footing on granular material.

To evaluate the effect of trapdoor type (i.e., subsoil movement mode) on the soil arching mobilization and degradation, two tests (T16 and T17) were conducted with the flexible trapdoor as compared with the rigid trapdoor (T14 and T15). They all were supported by six springs. Figures 5.3, 5.4, 5.7, and 5.8 present the pressure distribution on and beside the trapdoor during fill placement and under static surface footing loading in these tests. In the flexible trapdoor for both unreinforced and SL reinforced fill tests, the pressures on the trapdoor edges were significantly higher than those in the rigid trapdoor tests because the outer segments of the flexible trapdoor underwent smaller displacements than those in the rigid trapdoor tests. At the same time, since the middle segment of the flexible trapdoor underwent larger displacements than those in the rigid trapdoor tests, the pressures at TC on the flexible trapdoor were slightly lower than those in the rigid trapdoor. However, the overall average pressures on the flexible trapdoor tests were higher than those in the rigid trapdoor tests, which led to overall higher SARs and SRRs for these tests as shown in Figures 5.13(a), 5.13(c), 5.14(a), and 5.14(c). In conclusion, the mode of soil movement over the trapdoor during the fill placement and under localized footing loading affected the overall degree of soil arching. Use of a one segment rigid trapdoor to evaluate the degree of soil arching, which has been commonly done for the conventional trapdoor test in the past, overpredicts the degree of soil arching.

5.8 DEGRADATION PRESSURE

In this study, an Arching Full Degradation Pressure (AFDP) is proposed and defined as an applied footing pressure required to eliminate soil arching (i.e., the soil arching ratio equals to 1.0). Since the measured pressure on the trapdoor was not uniform during fill placement and under footing loading, it was assumed that the full degradation of center soil arching happened when the pressure at the trapdoor center (TC) in the trapdoor tests (T11-T17) was equal to that in the reference test (T10) (i.e., SAR_c = 1.0 based on the pressure measured at TC on the trapdoor for the unreinforced tests or above the geosynthetic for the reinforced tests). This concept was proposed by Al-Naddaf et al. (2017). Figure 5.10 presents the measured vertical pressures at the trapdoor center (TC) in tests T10-T17 and the corresponding center AFDPs. Figure 5.16 also shows that the vertical pressures at the center of the trapdoor were lower than that measured in the reference test T10 at the total applied pressure up to 90 kPa due to the soil arching effect. As the total pressure increased beyond 90 kPa, the vertical pressure at the center of the trapdoor increased at a faster rate and even exceeded that measured in the reference test T10.

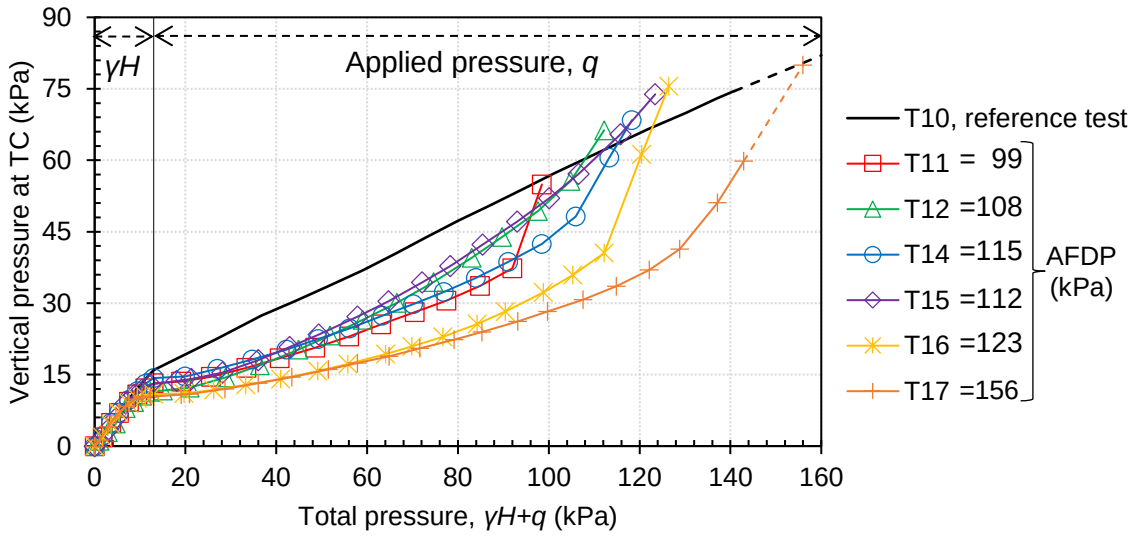

Figure 5.16 Measured vertical pressures at the trapdoor center (TC) in the trapdoor tests T11-T17 versus that at TC in the reference test T10 and their corresponding center AFDPs.

Since the pressure on the trapdoor is not uniform, the full degradation of the center soil arching does not mean the full degradation of soil arching above the trapdoor. Considering the definition of the soil arching ratio (SAR), given in Equation (5.1), the overall AFDP should be determined as the average pressure on the trapdoor with soil arching equal to that without soil arching. In other words, under this applied pressure, the overall soil arching ratio should be equal to 1.0. Therefore, the overall soil arching ratio was calculated based on the average pressure measured on the trapdoor for unreinforced fill tests or on the geosynthetic layer for reinforced fill tests (T11-T17) divided by that of the reference test (T10). Figure 5.14(a) presents the overall soil arching ratios versus the total pressure ($\gamma H+q$) for both unreinforced and SL reinforced fill tests. As discussed earlier, the overall SARs dropped to its minimum as the total pressure increased to 50 kPa. Under the application of static footing pressure and as the total pressure increased beyond 50 kPa, the overall SARs increased and reached unity. This result confirms that mobilized soil arching degraded under static footing loading as observed by Al-Naddaf et al. (2019). Figure

5.14(a) shows that the unreinforced fill tests T11, T14, and T16 had different trends for the overall SARs increasing from 0.39 to 0.47 (T11), 0.45 to 0.5 (T14), and 0.55 to 0.6 (T16) as the total pressure increased from 50.0 to 90.0 kPa. This result indicates that T11 (conducted with a four-spring-supported rigid trapdoor) has the lowest SAR among T14 and T16 (conducted with a six-spring-supported rigid trapdoor and a six-spring-supported flexible trapdoor, respectively). However, since soil arching depends on the mobilized shear stresses within the fill that rely on the soil relative displacement, T11 had a sudden large increase in the trapdoor displacement that caused the shear stresses to yield beyond the soil shear strength as the total pressure increased beyond 90 kPa; therefore, the overall AFDP for T11 was estimated to be 103 kPa by extrapolating the curve to the soil arching ratio equal to 1.0. The overall AFDPs for T14 and T16 were 138 and 120 kPa, respectively. The flexible trapdoor had a higher SAR and a lower AFDP than the rigid trapdoor because the non-uniform trapdoor displacement (i.e., less displacement in the outer trapdoor segments led to less soil arching) caused higher pressures on the trapdoor edges. Figure 5.14(a) shows that the use of SL geosynthetic reinforcement increased the soil arching ratio at the total applied pressure lower than 100 kPa; however, the soil arching ratios for these tests were lower than those in the unreinforced fill tests at the higher total applied pressure (higher than 100 kPa) thus an increase of the footing pressure required to fully degrade soil arching. For instance, the use of the SL geogrid increased the AFDP to 121 kPa in T12, 157 kPa in T15, and 137 kPa in T17. In other words, the use of single geosynthetic reinforcement increased the AFDP by 18%, 14%, and 14%, respectively as compared with those in the unreinforced fill tests when the four-spring-supported rigid trapdoor and the six-spring-supported rigid and flexible trapdoors were used.

Furthermore, Figures 5.14(b) and 5.14(c) present the stress reduction ratios for T11-T17 that show the contribution of the tensioned membrane effect of the geosynthetic to the reduction of the pressure on the trapdoor (i.e., subsoil in GRPS embankments). With the use of SL biaxial geogrid, the applied pressures required to increase SRR to 1.0 were to 174 kPa in T12, 220 kPa in T15, and 152 kPa in T17. In other words, the applied pressures required to degrade soil arching and eliminate the geosynthetic benefits were 69%, 59%, and 27% higher than those in the unreinforced fill tests when the four-spring-supported rigid trapdoor and the six-spring-supported rigid and flexible trapdoors were used respectively. Also, Figure 5.14(b) shows that the applied pressure required to degrade soil arching and eliminate the geosynthetic benefits in DL biaxial geogrid test (T13) was approximately 250 kPa, which is equivalent to a 143% increase as compared with that in the unreinforced fill test (T11). In the SL reinforced fill test, only a tensioned membrane effect dominated the geogrid behavior; while in the DL reinforced fill test, both the tensioned membrane and the beam behavior of the load transfer platform affected stress re-distribution; therefore, the degradation pressure was higher than that in the SL reinforced fill test. More reasons why the test with double reinforcement had a higher degradation pressure are: (1) under the increasing footing pressure, the normalized displacement became large and lateral movement of soil particles increased, which were more effectively restrained by the DL biaxial geogrid, so that the biaxial geogrid carried more tension across the geogrid as discussed earlier in the strain section; and (2) although the limited deflection of the geosynthetic layers minimized their tensioned membrane effect; however, they prevented the excessive displacement of the fill material and thus reduced the chance of yielding in the soil due to the shear stress which is responsible for soil arching.

5.9 ANALYTICAL SOLUTION FOR SOIL ARCHING

Terzaghi (1943) proposed a theoretical solution for describing the soil arching phenomenon based on the results and observations from his trapdoor tests in 1936. He developed an equation, Eq. (5.3), to estimate the vertical stresses above a yielding trapdoor when soil arching is mobilized under soil self-weight plus a uniform surcharge. Equation (5.3) assumes that a sufficient relative movement occurred within the fill material above the trapdoor to mobilize the shear stresses responsible for soil arching. Although Terzaghi (1943) realized that the actual slip planes where the shear stresses are generated are curved when the trapdoor was lowered, he assumed that two vertical slip planes passing through the outer edges of the trapdoor restrain the vertical movement of the yielding soil for simplification and calculation purposes. Also, these slip planes stop at the elevation of a horizontal plane, above which no relative displacement happens. Such a plane is called the equal settlement plane. The soil mass above the equal settlement plane is treated as a surcharge (i.e., no arching effect takes place above this plane). A brief description of Terzaghi's arching theory was provided in Chapter 2.

$$\sigma_v = \frac{B(\gamma - 2c/B)}{2K\tan\emptyset}\left(1 - e^{-2K\tan\emptyset\, h/B}\right) + q'e^{-2K\tan\emptyset\, h/B} \tag{5.3}$$

where σ_v = the vertical stress; B = the width of the trapdoor; γ = the unit weight of soil; c = the cohesion of soil; ϕ = the frictional angle of soil; K = the coefficient of lateral earth pressure; h = the depth from the equal settlement plane; and q' = the uniform surcharge at the soil surface.

The above equation is only valid for a uniform surcharge, and not valid for a localized surface load. In this study, an analytical solution is proposed based on Terzaghi's theory but for a localized footing load applied along the trapdoor centerline. In the proposed solution, Terzaghi's assumptions are applied; however, the equal settlement plane is assumed to exist at the surface of

the fill because the applied footing load will induce additional differential settlement in the fill that would increase the degree of soil arching. Figure 5.17 shows a free body diagram for a soil element within the yielding zone above the trapdoor, on which the normal stresses are assumed to be uniform across the horizontal sections. For the horizontal thrust on the soil element, a coefficient of lateral stress K is constant. Also, the effect of the footing load on the horizontal thrust on the soil element is considered by assuming that the footing pressure is distributed along the fill height with a distribution factor β. Cohesion c is assumed to exist along the slip planes. The vertical force equilibrium of the soil element at depth h below the fill height is given by Equations (5.4) and (5.5). Solving Eq. (5.4) or (5.5) by satisfying the boundary condition in Eq. (5.6) leads to Eq. (5.7), an equation to estimate the average vertical stress (σ_v) within the yielding soil zone above the trapdoor under localized footing loading.

$$\mathrm{B}\gamma \mathrm{d}h = -B\sigma_v + B(\sigma_v + \mathrm{d}\sigma_v) + 2\,(\mathrm{c} + \sigma_h\ \tan\emptyset)\,\mathrm{d}h \tag{5.4}$$

or

$$\frac{d\sigma_v}{dh} = \gamma - \frac{2c}{B} - \frac{2(\beta q + \sigma_v)K\ tan\,\emptyset}{B} \tag{5.5}$$

$$\sigma_v = q \quad and \quad \beta = 0 \quad for \quad h = 0 \tag{5.6}$$

$$\sigma_v = \frac{B(\gamma - 2c/B)}{2K\tan\emptyset}\left(1 - e^{-2K\tan\emptyset\ h/B}\right) + q\left(e^{-2K\tan\emptyset\ h/B} - \beta\right) \tag{5.7}$$

where σ_v = the vertical stress; B = the width of the trapdoor; γ = the unit weight of soil; c = the cohesion of soil; ϕ = the frictional angle of soil; σ_h = the horizontal stress [$\sigma_h = K(\beta q + \sigma_v)$]; K = the coefficient of lateral earth pressure; β = the distribution factor for the footing pressure calculated at h; h = the depth from the fill surface; H = the fill height; and q = the applied footing pressure at the soil surface.

It should be noted that both Terzaghi's and the proposed solutions yield the same equation and result if no localized footing pressure or a uniform surcharge (i.e., $\beta = 0$) is applied. Same as Terzaghi's solution, the proposed solution assumes that the fill weight and the footing load would induce sufficient (not large) relative movement in the fill that mobilizes soil arching. As discussed earlier, mobilized soil arching would degrade (i.e., yield under the shear stresses) under a high footing pressure that causes a large trapdoor displacement. Therefore, the proposed solution does not predict the vertical pressure on the trapdoor when soil arching degrades.

To verify the proposed solution with the measured pressures on the trapdoor in the tests conducted in this study, all parameters of this solution are based on the soil property, trapdoor width, and fill height except for K and β. The Rankine active earth pressure coefficient, K_a = (1- sin ϕ) / (1+ sin ϕ), was used here because a normalized trapdoor displacement of approximately 1.0% initiated the mobilization of soil arching in these tests. This is consistent with Marston and Anderson's (1913) suggestion of using K_a when soil arching is triggered by a small deformation. This K_a was also used by Al-Naddaf et al. (2018) for the soil arching calculation above the induced trench installation method of a concrete box culvert. The footing pressure distribution factor (β) was calculated using either Boussinesq's solution or the 2V:1H distribution mothed as demonstrated in Figure 5.18. When (β) was calculated based on the Boussinesq's solution, Equation (5.8) was used to obtain the distribution factor for six different points along the top of the trapdoor; then an average value was considered for (β). Also, Equation (5.9) was used to calculate the distribution factor (β) based on the 2V:1H distribution mothed.

$$\beta = \frac{1}{B}[\alpha + \sin\alpha \ \cos(\alpha + 2\delta)] \quad \text{At a specific point (A)} \tag{5.8}$$

$$\beta = \frac{B}{(B+z)} \tag{5.9}$$

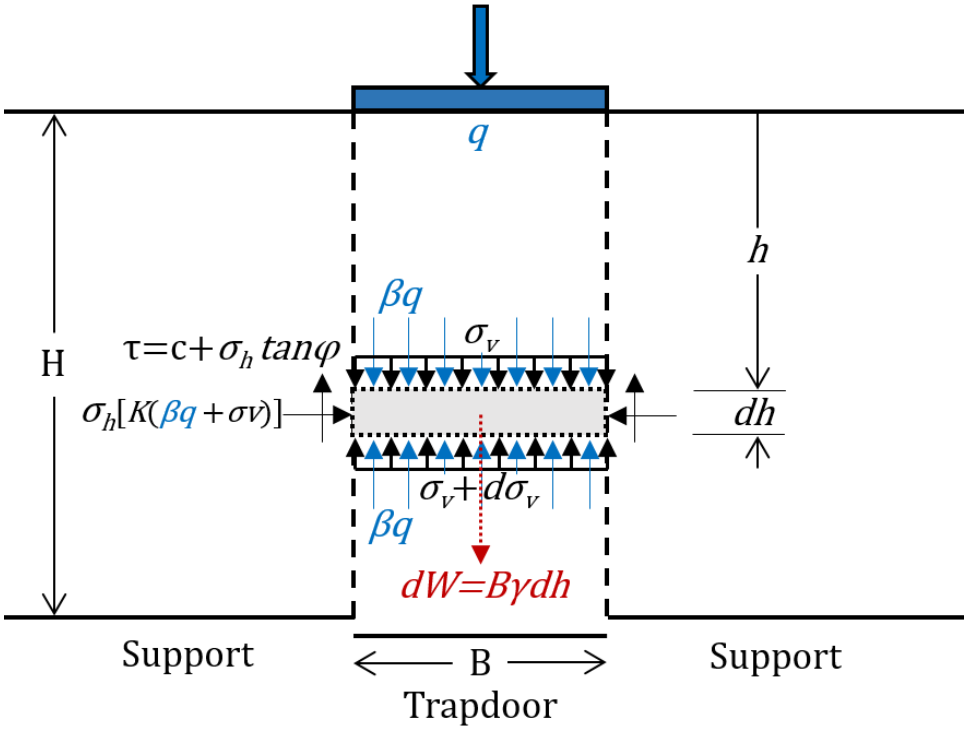

Figure 5.17 Forces on a soil element above the trapdoor under localized surface footing (modified from Terzaghi, 1943).

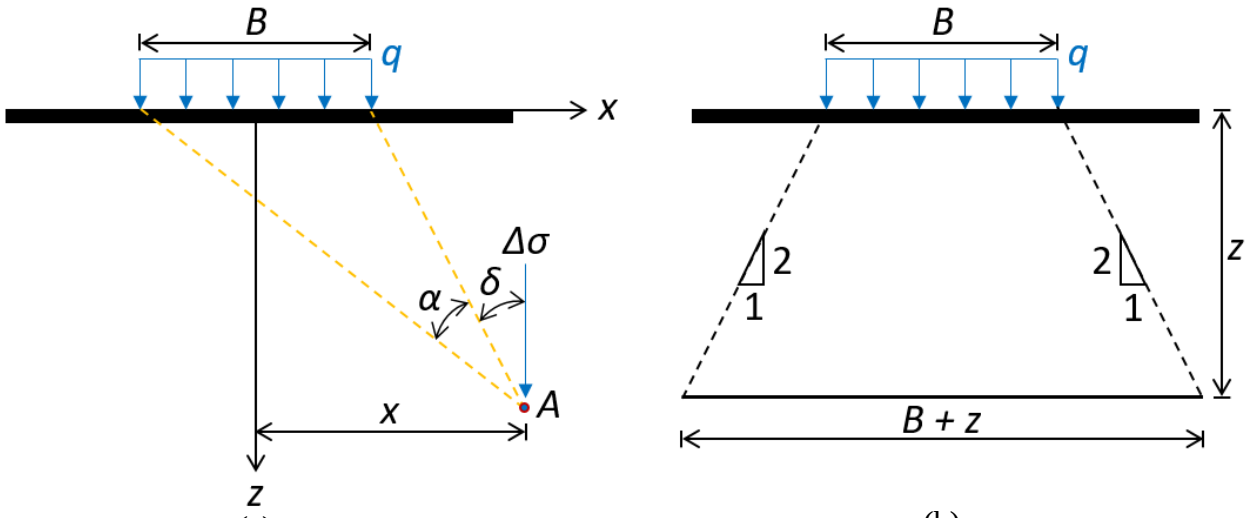

Figure 5.18 Footing pressure distribution methods: (a) Boussinesq's distribution; (b) 2V:1H distribution method

Figure 5.19 shows the comparison of the measured pressures on the trapdoor for the unreinforced tests (T11, T14, and T16) and on the geosynthetic for the reinforced tests (T12, T15, and T17) with the predicted pressures based on the proposed solution versus the total pressure ($\gamma H+q$). Since a small trapdoor displacement occurred (less than 1.0% of B) at the beginning of fill placement, Figure 5.19 shows that Terzaghi's solution or the proposed solution overestimated the vertical pressures on the trapdoor; however as the fill height increased, the predicted pressures match better with the measured pressures. Most importantly, the proposed solution well predicted the measured vertical pressures on the trapdoor under localized static footing loading.

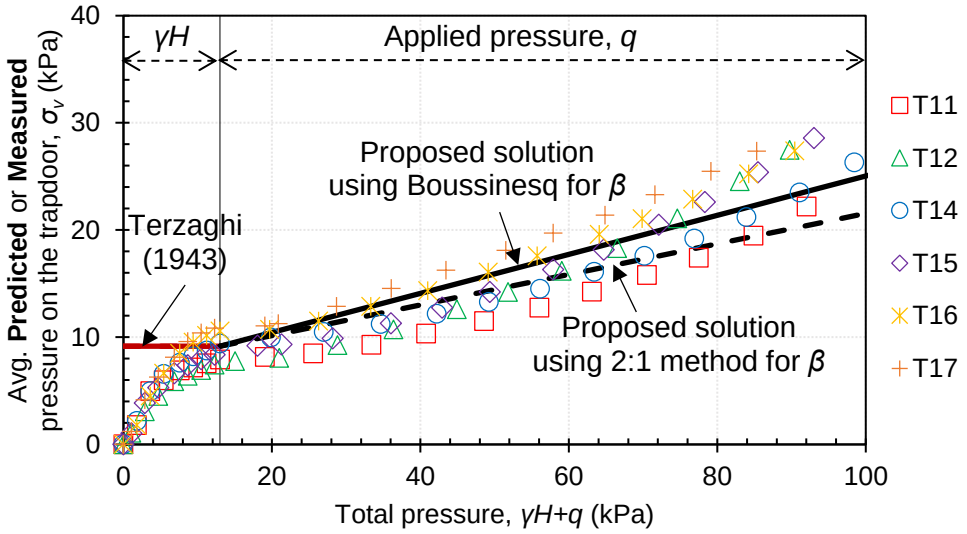

Figure 5.19 Measured and predicted average vertical pressures on the trapdoor under footing loading.

5.10 PRESSURE DISTRIBUTION UNDER CYCLIC FOOTING LOADING

The effects of soil arching and the contributions of geosynthetic reinforcement on the performance of GRPS embankments under localized static loading have been extensively discussed in previous sections to better understand these complex load transfer mechanisms. However, static loading does not represent the dominating loading type in transportation applications. This section discusses the soil arching mobilization and degradation under cyclic loading in an effort to better simulate traffic loading. In this study, four tests (T18-T21) were conducted under cyclic footing loading after placement of fill material, among which no trapdoor movement was allowed for one of the tests (T18). The other three tests were performed with a four-spring-supported rigid trapdoor (T19), a six-spring-supported rigid trapdoor (T20), and a six-spring supported flexible (T21) trapdoor, in which the trapdoor was allowed to move and soil arching was mobilized during the fill placement stage and under cyclic footing loading. Since the fill placement stages of these tests were completed under the same layout as those tested under static footing loading which were discussed earlier, the overburden stresses on and besides the trapdoor during the fill placement stage in these tests are not presented herein.

Figures 5.20 to 5.23 present the measured pressures at the center and the edges of the trapdoor, and the edges of the stationary support during the surface loading stage of tests T18-T21. In T18, the pressure on the trapdoor centerline (TC) increased the most as compared with those at other locations (TE and SE) as shown in Figure 5.20. Also, the amplitude for the measured pressure at TC was larger than those at other locations, TE and SE (SE had the smallest amplitude). The difference became even larger as the applied pressure increased as shown in Figure 5.20(b). In T19-T21 (the trapdoor was allowed to move), the pressure at SE increased the most and was higher than those at TC and TE due to the soil arching mobilization as shown in Figures 5.21 to 5.23.

Also, different from the reference test T18, the pressure at TC had a smaller amplitude than that at SE while the pressure at TE had the smallest amplitude. Since the shear stresses responsible for soil arching are concentrated along the slip planes between the trapdoor and the supports, the pressure at SE had the largest amplitude while that at TE had the smallest amplitude.

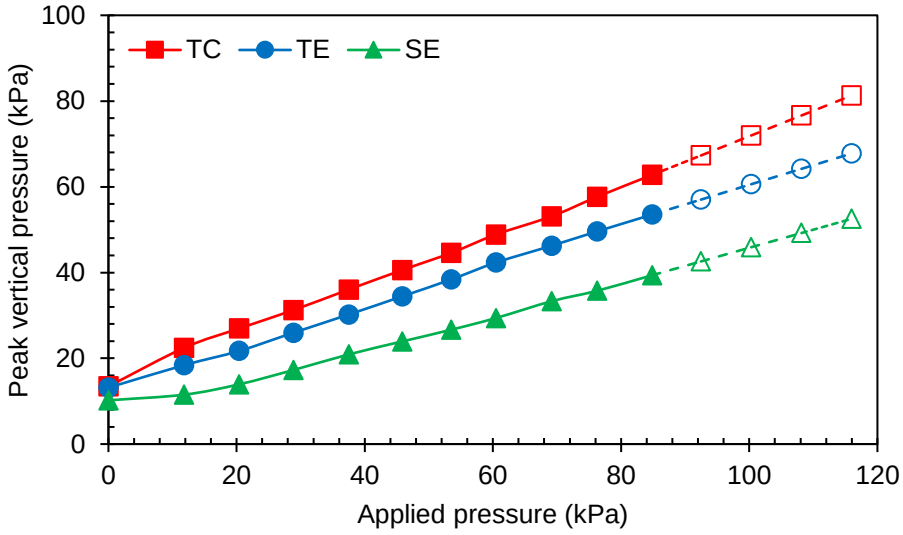

(a)

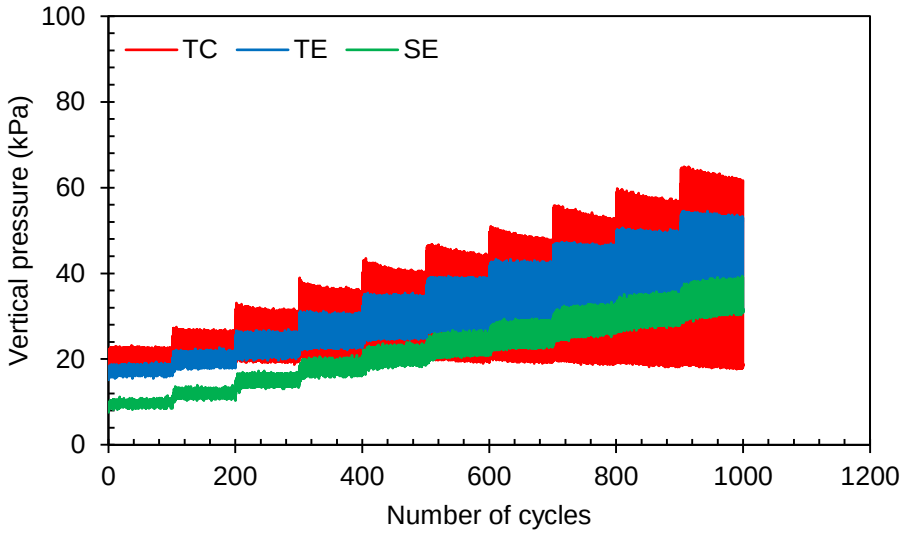

(b)

Figure 5.20 Measured vertical pressures on and besides the trapdoor under cyclic footing loading in T18 versus: (a) applied pressure and (b) number of cycles.

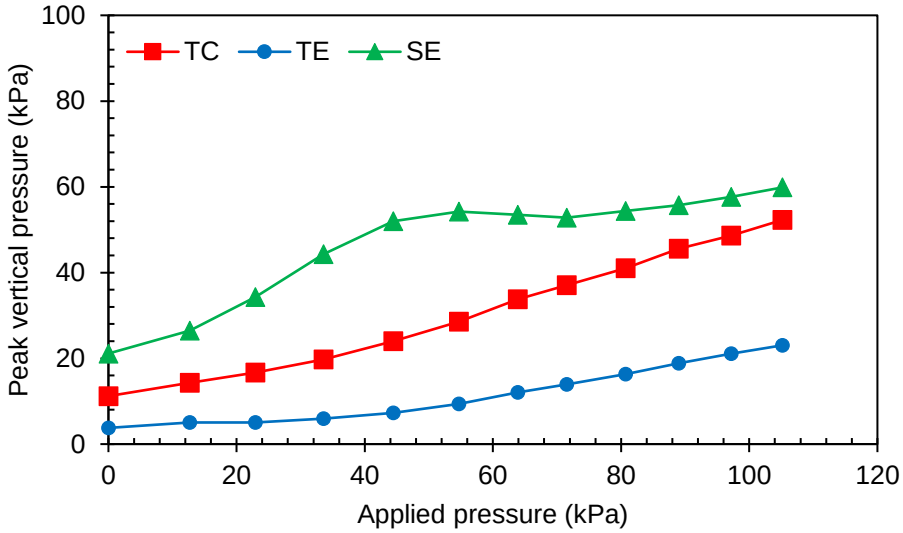

(a)

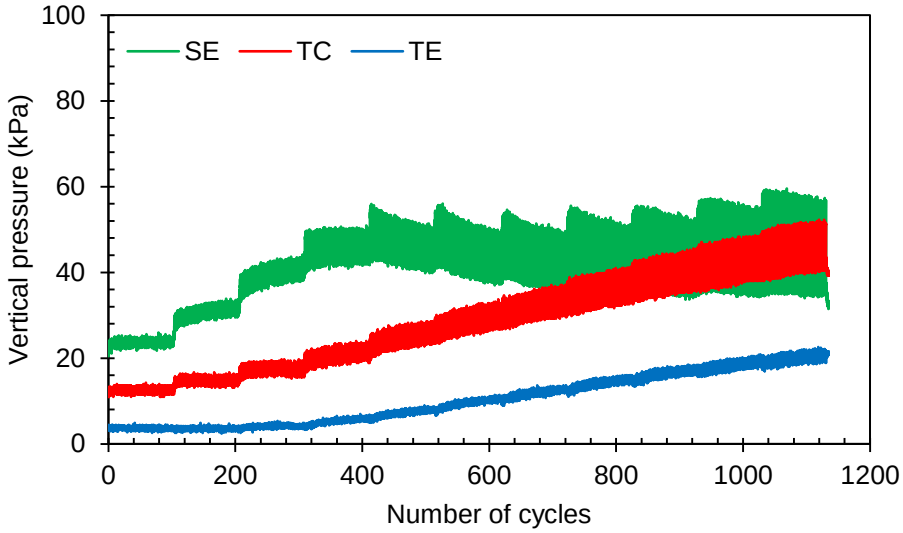

(b)

Figure 5.21 Measured vertical pressures on and besides the trapdoor under cyclic footing loading in T19 versus: (a) applied pressure and (b) number of cycles.

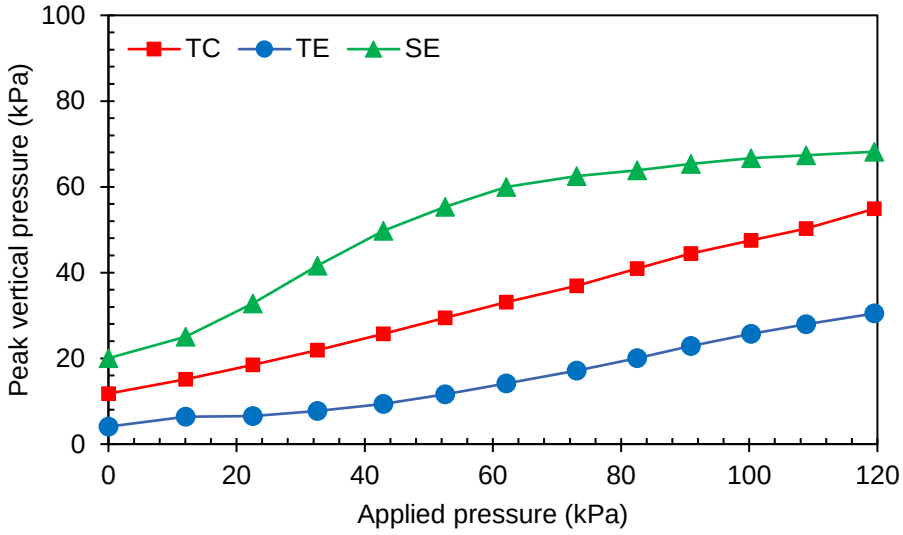

(a)

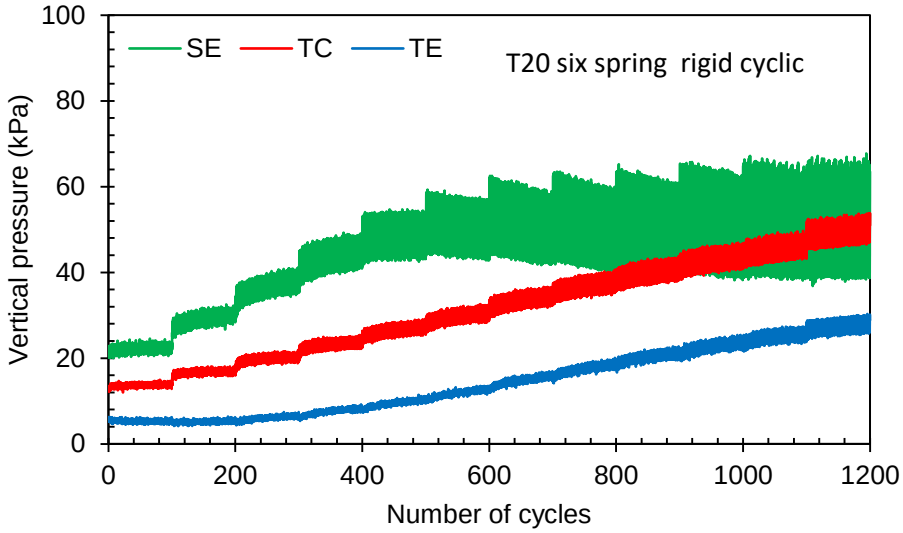

(b)

Figure 5.22 Measured vertical pressures on and besides the trapdoor under cyclic footing loading in T20 versus: (a) applied pressure and (b) number of cycles.

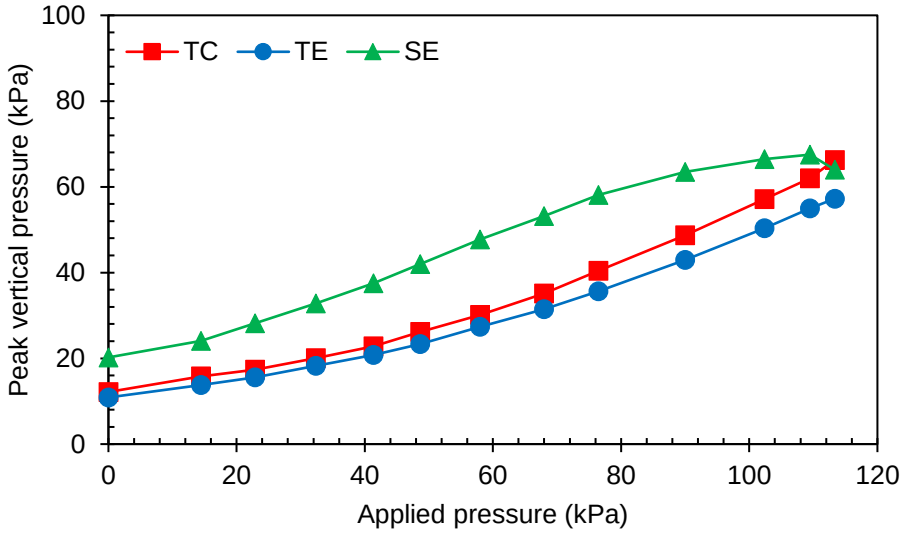

(a)

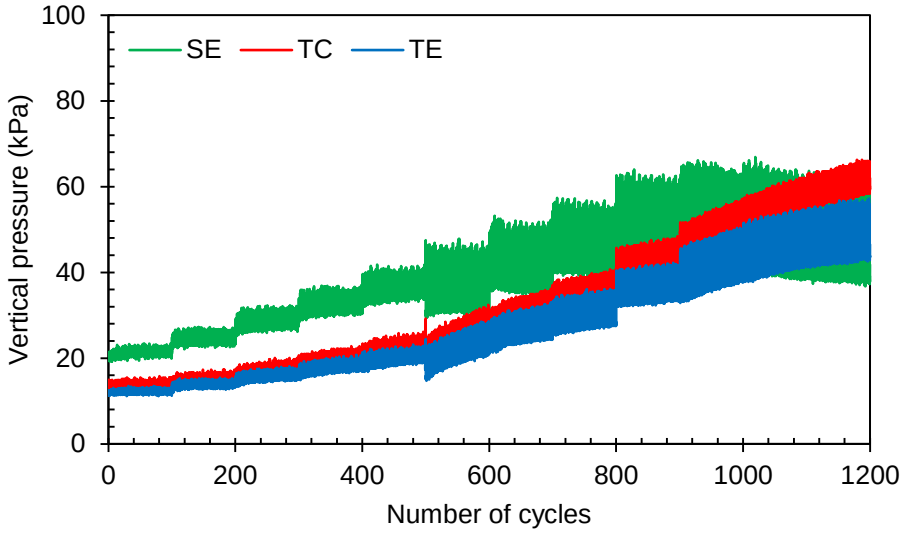

(b)

Figure 5.23 Measured vertical pressures on and besides the trapdoor under cyclic footing loading in T21 versus: (a) applied pressure and (b) number of cycles.

The effect of cyclic loading as compared to static loading can be explained in terms of the Dynamic Magnification Factor (DMF), which is defined as the ratio of the measured pressure under cyclic loading to that under static loading at the same magnitude of applied pressure as given in Equation (5.10). Figure 5.24 shows the DMF calculated based on the average vertical pressures

on the trapdoor with and without soil arching. In general, cyclic loading increased the pressure on the trapdoor as compared to static loading because the DMF was higher than 1.0. In the tests without soil arching, the DMF increased from 1.0 to 1.2 as the footing pressure increased to approximately 120 kPa. This behavior can be explained by the fact that the pressure under cyclic loading was distributed onto a narrower area than that under static loading. In other words, the pressure distribution angle would be smaller with the increased number of load cycles. This result is consistent with Giroud and Han's (2004) finding for the change in the distribution angle under cyclic loading in roadway applications. However, the effects of cyclic loading were more pronounced in the tests when soil arching was mobilized because the DMF increased from 1.0 to 1.4 as the footing pressure increased to approximately 80 kPa. This result indicates that soil arching was less effective in reducing the pressure on the trapdoor under cyclic loading as under static loading.

$$DMF = \frac{\sigma_{v(cyclic)}}{\sigma_{v(static)}} \tag{5.10}$$

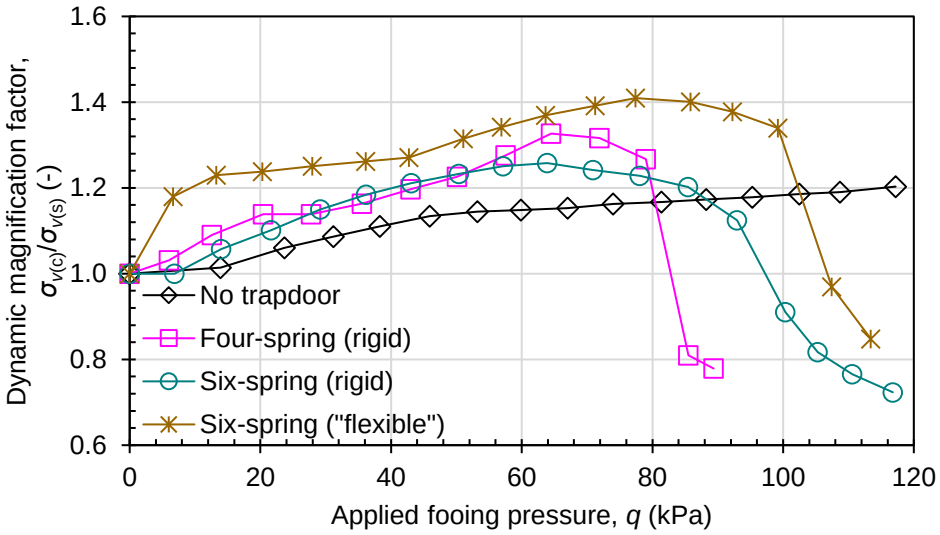

Figure 5.24 Dynamic magnification factors over the trapdoor with and without soil arching

Figure 5.24 also shows that the DMF for the tests with soil arching dropped after a certain applied pressure, this drop is corresponding to the sudden increase in the pressure over the trapdoor in the tests under static loading (i.e., $\sigma_{v(static)}$) as discussed earlier for the Figures 5.6 to 5.8.

Figure 5.25 presents the variation in the soil arching ratio (SAR) versus the normalized trapdoor displacement (δ/B) and the total pressure ($\gamma H+q$) in T19-T21. In these tests, the SAR was calculated based on Equation (5.1) and same as described earlier in Section 5.4. During the fill placement stage, soil arching was mobilized under soil-weight self only; thus the denominator of Equation (5.1) was the theoretical overburden stress (γH).Under cyclic footing loading, however, the denominator in Equation (5.1) was the average measured pressure on the trapdoor in the reference test, T18, in which no trapdoor movement was allowed. Figure 5.25 shows that soil arching was mobilized as the fill height increased to 720 mm in T19-T21. A higher degree of soil arching was reached as the cyclic footing pressure was increased to approximately 35 kPa (or 48 kPa for the total pressure). Although the minimum SARs under cyclic loading (0.41 in T19, 0.48 in T20, and 0.62 in T21) were less than those under static loading at the low applied pressure (48 kPa for the total pressure), the degree of soil arching under cyclic loading was higher (i.e., lower SAR) than that under static loading at the total pressure of more than 80 kPa. For instance, at the total pressure of 120 kPa, the SARs in T19, T20, and T21 were 0.55, 0.55, and 0.82, respectively, while those in T11, T14, and T16 were > 1.0, 0.81, and 1.02. Therefore, soil arching exhibited arching degradation and even collapse under static loading which was less pronounced under cyclic loading as the applied pressure increased beyond 80 kPa. This phenomenon can be explained by the fact that cyclic loading induced more differential displacement within the fill than static loading that generates more shear stresses thus more soil arching, which helps transfer the pressure away from the yielding base to the supports.

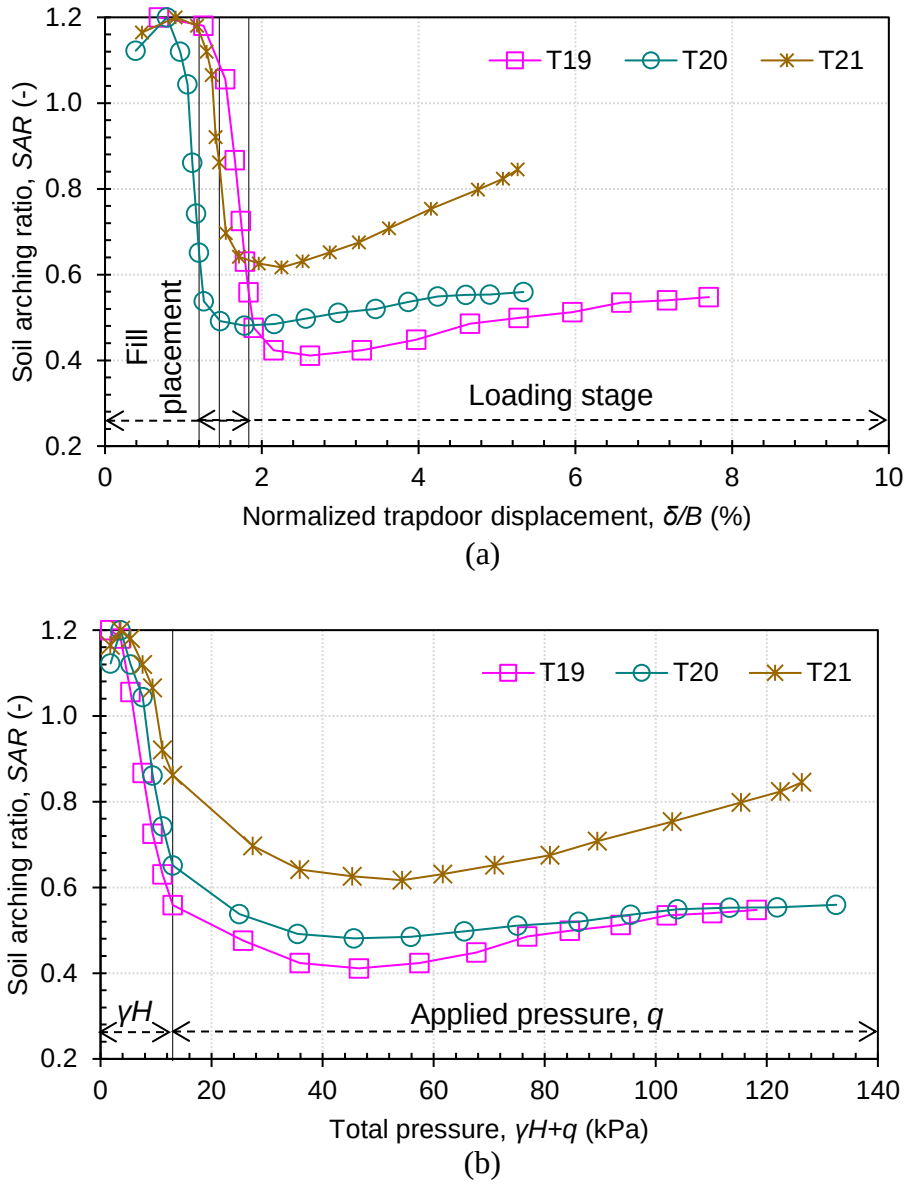

Figure 5.25 Soil arching ratios in the tests with a four-spring-supported rigid trapdoor, a six-spring-supported rigid trapdoor, and a six-spring-supported flexible trapdoor versus: (a) normalized trapdoor displacement and (b) total pressure.

CHAPTER 6 TWO-DIMENSIONAL NUMERICAL SIMULATION OF TRAPDOOR TESTS

This chapter presents the numerical models that simulate the trapdoor tests conducted in this study under static footing loading. The aim of these numerical simulations is to study the most critical condition of surface loading in terms of the footing width and location on the soil arching mobilization and degradation. Also, this study investigated the effects of the non-uniform trapdoor displacement (e.g., the use of the multi-segment trapdoor) and the fill height under footing loading on the degree of soil arching. This chapter discusses the selection of materials and the calibration of parameters used in these numerical models, including the properties of the fill material, the layout of the trapdoor, and the width and location of the footing. This chapter also discusses the interfaces and their properties between footing and fill material, trapdoor and fill material, support and fill material, and trapdoor and supports. After the calibration of the material properties, the numerical models were verified against the experimental results presented in Chapter 5.

6.1 NUMERICAL MODELING

6.1.1 Numerical Software

Fast Lagrangian Analysis of Continua (FLAC), a three-dimensional finite difference program, FLAC^{3D} Version 5.0, was used in this study. Although the trapdoor tests investigated in this study are plane-strain and two-dimensional, the 3D version of the FLAC software was used. The main reason is that these models will be expanded to three-dimensional models to simulate the field condition of pile-supported embankments in the future. FLAC^{3D} software uses an explicit finite difference method to solve problems with initial and boundary conditions. This software supports

several constitutive models, structural elements, interfaces, and boundary conditions to model various geotechnical materials and structures.

6.1.2 Typical Numerical Model

Figure 6.1 shows the layout of a typical numerical model, which includes fill material, trapdoor, a compressible medium underneath the trapdoor, supports, footing, and interfaces used to simulate the trapdoor test in this study.

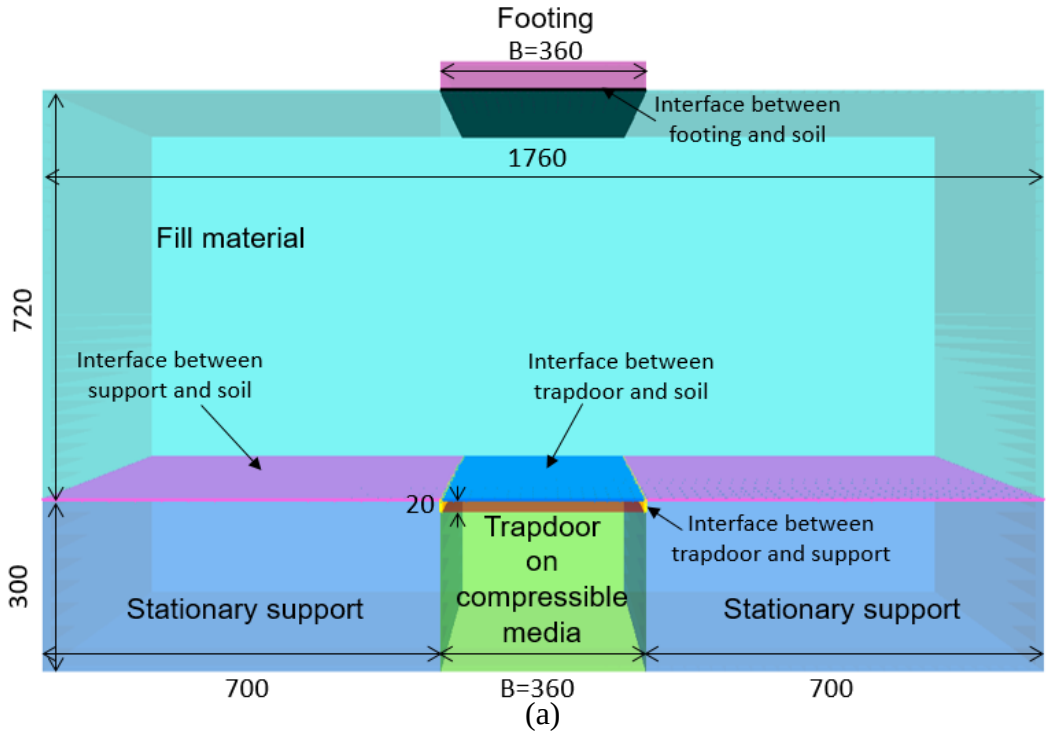

Figure 6.1 Typical numerical model for the trapdoor test: (a) the front view showing the model zones (all dimensions in millimeters) and (b) the 3D view showing the mesh size.

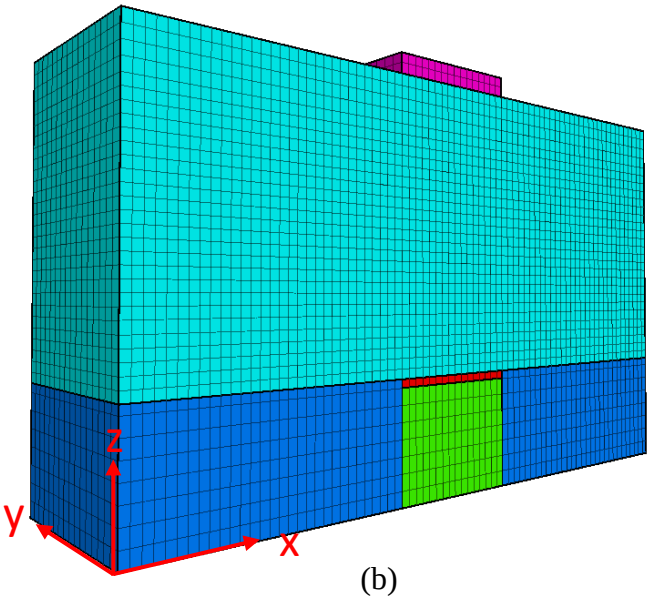

(b)

Figure 6.1 Typical numerical model for the trapdoor test: (a) the front view showing the model zones (all dimensions in millimeters) and (b) the 3D view showing the mesh size (Continued).

6.1.3 Constitutive Models

Two types of constitutive models were utilized in this study. The first constitutive model was the linearly elastic model that was employed to model the footing, the trapdoor, the compressible medium underneath the trapdoor, and the stationary supports. This constitutive model has a linear relationship between the stress and the axial strain, and the behavior of the materials mainly depends on two parameters: (1) elastic modulus E and (2) Poisson's ratio v. The second constitutive model was the linearly elastic-perfectly plastic model with a Mohr-Coulomb (MC) failure criterion, which was adopted to simulate the fill material in this study. This constitutive model has been intensively used to simulate fill materials in numerical modeling of pile-supported embankments and trapdoor problems (e.g., Russell and Pierpoint 1997; Kempton et al. 1998; Laurent et al. 2003; Chevalier et al., 2007; Han et al. 2007; Zhao and Cao 2012). The parameters of the Mohr-Coulomb model are the frictional angle ϕ, the cohesion c, the dilation angle ψ, the elastic modulus E, and Poisson's ratio v of the fill.

6.1.4 Interfaces

FLAC^{3D} provides different types of interfaces (e.g., bonded interface, slip while bonded, and Coulomb sliding) that can be used between the planes where the sliding or separation may happen to connect different zone faces together. In this study, the interaction of two different zones was controlled by a defined interface element. The interfaces between the footing and the fill, the trapdoor and the fill, the supports and the fill, and the trapdoor and the supports were characterized by the Coulomb sliding and shear bonding. The interface element is attached to the face of zone elements (target face) and the mechanical behavior of the interface is governed by the properties of friction, cohesion, dilation, normal and shear stiffness, and tensile and shear bond strengths as shown in Figure 6.2.

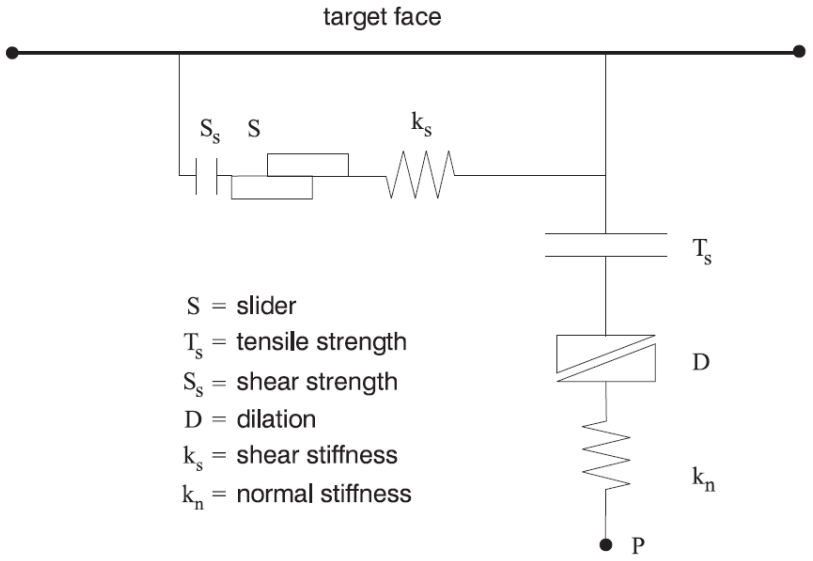

Figure 6.2 Components of the bonded interface constitutive model (Itasca 2014)

6.2 CALIBRATION OF PARAMETERS

Laboratory tests were conducted to determine the soil parameters required for the Mohr-Coulomb model.

6.2.1 Fill Material

The Kansas River sand was used in the experimental study and had a peak frictional angle of 38º based on three triaxial shear tests. The unit weight of this sand was 18.04 kN/m^3 at a relative density of 75%. The elastic modulus was determined from the initial slope of the deviator stress-axial stain curve to be 25 MPa. Poisson's ratio was assumed to be 0.3. Table 6.1 summarizes the parameters of the fill material. These parameters were used to model the triaxial tests as shown in Figure 6.3. Figure 6.4 shows that the numerical results are compared reasonably well with those of the triaxial shear tests.

Table 6.1 Properties of fill material used in the numerical models

Parameters	Unit	Value
Peak frictional angle (ϕ)	Degree	38
Cohesion (c)	kPa	0
Dilation angle (ψ)	Degree	0
Elastic modulus (E)	MPa	25
Poisson's ratio (ν)	-	0.3

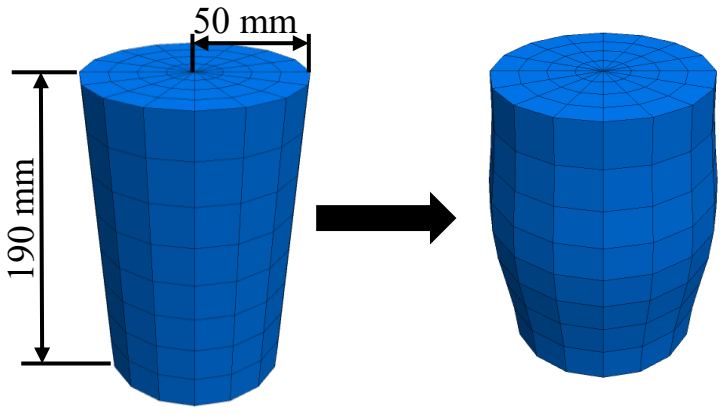

Figure 6.3 Numerical simulation of the triaxial test.

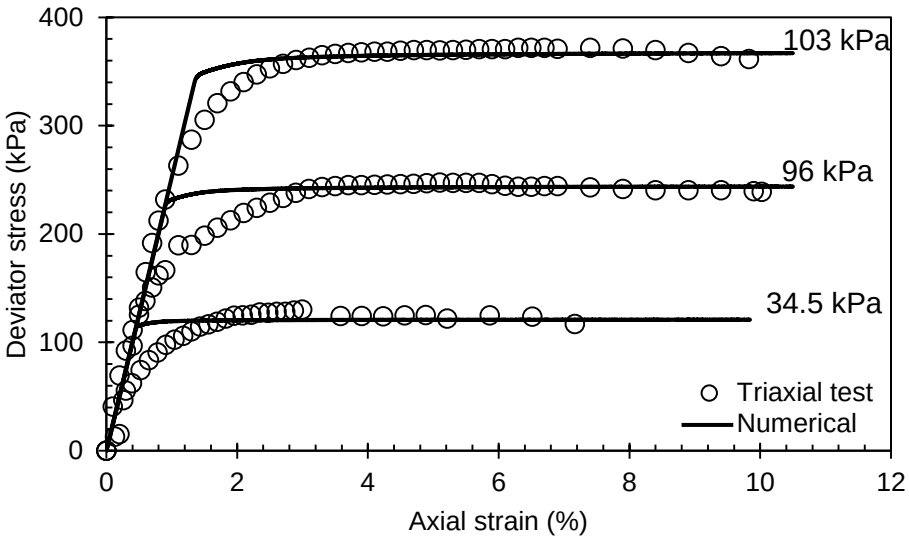

Figure 6.4 Numerical results versus triaxial shear test results.

6.3 VALIDATION OF NUMERICAL MODELS

To simulate trapdoor tests under static footing loading, the numerical models were built and verified with the experimental test results using the material properties and constitutive models discussed in the previous sections. The validation of the numerical models was achieved using three experimental tests T10, T11, and T14 by comparing their trapdoor displacements, footing displacements, and vertical pressures on and besides the trapdoor during fill placement and footing loading.

Figure 6.1 shows a typical numerical model, which was used to simulate a trapdoor test, including the fill material, the trapdoor on a compressible medium, the supports, the footing, and the interfaces. In the model, the nodes on the right and left boundaries were fixed in the x-direction only, and the nodes on the front and back boundaries were fixed in the y-direction only to simulate a plane-strain condition. The nodes at the bottom boundary were fixed in x, y, and z directions. The material properties and dimensions in the numerical model were the same as those in the

experimental test. For instance, since the material of the footing was steel, and the trapdoor and supports were wood, their properties in the numerical model were the same as those for the steel and wood. However, the compression springs that were utilized to support the trapdoor in the experimental test were simulated by a compressible elastic medium of the same total stiffness as the springs underneath the trapdoor. Table 6.2 summarizes the constitutive models, the material types, and their properties. The elastic modulus of the compressible medium was calculated based on the number of springs and their stiffness. This modulus was also checked against the results of the experimental tests with four-spring-supported (T11) and six-spring-supported (T14) rigid trapdoors during their fill placement as shown in Figure 6.5.

Table 6.2 Material properties used in the numerical models.

Zone	**Model**	**Type**	**Property**
Fill Material	Mohr-Coulomb	Soil (sand)	as in Table 6.1
Trapdoor	Linear elastic	Wood	E = 12.5 GPa; ν = 0.25
Compressible medium	Linear elastic	-	E = 0.32 or 0.48 MPa; ν = 0.3
Stationary supports	Linear elastic	Wood	E = 12.5 GPa; ν = 0.25
Footing	Linear elastic	Steel	E = 25 GPa; ν = 0.3

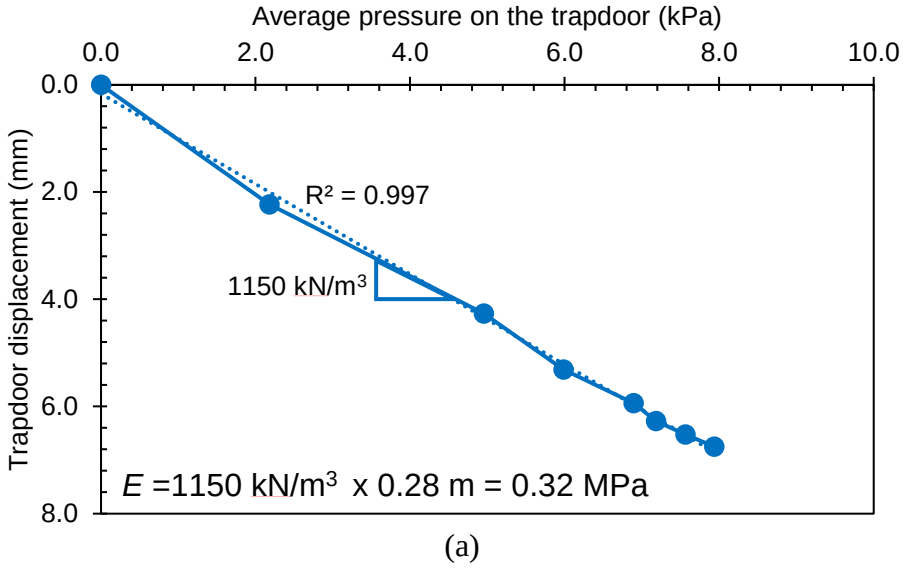

(a)

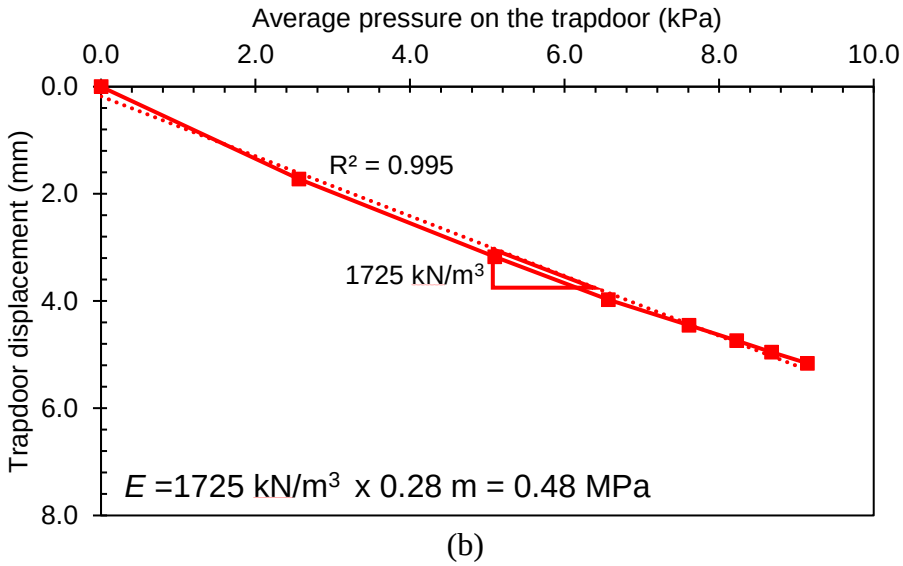

(b)

Figure 6.5 Average pressure on the trapdoor versus its displacement during fill placement stage of the experimental test: (a) T11; and (b) T14.

Four different interfaces were generated between the footing and the fill, the trapdoor and the fill, the supports and the fill, and the trapdoor and the supports. All the interfaces were assumed to have zero cohesion and dilation angle. The interface frictional angles were determined by multiplying the peak friction angle of the fill by the interaction coefficients, which were assumed

to be 0.6 between the soil and the steel (i.e., footing) and 0.8 between the soil and wood (i.e., trapdoor and supports). Therefore, the interface frictional angle between the footing and the fill was 23º while the interface frictional angle between the trapdoor or support and the fill was 30º. Furthermore, the interface frictional angle between the trapdoor and the supports was assumed to be 20º because a smooth plastic washer was used between the trapdoor and the supports in the experimental tests. The normal (k_n) and shear (k_s) stiffness values for all interfaces were calculated using Equation (6.1), which is suggested by Itasca (2014). It is worth mentioning that no interaction was allowed between the compressible medium and the supports by deleting the zone elements in-between.

$$k_n = k_s = max\left[\frac{\left(K+\frac{4}{3}G\right)}{\Delta Z_{min}}\right] \tag{6.1}$$

where K = the bulk modulus, G= the shear modulus, and Δz_{min} = the smallest element size of the adjacent zone perpendicular to the interface element.

To verify the model parameters without the soil arching effect and compare the numerical results with the reference test (T10) results, a numerical model was built and tested under static footing loading. Figure 6.6 shows a reasonable agreement of the footing displacement and the vertical pressures on and besides the trapdoor between the numerical results and the experimental results.

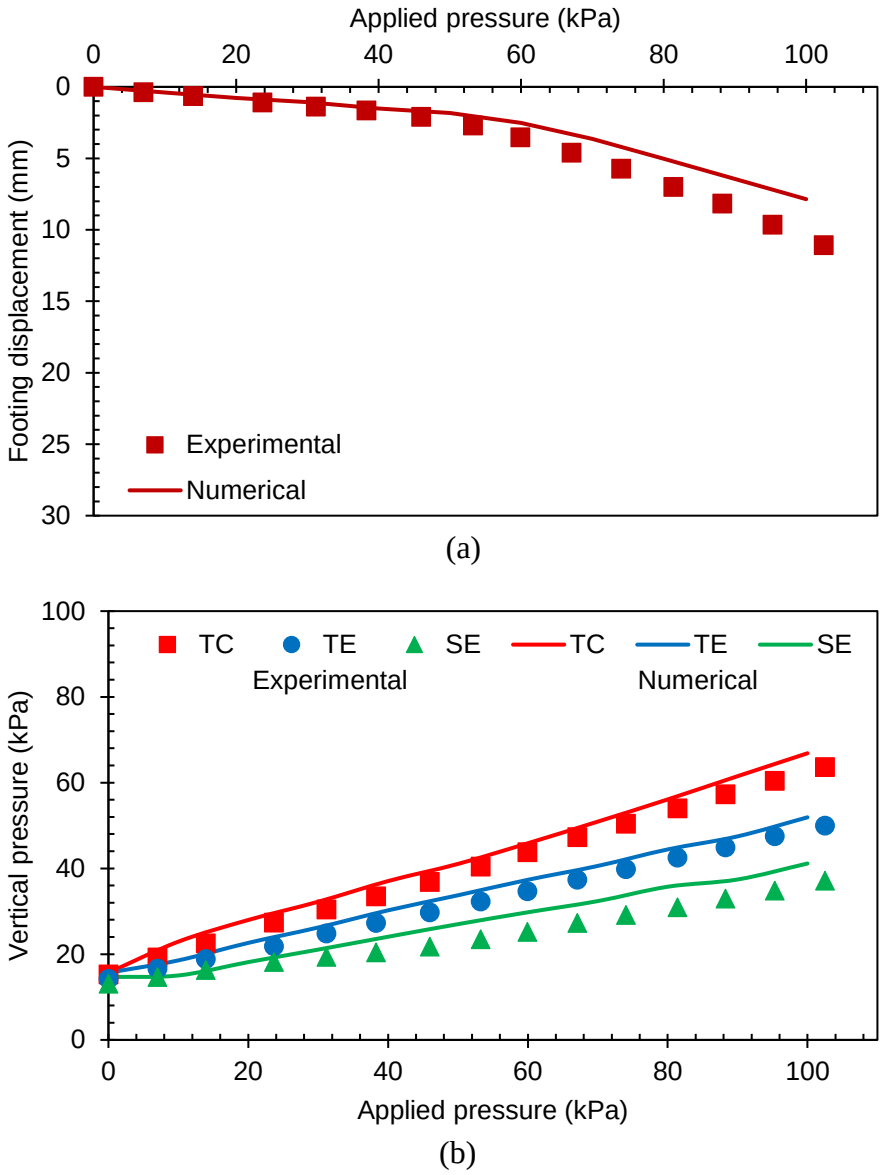

Figure 6.6 Numerical versus experimental results for T10 under static footing loading: (a) footing displacement and (b) vertical pressures on and besides the trapdoor.

In all numerical models with soil arching, the fill placement sequence was simulated with seven equal lifts, the trapdoor was allowed to settle based on its stiffness, and therefore the fill underwent differential settlement and mobilized soil arching. A compaction effort (i.e., a uniform vertical stress of 0.8 kPa) on the top of each fill lift was applied to simulate the fill placement sequence in the experimental tests. The magnitude of this effort (i.e., 0.8 kPa) was determined based on the increase in the vertical pressure after the application of compaction during the experimental tests. This effort was kept during the whole simulation. Following the fill placement, a monotonic footing pressure with each increment of 10 kPa was applied on the fill surface. Figures 6.7 to 6.9 show the numerical results for the model with the low stiffness trapdoor (i.e., 1150 kN/m^3 or E = 0.32 MPa) as compared with the experimental results. Figures 6.10 to 6.12 show the numerical results for the model with the high stiffness trapdoor (i.e., 1725 kN/m^3 or E = 0.48 MPa). These figures show that the numerical results matched reasonably well with the experimental data. However, as the applied pressure increased beyond 80 kPa for the low stiffness trapdoor test and 95 kPa for the high stiffness trapdoor test as shown respectively in Figures 6.8 and 6.10, the trapdoor and footing displacement results of the experimental tests were higher than those of the numerical models. The increase in the trapdoor and footing displacements of the experimental tests was due to soil arching degradation that caused a sudden increase in the pressure on the trapdoor. The numerical model with the high stiffness trapdoor was adopted for the following parametric study.

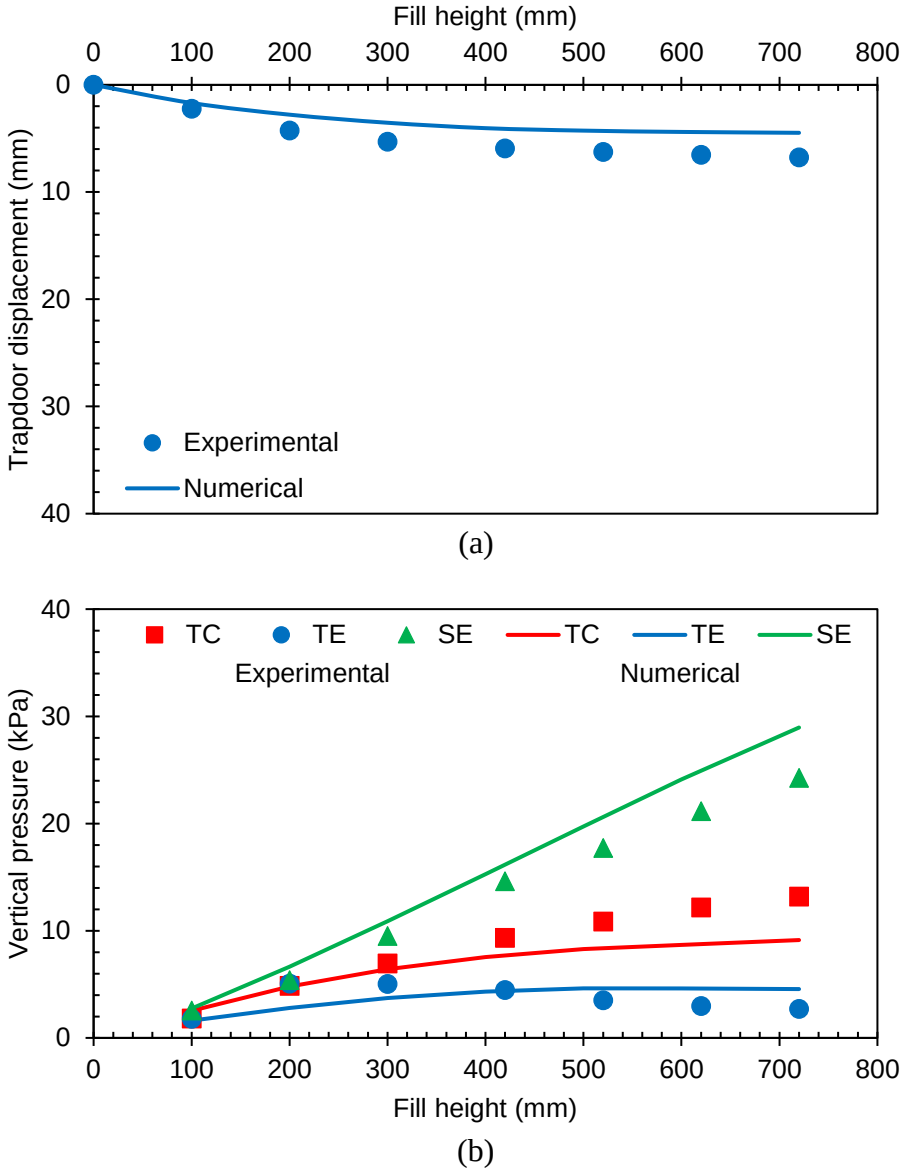

Figure 6.7 Numerical versus experimental results for T11 during the fill placement: (a) trapdoor displacement and (b) vertical pressures on and besides the trapdoor.

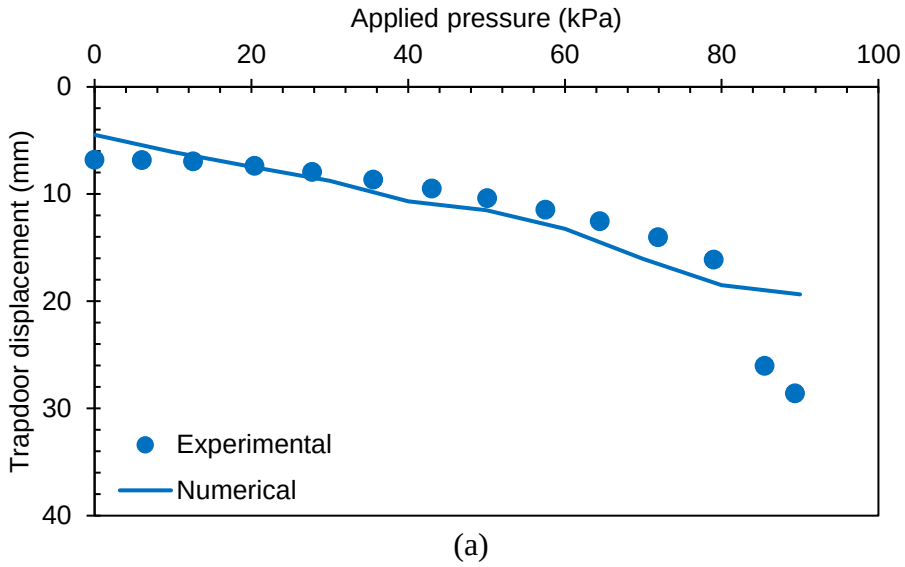

(a)

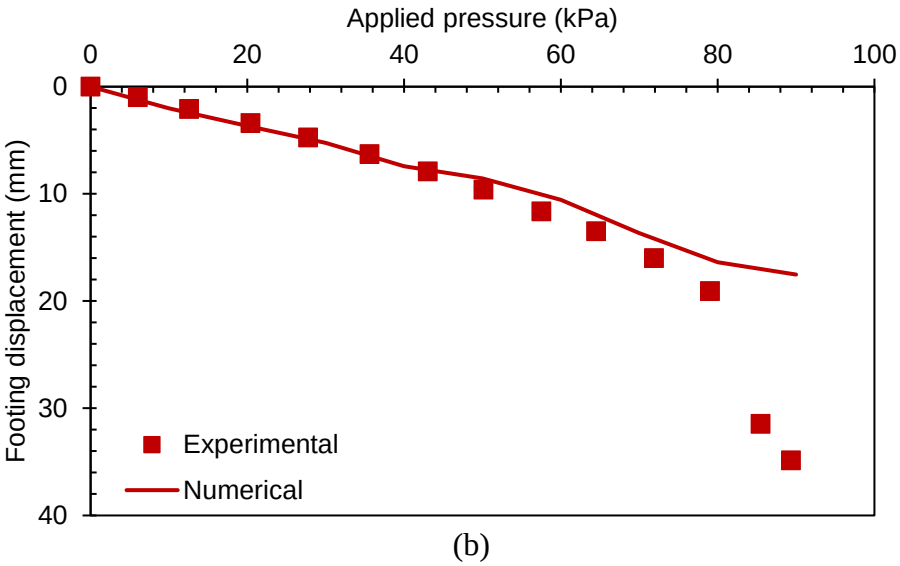

(b)

Figure 6.8 Numerical versus experimental results for T11 under static footing loading: (a) trapdoor displacement and (b) footing displacement.

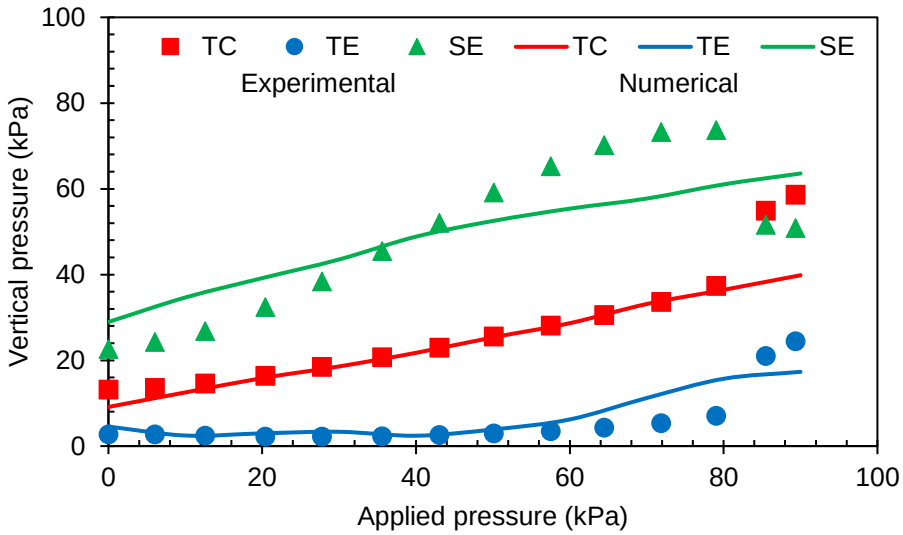

Figure 6.9 Numerical versus experimental results for vertical pressures on and besides the trapdoor in T11 under static footing loading.

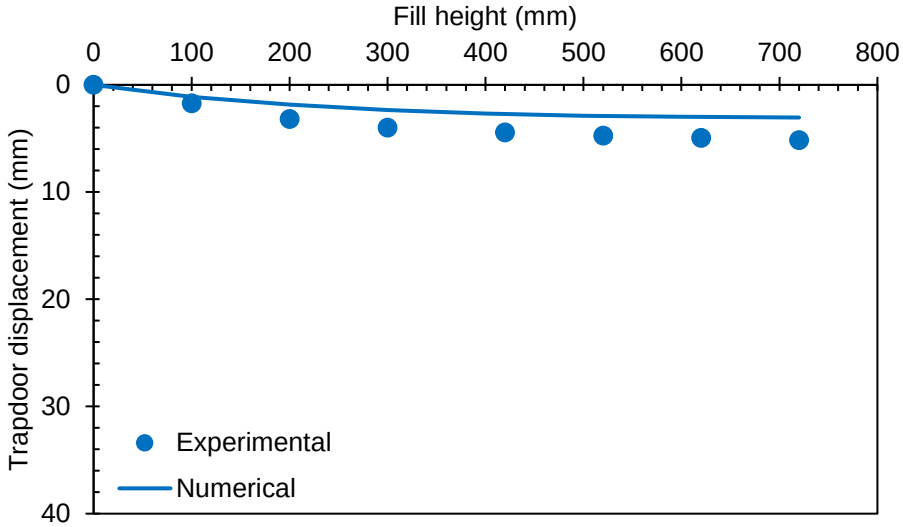

(a)

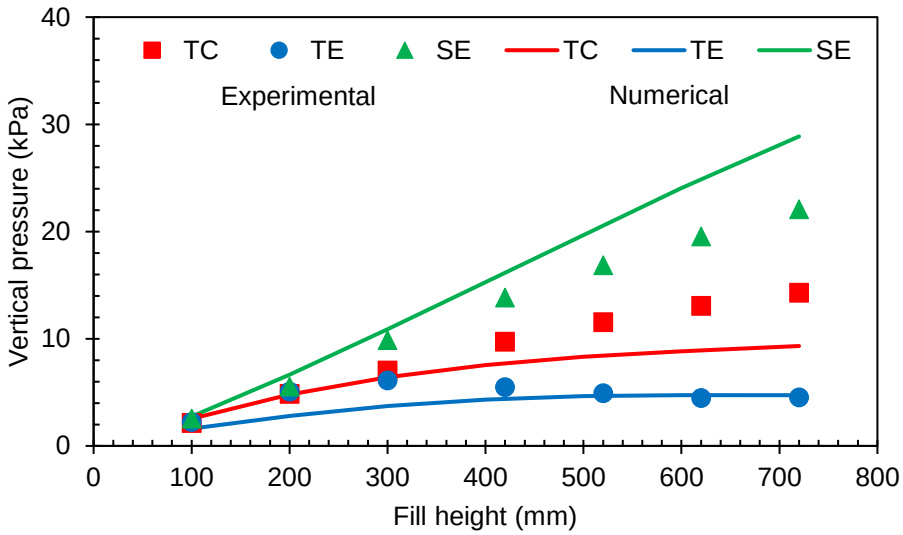

(b)

Figure 6.10 Numerical versus experimental results for T14 during the fill placement: (a) trapdoor displacement and (b) vertical pressures on and besides the trapdoor.

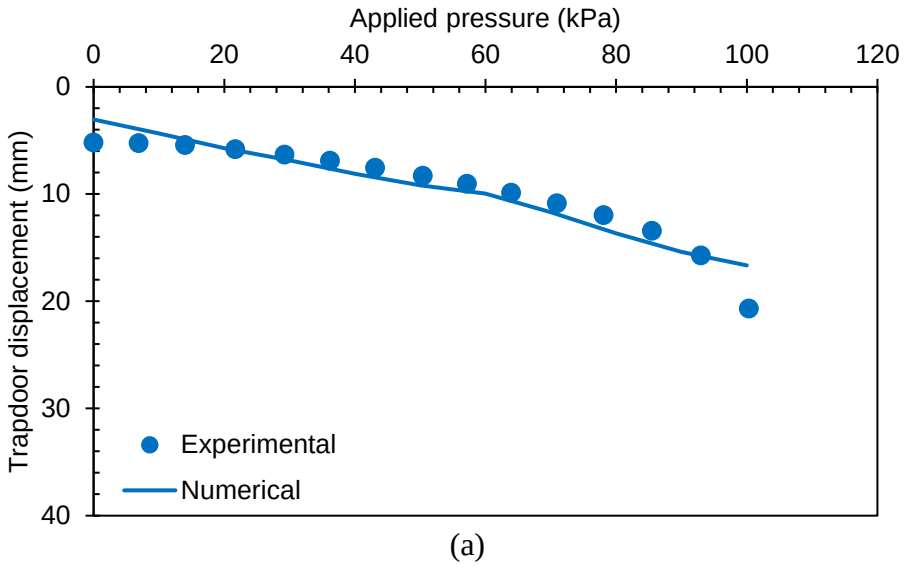

(a)

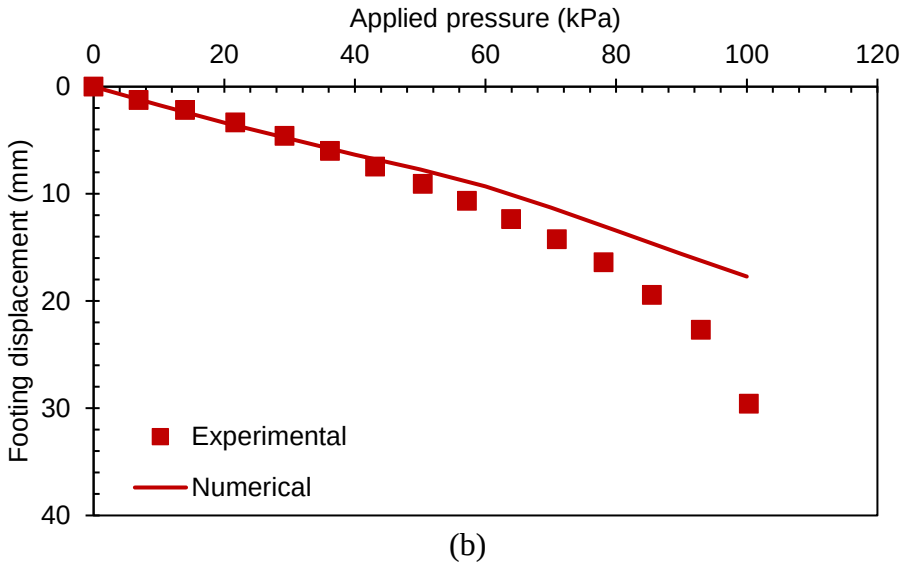

(b)

Figure 6.11 Numerical versus experimental results for T14 under static footing loading: (a) trapdoor displacement and (b) footing displacement.

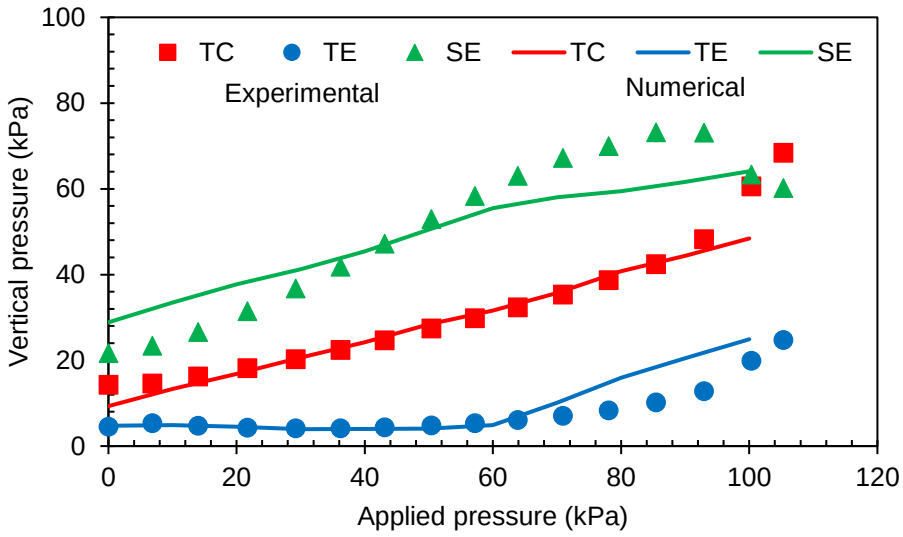

Figure 6.12 Numerical versus experimental results for vertical pressures on and besides the trapdoor in T14 under static footing loading.

6.4 PARAMETRIC STUDY

For the baseline model, the footing width and location from the model centerline were 1B and 0.0B, respectively, where B is the trapdoor width and equals 360 mm. The ratio of the fill height to the trapdoor width was 2 (i.e., H/B =2). This baseline model had the material properties described in Table 6.2 with an elastic modulus for the compressible medium underneath the trapdoor of 0.48 MPa (i.e., 1725 kN/m^3). The same boundary conditions and interface properties that were explained and employed in the previous section were used in the parametric study. The load was applied on the top of the footing by means of equal pressure increments to simulate the procedure used in the experimental work. The finite difference mesh of the numerical model is shown in Figure 6.1(b).

A parametric study was conducted to investigate the parameters that may have an important influence on soil arching under surface loading, including fill height, footing width, footing

location, and trapdoor layout. The parametric study was performed by changing one parameter while keeping all other parameters the same.

6.4.1 Effect of Fill Height

This section discusses the effect of fill height on soil arching under surface footing loading. Since soil arching depends on the shear stresses mobilized in the fill, the height of the fill is expected to have an important effect on the stress transfer from the subsoil (i.e., the trapdoor in this study) to the adjacent supports, especially under localized loading. To investigate the effect of the fill height with the presence of localized loading on soil arching, three models with different fill heights (e.g., H/B = 1, 2, and 3) and a footing width of 1B were analyzed as shown in Figure 6.13. More discussion about the effect of the fill height with different footing widths will be presented in Section 6.4.2.

Figure 6.14 presents the vertical pressures on and besides the trapdoor for the models with H/B = 1, 2, and 3 during their fill placement. Figure 6.14 shows that the pressures on the trapdoor increased at a faster rate at the low fill height (e.g., H/B = 1) than that at the high fill height (e.g., H/B = 3). The pressures on the trapdoor became approximately constant as the fill height increased beyond 600 mm, indicating that the fill weight plus the compaction effort were transferred to the stationary supports only after this height. This observation is consistent with that for the experimental work. In conclusion, the degree of soil arching increased as the fill height increased since the difference between the pressure on the trapdoor and the overburden pressure increased.

Figures 6.15 and 6.16 show the vertical pressures on and besides the trapdoor for these models under static footing loading. These figures show that the model with H/B = 3 had the lowest average vertical pressure on the trapdoor as compared with other cases (i.e., H/B = 1 and 2).

Consequently, the pressure at the support edge (SE) was the highest for the model with H/B = 3 due to the high degree of soil arching within the fill. Since the model with the low fill height (H/B = 1) had the lowest degree of soil arching, the additional pressure from the footing loading caused a faster increase in the pressure on the trapdoor with an obvious turning point at an applied pressure of 50 kPa, which might correspond to yielding and even collapse of soil arching. At a footing pressure of 100 kPa, the reduction of the fill height from H/B = 2 (baseline case) to H/B = 1 increased the average pressure on the trapdoor by approximately 97%. On the other hand, the increase of the fill height from H/B = 2 (baseline case) to H/B = 3 reduced the average pressure on the trapdoor by approximately 31%. Therefore, the fill needs to be sufficiently high to control the level of stresses exerted on the trapdoor (e.g., subsoil in real applications) and minimize the effect of footing loading. Figure 6.17 presents the trapdoor and footing displacements of these numerical models under static footing loading. This figure shows that the model with H/B = 1 had the largest trapdoor and footing displacements as compared with other cases.

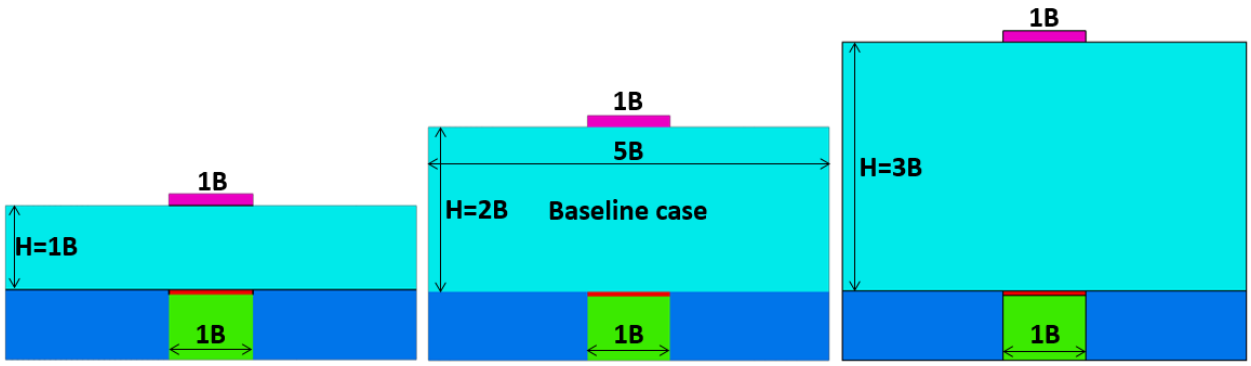

Figure 6.13 Model configurations with different fill heights.

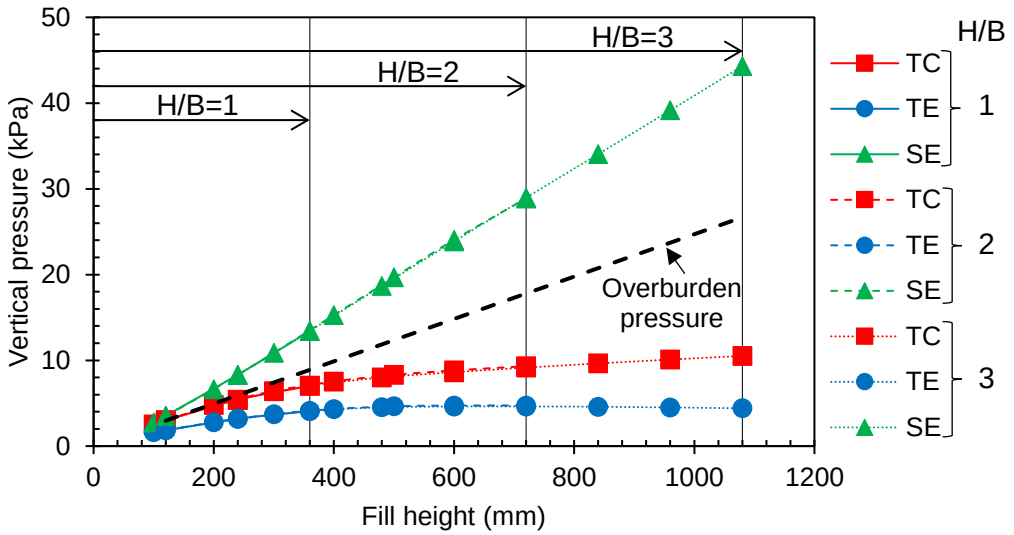

Figure 6.14 Vertical pressures on and besides the trapdoor for different fill heights during their fill placement.

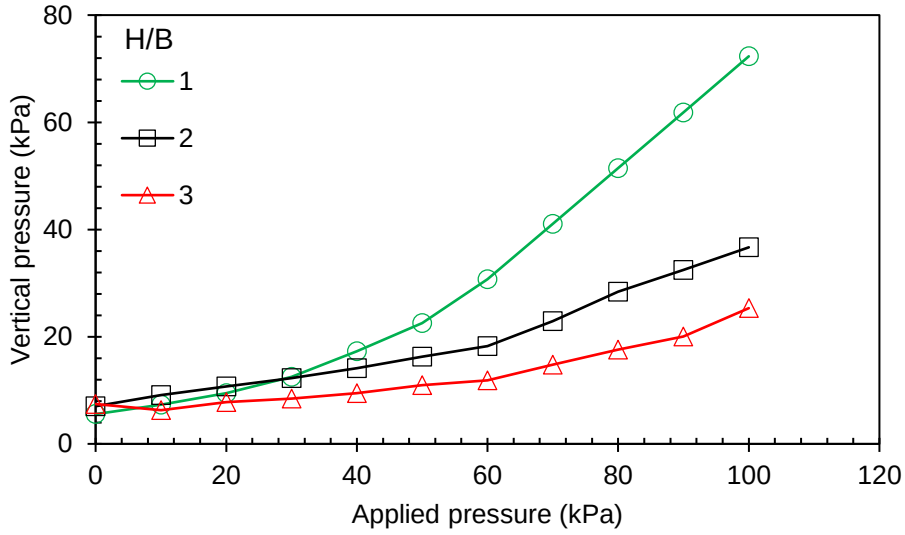

Figure 6.15 Average vertical pressures on the trapdoor for different fill heights under footing loading.

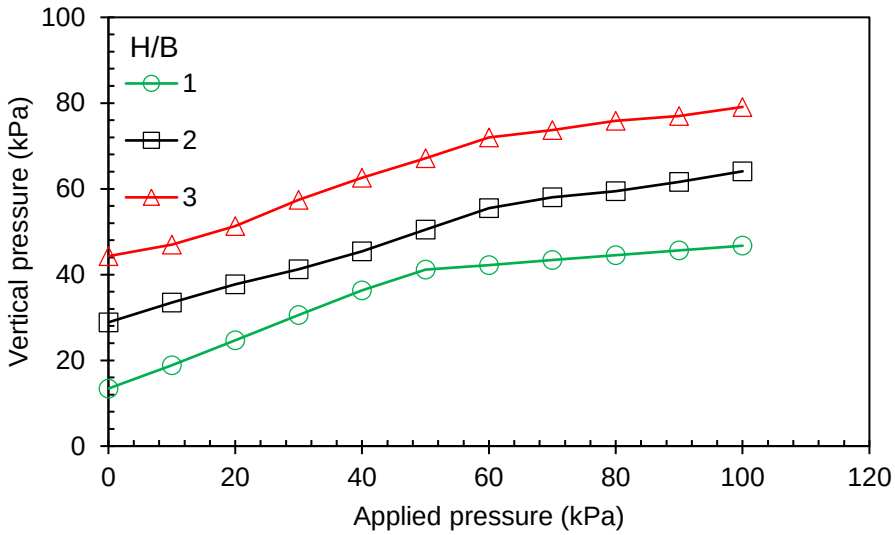

Figure 6.16 Vertical pressures at the support edge (SE) for different fill heights under footing loading.

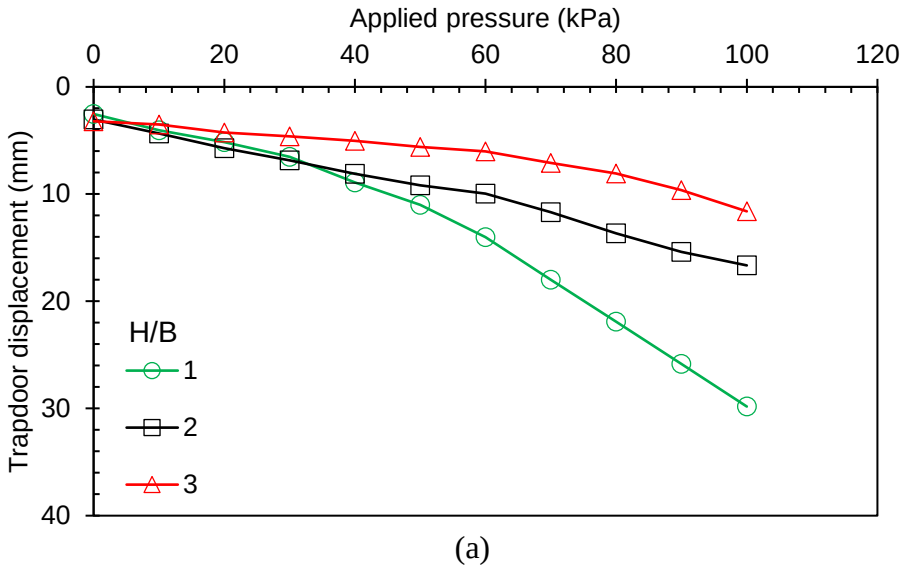

(a)

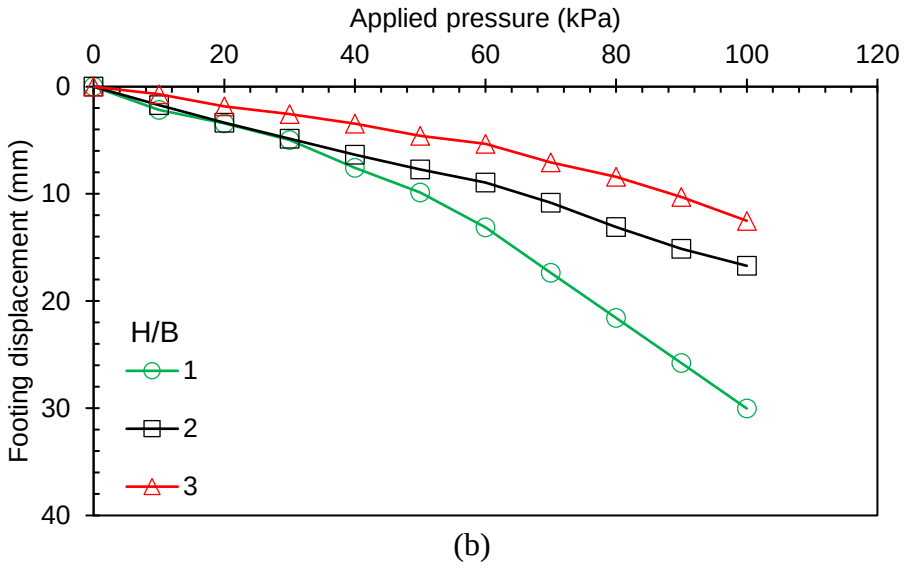

(b)

Figure 6.17 Displacements in the models with different fill heights under static footing loading for: (a) the trapdoor; and (b) the footing.

6.4.2 Effect of Footing Width

This section evaluates the effect of footing width on soil arching as compared with the baseline case that had the footing width of 1B. The footing widths varied from 0.25B, 0.5B, 1B, 1.5B, 2B to 5B as shown in Figure 6.18. The footing width of 5B is to simulate a uniform surcharge condition since the footing width is equal to the model width. Chapter 5 discussed the soil arching degradation under static footing loading based on a single footing width (i.e., 1B) and a single ratio of fill height to trapdoor width (i.e., H/B = 2). However, the effect of the footing width on the soil arching degradation is not known. In addition, the effect of footing width on different fill heights (e.g., H/B = 1, 2, and 3) is also discussed in this section. Since the fill heights of the numerical models in this section were the same for each H/B ratio, their results during fill placement were already discussed in the previous section and are not presented herein.

Figures 6.19 and 6.20 show the vertical pressures on and besides the trapdoor under static footing loading for the models with H/B = 2 and different footing widths. Figure 6.19 shows that the model with a footing width of 0.5B had the highest vertical pressure on the trapdoor as compared with all other cases. The baseline case with a footing width of 1B had the second highest pressure on the trapdoor followed by the cases with footing widths of 0.25B, 1.5B, 2B, and 5B (uniform). For the models with the footing width larger than 1B, the magnitudes of their pressures at the support edge (SE) were in the order from the cases with the footing widths of 5B (highest) to 2B, 1.5B, and 1B (lowest) due to the soil arching effect. Using an applied footing pressure of 60 kPa as an example for comparisons, Figure 6.21 shows a distinguish arch forming above the trapdoor, which transferred the pressure onto the adjacent supports, within two slip planes extended from the trapdoor edges to the fill surface for the cases with the footing width larger than 1B. On the other hand, when a footing width smaller than 1B was used, no clear arch can be seen

above the trapdoor; however, the two slip planes extended from the trapdoor edges toward the fill surface limited the distribution of the footing pressure within the trapdoor range thus minimizing the applied pressure transferred onto the adjacent supports as shown in Figure 6.21. As a result, both the models with footing widths of 0.25B and 0.5B had the lowest pressures on the support edge as shown in Figure 6.20. In summary, increasing the footing width from 1B (baseline case) to 1.5B, 2B, and 5B (uniform) reduced the average pressure on the trapdoor at an applied footing pressure of 60 kPa by approximately 34%, 45%, and 50%, respectively. On the other hand, reducing the footing width from 1B to 0.5B and 0.25B increased and reduced the average pressure on the trapdoor at the same applied pressure by approximately 47% and 11% reduction, respectively. Figure 6.22 presents the relationship between the trapdoor or footing displacement and the applied pressure for these numerical models under static footing loading. This figure shows that the model with the footing width of 0.5B had the largest trapdoor and footing displacements as compared with all other cases.

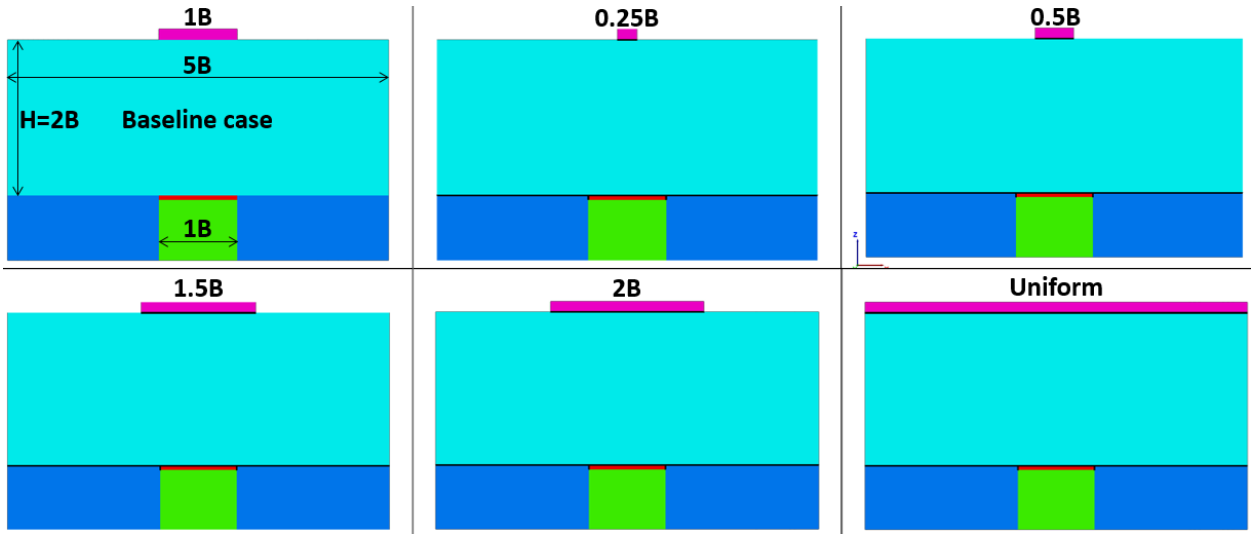

Figure 6.18 Model configurations with different footing widths when H/B = 2.

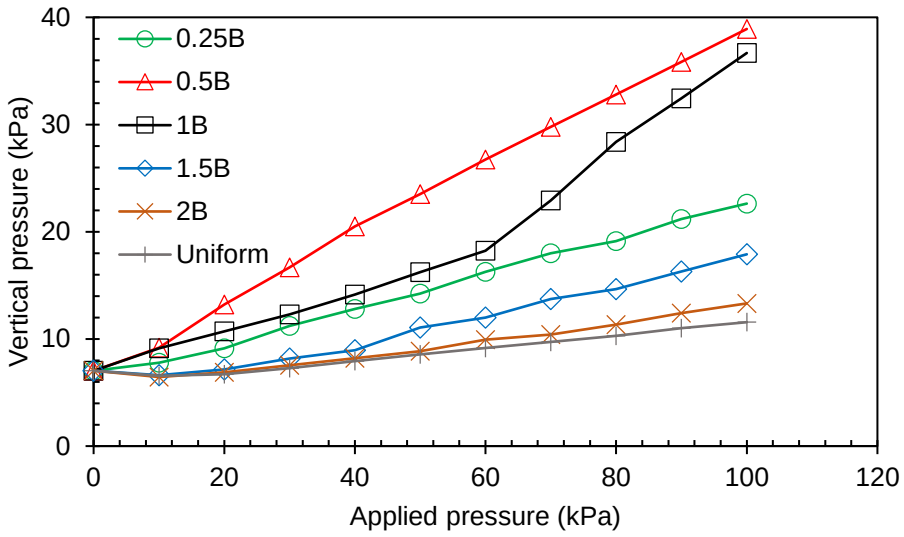

Figure 6.19 Average vertical pressures on the trapdoor under footing loading for different footing widths when H/B = 2.

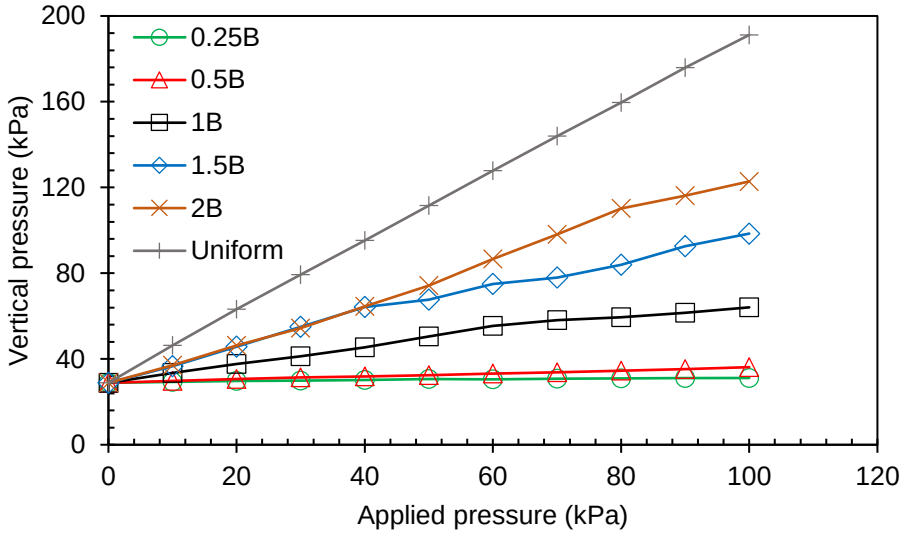

Figure 6.20 Vertical pressures at the support edge (SE) under footing loading for different footing widths when H/B = 2.

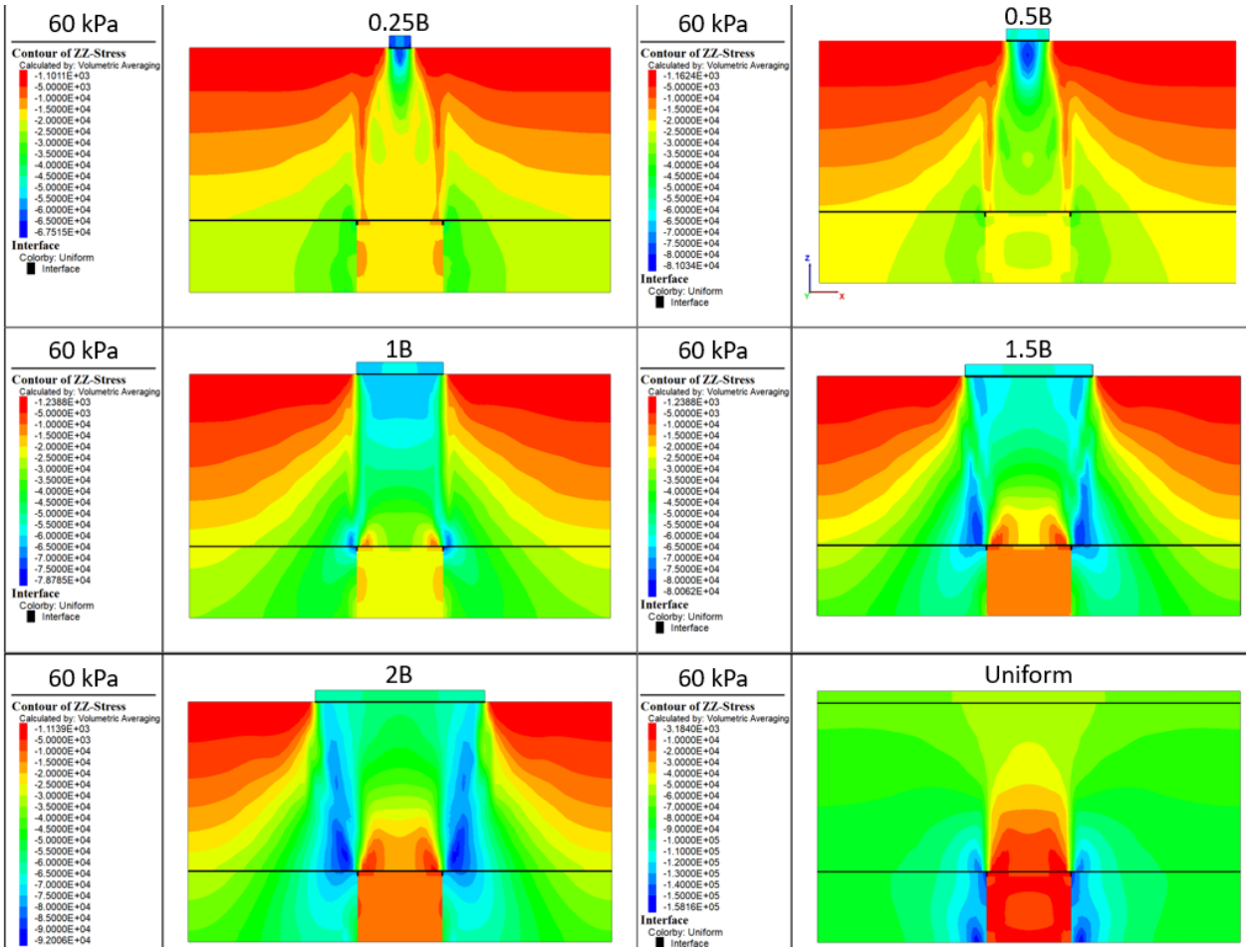

Figure 6.21 Pressure contours for different footing widths under the footing pressure of 60 kPa.

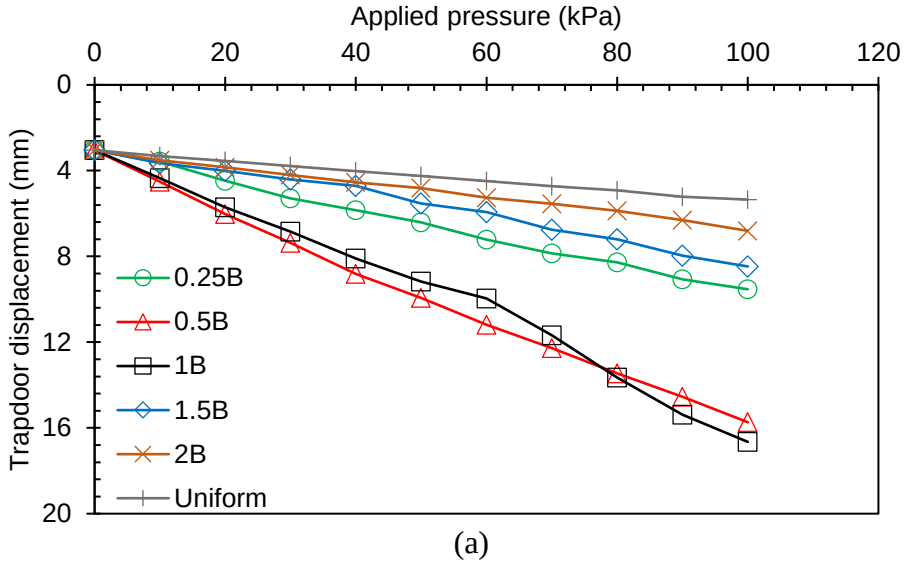

(a)

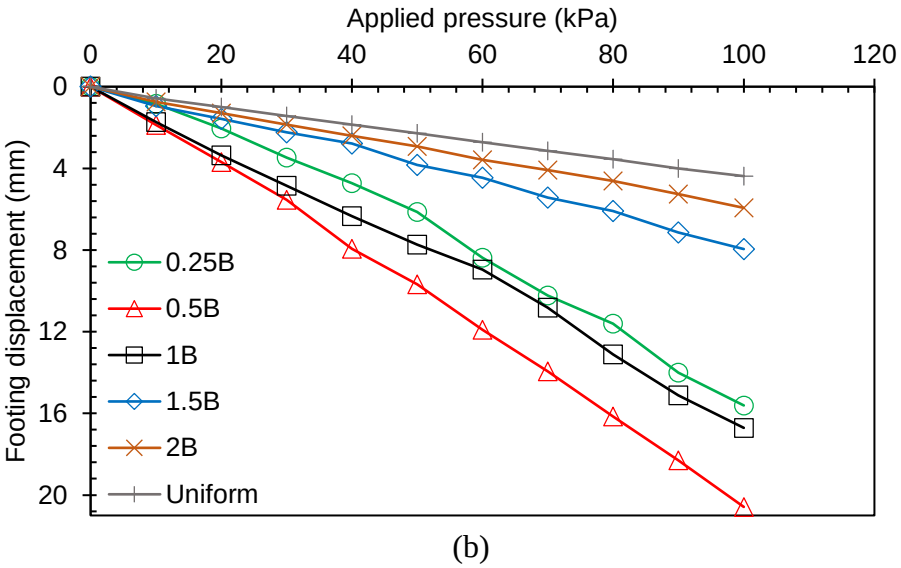

(b)

Figure 6.22 Displacements under footing loading in the numerical models with different footing widths when H/B = 2 for: (a) the trapdoor; and (b) the footing.

To confirm whether the model width (i.e., side boundary locations) affected the numerical results when the footing width was larger than 1B, the width of the model with the footing width of 2B was enlarged such that the ratio of the footing width to the model width equal to 1/5 as shown in Figure 6.23. This ratio is the same as that for the baseline case. It is worth mentioning

that when the model width was equal to the footing width, it became a uniform surcharge case, which does not have any boundary effect issue. Figures 6.24 and 6.25 present the vertical pressures on and besides the trapdoor under footing loading for these two different model widths (i.e., 5B and 10B) with a footing width of 2B and H/B = 2. These figures indicate that both models behaved similarly under a low applied pressure (lower than 50 kPa) and had a negligible difference as the pressure increased beyond 50 kPa. Therefore, the boundary had a minor effect on the numerical results when the footing with the width of 2B or smaller was placed in the numerical model with the width of 5B.

Figure 6.23 Model configurations with footing width of 2B and different model lengths.

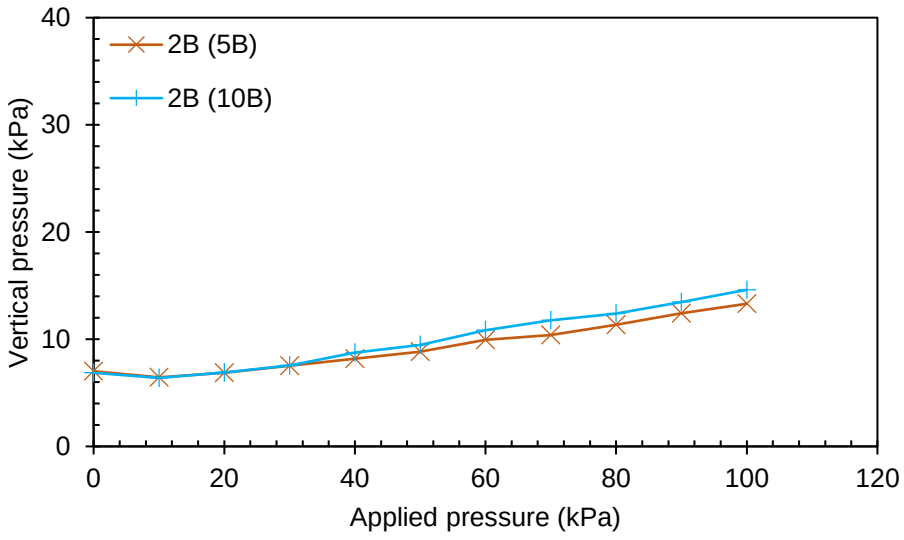

Figure 6.24 Average vertical pressures on the trapdoor under footing loading for different model widths with the footing width of 2B and H/B = 2.

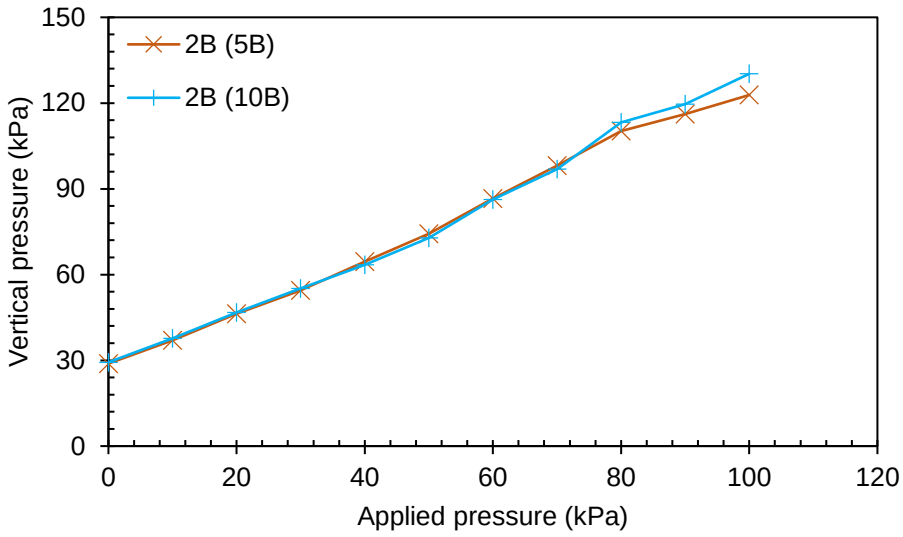

Figure 6.25 Vertical pressures at the support edge (SE) under footing loading for different model widths with the footing width of 2B and H/B = 2.

This study also investigated the effect of footing width when the ratios of fill height to trapdoor width (H/B) were equal 1 and 3. Figures 6.26 to 6.27 and 6.28 to 6.29 show the vertical pressures on and besides the trapdoor for H/B = 1 and 3, respectively at different footing widths. These figures show that the footing width of 1B was the most critical width because it resulted in the highest pressure on the trapdoor for both H/B = 1 and 3. As the footing width increased from 1B to 5B, less pressure was exerted on the trapdoor and more pressure was transferred onto the supports for both H/B ratios. However, as the footing width decreased from 1B to 0.25B, less pressure exerted on the trapdoor and the supports for both H/B ratios. In addition, for the same footing width, the pressure on the trapdoor increased as the fill height decreased.

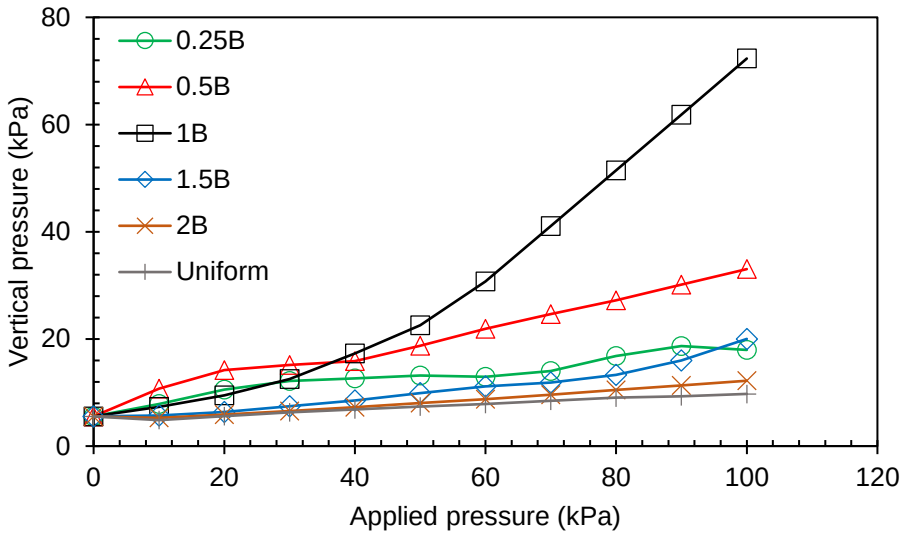

Figure 6.26 Average vertical pressures on the trapdoor under footing loading for different footing widths when H/B = 1.

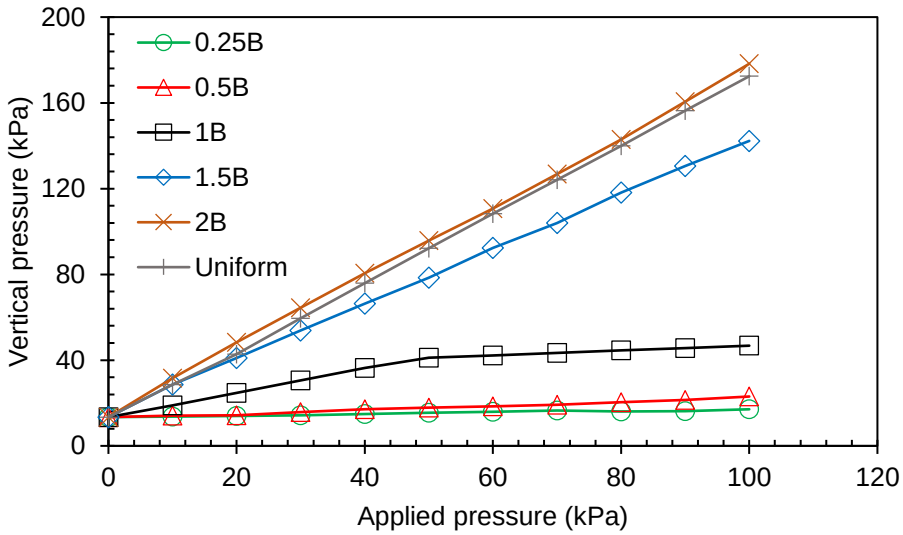

Figure 6.27 Vertical pressures at the support edge (SE) under footing loading for different footing widths when H/B = 1.

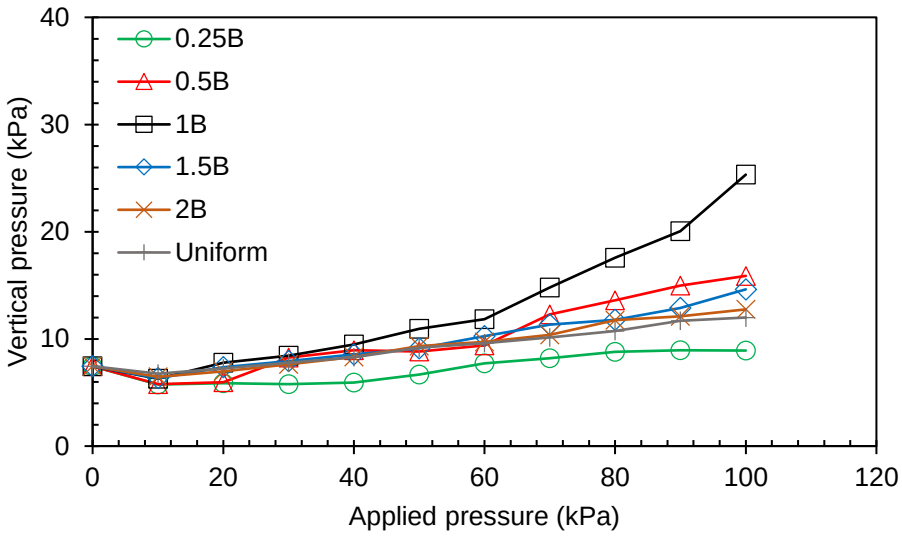

Figure 6.28 Average vertical pressures on the trapdoor under footing loading for different footing widths when H/B = 3.

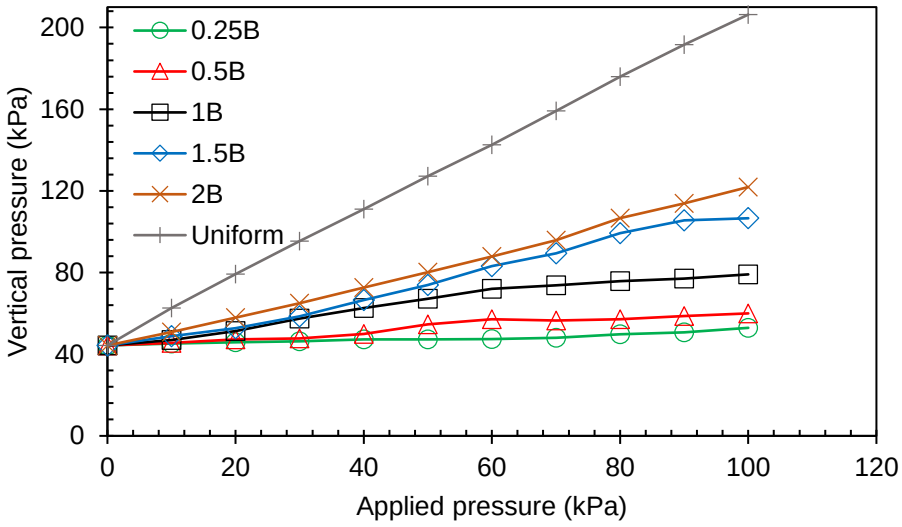

Figure 6.29 Vertical pressures at the support edge (SE) under footing loading for different footing widths when H/B = 3.

6.4.3 Effect of Footing Location

This section presents and discusses the results of the numerical analysis performed with different footing locations (offsets) from the model (or trapdoor) centerline. The investigated footing offsets, which are measured from the footing centerline to the trapdoor centerline, were 0.0B (baseline case), 0.25B, 0.5B, 0.75B, and 1B as shown in Figure 6.30. All the models were analyzed with a footing width of 1B and a fill height to trapdoor width ratio (H/B) of 2. The aim of this parametric study is to determine the most critical footing location with respect to the trapdoor location that would cause soil arching to degrade. The numerical results during fill placement for these models have been discussed in the previous section and are not presented herein.

Figures 6.31 and 6.32 show the vertical pressures on and besides the trapdoor for the investigated footing offsets and H/B = 2 under static footing loading. Figure 6.31(a) shows that the model with a footing offsets of 0.0B (baseline case), where the footing and trapdoor centerlines were aligned, had the highest vertical pressure on the trapdoor centerline (TC) as compared with all other cases. As the footing offset increased to 1B, less pressure reached the trapdoor centerline. For instance, increasing the footing offset from 0.0B (baseline case) to 0.25B, 0.5B, 0.75B and 1B reduced the pressure on the trapdoor centerline (TC) at an applied footing pressure of 100 kPa by approximately 9%, 33%, 53%, and 63%, respectively. Furthermore, when the footing was located with an offset from the model centerline, the shape of the soil arch above the trapdoor was significantly affected and had a non-uniform pressure distribution on and besides the trapdoor as shown in Figure 6.33. As a result, higher pressures were observed on the trapdoor edge (TE-Right side (R)) and the support edge (SE-Right side (R)) that were closer to the footing centerline than those that were away from the footing centerline. Figures 6.31(b) and 6.32 present the pressures at TE-R and SE-R, respectively. These figures show less pressure was exerted on the trapdoor edge

and more pressure was transferred onto the support edge as the footing offset increased to 1B. Figure 6.34 presents the trapdoor and footing displacements of these numerical models under static footing loading, which shows that the model with 0.0B footing offset had the largest trapdoor and footing displacements as compared with all other cases.

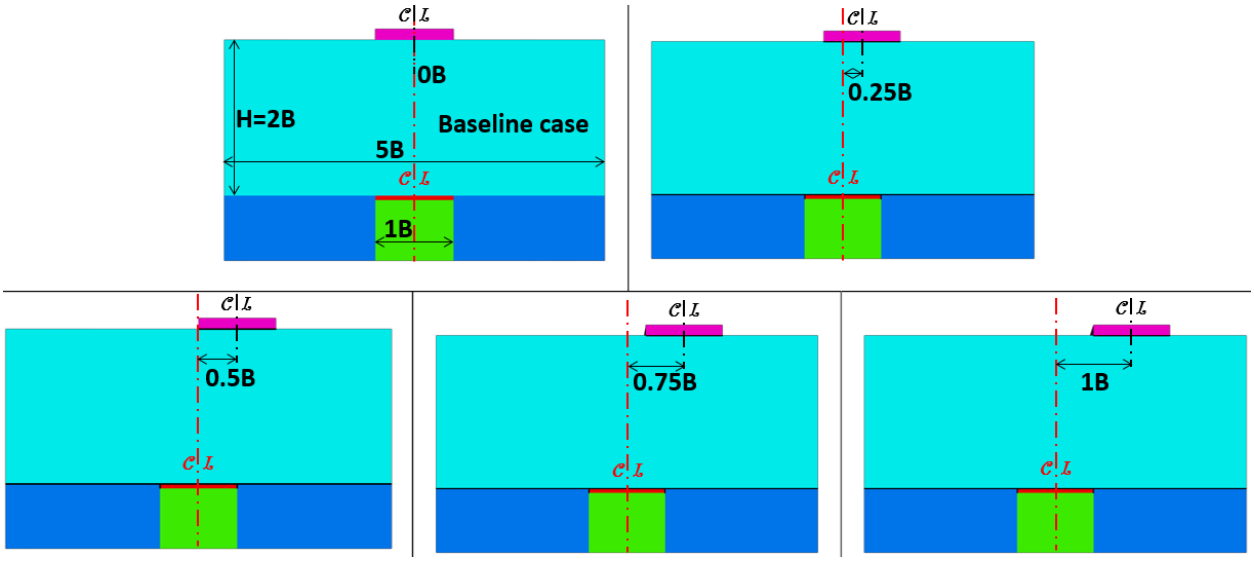

Figure 6.30 Model configurations with different footing offset from the model centerlines when H/B = 2.

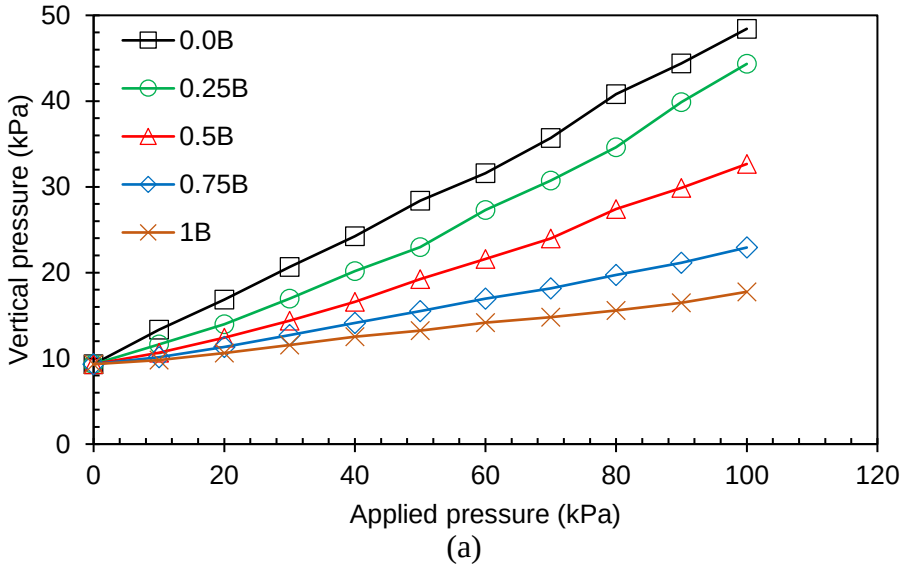

(a)

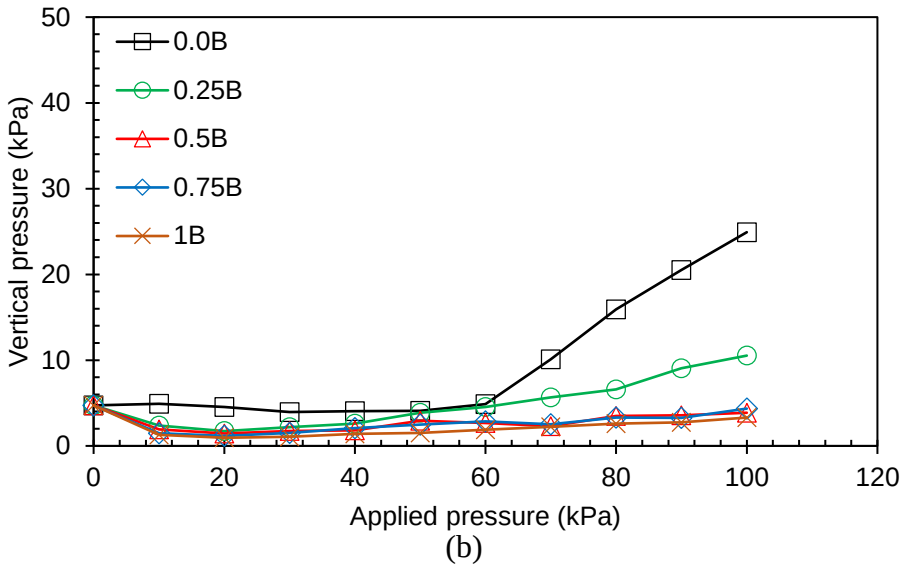

(b)

Figure 6.31 Average vertical pressures on the trapdoor under footing loading for different footing offsets when H/B = 2 at: (a) TC; and (b) TE-R.

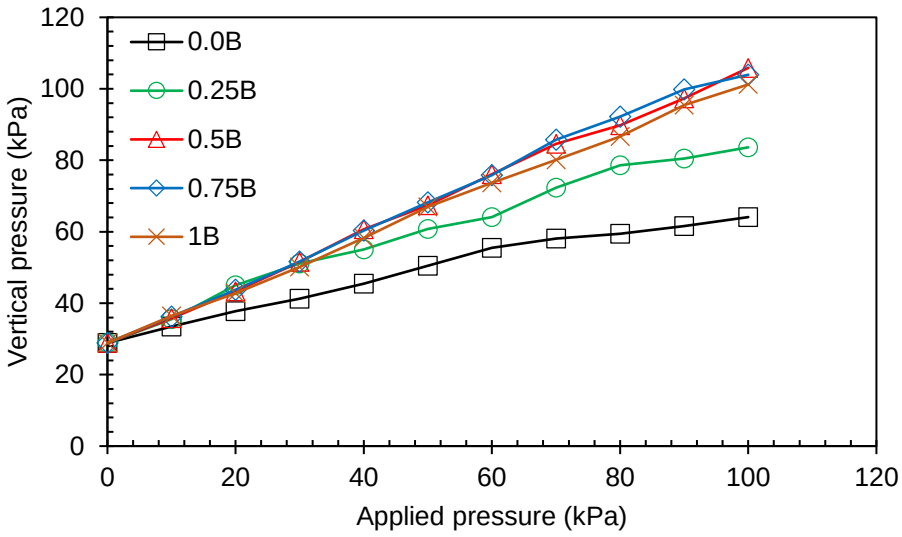

Figure 6.32 Vertical pressures at the support edge (SE-R) under footing loading for different footing offsets when H/B = 2.

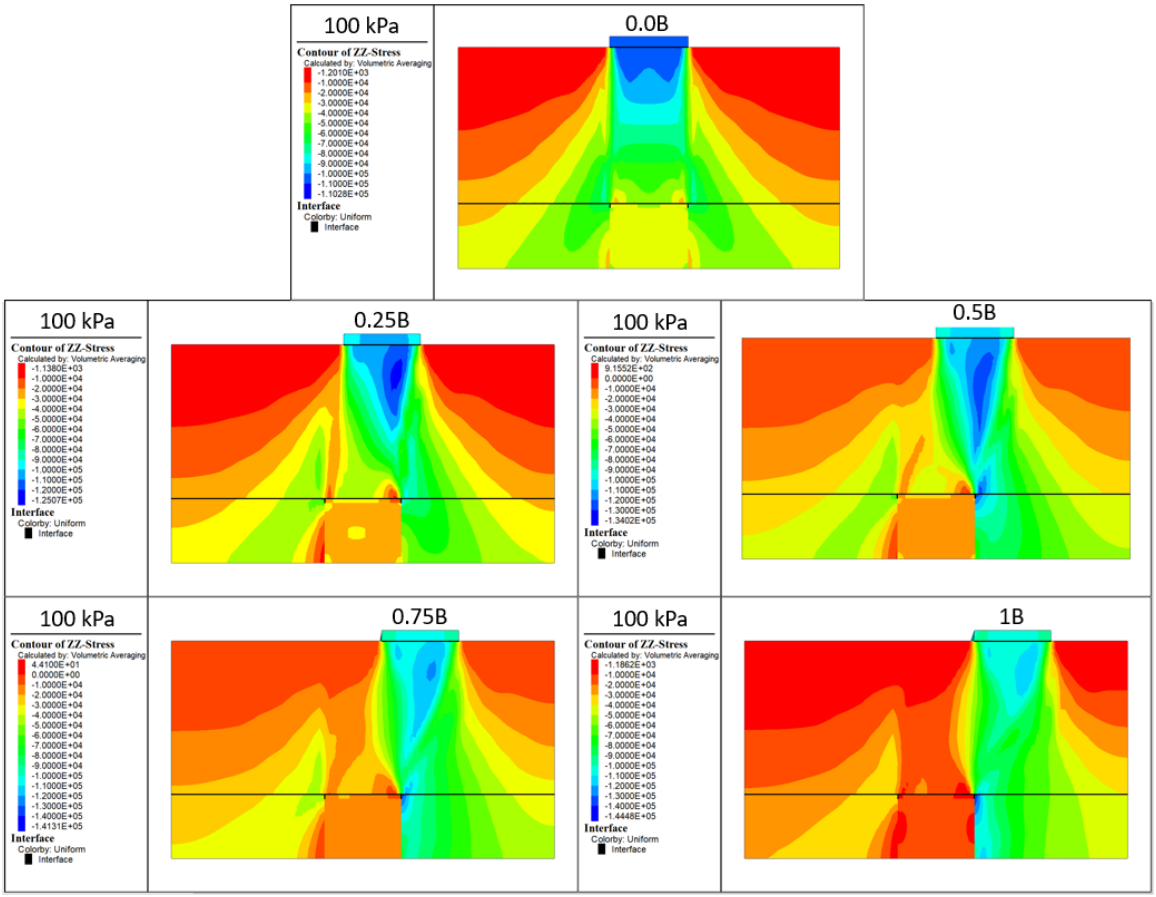

Figure 6.33 Pressure contours for different footing offsets under 100 kPa footing pressure.

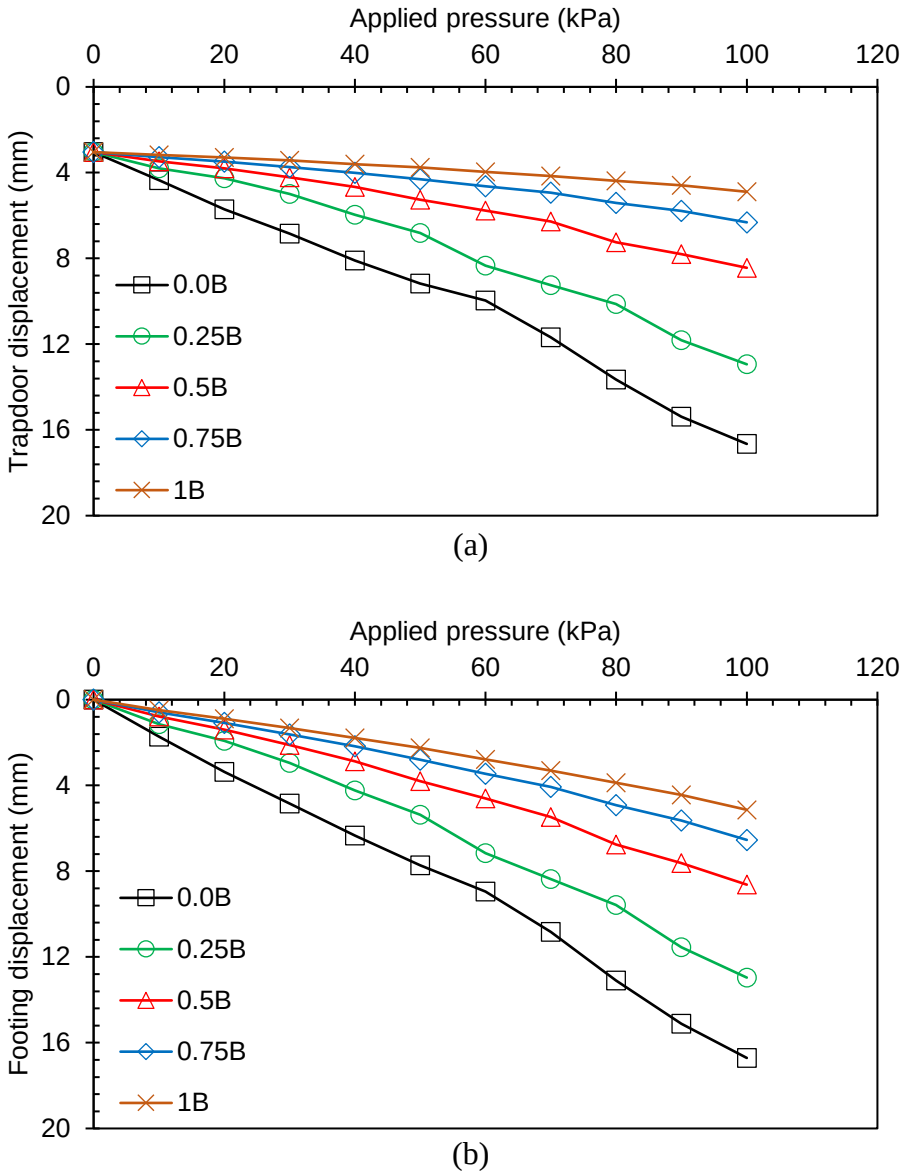

Figure 6.34 Displacements under footing loading in the numerical models with different footing offsets when H/B = 2 for: (a) the trapdoor; and (b) the footing.

To further check whether the model width (i.e., the right side of the boundary location) has affected the numerical results when the footing offset was larger than 0.0B, the model with the footing offset of 1B was selected for analysis, in which that the minimum distance between the boundary and the footing edge is 2B as shown in Figure 6.35. This distance is the same as that for

the baseline case. Figures 6.36 and 6.37 present the vertical pressures at TC, TE-R, and SE-R under footing loading for the two different model widths (i.e., 5B and 6B). These figures indicate that both models behaved similarly; therefore, the results of the models with the footing offset larger than 0.0B are valid.

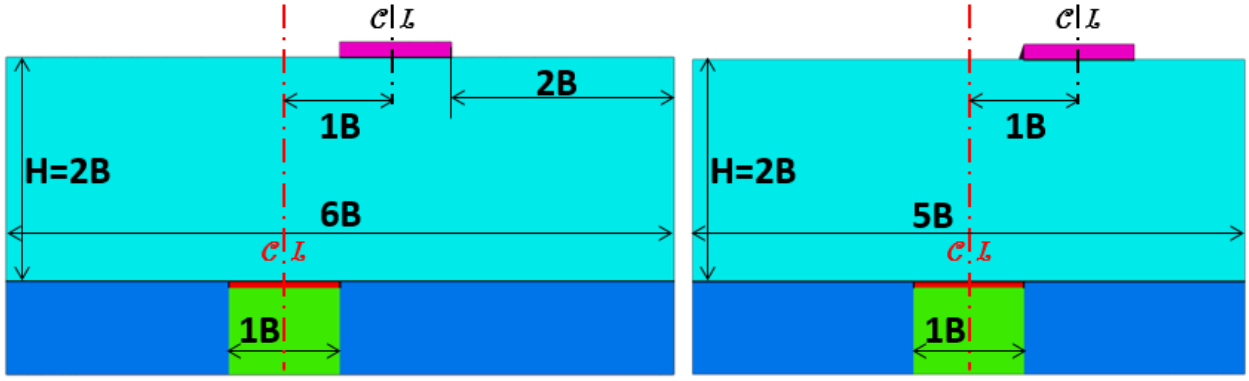

Figure 6.35 Model configurations with the footing offset of 1B and different model widths.

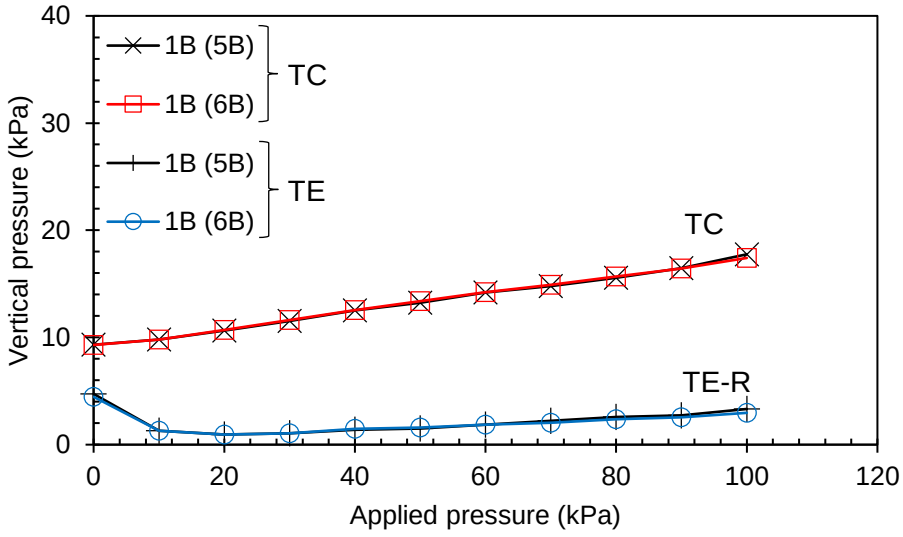

Figure 6.36 Average vertical pressures on the trapdoor under footing loading for different model widths and the footing offset of 1B when H/B = 2.

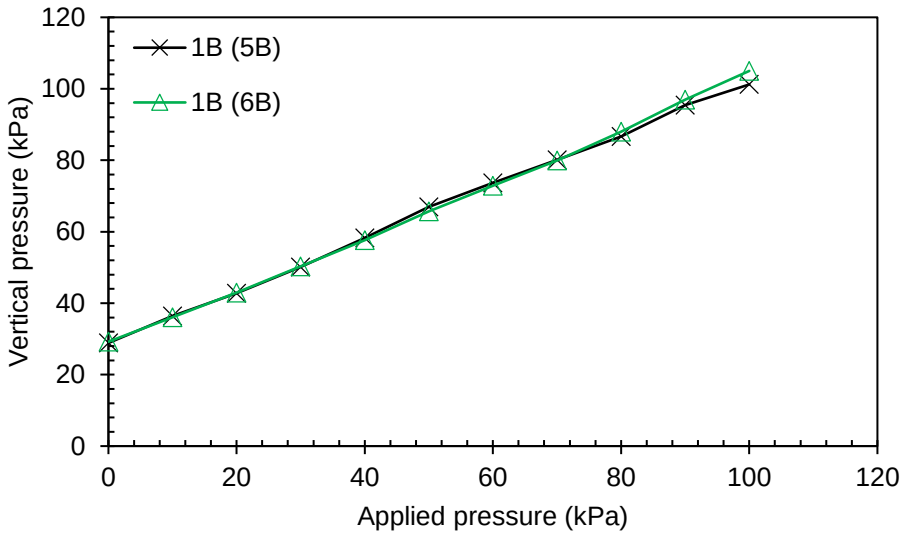

Figure 6.37 Vertical pressures at the support edge (SE-R) under footing loading for different model lengths and the footing offset of 1B when H/B = 2.

6.4.4 Flexible Trapdoor

The effect of trapdoor flexibility on soil arching was investigated experimentally in Chapter 5 where a three-segment trapdoor was utilized. The pressure distribution on the three-segment trapdoor was more uniform than that on a one-segment rigid trapdoor. One main conclusion from Chapter 5 is that the rigid trapdoor resulted in more soil arching than the flexible trapdoor. This conclusion was drawn based on the three-segment trapdoor due to experimental limitations. It is a question whether the increase of the number of trapdoor segments would affect soil arching. A numerical study was conducted to investigate the effect of the number of trapdoor segments (i.e., nine-segment) on soil arching. The motive behind this study is that the displacement mode in a multi-segment trapdoor is closer to that in the subsoil between rigid supports in real applications (e.g., PS or GRPS embankments). Figure 6.38 depicts the model configurations of the three-segment and nine-segment trapdoor layouts.

Prior to the numerical analysis with the nine-segment trapdoor, the numerical model with a three-segment trapdoor (as shown in Figure 6.38(a)) was built and validated against the experimental results of T16 as shown in Figure 6.39. This model was generated by creating three separate zones (each zone with a width of B/3) for the trapdoor and the compressible medium underneath the trapdoor. All other zones were the same as those in the model with a one-segment trapdoor. The interaction between the trapdoor segments was controlled by interface elements of the same property as that used between the trapdoor and the supports. On the other hand, no interaction was allowed between the compressible medium zones as in the experimental test. Figure 6.39 shows a good agreement between the vertical pressures on and besides the three-segment trapdoor in the numerical analysis and T16 under static footing loading. The same technique was taken for the numerical model with the nine-segment (segment width is B/9) trapdoor.

Figures 6.40 and 6.41 present and compare the numerical results of both models (i.e., three-segment and nine-segment trapdoors) during fill placement and under footing loading, respectively. Figure 6.40 shows that both models had approximately the same vertical pressures on the trapdoor and slightly lower pressures at the support edge for the nine-segment trapdoor than that for the three-segment trapdoor during fill placement. As the footing pressure increased, the pressure on the trapdoor for the nine-segment trapdoor was higher than that for the three-segment trapdoor, and consequently, less pressure was transferred to the support edges. However, more uniform pressure distribution on the nine-segment trapdoor was observed as compared to that on the three-segment trapdoor. In summary, increasing the number of trapdoor segments reduced soil arching due to the increased non-uniformity of the trapdoor displacement, which increased differential settlement between the trapdoor segments.

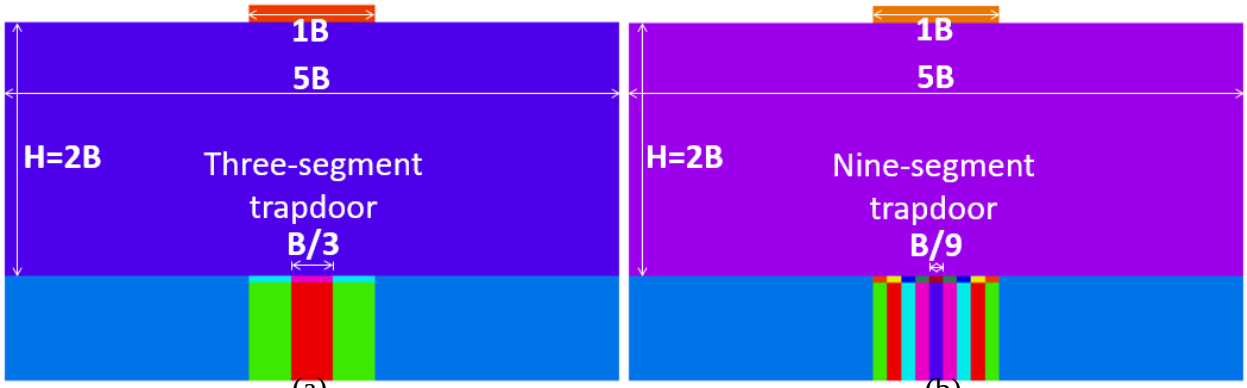

(a) (b)

Figure 6.38 Model configurations with multi-segment trapdoor layout: (a) three-segment trapdoor; and (b) nine-segment trapdoor.

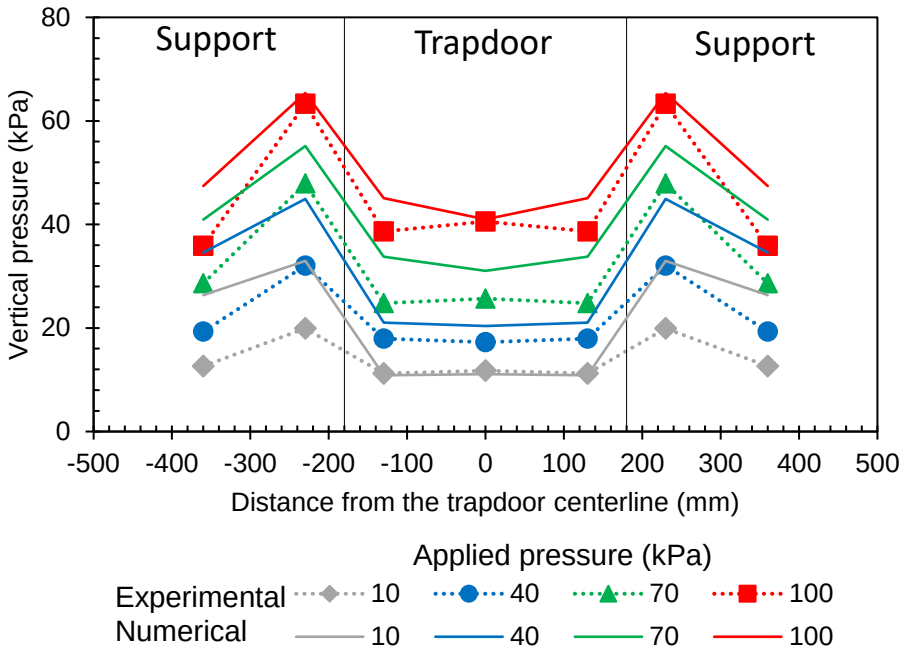

Figure 6.39 Numerical model validation against T16 under static footing loading for the vertical pressures on and besides the trapdoor.

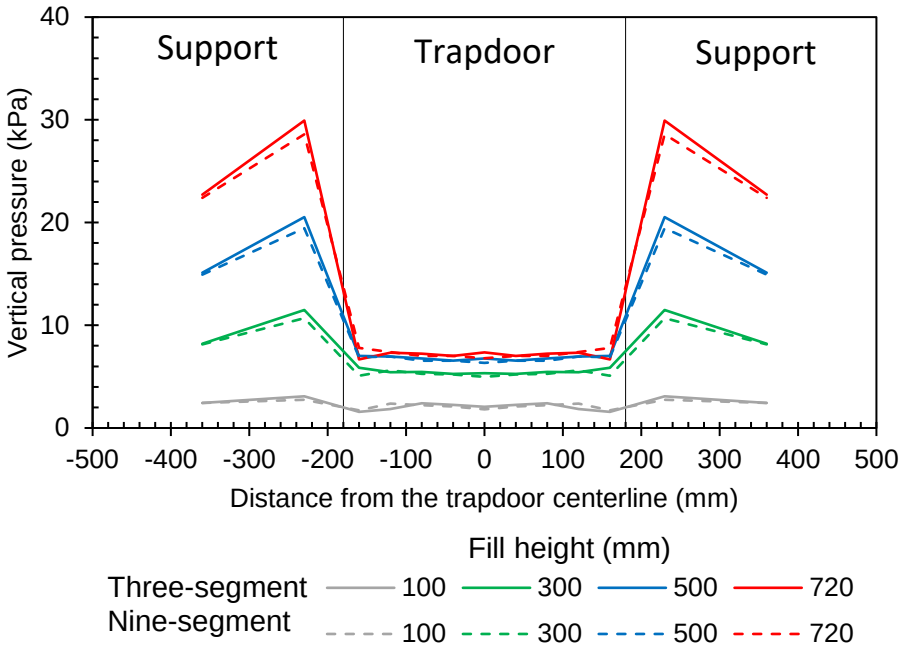

Figure 6.40 Vertical pressures on and besides the trapdoor for the models with different trapdoor segments during fill placement.

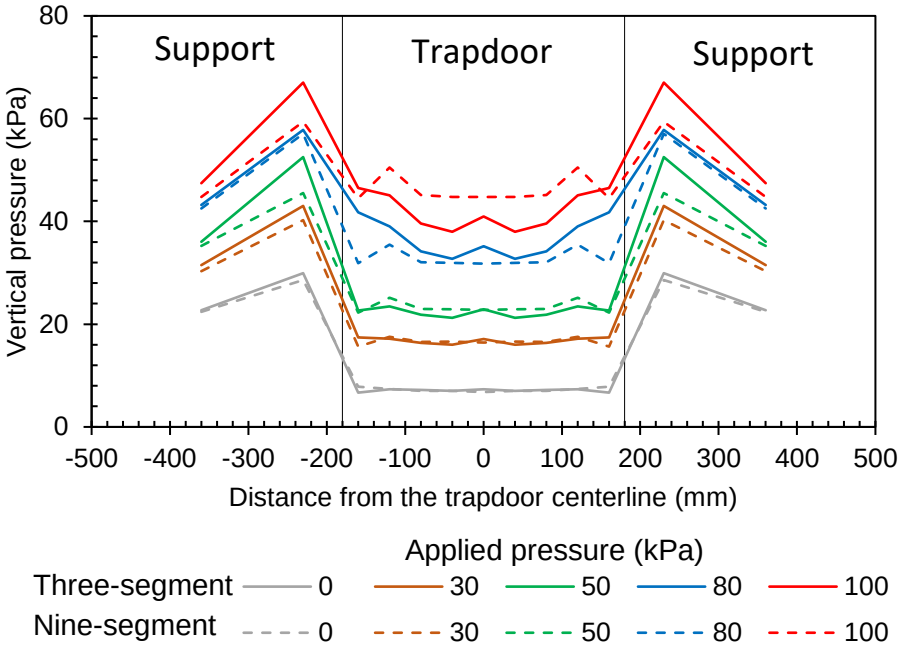

Figure 6.41 Vertical pressures on and besides the trapdoor for the models with different trapdoor segments under static footing loading.

6.5 COMPARISONS WITH ANALYTICAL SOLUTION

This section compared the proposed analytical solution in this study for soil arching presented in Equation (5.7) and discussed in Section 5.9 with the numerical results. The analytical solution is to predict the vertical stresses above a yielding trapdoor where soil arching is mobilized under its self-weight plus surface footing loading-induced stress along the trapdoor centerline.

Eight numerical models that had different fill height to trapdoor width ratios (H/B = 1, 2, and 3) and different footing widths (0.25B, 0.5B, 1B, 1.5B, 2B, and 5B (uniform)) were selected and are compared with the analytical solution. For the analytical solution, all parameters in Equation (5.7) are based on the soil properties (φ, c, and γ), trapdoor width (B), and fill height (H) except for K and β. The footing pressure distribution factor (β) was calculated using Boussinesq's solution based on the layout and/or dimensions of each model. The Rankine active earth pressure coefficient, $K_a = (1- \sin \phi) / (1+ \sin \phi)$, was used for the coefficient of lateral earth pressure (K) for all eight models. In addition to the Rankine active earth pressure coefficient (K_a), a K value based on the Mohr circle, which was derived by Tien (1996) and expressed as $K_m = (1- \sin^2 \phi) / (1+ \sin^2 \phi)$, was used for the model with the footing width of 0.25B and 5B (uniform). For the model with footing width of 5B (uniform), a K value of 1 was also used as suggested by Terzaghi (1943).

Figure 6.42 shows the comparison between the average vertical pressures on the trapdoor computed by the numerical models and those predicted using the analytical solution for the models with H/B of 1, 2, and 3 and a footing width of 1B. For a low fill height (H/B = 1) as shown in Figure 6.42(a), the predicted vertical pressure matches well the numerical result at the applied footing pressure lower than 40 kPa. However, as the applied footing pressure increased, soil arching degraded and the vertical pressure on the trapdoor in the numerical model increased rapidly, which was not well predicted by the analytical solution. This comparison indicates, also

as discussed earlier in Section 5.9, the analytical solution could not predict the vertical pressure on the trapdoor when soil arching degraded. For high fill heights (H/B = 2 and 3), the vertical pressures predicted by the analytical solution compared reasonably well with those on the trapdoor computed by the numerical models as shown in Figures 6.42(b) and 6.42(c).

Furthermore, Figure 6.43 shows the comparison between the average vertical pressures on the trapdoor computed by the numerical models and those predicted based on the analytical solution for the models with different footing widths (i.e., 0.25B, 0.5B, 1.5B, 2B, and 5B (uniform)) at H/B = 2. In general, the vertical pressures predicted by the analytical solution are compared reasonably well with those computed by the numerical models. However, the vertical pressures for the models with the footing widths of 0.5B, 1B, 1.5B, and 2B computed by the numerical method are compared well with those predicted by the analytical solution using K_a. For the models with the footing widths of 0.25B and 5B (uniform), the numerical results are compared well with those predicted by the analytical solution using K_m and K = 1, respectively. Since the analytical solution is a frictional model (stress redistribution depends on the frictional forces around the vertical planes of sliding), the value of K is detrimental for the estimation of soil arching due to its effect on the calculation of the shear stresses along the planes of sliding. The mobilization of shear stresses significantly relies on the differential displacement throughout the fill. In the model with a footing width of 0.25B, the pressure distribution underneath the footing was mostly concentrated above the trapdoor, as shown in Figure 6.21, inducing large displacement in the trapdoor as shown in Figure 6.22. Large displacement in the trapdoor indicates significant differential displacement and more shear stresses throughout the fill. Therefore, a K value of K_m = 0.45, which is higher than K_a = 0.238, for the analytical solution was needed to better predict the vertical pressure on the trapdoor computed by the numerical model since it resembles the condition

of shear stresses mobilized in this test. As stated in Section 5.9, the analytical solution and Terzaghi's (1943) solution yield the same result for the vertical pressure on the trapdoor when the soil arching is mobilized under a uniform surcharge loading condition. Therefore, in the model with a footing width (5B) equal to the model width (i.e., uniform surcharge condition), the analytical solution with a *K* value of 1 best predicted the vertical pressure on the trapdoor computed by the numerical model. This *K* value (K = 1) was suggested by Terzaghi (1943) and was later confirmed by Han et al. (2017) as they compared Terzaghi's solution to several experimental and numerical investigations of soil arching in the trapdoor test under soil-self weight.

In conclusion, both the experimental data in Chapter 5 and the numerical results in this chapter validated the proposed analytical solution for soil arching over a yielding trapdoor under localized and uniform surface footing loading.

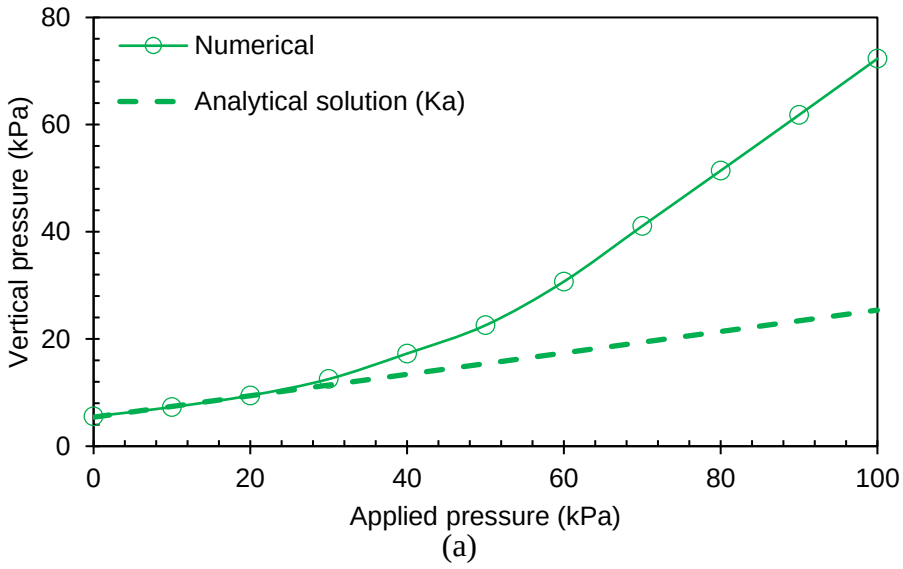

Figure 6.42 Comparisons between the numerical results and the analytical solution for the models with a footing width of 1B at: (a) H/B = 1; (b) H/B = 2; and (c) H/B = 3.

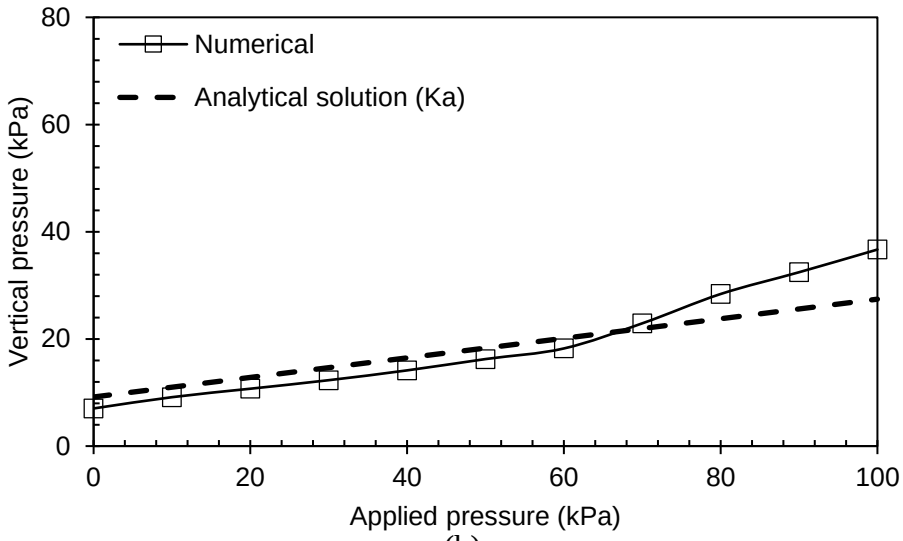

(b)

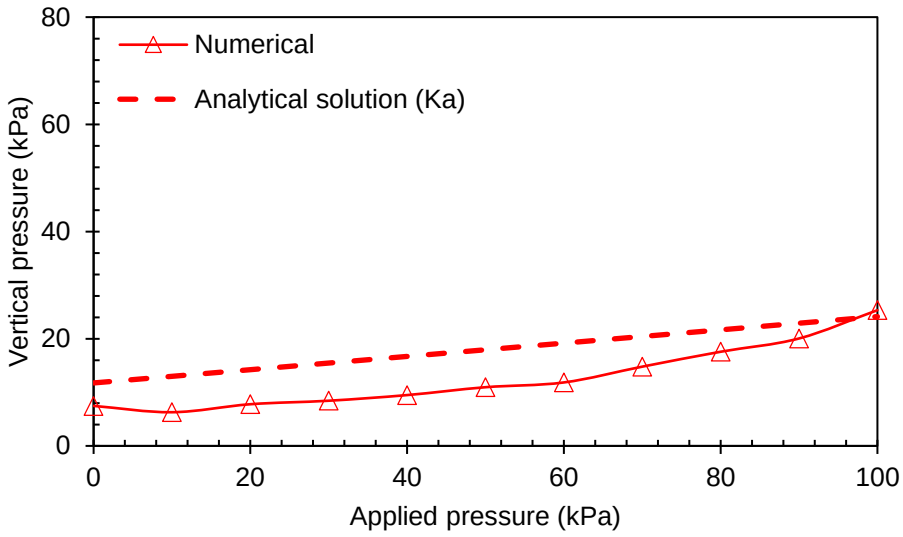

(c)

Figure 6.42 Comparisons between the numerical results and the analytical solution for the models with a footing width of 1B at: (a) H/B = 1; (b) H/B = 2; and (c) H/B = 3 (continued).

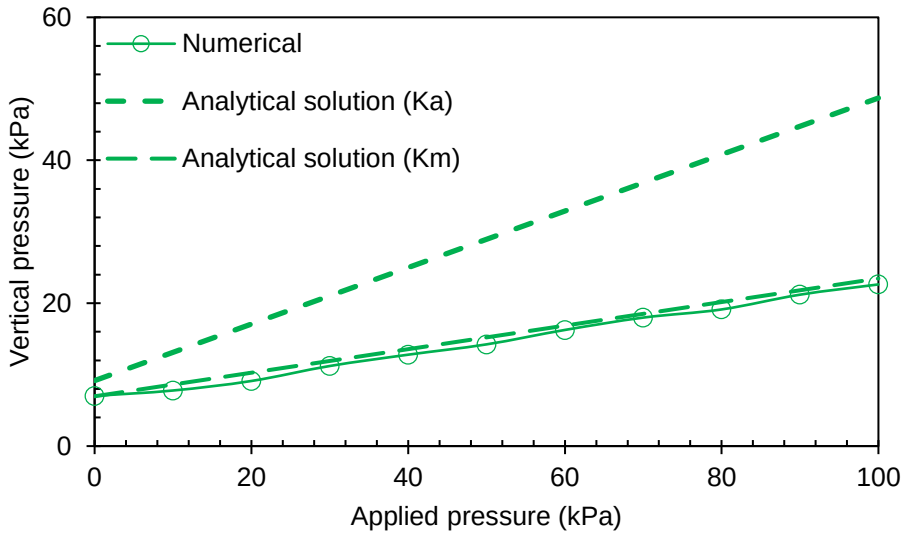

(a)

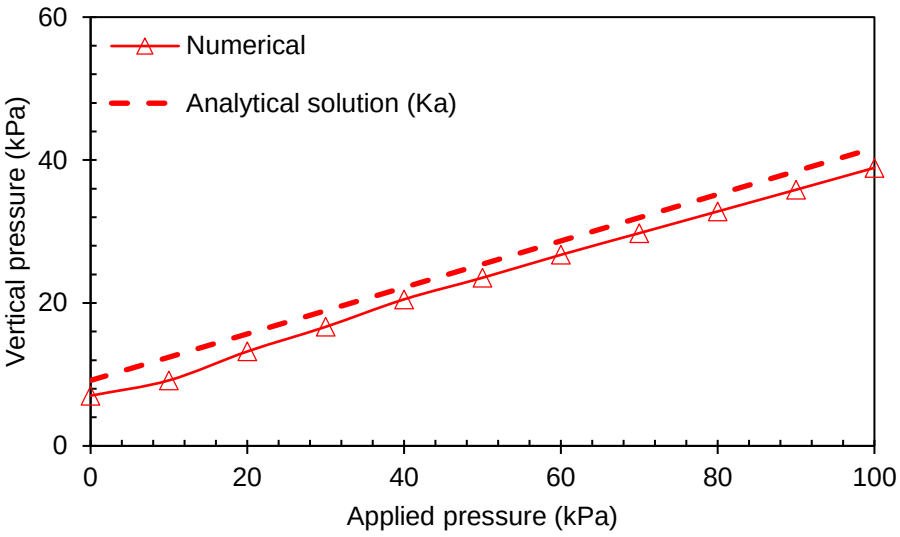

(b)

Figure 6.43 Comparisons between the numerical results and the analytical solution for the models with the footing widths of: (a) 0.25B; (b) 0.5B; (c) 1.5B; (d) 2B; and (e) 5B, at H/B = 2.

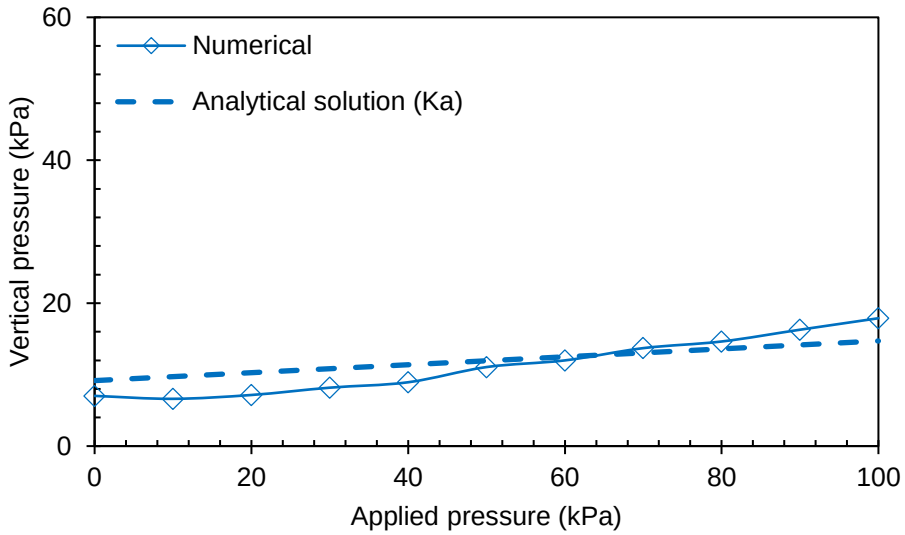

(c)

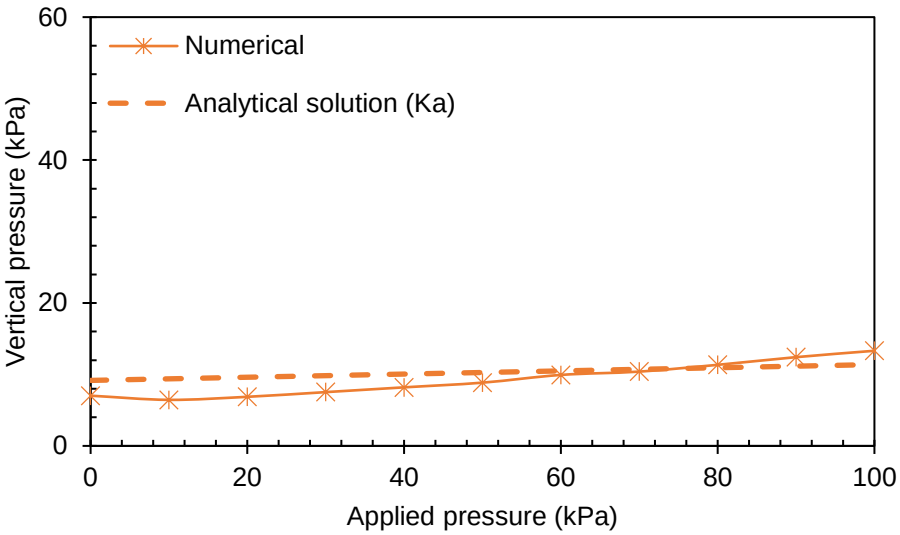

(d)

Figure 6.43 Comparisons between the numerical results and the analytical solution for the models with the footing widths of: (a) 0.25B; (b) 0.5B; (c) 1.5B; (d) 2B; and (e) 5B at H/B = 2 (Continued).

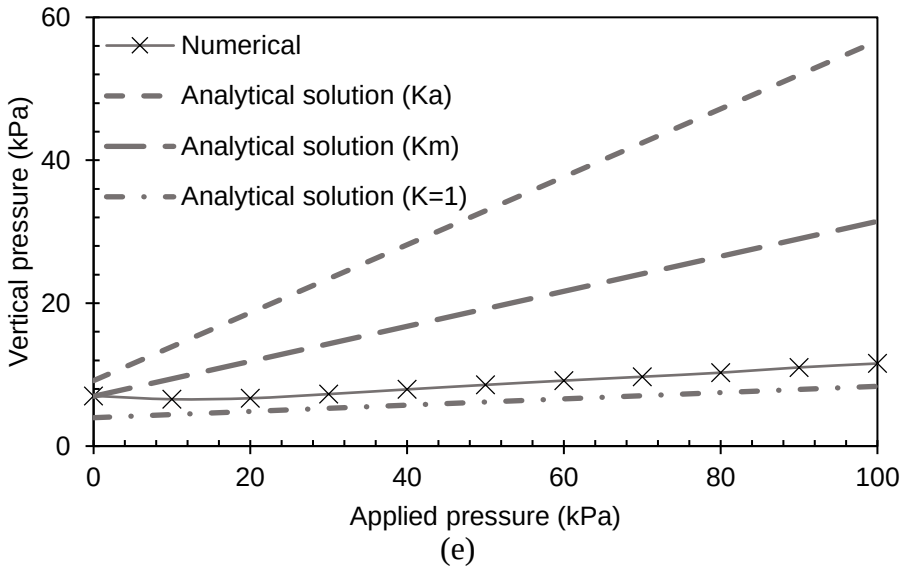

(e)

Figure 6.43 Comparison between the numerical results and the analytical solution for the models with the footing widths of: (a) 0.25B; (b) 0.5B; (c) 1.5B; (d) 2B; and (e) 5B at H/B = 2 (Continued).

CHAPTER 7 CONCLUSIONS AND RECOMMENDATIONS

7.1 CONCLUSIONS

In this research, laboratory tests were conducted to investigate the load transfer mechanism (i.e., specifically soil arching) over a reduced scale buried culvert as well as the benefit of Expanded Polystyrene (EPS) geofoam installed above the culvert in reducing the vertical pressure on it. Additionally, soil subsidence and/or consolidation of foundation (soft) soil in-between two stationary supports were simulated using the trapdoor test setup to investigate both soil arching and geosynthetic tensioned membrane when geosynthetic was used. In these tests, the stability of soil arching under surface footing loading was evaluated. Both static and cyclic footing loads were utilized to simulate traffic loading. All physical model tests were conducted under a plane strain condition. To comprehensively assess the effect of localized surface loading with different configurations on the soil arching, numerical models simulating trapdoor tests were built and validated against the results of the experimental tests. A series of parametric studies were conducted to investigate the effects of several parameters on the soil arching degree. Based on the experimental and numerical results, the following main conclusions can be made:

7.1.1 Study of Soil Arching with Geofoam on Culvert

Soil arching is a common phenomenon in many geotechnical applications, and it contributes to the degree of the load transfer on buried structures. Seven reduced-scale model tests were conducted under a plane strain condition in this study to evaluate the vertical pressure on the top of a rigid concrete culvert constructed with the positive projection embankment (PPE) and the induced trench installation (ITI) on an unyielding foundation under footing loads. Expanded Polystyrene

(EPS) geofoam, a lightweight material, was utilized as a compressible inclusion above the concrete culvert in the ITI tests. The effects of EPS geofoam, including its stiffness and thickness, on the distribution of vertical stresses on the culvert, were evaluated and discussed. The experimental results were also compared with the analytical solutions. From this study, the following conclusions can be drawn:

1. Negative soil arching was mobilized under the embankment weight in the PPE test and increased the measured vertical pressure on the culvert by 13% as compared with the overburden pressure. The installation of an EPS geofoam eliminated the increase of the vertical pressure on the culvert in the ITI tests due to the embankment weight despite the geofoam underwent a small compression.
2. As the footing load increased in the PPE test, the relative settlement induced by the footing load increased the degree of negative soil arching and caused the vertical pressure to increase by 37% as compared with that calculated without a buried structure under an applied footing pressure of 130 kPa.
3. When an EPS geofoam was installed above the culvert in the ITI tests, positive soil arching was mobilized so that the vertical pressure on the geofoam decreased and that on the surrounding soil increased. However, soil arching was found to be partially mobilized based on the measured soil arching ratio due to the low modulus ratio of soil to geofoam that caused limited compression of the geofoam (i.e., limited relative displacement).
4. The stiffness of the EPS geofoam contributed to positive soil arching. The low-stiffness (i.e., low density) geofoam underwent larger compression, causing lower vertical pressure on the culvert than the high stiffness geofoam. Within the range of geofoam stiffness, the low-density geofoam reduced the vertical pressure on the culvert by 45% as compared with

that in the PPE while the high-density geofoam reduced the vertical pressure by 31% as compared with that in the PPE at an applied footing pressure of 130 kPa.

5. The measured vertical pressure on the culvert decreased more when a thin geofoam was used than a thick geofoam. This finding is different from what other researchers reported, who found that a thick geofoam is more effective in reducing the pressure on the culvert under a uniform surface pressure. In this study, the thick geofoam showed a stiffer behavior than the thin geofoam of the same density. An optimum geofoam thickness may exist, which deserves further investigations.
6. When a footing load is applied on the surface, the vertical pressure on the top of the culvert depends on soil arching within the embankment fill and the distribution of the footing load. The calculated vertical pressures on the top of the culvert using the Marston solution for soil arching for the soil self-weight and the Boussinesq's solution or the 2:1 distribution method for the footing load distribution were in good agreement with those measured in this study.
7. Cyclic loading minimized the soil arching effect induced by the compressible geofoam and geofoam density showed no effect on the vertical pressure over the culvert under cyclic loading.

7.1.2 Study of Soil Arching with Spring-based Trapdoor

This chapter presents twelve physical model tests that were conducted under a plane-strain condition to evaluate the soil arching mobilization and degradation in unreinforced and geosynthetic-reinforced fill under localized surface loading. The trapdoor test setup was utilized in these tests to simulate the settlement of a subsoil between two supports and investigate the soil

arching behavior within the fill. Following the fill placement, either static or cyclic surface loading was applied on the top of the fill to simulate a traffic load and to assess its effect on the soil arching behavior. The effect of geosynthetic reinforcement on the soil arching behavior was investigated for both single layer (SL) and double layer (DL) of geosynthetic reinforcement. The soil arching mobilization and degradation were evaluated based on the soil arching ratio while the geosynthetic benefit was evaluated based on the stress reduction ratio. The following conclusions can be drawn from this study:

1. Soil arching developed under soil self-weight as the fill height increased and trapdoor displacement increased in both unreinforced and geosynthetic-reinforced fill so that the pressure on the trapdoor or the geosynthetic reinforcement decreased and that on the supports increased.
2. Under static footing loading, the degree of soil arching increased at the low applied total pressure of approximately 50 kPa (or small trapdoor displacement δ/B = 2.0%); however, under higher footing loading that caused a larger trapdoor displacement, soil arching degraded or stress recovered.
3. In the geosynthetic-reinforced fill tests, less soil arching (based on the measured pressure on the geosynthetic) was mobilized during fill placement than that in the unreinforced fill tests because the deflected geosynthetic changed the shape of soil displacement above the geosynthetic and reduced the total amount of soil movement even though the trapdoor had approximately the same movement as that in the unreinforced fill tests. A smaller amount of soil movement minimized soil arching mobilization.
4. Based on the measured strains in the geogrid, the maximum tensile strain was at the trapdoor edges during fill placement in the SL reinforced tests, which indicates the

mobilization of tensioned membrane in the geosynthetic and transfer of the vertical pressure on the reinforcement to the adjacent supports. Also, during the fill placement, the load transfer platform formed by double layer of geosynthetic reinforcement as well as the soil in between functioned as a beam because the maximum tensile strain existed at the support edges and trapdoor centerline in the lower geogrid layer; and a compressive strain occurred across the trapdoor in the upper geogrid layer. Under footing loading, however, the overall strains along the geogrid layers in both SL and DL reinforced tests were tensile strains, with higher tensile strains at the support edges as compared with those over the trapdoor; therefore, the tensioned membrane effect was the dominating mechanism in the reinforcement layers that helped transfer the vertical load to the adjacent supports.

5. In the SL reinforced fill tests, the results show that the geosynthetic reinforcement reduced the measured pressure on the trapdoor as compared with the case without a geosynthetic due to more tensioned membrane effect in the geosynthetic as the trapdoor displacement increased under footing loading. The results also show that the geosynthetic helped transfer more fill and surface loads onto the supports and reduced the rate of stress recovery under increasing surface loading, thus helped maintain more stable arching.
6. In this study, an Arching Full Degradation Pressure (AFDP) is defined as an applied footing pressure required to eliminate soil arching (i.e., the soil arching ratio equals 1.0). Soil arching degradation first happened at the center and then extended to the area above the trapdoor. The use of geosynthetic reinforcement reduced the soil arching ratio and increased the footing pressure required to fully degrade soil arching and eliminate the geosynthetic benefits. The use of geosynthetic reinforcement increased the degradation pressure on the trapdoor by 69%, 59%, and 27% as compared with those of the

unreinforced fill tests when the four-spring-supported rigid trapdoor, the six-spring-supported rigid trapdoor, and the six-spring-supported flexible trapdoor, respectively, were used. In addition, a higher applied pressure was required to degrade soil arching and eliminate the geosynthetic benefits in DL biaxial geogrid test. The degradation pressure required for the DL geogrid-reinforced fill test was 143% higher than that for the unreinforced fill test. This degradation pressure was higher than that in the SL reinforced fill test, since only the tensioned membrane governed the geogrid behavior in the SL reinforced fill test, while in the DL reinforced fill test, both the tensioned membrane and the beam behavior of the load transfer platform existed.

7. The total pressures on the trapdoor in the low-stiffness trapdoor tests were lower than those in the high-stiffness trapdoor tests because the low-stiffness trapdoor had more displacement and soil arching than the high-stiffness trapdoor. Therefore, both SARs and SRRs in the low-stiffness trapdoor tests were less than those in the high-stiffness trapdoor tests under the total applied pressure up to 90 kPa or its corresponding normalized displacement up to 4.5%. As the total applied pressure increased beyond 90 kPa, a much faster displacement rate with the low-stiffness trapdoor occurred and caused soil arching to degrade and the SARs to increase faster than those with the high-stiffness trapdoor.
8. In the one-segment rigid trapdoor tests, the trapdoor underwent uniform displacement that caused a non-uniform pressure distribution (i.e., higher pressure at the center and lower pressure at the edges), which is similar to that under a rigid footing on granular material. On the other hand, the three-segment flexible trapdoor had a non-uniform displacement (i.e., larger displacement at the center and smaller displacement at the edges) and a more uniform pressure distribution; therefore, it behaved more like a flexible footing on granular

material. The average measured pressures on the flexible trapdoor were higher than those on the rigid trapdoor, which led to higher SARs and SRRs for these tests. In conclusion, the mode of soil movement over the trapdoor during the fill placement and under localized footing loading affected the overall arching degree. Use of a rigid trapdoor overpredicts the degree of soil arching degree.

9. In this study, an analytical solution is proposed based on Terzaghi's theory but for a localized footing load applied along the trapdoor centerline. The analytical solution well predicted the measured vertical pressures on the trapdoor under localized footing loading within the range of the tests conducted in this study.
10. Cyclic loading increased the pressure on the trapdoor as compared to static loading, which resulted in the DMF higher than 1.0. In the tests without soil arching, the DMF increased from 1.0 to 1.2 as the footing pressure increased to approximately 120 kPa. However, the effect of cyclic loading was more pronounced in the tests when soil arching was mobilized because the DMF increased from 1.0 to 1.4 as the footing pressure increased to approximately 80 kPa. This result indicates that soil arching was less effective in reducing the pressure on the trapdoor under cyclic loading as under static loading. Although the minimum SARs under cyclic loading were less than those under static loading at the low applied pressure (i.e., 48 kPa for the total pressure), the degree of soil arching under cyclic loading was higher (i.e., lower SAR) than that under static loading at the higher applied pressure. Soil arching exhibited arching degradation and even collapse under static loading which was less pronounced under cyclic loading as the applied pressure increased beyond 80 kPa. This phenomenon can be explained by the fact that cyclic loading induced more differential displacement within the fill than static loading that generates more shear

stresses and soil arching, which helps transfer more pressure away from the yielding base to the supports.

7.1.3 Numerical Simulation of Trapdoor Tests

This chapter presented two-dimensional numerical simulations of the trapdoor tests conducted in this study under static footing loading using the FLAC^{3D} software. The aim of the numerical simulations was to study the effects of: (1) fill height, (2) footing width and location, (3) non-uniform (e.g., multi-segment trapdoor) trapdoor displacement, on soil arching mobilization and degradation. This chapter discussed the selection of materials, constitutive models, interface elements, and boundary conditions for the numerical models and presented the calibration of the parameters used for the numerical models. After the calibration of the material properties, the numerical models were verified against the experimental results presented previously in Chapter 5. In addition, the numerical results were compared with the proposed analytical solution for soil arching considering localized surface loading. The following conclusions can be made based on the numerical parametric study presented in this chapter and the comparisons of the numerical results with the analytical solution:

1. For the fill heights investigated in this study (i.e., H/B = 1, 2 (baseline case), and 3), the degree of soil arching increased as the fill height increased due to additional shear stresses mobilized within the fill. Under footing loading, the model with H/B = 1 had the highest vertical pressure on the trapdoor followed by the models with H/B = 2 and 3, respectively. For instance, at a footing pressure of 100 kPa, reducing the fill height from H/B = 2 to H/B = 1 increased the average pressure on the trapdoor by approximately 97%, while increasing

the fill height from H/B = 2 to 3 reduced the average pressure on the trapdoor by approximately 31%.

2. For the footing widths investigated (i.e., 0.25B, 0.5B, 1B (baseline case), 1.5B, 2B, and 5B (uniform)) at H/B = 2, the model with a footing width of 0.5B had the highest vertical pressure on the trapdoor among all the cases. For example, reducing the footing width from 1B to 0.5B or 0.25B increased or reduced the average pressure on the trapdoor by approximately 47% and 11%, respectively, at an applied footing pressure of 60 kPa. On the other hand, increasing the footing width from 1B to 1.5B, 2B, and 5B (uniform) reduced the average pressure on the trapdoor by approximately 34%, 45%, and 50%, respectively, at the same applied pressure.
3. The footing width of 1B was the most critical width that induced the highest pressure on the trapdoor when H/B = 1 and 3. As the footing width increased, less pressure was exerted on the trapdoor and more pressure was transferred onto the supports for both H/B ratios. In addition, for the same footing width, the pressure on the trapdoor induced by surface footing loading increased as the fill height decreased.
4. For the footing offsets investigated (i.e., 0.0B (baseline case), 0.25B, 0.5B, 0.75B, and 1B), the model with a footing offset of 0.0B had the highest vertical pressure on the trapdoor centerline (TC) among all the cases. Also, as the footing offset increased to 1B, less pressure reached the trapdoor centerline. For instance, increasing the footing offset from 0.0B to 0.25B, 0.5B, 0.75B and 1B reduced the pressure on the trapdoor centerline by approximately 9%, 33%, 53%, and 63%, respectively, at an applied pressure of 100 kPa. At the same time, as the footing offset increased to 1B, less pressure was exerted on the trapdoor edge and more pressure was transferred onto the support edge.

5. For the multi-segment (i.e., three-segment and nine-segment) trapdoor models, both models had approximately the same vertical pressures on the trapdoor. The nine-segment trapdoor resulted in a slightly lower pressure at the support edge than the three-segment trapdoor during fill placement. As the footing pressure increased, the pressure on the nine-segment trapdoor was higher than that on the three-segment trapdoor, and consequently, less pressure was transferred onto the support edges. At the same time, more uniform pressure distribution on the nine-segment trapdoor was observed as compared to that on the three-segment trapdoor. Increasing the number of trapdoor segments reduced the degree of soil arching due to the increased non-uniformity of trapdoor displacement and more differential settlements between the trapdoor segments. More differential settlement segments increased the number of shear surfaces between the trapdoor segments that changed the mode of soil arching such that the pressure was transferred from the inner (middle) trapdoor to those on the sides.
6. The numerical results for different fill height to trapdoor width ratios (H/B = 1, 2, and 3) and different footing widths (0.25B, 0.5B, 1B, 1.5B, 2B, and 5B (uniform)) were selected for comparison with the analytical arching solution presented in Chapter 5. Generally, the analytical solution predicted the average vertical pressures on the trapdoor reasonably well with all the numerical results. The vertical pressures on the trapdoor predicted by the analytical solution using K_a were close to the numerical results for the models with the footing width of 1B at H/B = 1, 2, and 3 or with footing widths of 0.5B, 1.5B, and 2B at H/B = 2. The vertical pressures on the trapdoor predicted by the analytical solution using K_m *and* $K=1$ were close to the numerical results for the models with the footing widths of 0.25B and 5B (uniform), respectively. In addition to the experimental data in Chapter 5,

the numerical results further validated the proposed analytical solution for soil arching over a trapdoor (or a yielding soil zone) under localized surface static footing loading.

7.2 RECOMMENDATIONS FOR FUTURE STUDY

The following are recommended for future study to better understand the behavior of soil arching under surface loading:

1. The results and findings from this study were based on reduced-scale physical models and numerical models and can be verified through field studies.
2. Since both experimental study and numerical analysis evaluated the soil arching under localized footing loading in a single trapdoor test configuration, interaction of multiple trapdoors (i.e., yielding of multiple soil zones) on soil arching is recommended.
3. Also, both experimental study and numerical analysis were under 2D plane-strain condition, which their findings are relevant for the case of pile-supported embankments with piles arranged in beam pattern; nevertheless, investigation of soil arching under a 3D condition is recommended to better understand soil arching when piles are arranged in square or triangular pattern.
4. The proposed analytical solution in this study can predict the vertical stresses on a yielding soil zone when soil arching is mobilized under soil self-weight plus a localized footing loading but it does not predict the vertical stresses when the soil arching degrades under increasing footing loading. Therefore, a theoretical model or solution is needed to predict the process of soil arching collapse including the full degradation load under surface loading.

REFERENCES

ACPA (2011). *Concrete Pipe Design Manual*, American Concrete Pipe Association, Vienna, Va.

Adachi, T., Kimura, M., and Tada, S. (1989). "Analysis on the preventive mechanism of landslide stabilizing piles." *Proceedings of the 3rd International Symposium of numerical models in geotechnics, Niagara Falls, Canada, 8-11 May*, Elsevier Applied Science Publishers Limited, 15(3), 691-698.

Agaiby, S. W. and Jones, C. J. (1995). "Design of reinforced fill systems over voids." *Canadian Geotechnical Journal*, 32(6), 939-945.

Agaiby, S. W. and Jones, C. J. (1996). "Design of reinforced fill systems to support footings overlying cavities." *Geotextiles and Geomembranes*, 14(1), 57-72.

Ahmed, M. (2016). *Experimental Investigations into the Role of Geosynthetic Inclusions on the Earth Pressure Acting on Buried Structures*. Ph.D. Thesis, McGill University, Montreal, Quebec, Canada.

Al-Naddaf, M. (2017). *Investigation of Soil Arching Stability under Static and Cyclic Surface Loading Using Trapdoor Model Tests*. Master's thesis, The University of Kansas, Lawrence, KS.

Al-Naddaf, M., Han, J., Jawad, S., Abdulrasool, G., and Xu, C. (2017). "Investigation of stability of soil arching under surface loading using trapdoor model tests." *Proceedings of the 19th International Conference on Soil Mechanics and Geotechnical Engineering*, Korea, 889-892

Al-Naddaf, M., Han, J., Xu, C., and Rahmaninezhad, S. M. (2018). "Effect of geofoam on vertical stress distribution on buried structures subjected to static and cyclic footing loads." *Journal of Pipeline Systems Engineering and Practice*, ASCE, 10(1), 04018027.

Al-Naddaf, M., Han, J., Xu, C., Jawad, S., and Abdulrasool, G. (2019). “Experimental investigation of soil arching mobilization and degradation under localized surface loading.” *Journal of Geotechnical and Geoenvironmental Engineering*, ASCE, (Accepted).

Ariyarathne, P. and Liyanapathirana, D. (2015). "Review of existing design methods for geosynthetic-reinforced pile-supported embankments." *Soils and Foundations*, 55(1), 17-34.

ASTM (2011). "Standard practice for classification of soils for engineering purpose." *ASTM-D2487-11*, West Conshohocken, PA.

ASTM (2016). "Standard test method for compressive properties of rigid cellular plastics." *ASTM D1621-16*, West Conshohocken, PA.

Atkinson, J., and Potts, D. (1977). "Stability of a shallow circular tunnel in cohesionless soil." *Geotechnique*, 27(2), 203-215.

Bell, A., Jenner, C., Maddison, J., and Vignoles, J. (1994). "Embankment support using geogrids with vibro concrete columns." *Proc., Proceedings, 5th International Conference on Geotextiles, Geomembranes, and Related Products*, 335-338.

Bennett, R. M., Wood, S. M., Drumm, E. C., and Rainwater, N. R. (2005). "Vertical loads on concrete box culverts under high embankments." *Journal of Bridge Engineering*, ASCE, 10(6), 643-649.

Bertin, Y. (1978). *A Centrifuge Study of the Collapse of Hemispherical Cavities in Soil.*, M.Sc. Thesis, University of Florida, Gainesville, Florida.

Bhandari, A. (2010). *Micromechanical Analysis of Geosynthetic-Soil Interaction Under Cyclic Loading.* Ph.D. Dissertation, the University of Kansas.

Bhandari, A. and Han, J. (2018). “2D physical modeling of soil displacements above trapdoors.” *Geotechnical Research*, 5(2), June, 68-80.

Bloomquist, D., Boyd, A., Chen, Y., and Crosby, M. (2009). *Load Response Comparison Between Fiber and Steel Reinforced Concrete Pipe-Phase Two*. Report developed for the Florida Department of Transportation, University of Florida, Gainesville, FL.

Bosscher, P. J., and Gray, D. H. (1986). "Soil arching in sandy slopes." *Journal of Geotechnical Engineering*, 112(6), 626-645.

British Standard 8006. (2010). *Code of Practice for Strengthened/Reinforced Soils and Other Fills.* British Standard Institution, London, UK.

Broms, B., and Wong, I. (1985). "Embankment piles." *Proc., Proceedings of 3rd International Geotechnical Seminar—Soil Improvement Methods*, Singapore: Nanyang Technological Institute, 167-178.

Brown, C. B. (1967). "Forces on rigid culverts under high fills." *Journal of the Structural Division* ASCE, 93(1), 195-215.

Card, G. and Carter, G. (1995). "Case history of a piled embankment in London's Docklands." *Geological Society, London, Engineering Geology Special Publications*, 10(1), 79-84.

Carlsson, B. (1987). "Reinforced soil, principles for calculation." *Terratema AB*, Linköping (in Swedish).

Chen, B. and Sun, L. (2013a). "Performance of a reinforced concrete box culvert installed in trapezoidal trenches." *Journal of Bridge Engineering*, ASCE, 19(1), 120-130.

Chen, B. and Sun, L. (2013b). "The impact of soil properties on the structural integrity of high-fill reinforced concrete culverts." *Computers and Geotechnics*, 52(1), 46-53.

Chen, H. L., Chen, S. E., and Kiger, S. A. (1991). "An experimental study of dynamic soil arching." *Proceedings of the 62nd Shock and Vibration Symposium*, (1), (Defense Nuclear Agency, Springfield, Virginia), 190-198.

Chevalier, B., Combe, G., and Villard, P. (2007). "Experimental and numerical studies of load transfers and arching effect in the trap-door problem." *Laboratoire Sols, Solides, Structures*.

Chen, R., Chen, Y., Han, J., and Xu, Z. (2008). "A theoretical solution for pile-supported embankments on soft soils under one-dimensional compression." *Canadian Geotechnical Journal*, 45(5), 611-623.

Collin, J. (2003). *NHI Ground Improvement Manual–Technical Summary# 10: Column Supported Embankments*. National Highway Institute, Arlington, Va.

Dancygier, A., and Karinski, Y. (1999). "A simple model to assess the effect of soil shear resistance on the response of soil-buried structures under dynamic loads." *Engineering Structures*, 21(12), 1055-1065.

Dasgupta, A. and Sengupta, B. (1991). "Large-scale model test on square box culvert backfilled with sand." *Journal of Geotechnical Engineering*, 117(1), 156-161.

Delmas, P. (1979). *Sols Renforcés par Géosynthétiques-Premières études.*, Ph.D. Dissertation, Université Scientifique et Médicale de Grenoble.

Demerdash, M. A. (1996). *An Experimental Study of Piled Embankments Incorporating Geosynthetic Basal Reinforcement*. Ph.D. Dissertation, the University of Newcastle-upon-Tyne, 158 p.

Einstein, H. H., and Schwartz, C. W. (1979). "Simplified analysis for tunnel supports." *Journal of Geotechnical and Geoenvironmental Engineering*, ASCE, 109(1), 15-39.

Evans, C. H. (1983). *An Examination of Arching in Granular Soils.*, M.Sc. Thesis, Massachusetts Institute of Technology, 235p.

Feld, J. (1948). "Early history and bibliography of soil mechanics." *Proc., communication présentée à Second International Conference on Soil Mechanics and Foundation Engineering*, Rotterdam, (1), 1-7.

Finn, W. L. (1963). "Boundary value problems of soil mechanics." *Journal of Soil Mechanics and Foundation Division,* ASCE, 89(5), 39-72.

Gabr, M., and Han, J. (2005). "Geosynthetic reinforcement for soft foundations: US perspectives." *International Perspectives on Soil Reinforcement Applications.* ASCE, 1-17.

Gabr, M., and Hunter, T. (1994). "Stress-strain analysis of geogrid-supported liners over subsurface cavities." *Geotechnical & Geological Engineering*, 12(2), 65-86.

Getzler, Z., Komornik, A., and Mazurik, A. (1968). "Model study on arching above buried structures." *Journal of Soil Mechanics & Foundations Div.*, 94(5), 1123-1142.

Giroud, J. P. (1984). "Geotextiles and Geomembranes Definitions, Properties and Design: Selected Papers, Revisions and Comments." Industrial Fabrics Association International,404p.

Giroud, J., Bonaparte, R., Beech, J., and Gross, B. (1990). "Design of soil layer-geosynthetic systems overlying voids." *Geotextiles and Geomembranes*, 9(1), 11-50.

Giroud, J., and Han, J. (2004). "Design method for geogrid-reinforced unpaved roads. I. Development of design method." *Journal of Geotechnical and Geoenvironmental Engineering*, 130(8), 775-786.

Gourc, J., and Villard, P. (2000). "Reinforcement by membrane effect: Application to embankments on soil liable to subsidence." *Proc., Proceedings of the 2nd Asian Geosynthetics Conference*, (1), 55-72.

Han, J. (1999). "Design and construction of embankments on geosynthetic reinforced platforms supported by piles." *Proceedings of 1999 ASCE/PaDOT Geotechnical Seminar*, 66-84.

Han, J. (2015). *Principles and Practice of Ground Improvement*, John Wiley & Sons, Hoboken, New Jersey, USA, June, 432p.

Han, J., and Bhandari, A. (2009). "Evaluation of geogrid-reinforced pile-supported embankments under cyclic loading using discrete element method." *Proc., US-China Workshop on Ground Improvement Technologies*, 73-82.

Han, J., Bhandari, A., and Wang, F. (2011). "DEM analysis of stresses and deformations of geogrid-reinforced embankments over piles." *International Journal of Geomechanics*, 12(4), 340-350.

Han, J., and Gabr, M. (2002). "Numerical analysis of geosynthetic-reinforced and pile-supported earth platforms over soft soil." *Journal of geotechnical and geoenvironmental engineering*, ASCE, 128(1), 44-53.

Han, J., Oztoprak, S., Parsons, R. L., and Huang, J. (2007). "Numerical analysis of foundation columns to support widening of embankments." *Computers and Geotechnics*, 34(6), 435-448.

Han, J., Wang, F., Al-Naddaf, M., and Xu, C. (2017). "Progressive development of two-dimensional soil arching with displacement." *International Journal of Geomechanics*, 10.1061/(ASCE)GM.1943-5622.0001025, 04017112.

Han, J., Wang, F., Xu, C., and Al-Naddaf, M. (2016). "Fully-mobilized soil arching versus partially-mobilized soil arching." *Proc., 2016 Int. Conf. on Transportation Infrastructure and Materials*, DEStech Publications, Lancaster, PA.

Handy, R. L. (1985). "The arch in soil arching." *Journal of Geotechnical Engineering*, 111(3), 302-318.

Harris, G. (1974). "A sandbox model used to examine the stress distribution around a simulated longwall coal-face." *Proc., International Journal of Rock Mechanics and Mining Sciences & Geomechanics Abstracts*, Elsevier, 325-335.

Helwany, S. M., and Chowdhury, A. (2000). *Dynamic Lateral Earth Pressure on Underground Structures*. Research Report, submitted to Air Force Office of Scientific Research, 68p.

Hewlett, W. (1984). *The Analysis and Design of Bridge Approach Support Piling*. Part I project report, Cambridge University Engineering Department.

Hewlett, W., and Randolph, M. (1988). "Analysis of piled embankments." *Ground Engineering*, 21(3), 12-18.

Holmberg, S. (1979). "Bridge approaches on soft clay supported by embankment piles." *Geotechnical Engineering*, 10(1).

Holtz, R., and Massarsch, K. (1976). "Improvement of the stability of an embankment by piling and reinforced earth." *Proc., Sechste Europaeische Konferenz Fuer Bodenmechanik und Grndbau, (1)*.

Hong, W. P., Hong, S., and Kang, T. H.-K. (2016). "Lateral earth pressure on a pipe buried in soft grounds undergoing lateral movement." *Journal of Structural Integrity and Maintenance*, 1(3), 124-130.

Huang, J., Han, J., and Collin, J. G. (2005). "Geogrid-reinforced pile-supported railway embankments-three dimensional numerical analysis." *Journal of Transportation Research Board*, 1936, 221-229.

Iglesia, G. R., Einstein, H. H., and Whitman, R. V. (2014). "Investigation of Soil Arching with Centrifuge Tests." *Journal of Geotechnical and Geoenvironmental Engineering*, 140(2), 04013005.

Itasca. (2014). Fast Lagrangian Analysis of Continua in 3 Dimensional (Flac3D) Software Manual.

Jang, D., and Montero, C. (1993). "Design of linear systems under vertical expansions: an alternative to geogrids." *Proceedings of Geosynthetics*, Canada Vancouver, BC:[sn], (3), 1487-1510.

Janssen, H. (1895). "Versuche über getreidedruck in silozellen." *Zeitschr. d. Vereines deutscher Ingenieure*, 39(35), 1045-1049.

Jenck, O., Dias, D., and Kastner, R. (2007). "Two-dimensional physical and numerical modeling of a pile-supported earth platform over soft soil." *Journal of Geotechnical and Geoenvironmental Engineering*, 133(3), 295-305.

Jones, C., Lawson, C., and Ayres, D. (1990). "Geotextile reinforced piled embankments." *Proc., of the 4th International Conference on Geotextiles, Geomembranes and Related Products*, Rotterdam, 155-160.

Kakrasul, J.I., Han, J., Rahmaninezhad, S.M., and Weldu, M. (2016). "Model tests of geosynthetic-reinforced earth walls with limited-space retained fill. " *3rd Pan-American Conference on Geosynthetics (GeoAmericas)*, Miami, FL., 2(1), 1279-1286.

Kang, J., Parker, F., Kang, Y. J., and Yoo, C. H. (2008). "Effects of frictional forces acting on sidewalls of buried box culverts." *International Journal for Numerical and Analytical Methods in Geomechanics*, 32(3), 289-306.

Kempfert, H., Göbel, C., Alexiew, D., and Heitz, C. (2004). "German recommendations for reinforced embankments on pile-similar elements." *Proc., EuroGeo3-third European*

Geosynthetics Conference, Geotechnical Engineering with Geosynthetics, Deutsche Gesell schaft fur Geotechnik, Munich, Germany, 279-284.

Kempton, G., Russel, D., Pierpoint, N. D., and Jones, C. J. F. P. (1998). "Two- and three-dimensional numerical analysis of the performance of piled embankments." *Proc., 6th Int. Conf. on Geosynthetics*, Atlanta, 767–772.

Key, A. J. (1999). *Behaviour of Two Layer Railway Track Ballast under Cyclic and Monotonic Loading*. Ph.D. thesis, University of Sheffield, Sheffield, UK.

Kezdi, A. (1975). "Lateral earth pressure." *Foundation engineering handbook, Van Nostrand Reinhold Company*, New York, 197-220.

Kim, K. and Yoo, C. H. (2005). "Design loading on deeply buried box culverts." *Journal of Geotechnical and Geoenvironmental Engineering*, 10.1061/(ASCE)1090-0241(2005)131:1(20), 20-27.

King, D. J., Bouazza, A., Gniel, J. R., Rowe, R. K., and Bui, H. H. (2017). "Serviceability design for geosynthetic reinforced column supported embankments." *Geotextiles and Geomembranes*, 45(4), 261-279.

Koutsabeloulis, N., and Griffiths, D. (1989). "Numerical modelling of the trap door problem." *Geotechnique*, 39(1), 77-89.

Ladanyi, B., and Hoyaux, B. (1969). "A study of the trap-door problem in a granular mass." *Canadian Geotechnical Journal*, 6(1), 1-14.

Laurent, Y., Dias, D., Simon, B., and Kastner, R. (2003). "A 3D finite difference analysis of embankments over pile-reinforced soft soil." *Proc., Int. Workshop on Geotechnics of Soft Soils—Theory and Practice*, VGE, Noordwijkerhout, The Netherlands, 271–276.

Liedberg, N. (1997). "Load reduction on a rigid pipe: pilot study of a soft cushion installation." *Journal of the Transportation Research Board* (1594), Transportation Research Record, Washington, D.C., 217-223.

Low, B., Tang, S., and Choa, V. (1994). "Arching in piled embankments." *Journal of Geotechnical Engineering*, 120(11), 1917-1938.

Magnan, J. P. (1994). "Methods to reduce the settlement of embankments on soft clay: a review." *Proc., Vertical and Horizontal Deformations of Foundations and Embankments*, ASCE, 77-91.

Marston, A. (1930). "The theory of external loads on closed conduits in the light of the latest experiments." *Highway Research Board Proc.,* Transportation Research Board, Washington, DC.

Marston, A. and Anderson, A. (1913). *The Theory of Loads on Pipes in Ditches: And Tests of Cement and Clay Drain Tile and Sewer Pipe*, Iowa State College of Agriculture and Mechanic Arts, Ames, Iowa.

McAffee, R. and Valsangkar, A. (2005). "Performance of an induced trench installation." *Journal of the Transportation Research Board* (1936), Transportation Research Record, Washington, D.C., 230-237.

McAffee, R. P. and Valsangkar, A. J. (2008). "Field performance, centrifuge testing, and numerical modelling of an induced trench installation." *Canadian Geotechnical Journal*, 45(1), 85-101.

McGuigan, B. L. and Valsangkar, A. J. (2010). "Centrifuge testing and numerical analysis of box culverts installed in induced trenches." *Canadian Geotechnical Journal*, 47(2), 147-163.

McGuigan, B. L. and Valsangkar, A. J. (2011). "Earth pressures on twin positive projecting and induced trench box culverts under high embankments." *Canadian Geotechnical Journal*, 48(2), 173-185.

McNulty, J. W. (1965). *An Experimental Study of Arching in Sand*. Rep. No.I-674, US Army Engineer Waterways Experiment Station, Corps of Engineers, Vicksburg, Mass.,170.

Meguid, M., Hussein, M., Ahmed, M., Omeman, Z., and Whalen, J. (2017). "Investigation of soil-geosynthetic-structure interaction associated with induced trench installation." *Geotextiles and Geomembranes*, 45(4), 320-330.

Miki, H. (1997). "Design of deep mixing method of stabilization with low improvement ratio." *Proc., of the first seminar on ground improvement in highways,* Bangkok, Thailand, 197-204.

Oshati, O. S., Valsangkar, A. J., and Schriver, A. B. (2012). "Earth pressures exerted on an induced trench cast-in-place double-cell rectangular box culvert." *Canadian Geotechnical Journal*, 49(11), 1267-1284.

Penman, A., Charles, J., Nash, J., and Humphreys, J. (1975). "Performance of culvert under Winscar dam." *Geotechnique*, 25(4), 713-730.

Rahmaninezhad, S. M., Han, J., Weldu, M., and Kakrasul, J. I., (2016). "Effects of methods of applying normal stresses in pullout tests on pressure distributions and pullout resistance, " *3rd Pan-American Conference on Geosynthetics (GeoAmericas)*, Miami, FL., 2(1), 1308-1315.

Rahmaninezhad, S., Yasrobi, S. S., and Eftekharzadeh, S. (2009). "Effects of compaction in the subgrade of the reinforced sand backfills with geotextile on bearing capacity." *International Journal of Civil Engineering*, 12, 320-328.

Reichman, O., and Smith, S. C. (1990). "Burrows and burrowing behavior by mammals." Chapter 5, in *Current Mammalogy*, H.H. Genoways (ed.), Plenum Press, New York and London, 197-244.

Reid, W., and Buchanan, N. (1984). "Bridge approach support piling." *Piling and ground treatment*, Thomas Telford Publishing, 267-274.

Rui, R., Han, J., van Eekelen, S.J.M., and Wang, Y., (2019). "Experimental investigation of soil arching evolution in unreinforced and geosynthetic-reinforced pile-supported embankments." ASCE Journal of Geotechnical and Geoenvironmental Engineering, 145(1), 04018103-1 to 11.

Rui, R., van Tol, A., Xia, Y., van Eekelen, S., and Hu, G. (2016). "Investigation of Soil-Arching Development in Dense Sand by 2D Model Tests." *Geotechnical Testing Journal* 39, no. 3 (2016): 415-430. doi: https://doi.org/10.1520/GTJ20150130.

Russell, D., and Pierpoint, N. (1997). "An assessment of design methods for piled embankments." *Ground Engineering*, 30(10), 39-44.

Shenton, M. (1975). "Deformation of railway ballast under repeated loading conditions." *Railroad Track Mechanics and Technology (Kerr ed.)*, Princeton University, 387–404.

Sladen, J. and Oswell, J. (1988). "The induced trench method—a critical review and case history." *Canadian Geotechnical Journal*, 25(3), 541-549.

Spangler, M. (1948). "Underground conduits-an appraisal of modern research." *Transactions of the American Society of Civil Engineers*, 113(1), 316-345.

Spangler, M. (1950). "Field measurements of the settlement ratios of various highway culverts." *Iowa Engineering Experiment Station Bulletin* 170, Ames, Iowa.

Spangler, M. (1964). "Protection of underground structures by arch action associated with the imperfect ditch method of construction." *Proc., of the Symposium on Soil-Structure Interaction,* the University of Arizona, Tucson, Arizona, 531-546.

Spangler, M., and Handy, R. (1973). "Loads on underground conduits." *Soils Engineering*, New York, (3), 658-686.

Sun, L., Hopkins, T., and Beckham, T. (2011). "Long-term monitoring of culvert load reduction using an imperfect ditch backfilled with geofoam." *Journal of the Transportation Research Board* (2212), Transportation Research Record, Washington, D.C., 56-64.

Sun, L., Hopkins, T. C., and Beckham, T. L. (2009). *Reduction of Stresses on Buried Rigid Highway Structures Using the Imperfect Ditch Method and Expanded Polysterene (Geofoam).* Kentucky Transportation Center, Report No. KTC-07-14-SPR- 228-01-1F. The University of Kentucky, Lexington, KY.

Terzaghi, K. (1936*).* "Stress distribution in dry and in saturated sand above a yielding trap-door." *Proceedings of Frist International Conference on Soil Mechanics and Foundation Engineering*, Cambridge, Massachusetts, 307-311.

Terzaghi, K. (1943). *Theoretical Soil Mechanics*, John Wiley & Sons, New York, 66-76.

Tien, H. J. (1996). “A literature study of the arching effect.” Master’s thesis, Massachusetts Institute of Technology, Cambridge, MA.

Tsur-Lavie, Y., Denekamp, S., and Fainstein, G. (1988). "Surface subsidence associated with long wall mining: Two and three dimensional boundary element model." *Geological Society, London, Engineering Geology Special Publications*, 5(1), 225-231.

Van Eekelen, S. J., Bezuijen, A., Lodder, H., and Van Tol, A. (2012). "Model experiments on piled embankments. Part I." *Geotextiles and Geomembranes*, 32, 69-81.

Van Eekelen, S. J., Bezuijen, A., and Van Tol, A. (2013). “An analytical model for arching in piled embankments.” *Geotextiles and Geomembranes*, 39, 78–102. https://doi.org/10.1016/j.geotex mem.2013.07.005.

Van Eekelen, S. J. M., Bezuijen, A., Van Tol, A. F., (2011). “Analysis and modification of the British Standard BS 8006 for the design of piled embankments.” *Geotextiles and Geomembranes*, 29, 345–359.

Vaslestad, J., Johansen, T. H., and Holm, W. (1993). "Load reduction on rigid culverts beneath high fills: long-term behavior." *Journal of the Transportation Research Board (1415)*, Transportation Research Record, Washington, D.C., 58-68.

Wang, F., Han, J., Miao, L.-C., and Bhandari, A. (2009). "Numerical analysis of geosynthetic-bridged and drilled shafts-supported embankments over large sinkholes." *Geosynthetics International*, 16(6), 408-419.

Wang, M., Feng, Y., and Jao, M. (1996). "Stability of geosynthetic-reinforced soil above a cavity." *Geotextiles and Geomembranes*, 14(2), 95-109.

Wu, T., and Leonards, G. (1985). "Characterization of soil arching above buried conduits." *Advances in Underground pipeline engineering*, ASCE, 396-407.

Zarnani, S., El-Emam, M. M., and Bathurst, R. J. (2011). "Comparison of numerical and analytical solutions for reinforced soil wall shaking table tests." *Geomechanics and Engineering*, 3(4), 291-321.

Zhao, M., and Cao, W. P. (2012). "A Numerical Analysis of Soil Arching in Piled Embankments." *Advanced Materials Research Vols. 468-471*, (2012) Trans Tech Publ, 638-642.